Heavy Metal Extraction Using Advanced Liquid - Liquid Style Partitioning Systems

A thesis submitted to The University of Manchester for the degree of Doctor of Philosophy in the Faculty of Engineering and Physical Sciences

2015

Kate Tucker

School of Chemistry

Table of Contents

List of Figures

List of Tables

List of Symbols

Symbol	Description
δ	Chemical shift
^{o}C	Degrees Celsius
%	Percentage
cm	Centimetre
g	Gram
kg	Kilogram
M	Mol dm^{-3}
MBq	Mega Becquerel
MHz	Mega Hertz
uM	Micromolar
mL	Millilitre
mM	Millimolar
nM	Nanomolar
nm	Nanometre
ppm	Parts per million

List of Abbreviations

Abbreviation	Description
AHA	Acetohydroxamic Acid
An	Actinides
ANL	Argonne National Lab
BTBP	*bis*-triazinyl bipyridines
BTP	Bis-triazinylpyridine
BTPhen	Bis-triazinylphenanthroline
C5-BTBP	6,6'-bis-(5,6-dipentyl-[1,2,4]triazin-3-yl)-[2,2']bipyridinyl
CCI	Cation Cation Interactions
CDTA	1, 2-cyclohexanediaminetetraacetic acid
c.f.	Confer, Latin: "compare"
CMPO	Octylphenyl-N,N-diisobutylcarbamoylmethylphosphine oxide
$CyMe_4BTBP$	6,6'-Bis(5,5,8,8-tetramethyl-5,6,7,8-tetrahydrobenzo[1,2,4]-triazin-3-yl)-[2,2']-bipyridine
D	Distribution Ratio
DEHiBA	N,N-di(2-ethylhexyl)isobutyramide
DIAMEX	DIAMide Extraction
DMDBTDMA	Dimethyldibutyltetradecylmalonamide
DMDOHEMA	Dimethyldioctylhexylethoxymalonamide
e.g.	Exempli gratia, Latin: "for example"
et al.	Et alii, Latin: "and others"
EURO-GANEX	EUROpean Group ActiNide Extraction
EXAFS	Extended X-Ray Absorption Fine Structure
FBR	Fast breeder reactor
FP	Fission Products
GANEX	Group ActiNide Extraction
GDF	Geological Disposal Facility
HCl	Hydrochloric Acid

$HClO_4$	Perchloric Acid
HEDTA	Hydroxyethyl-ethylenediamine-triacetic acid
HLW	High Level Waste
HNO_3	Nitric Acid
HPT	Hydrogenated Polypropylene Tetramer
ICP-MS	Inductively Coupled Plasma Mass Spectrometry
ICP-OES	Inductively Coupled Plasma Optical Emission Spectrometry
ILW	Intermediate Level Waste
IR	Infra Red
i-SANEX	Innovative Selective Actinide EXtraction
Ln	Lanthanide
LOC	Limiting Organic Concentration
LSC	Liquid Scintillation Counting
LWR	Light Water Reactor
MA	Minor Actinides
MOX	Mixed Oxide Fuel
Na_2CO_3	Sodium Carbonate
NaOH	Sodium Hydroxide
NFC	Nuclear Fuel Cycle
nIR	near Infra Red
NMR	Nuclear Magnetic Resonance
NOM	Natural Organic Matter
NPH	Normal Paraffinic Hydrocarbon
PTFE	Polytetrafluoroethylene
PUREX	Plutonium and Uranium Recovery by EXtraction
PWR	Pressurised Water Reactor
QEXAFS	Quick Extended X-Ray Absorption Fine Structure
REDOX	REDuction and OXidation
SANEX	Selective ActiNide Extraction
SNF	Spent Nuclear Fuel
SO_3-Ph-BTP	Sulfonated BTP
SX	Solvent Extraction
TBP	Tributyl Phosphate

TODGA	N,N,N′,N′-tetraoctyl diglycolamide
TRU	TRansUranics
TRUEX	*TRansUranic EXtraction*
UREX	URanium EXtraction
UV/vis	Ultra violet / visible
VT	Variable Temperature
XANES	X-ray absorption near edge structure
XAS	X-ray absorption spectroscopy

Abstract: Heavy Metal Extraction Using Advanced PUREX Style Partitioning Systems

The University of Manchester, Kate Tucker, Doctor of Philosophy, 2015

Understanding the behaviour of heavy metals involved in the nuclear fuel cycle is of paramount importance to the reprocessing and storage of spent nuclear fuel. These studies have attempted to obtain a greater understanding of the fundamental chemistry of these systems, by investigating extraction performance and speciation in current (PUREX) and proposed (GANEX) extraction processes. Various complexes have been shown to exist in the post-extracted organic fraction of the systems analysed. For Zr(IV), U(VI) and Np(VI) separated from aqueous nitric and hydrochloric using TBP, the complexes $[Zr(NO_3/Cl)_4(TBP)_4]$, $[UO_2(NO_3/Cl)_2(TBP)_2]$ and $[NpO_2(NO_3/Cl)_2(TBP)_2]$ formed, respectively. For Zr(IV) separated from aqueous mixtures of HNO_3 and HCl at equal concentration, a preference was shown to $[Zr(Cl)_4(TBP)_4]$ over the analogous nitrate complex. For U(VI) separated from aqueous mixtures of HNO_3 and HCl, a preference was shown to $[UO_2(Cl)_2(TBP)_2]$, even at high aqueous nitrate concentrations. NMR data for Pu(IV) separated from aqueous HNO_3, HCl and mixtures of both, using TBP were presented, where possible complexation was observed. It is thought that $[Pu(NO_3)_4(TBP)_4]$ or $[PuCl_4(TBP)_4]$ species existed within the organic fraction for Pu(IV) separated from aqueous HNO_3 and HCl, respectively. These systems showed high distribution ratios where an increase was observed with increasing aqueous acid concentration overall.

Distribution ratio data were presented for the lanthanide series separated from aqueous nitric acid, using the proposed GANEX solvent system(s). The lanthanides analysed showed an increase in distribution ratio with increasing aqueous nitric acid concentration and with increasing TODGA concentration in the organic fraction. Heavier lanthanides were observed to give higher distribution ratios overall. The best distribution ratios were observed for lanthanides separated using 0.2 M TODGA with 1-octanol (5 % by volume) over the nitric acid concentration range analysed. For lanthanides separated using 0.5 M DMDOHEMA, an optimum distribution ratio was observed at around 6 M aqueous nitric acid concentration. The distribution ratio data for lanthanides separated from a range of DMDOHEMA concentrations, were observed to increase with increasing organic DMDOHEMA concentration. The distribution ratios observed for isotopes of Np, Am, Eu and Pu separated using 0.2 M TODGA, increased with increasing aqueous nitric acid concentration. The same trend was observed for the aforementioned isotopes separated using 0.5 M DMDOHEMA. However, pertechnetate separated using 0.2 M TODGA from aqueous nitric acid, showed a decrease in the distribution ratios observed over the acid concentration range analysed. This was contrary to pertechnetate separated from aqueous nitric acid using 0.5 M DMDOHEMA, where a small increase in distribution ratio was observed over the concentration range analysed. For Np(VI) separated from some proposed GANEX solvents, the 0.2 M TODGA/0.5 DMDOHEMA combination gave the best distribution of neptunium into the organic fraction. For Np(VI) separated using 0.5 M DMDOHEMA, the complex $[Np(DMDOHEMA)_2(NO_3)_4]$ was observed. Additional attempts to analyse Np(VI) behaviour under GANEX style conditions via EXAFS, were not successful due to immediate reduction of the Np(VI) on the beam line.

Declaration

No portion of the work referred to in this thesis has been submitted in support of an application for another degree or qualification of this or any other university or other institute of learning.

Copyright Statement

Acknowledgements

I would like to express gratitude to my supervisors, Dr's Steph Cornet (initially), Sarah Heath and Clint (Clinton!) Sharrad, for their advice and guidance throughout this Ph.D. My thanks also goes to Dr Robin Taylor for all the helpful science discussions over the last few years.

Thanks to my friends in radiochemistry, past and present, for making this whole experience more bearable: Carlos, Saif, Rajib, Raj, Nigel, Tony, Sherriff, Cloz, Maddie, Chris, Simon, Ally, Goti, Daisy, Waage, Matt, Rosie, Hamza, Pete, Chard, Hugues, Tim and especially to Deborah, Adam, Ryan and Kurt for making me laugh in the lab for the last 3.5 years! And to Chewy – hope you're happy somewhere buddy.

Thanks to Lucy, Pilks and Perri for their support, encouragement and to all the light lunch entertainment – I'm not going to miss "tell me your news" AT ALL! And Lucy, I don't know what i would have done without your magical word skills!!

My thanks to Kurt and Dan for all their help with EXAFS processing and to Dan W, Dan C and Clint for running my samples at DIAMOND whilst I went to Glastonbury!! A big thanks to Tim for all his help at the ANKA beam line, and for being a good beer buddy too.

A very big thank you to everyone in Karlsruhe for all your help and for being so accommodating during our times there – I especially thank Kathy, Jorg, Peter, Andreas, Christian, Nicole, Bjorn and Sasha.

Major thanks to my wonderful friends Tam and Sean for all the (highly educational) fun, Riesling, Philadelphia and RiRi in both Manchester and in Karlsruhe. Viva la Party Flat!

I'd like to say a massive thank you to Dr Nick Bryan for generally being a legend; I don't think I would have even made it past undergraduate without you. My thanks and appreciation also goes to Professor Francis Livens, for being a great source of intellect and guidance during this Ph.D... and for the free lunches at Christies.

Ralph and Andy, thank you for all your help with the NMR over the years– I don't know what I would have done without you both.

I would like to thank my DTC cohort for being such amazing friends over the last few years – Neda, Josh, Sam, Heathcliff, Tim, Chris, Gilly and especially Gerald and Lizzie, it's been an absolute pleasure. My thanks also goes to Vicky Turner looking after us so well.

To all my wonderful friends for their support, especially Em and Alex for keeping a smile on my face, and to A.J., Rob and Liv for understanding the trials and tribulations of a Ph.D better than anyone, which without a doubt, kept me going.

Finally I would like to say an enormous thank you to my Mum, Dad, Gran and Sister, for their endless support, and for always trying to instil positivity in me, even in the most rocky of times. Finally, I thank Jon who had to put up with me during the worst part of all this, and who's logic was consistently infallible!

The first principal is that you must not fool yourself and you are the easiest person to fool.
- Richard Feynman

1 Introduction

1.1 Nuclear Fuel Cycle

The nuclear fuel cycle (NFC) consists of a series of different industrial processes that allow electricity to be produced via the fission of, most commonly, uranium-235. The nuclear fuel cycle can be split in to three components: the front end, where the fuel is prepared for use, the service period, in which the fuel is used during reactor operation, and the back end where the spent nuclear fuel (SNF; see below) is reprocessed and/or disposed of. The front end refers to processes pertaining to the placement of the fuel into the reactor core, schematically shown in Figure 1. The initial stage involves the mining and extraction of uranium ore which is most commonly found in the form of pitchblende, UO_2. Open pit mining or underground mining techniques are employed depending on the geological environment but open pit mining can go no deeper than one hundred metres below the surface. Open pit mining has the advantage of minimal surface disturbance and waste, with a reduced cost in comparison to underground mining.

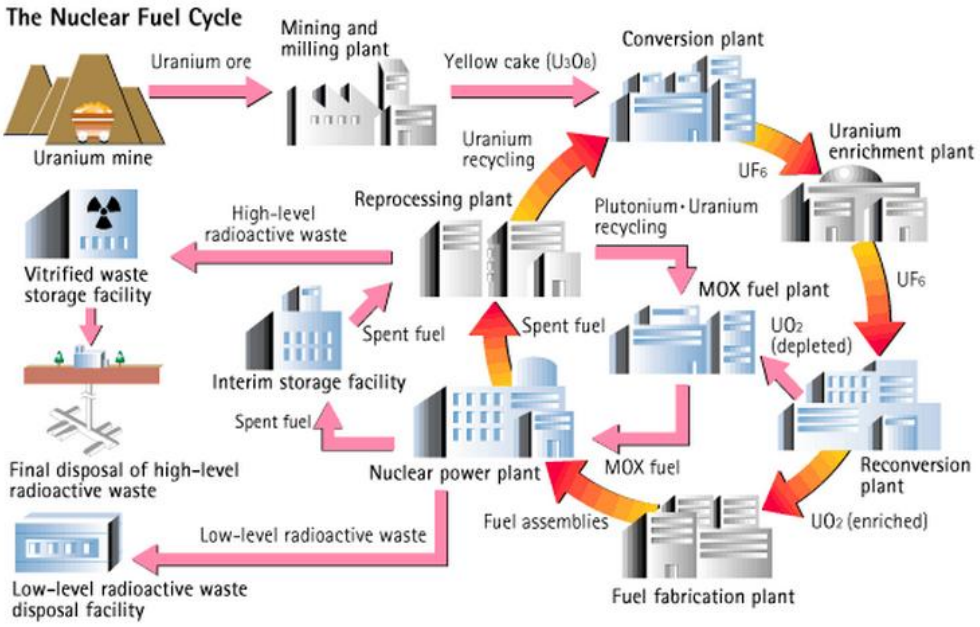

Figure 1: Nuclear fuel cycle demonstrating both open and closed routes.[1]

The most common practice utilised for the extraction of UO_2 from the ground is the method of *in-situ* leaching whereby the ore is dissolved *in-situ* and pumped to the surface for full recovery. Mainly, sulphuric acid (H_2SO_4) is pumped in to the ore to dissolve the pitchblende, with prior consideration to the surrounding geochemistry. The resultant leachate is then subjected to a solvent extraction process (Equations 1 and 2) which exploits the ability of tertiary amines to extract uranyl, leaving the impurities in the aqueous phase:

$$2R_3N + H_2SO_{4\,(aq)} \rightarrow (R_3NH)_2SO_4 \qquad (1)^2$$

$$2(R_3NH)_2SO_4 + [UO_2]^{2+} \rightarrow [(R_3NH)_4UO_2(SO_4)_2]^{2+} \qquad (2)^2$$

Ammonia is further added to the uranyl containing organic phase to precipitate, ammonium diuranate, $(NH_4)_2U_2O_7$, which is isolated and dry roasted at around 200°C to produce solid U_3O_8, known as yellowcake.

For most nuclear fission reactors (e.g. pressurised water reactors (PWR)) the uranium fuel needs to be enriched to increase the fissile ^{235}U content of the fuel. In order to achieve this, the yellowcake is converted to UF_6 which sublimes at 64°C allowing gas phase mass separation methods to be employed. There are two common conversion processes: the wet and the dry. In the wet process, the yellowcake is dissolved in concentrated nitric acid yielding $UO_2(NO_3)_2$ which is subsequently fed in to a continuous solvent extraction stream of kerosene, containing the extractant tributyl phosphate (TBP). This forces the formation of the complex $[UO_2(NO_3)_2(TBP)_2]$ which is retained within the organic fraction. This process is achieved at temperatures below 60^oC due to the thermal degradation of the TBP. The $UO_2(NO_3)_2$ species is precipitated from the organic fraction using ammonium hydroxide (NH_3OH) to form ammonium diurinate ($(NH_4)_2U_2O_7$) which is further reduced to UO_2 using H_2.

The pure UO_2 undergoes hydrofluorination using UF_4 and subsequently fluorination using F_2 to form gaseous UF_6. The UF_6 is subjected to enrichment usually via a form of centrifugation or diffusion, where the heavier $^{238}UF_6$ compound is separated from the lighter $^{235}UF_6$ compound. Enrichment of ^{235}U to around 4 % isotopic content is required for optimal nuclear reactor operation. Once enriched, the UF_6 is converted into ceramic UO_2 fuel pellets.

1.2 Nuclear Fuel

Upon formation, the ceramic UO_2 pellets are placed into the reactor core, usually in some form of cladding. Ceramic pellets are employed due to their high melting points (around 3000 ^oC) as well as their durability in extreme conditions. Zirconium alloys were selected for use as nuclear fuel cladding due to their low neutron capture cross section, high ductility and corrosion resistance. Collectively, the fuel rods (UO_2 pellets encased with zirconium alloy cladding) are known as fuel assemblies; some reactors may contain up to 264 rods per fuel assembly. These fuel assemblies allow sufficient heat transfer to the cooling water surrounding the reactor core as well as containing any radioactive gas emission from the fuel pellets. From reaction initiation, the fuel will continue the fission process until it is no longer of optimum use within the reactor. It is then known as spent nuclear fuel. The zircalloy cladding is separated and disposed of as intermediate level waste (ILW). The ILW (contaminated cladding, equipment etc) is usually cemented in to large steel drums and stored above ground in specified locations.

1.3 Spent Nuclear Fuel

The processes involved during the NFC fabricate a large range of products. Spent Nuclear Fuel (SNF) consists of the original reactor fuel as well as the many decay products produced during the lifetime of the fuel within the reactor. The last 50 years or so have seen the development of many methodologies to recycle SNF for further use, this is known as reprocessing. By reprocessing SNF, the fuel cycle becomes a closed process. Stemming from the Cold War, reprocessing technologies were developed in an attempt to separate the uranium and plutonium (produced from neutron capture by ^{238}U to give ^{239}U, followed by decay to ^{239}Np and then to ^{239}Pu)

for the nuclear weapons programme. Consequently, there now remains a significant quantity of legacy plutonium in storage in several locations worldwide, most notably in the UK at the Sellafield site.[3] These plutonium stockpiles are a significant proliferation concern due to their highly fissionable nature. However, this legacy plutonium could be converted to mixed oxide fuels (MOX) which are invaluable for use in fast breeder reactors (FBRs) or in high temperature reactors. MOX fuel is currently used in some PWRs in France. Conversion of current plutonium stockpiles would not only create a large fuel store but also reduce the proliferation risks associated with accumulating pure plutonium.

The production of various poisons within the reactor as the fuel is burned defines the point at which the spent fuel is removed for reprocessing or disposal. Upon removal, the SNF is sent to storage pond facilities which have been deemed the safest method to allow radiation levels to diminish. The fuel can remain here for a number of years until sufficiently safe to undergo reprocessing and/or subsequent permanent disposal of the waste products. The SNF is either fully disposed of as waste (open fuel cycle) or further reprocessed (closed fuel cycle). The SNF is retained in the storage pond facilities until a significant proportion of the plutonium-241 ($t\text{-}_{1/2}$ = 14 years) and subsequently strontium-90 and cesium-137 ($t\text{-}_{1/2}$ = 29 and 30 years respectively) have decayed.[4]

The estimated isotopic composition of SNF from a PWR is as follows: uranium ~ 95.6 %, fission products ~ 2.9 %, plutonium ~ 0.9 %, minor actinides ~ 0.1 %, iodine and technetium ~ 0.1 %, caesium and strontium 0.3 %, other fission products ~ 0.1 %.[5] Plutonium and minor actinide isotopes generally occur in SNF via neutron absorption of uranium. Fission products, both long and short-lived, contribute to around 95 % of the total radioactivity of the SNF during an average lifetime within the reactor, but only 3 % of the total waste by volume.

The long term radiotoxicity of the reprocessed SNF indicates a growing necessity to improve on the methodologies for nuclear fuel reprocessing in order to reduce the overall radiotoxicity of the proposed waste form for long term storage. Of late, it has been proposed that some isotopes found in the reprocessed waste form are of wider use and therefore it is favourable to harness their capabilities; for example, americium recovery for use in long term space battery production.[6]

The current reprocessing technology must improve to retain compatibility with the various proposed fuel types and fuel cycles, which will create the most effective route for the recovery of useful materials from SNF. Currently, removal of desired materials from SNF via reprocessing leaves a liquor which has been termed high level waste (HLW). This HLW is currently stored in designated intermediary areas but is intended for long term permanent disposal. The removal and use of the more long term radiotoxic actinide isotopes in the SNF, leaving a less radiotoxic liquor that will decay to safe activity levels relatively quickly will provide simpler management options for long term disposal. The currently proposed option for safe management of non-recyclable radioactive waste is a deep Geological Disposal Facility (GDF).[7]

With the separation of long lived fission products, such as ^{99}Tc, a significant contributor to the radiotoxicity in spent nuclear fuel, it has been proposed they undergo transmutation and possibly incorporated into targets for destruction reactors.[8] The process of transmutation serves to convert long lived fission products or species of high radiotoxicity to stable isotopes of low or no radiotoxicity, usually by a form of artificial nuclear reaction.

1.4 Solvent Extraction within the Nuclear Industry

From the onset of the nuclear industry, solvent extraction processes have dominated the recovery of metals from their sources. Solvent extraction, SX, is known for its relatively simplistic mechanism and ease of reproducibility on a macro scale. Its premise implies an increased solubility of the extractant within the organic phase and a significantly decreased solubility throughout the aqueous phase. Solvent extraction techniques have been developed which contribute to the purification of uranium

during the milling and conversion steps of the nuclear fuel cycle. Towards the end of World War 2, the isolation of plutonium for weapons production was of particular interest; the Plutonium and Uranium Recovery by EXtraction (PUREX) (see Section 1.5.1) process was designed with this in mind.[9] Reprocessing of SNF for the recycling of reusable uranium is also a premise of the PUREX process. In addition, proposed recycling of minor actinides which contribute to an improved nuclear waste management arrangement, also utilise solvent extraction techniques. A number of fundamental principles will dictate the sustainability of a solvent extraction process, which include thermodynamics, kinetics, cost effectiveness, waste management and maloperation concerns like precipitation and third phase formation.

Solvent extraction processes consider the parameters of distribution ratio, D, and separation factor, SF. The parameter of distribution ratio, D, simply considers how well a species is extracted from one phase to another. Amidst liquid-liquid extraction techniques, the distribution ratio (Equation 3) is equal to the concentration of a solute, X, in the organic fraction divided by its concentration in the aqueous fraction:

$$D = [X]_{org} / [X]_{aq} \quad (3)$$

Provided the solute does not chemically interact with either phase, the solute will distribute itself between each phase until equilibrium is reached. Each phase can then undergo further analysis.

The term separation factor (SF, γ) is also strongly associated with solvent extraction in the nuclear industry. This term is applicable whenever a mixture of two or more solutes, have been partitioned into two phases. The separation factor is then the ratio of one solute to the other in one fraction (Equation 4), divided by the corresponding ratio in the other fraction.[10] In systems where the separation of trivalent actinides from trivalent lanthanides is desirable, one large and one small distribution ratio will allow the separation of the solutes.

$$\gamma = D_A / D_B \quad (4)$$

Increased loading of an organic (predominantly paraffinic) solvent with metals can cause issues within the nuclear reprocessing industry. The loading of heavy metals into an organic diluent can cause the precipitation of coordinated metal solvates. This is highly unfavourable during a liquid-liquid extraction. At certain parameters, a loaded organic fraction can sporadically form a secondary phase, termed the third phase.[11] Third phase formation is known to also occur at high acid as well as high metal concentrations. During third phase formation, the organic phase splits into a heavy and a light fraction in which the metal concentration is significantly higher within the heavy fraction, leaving the light fraction containing mostly solvent. Within nuclear reprocessing where large quantities of fissile material (e.g. ^{239}Pu) are handled, metal enriched third phase formation is highly undesirable as it can result in serious criticality issues.[12] An amount of fissile material in which a nuclear chain reaction can be sustained is deemed a critical mass. Criticality could arise within SNF reprocessing if, during third phase formation, enough fissile material was forced into close proximity. This must be avoided at all costs.

Previous studies have endeavoured to outline the third phase boundaries in various systems and further, to clarify its characteristics. Several methods have been proposed to reduce the propensity of third phase formation: improvement of the lipophilicity of the extractant and/or change the nature of the diluent to either increase its polarity, decrease its molecular size or increase the branch length of the alkyl chain.[13] Typically third phase data is presented in terms of limiting organic concentration (LOC), which is deemed to be the maximum metal concentration within the organic phase just prior to the visual formation of a third phase.

The extraction of both uranium and plutonium as well as the extraction of Minor Actinides (MA) is currently being considered. Processes whereby plutonium is not isolated from the uranium and/or MA are thought to be more proliferation resistant and are therefore encouraged. The removal of the aforementioned MA from the waste streams of reprocessed nuclear material reduces the overall radiotoxicity and volume, allowing condensed storage times of the remaining waste effluent. The separated MA can potentially be used as fuel or transmuted into safer, less radiotoxic isotopes.

1.5 Solvent Extraction Methods

1.5.1 Plutonium and Uranium Recovery by EXtraction – PUREX

There are numerous solvent extraction processes that are in various stages of development for the partitioning of SNF, but the only established plant-scale process is the Plutonium and Uranium Recovery by EXtraction (PUREX) process which uses the extractant TriButyl Phosphate (TBP; Figure 2) in a kerosene diluent. Reprocessing of spent nuclear material begins with the dissolution of the irradiated fuel pellets into concentrated nitric acid (~ 7 M). Upon dissolution of the fuel pellets, any undissolved material, such as metal cladding, is removed and disposed of as intermediate level waste (ILW).

For the PUREX process, tributyl phosphate (TBP) is used due to its preferential separation of uranium and plutonium over the other heavy metals present. The TBP forms complexes with uranyl nitrate and plutonium nitrate which are soluble within the organic phase. Neptunium can also be extracted for the production of ^{238}Pu used in thermo-electric generators.[14] The resultant aqueous phase, containing the residual fission products, is reduced in volume by way of evaporation and the resultant material mixed with glass frit at high temperatures (around 1000^{o}C). The molten liquid is then encased in canisters and sealed for storage. This is vitrified waste and requires careful storage.

During the PUREX process, the organic, TBP containing phase is passed over an aqueous nitric acid phase, containing dissolved SNF. The two phases are contacted in a counter current direction in a specifically engineered vessel, such as a mixer settler or pulse column. The level of uranium and plutonium extraction is a direct function of aqueous nitric acid concentration, with optimum conditions around 7 M nitric acid. Extraction of the uranium and plutonium from SNF, occurs by the formation of charge neutral complexes with U(VI) and Pu(IV) of the formulation $[UO_2(NO_3)_2(TBP)_2]$ and $[Pu(NO_3)_4(TBP)_2]$, respectively (see Figure 2).[15] The coordination of TBP to uranium or plutonium occurs via an interaction between the lone oxygen on the phosphate group and the metal centre.

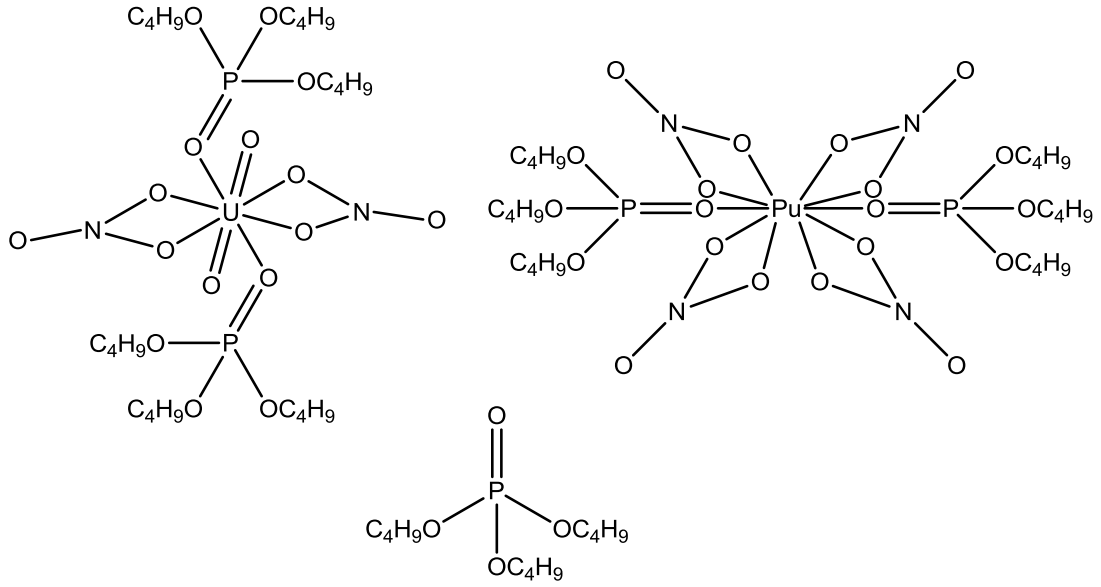

Figure 2: Structures of $[UO_2(TBP)_2(NO_3)_2]$, $[Pu(NO_3)_4(TBP)_2]$ and TBP.

SNF designated for PUREX reprocessing is removed from the reactor, and cooled in a storage pool before any further handling. The SNF encased in its cladding is either dissolved in aqueous nitric acid and the solids, mostly cladding are separated as solid waste, or the cladding is sheared before dissolution. The remaining raffinate undergoes a 1st extraction cycle within PUREX to remove U and Pu. From this, the aqueous phase (known collectively as HLW), containing Fission Products (FP) and Minor Actinides (MA) is separated as aqueous waste where it is reduced in volume by way of evaporation and denitration and the remaining residue sent for vitrification. Several locations throughout the world, including Sellafield, use a vitrification process to form a stable, HLW containing borosilicate glass waste-form, suitable for long-term storage.[16] The PUREX process is dependent on the knowledge and control of the REDuction and OXidation (REDOX) chemistry of the metals present in dissolved SNF, in particular uranium and plutonium. After the primary extraction cycle, the resultant organic phase is treated with a reducing agent, typically ferrous sulfamate (U(IV) can also be used as a reductant in these systems), to manipulate the plutonium valence state from Pu(IV) to the Pu(III) which allows for back extraction of plutonium in to a fresh aqueous phase. This occurs during the 2nd and 3rd cycles and gives a separate organic uranyl containing stream and a separate aqueous plutonium containing stream. The isolated plutonium is then precipitated from the aqueous fraction by use of oxalate, and subsequently treated to

give solid PuO_2.[17] The now plutonium scarce, uranium containing organic phase is back extracted in to the aqueous fraction through contact with dilute nitric acid. The uranium species is further reduced to UO_2, where it can be reused as fuel (directly or in MOX), or treated with HF/F_2 to produce UF_6 for further enrichment.

Metal extractability in a two phase system is a function of the affinity for each extractant to the metal species in question. TBP has previously been determined as the most effective extractant for uranium[18] and plutonium[19] recovery, as well as being agreeable in regard to factors such as cost and availability. The TBP has less affinity for trivalent actinides and fission products dissolved into the aqueous nitric acid phase of SNF, making it favourable within the premise of the PUREX process.[20] TBP as an extractant has been found, on exposure to high concentration nitric acid, to exhibit a low hydrolysis rate hence thermal degradation is slow and can thus be neglected with respect to the PUREX reaction conditions.

Figure 3 illustrates the life of uranium LWR spent fuel from the fuel assembly to the reprocessed products, isolated during PUREX. The PUREX process was not initially designed to consider such things like effluent treatment and vitrification, as shown in Figure 3. These however, are important off processes necessary for safe overall reprocessing conditions. It is quite clear that any changes in initial fuel type and therefore subsequent SNF composition will directly affect the ability of the process to continue at its optimum, unless the processes are fully understood and adjusted accordingly.

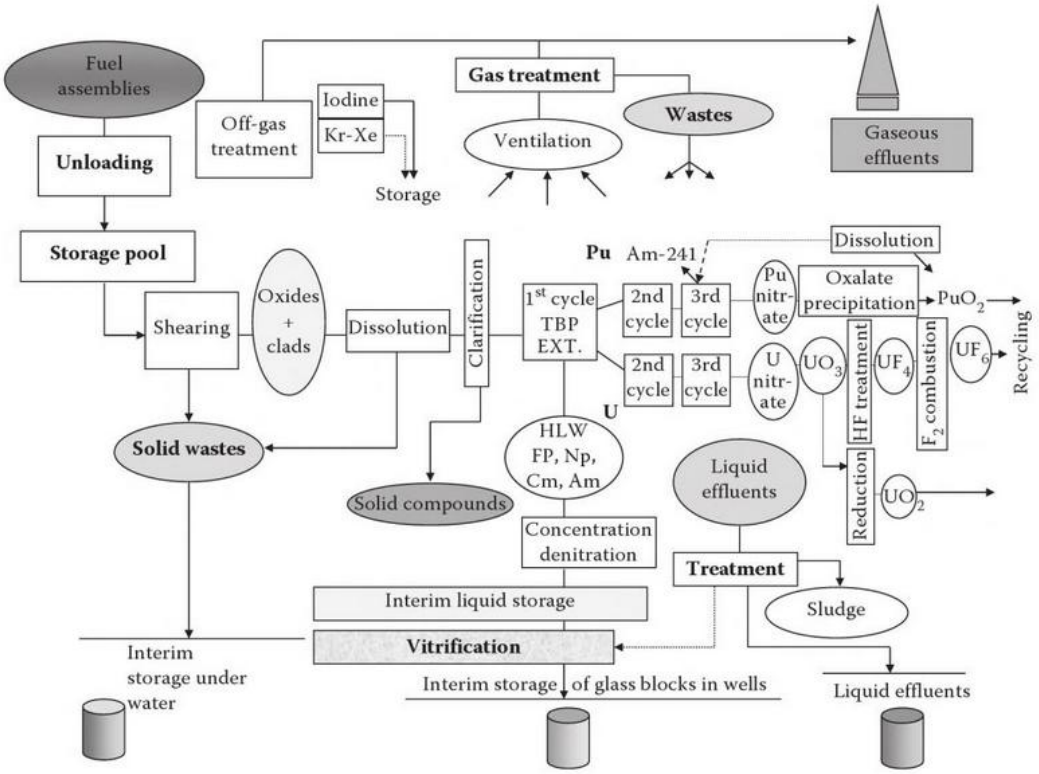

Figure 3: Management of LWR spent fuel.[21]

The extracted plutonium and uranium products from the reprocessed waste streams of SNF are presently conditioned for reuse, either as a pure uranium fuel or as mixed oxide (MOX) fuel. The PUREX process was not designed to extract the MA (neptunium, americium and curium) produced during the lifetime of the fuel within the reactor.

Within the bounds of the PUREX process, a high plutonium loading may lead to third phase formation which is highly undesirable under this large scale industrial process. For systems analysed using a TBP (30 % by volume) in dodecane organic phase with the addition hydrogenated polypropylene tetramer (HPT) (commonly used for its resistance to third phase formation), it has been shown that no third phase was observed where the initial aqueous nitric acid concentration was above 5 M with plutonium loadings below 0.55 M.[12]

Additional data has reported that solutions of 0.063 M Pu(IV) in 10 M aqueous nitric acid formed an observable third phase when contacted with TBP (20 % by volume) in kerosene.[22] Kolarik *et al.* reported a LOC of 0.325 M plutonium at 7 M aqueous nitric acid with TBP (30 % by volume) in dodecane diluent at 25^{o}C.

For PUREX based systems reported, previous data suggest that for Pu(IV) the LOC decreases with increasing acid concentration below 2 M aqueous nitric acid; above 2 M a significant increase in the LOC is noted. At higher acidities, > 3 M, the concentration of nitric acid extracted into the organic fraction is considerable and might therefore explain the differences in LOC at higher acidities compared to low acidities.[23]

Third phase formation in uranium containing systems has also been studied but is thought to form at much higher nitric acid concentrations. Solovkin *et al.* observed third phase formation in PUREX based, U(VI) containing systems with > 8.7 M aqueous nitric acid, but did not give a clear indication of the LOC of uranium in these conditions.[23] There is limited data on the LOC of uranium in PUREX type systems, however it is established that higher concentrations of uranium are required to form third phase compared to those of plutonium.

1.5.2 PUREX Alternatives

Over mounting proliferation concerns over separated plutonium streams during the PUREX process, modified PUREX style processes were proposed which prevented a separate plutonium stream being isolated.

1.5.3 URanium EXtraction – UREX

The URanium EXtraction (UREX) process (Figure 4) is much like PUREX, however to the initial feed of dissolved SNF, acetohydroxamic acid (AHA; Figure 5)[24] is added as a scrub solution to complex Pu(IV) and reduce Np(VI) to inextractable Np(V).[25] The uranium is still separated by complexation with TBP while the plutonium is not available for use as a fuel. The UREX process retains the plutonium and neptunium within the aqueous fraction via complexation with salt free AHA.

The resultant organic fraction containing uranium and technetium is separated to undergo further treatment. The technetium is separated using 5.5 M nitric acid in one stream and the uranium stripped at 60°C using 0.01 M nitric acid. The remaining raffinate contains Pu, Np, Am, Cm and FP, making it more proliferation resistant than a lone plutonium waste stream. The spent solvent is sent for solvent washing.

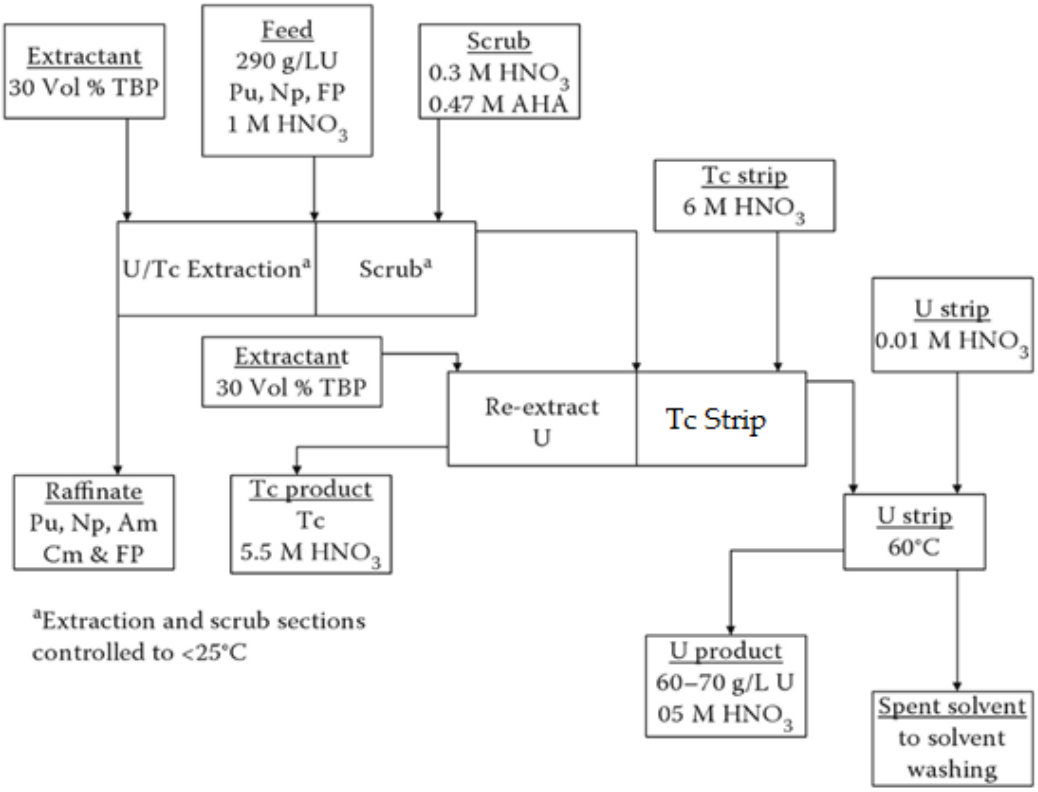

Figure 4: UREX flowsheet.[26]

The UREX flowsheet, Figure 4, was successfully tested at Argonne National Lab (ANL), using centrifugal contactors and simulated solutions.[26]

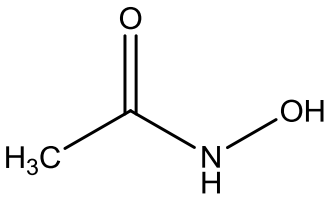

Figure 5: Structure of acetohydroxamic acid.

1.5.4 TRansUranic EXtraction – TRUEX

The TRansUranium EXtraction (TRUEX) process, Figure 6, developed at Argonne National Lab (ANL), was conceived for the extraction and recovery of transuranic elements from various waste liquors.[27] Similar to PUREX, TRUEX employs an organic diluent with TBP but also incorporates octyl(phenyl)-N,N-diisobutylcarbamoylmethylphosphine oxide (CMPO), Figure 7, to provide an effective extraction route for tri, tetra and hexavalent actinides over a wide range of acidities (0.5 to 6 M HNO_3). The combination of both TBP and CMPO has been labelled an "all purpose" extraction system with particular favourability to an increased metal loading capacity without third phase formation.[28]

TRUEX has demonstrated considerable promise with regard to the extraction of all *f*-elements problematic to HLW raffinate and could contribute significantly to the management of spent nuclear fuel. The TRUEX process comprises of four operations: extraction, scrubbing of the organic phase, one or more stripping steps and solvent cleanup.[29] CMPO was chosen for the extraction operation for its propensity to extract trivalent actinides, such as americium and curium, from a range of concentrations of nitric acid. Only a small concentration of CMPO is needed in combination with the PUREX solvent to successfully extract the transuranics, without the formation of a third phase.[30] The TRUEX flowsheet shows the isolation of Am, Cm and the lanthanide elements using the TRUEX solvent - CMPO and TBP in a Normal Paraffinic Hydrocarbon (NPH). These elements are isolated after strip 1. The remaining plutonium and neptunium are isolated in the second stripping stage using HNO_3 and HF. The remaining raffinate post plutonium/neptunium removal (strip 2) is fed back to the TRUEX feed with the solvent washed using Na_2CO_3. The aqueous raffinate separated after the initial extraction step contains up to 80 % technetium and is sent for immobilization by vitrification.

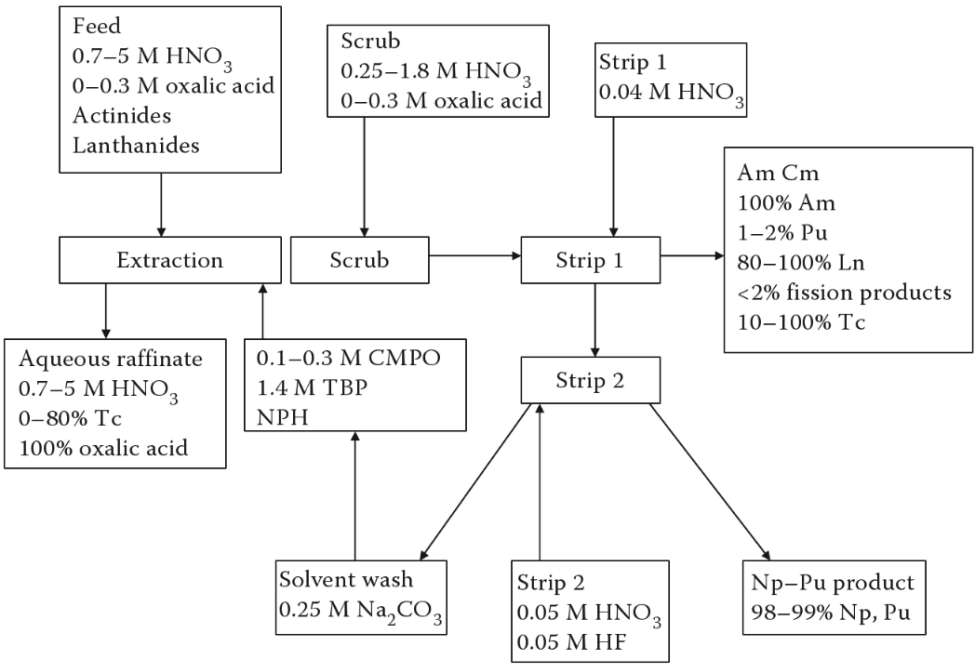

Figure 6: TRUEX flowsheet.[31]

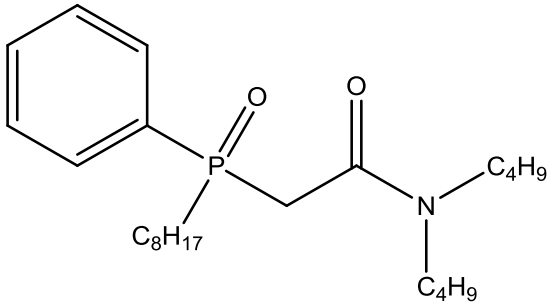

Figure 7: Structures of CMPO.

The TRUEX process however, requires further separation of trivalent actinides from lanthanides, thus making TRUEX most effective in combination with an additional process.

1.6 Processes for MA/Lanthanide (Ln) Separations

1.6.1 DIAMide EXtraction – DIAMEX

The DIAMide EXtraction (DIAMEX) process was initially proposed in 1987 where trivalent actinides and lanthanides are co-extracted directly from the high activity raffinate (HAR) obtained after the removal of uranium and plutonium by the PUREX

process. This process was initially proposed utilising malonamide extractants, most notably dimethyldibutyltetradecylmalonamide (DMDBTDMA; Figure 8).[32] Currently, the preferred DIAMEX formula utilises dimethyldioctylhexylethoxy-malonamide (DMDOHEMA; Figure 8) in an aliphatic diluent for the extraction of MA and trivalent lanthanides (see flowsheet presented in Figure 9).[33] The DIAMEX process has the advantage of avoiding the formation of organic waste streams that contain anything other than carbon, nitrogen, oxygen and hydrogen, allowing them to be safely incinerated without the formation of solid secondary wastes needing further treatment and disposal. Co-extraction of the fission products, zirconium, molybdenum and palladium, is prevented using oxalic acid and hydroxyethyl-ethylenediamine-triacetic acid (HEDTA; Figure 8). However, the extraction of actinides using amides does suffer from the drawback of third phase formation, necessitating the use of a modifier at high acid and metal loading concentrations.[34]

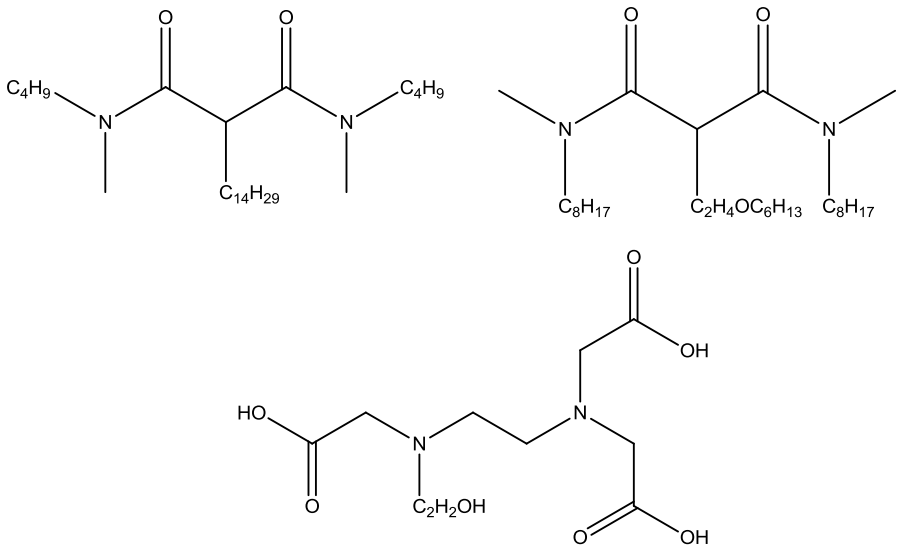

Figure 8: Structures of DMDBTDMA, DMDOHEMA and HEDTA.

The proposed DIAMEX flowsheet, Figure 9, uses DMDOHEMA in Hydrogenated Polypropylene Tetramer (HPT) to extract the trivalent actinides and lanthanides which are subsequently back extracted using 0.1 M HNO_3. The resultant aqueous raffinate contains less than 1 % MA with the majority FP for high level waste disposal via vitrification. Physical hot tests were carried out at the Institute for Transuranium Elements (ITU), Germany, on high active concentrate (HAC) where the results gave 99.9 % recovery for An(III) and Ln(III).[33]

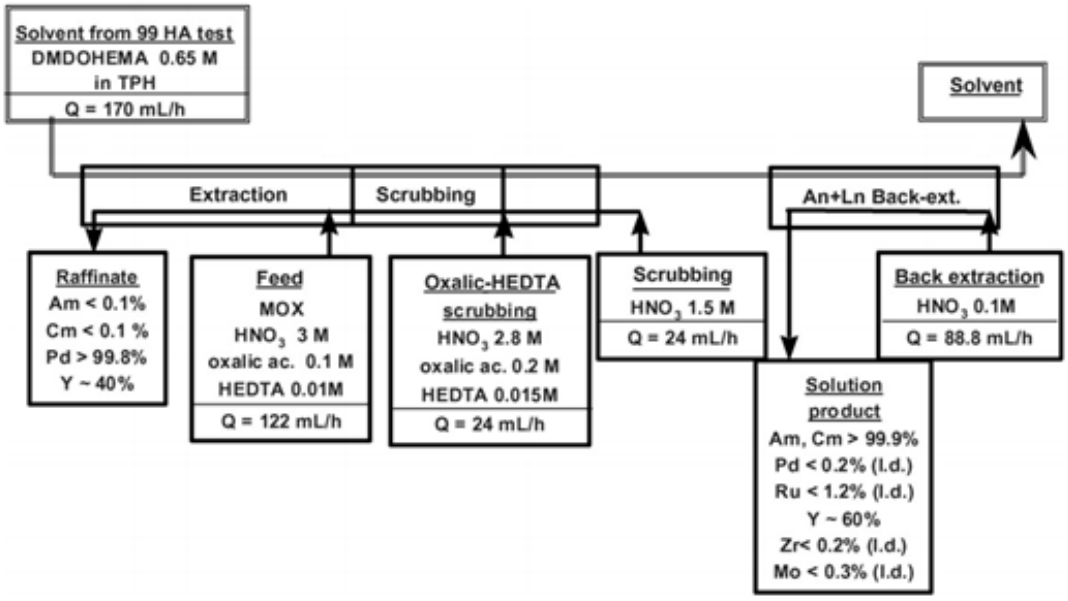

Figure 9: DIAMEX flowsheet.[33]

1.6.2 Selective ActiNide EXtraction - SANEX

The proposed Selective ActiNide EXtraction (SANEX) process, still currently in development, allows for the reusable actinides to be separated from the trivalent lanthanides, post DIAMEX conditioning. The large neutron cross section of the lanthanides will poison any further use for the actinides as fuels therefore it is desirable to separate them and subsequently dispose of them separately.[35] Nitrogen donating ligands have been suggested as effective actinide lanthanide separation extractants, such as the bis-triazinylpyridine (BTP), bis-triazinyl bipyridines (BTBP) and bis-triazinylphenanthroline (BTPhen) derivatives (Figure 10), proposed for their high affinity for trivalent actinides.[36] Flowsheets have subsequently been produced that outline a number of sections: extraction, back extraction of trivalent lanthanides, back extraction to recover trivalent actinides and potentially an organic scrubbing to remove any extracted Pd(II).

The extractant 6,6'-Bis(5,5,8,8-tetramethyl-5,6,7,8-tetrahydrobenzo[1,2,4]-triazin-3-yl)-[2,2']-bipyridine ($CyMe_4BTBP$), Figure 10, has shown promise for the extraction of Am(III) at high nitric acid concentrations with, in addition, a high separation factor from Eu(III) of around 50.[37] Further, the extraction of Am(III) using

$CyMe_4BTBP$ is fast, in the order of minutes, and is retained within the organic fraction over long periods of time.

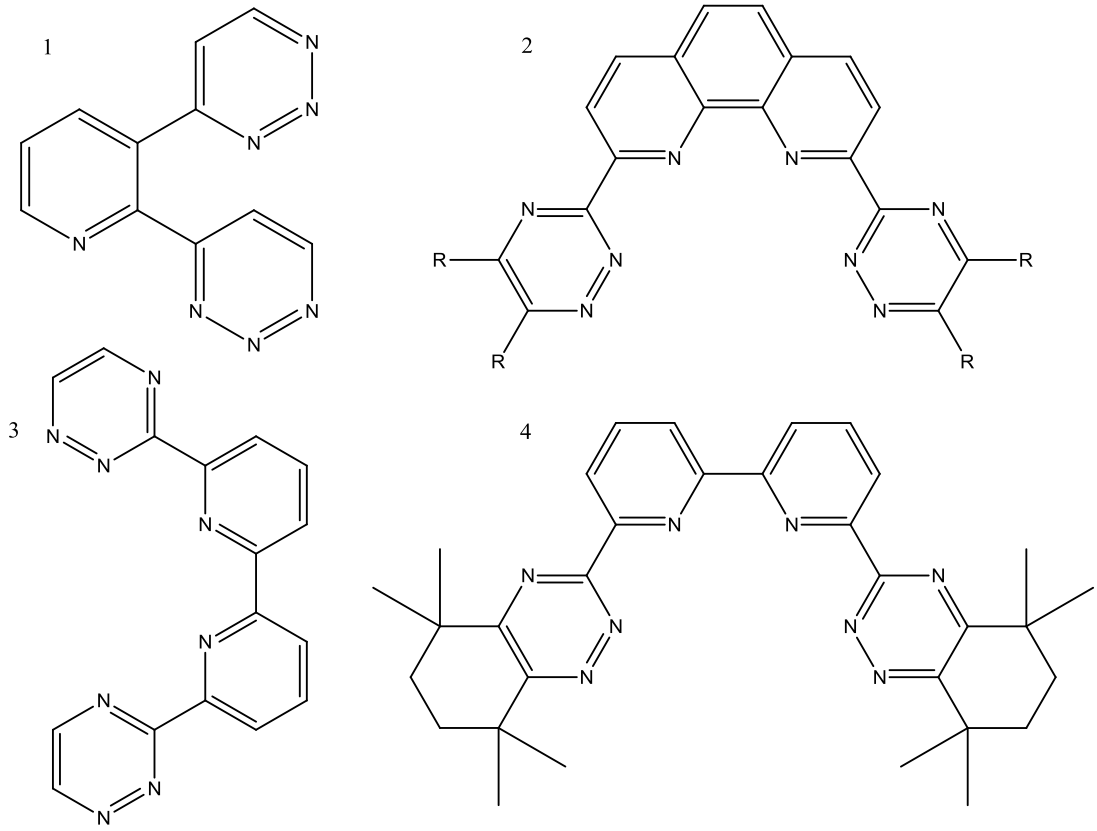

Figure 10: Structures of 1) BTP, 2) BTPhen, 3) BTBP and 4) CyMe4BTBP.

An alternative option proposed for MA/Ln separations is the 1-cycle SANEX process where the minor actinides are selectively extracted directly from the PUREX raffinate, avoiding the need to employ DIAMEX.[38] $CyMe_4$-BTBP has also been employed in this version of SANEX.[39] Extractants containing 'soft' donor ligands such as nitrogen (in this case the soft term is considered relative to oxygen donor ligands, which are harder by comparison), are favoured for their preferential interaction with actinides *vis-à-vis* lanthanides.[40] This separation can be, however, kinetically slow, therefore, the use of a phase transfer agent, (e.g. N,N,N',N'-tetraoctyl diglycolamide (TODGA)[41]; Figure 11) has been suggested. This may imply that the FP present in the aqueous phase impact the extraction of the MA. Previous tests have employed a 0.015 M $CyMe_4$-BTBP and 0.005 M TODGA in a 40:60 % mix of hydrogenated tetrapropylene (HTP) and 1-octanol, respectively.[41]

Another alternative process for MA/Ln separations while still avoiding the need for DIAMEX is the innovative SANEX (*i*-SANEX) process which utilises a DIAMEX type process to co-extract the trivalent actinides and lanthanides initially, then a hydrophilic BTP type ligand is used to selectively strip the trivalent actinides from lanthanides, in a once through process . The *i*-SANEX process uses a diglycolamide, N,N,N',N'-tetraoctyl diglycolamide (TODGA; Figure 11), to co-extract the trivalent actinides and lanthanides from the PUREX raffinate.[42] The tridentate ligand TODGA has shown promise for the extraction of An/Ln (III) and An (IV, VI) and is found to have good radiolytic and hydrolytic stability.[43] The suggested *i*-SANEX process will likely employ oxalic acid for the suppression of zirconium and palladium extraction as TODGA readily extracts these problematic fission products too.

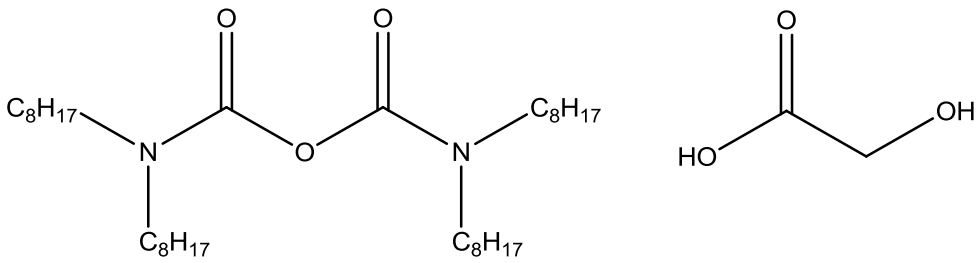

Figure 11: Structures of TODGA and glycolic acid.

The trivalent lanthanides are selectively stripped from the trivalent actinides using BTP type ligands.[44] The proposed *i*-SANEX flowsheet illustrated in Figure 13, utilises a hydrophilic sulfonated BTP type ligand (SO_3-Ph-BTP, Figure 12) to strip the actinides. The lanthanides are stripped from the organic fraction using glycolic acid (Figure 11). The spent solvent is recycled.

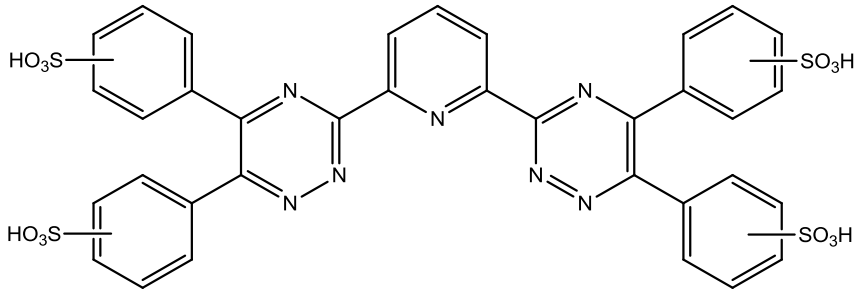

Figure 12: Structure of SO_3-Ph-BTP

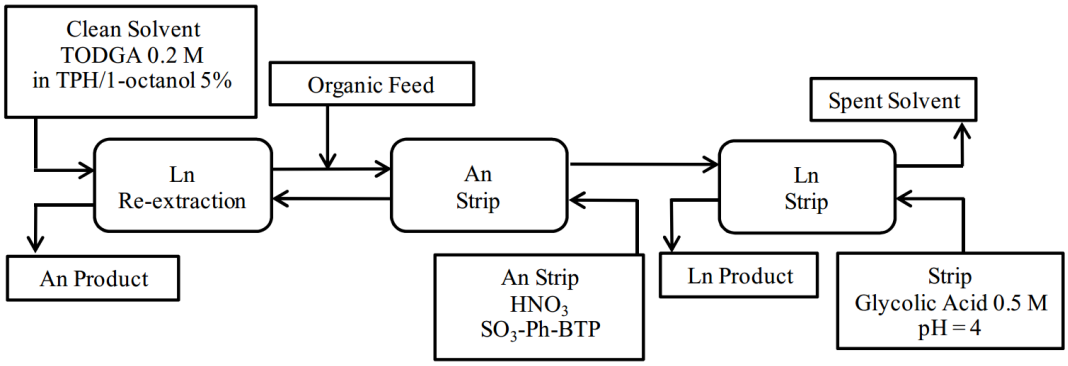

Figure 13: *i*-SANEX flowsheet.[45]

1.6.3 Group ActiNide EXtraction – GANEX

Currently of interest are reprocessing technologies that facilitate the complete and simultaneous removal of the actinides from the dissolved spent fuel. The Group ActiNide EXtraction (GANEX) process, aiming to replace the PUREX process,[46] is a single process that has been proposed which separates the actinides from both the lanthanides and the fission/corrosion products and can be achieved either directly from the dissolved spent fuel or from the post uranium extraction stream.[47] The *concept* of group actinide extraction uses complementary extractants within the same system to allow uranium, plutonium and MA to be removed concurrently for the potential use in Generation IV fast neutron reactors. Within the GANEX process, there is no separate plutonium stream, hence it is therefore considered more proliferation resistant than the original PUREX process.

The intention is a solvent system that can be used to extract all actinides from the initial dissolution solution, in a once through process. The bulk uranium removal would occur prior to this using a ligand such as DEHiBA (Figure 14). A number of differing combinations of extractants have been proposed for this group actinide removal stage. It is important to note however, that a mixture of extractants will be employed, each with a different purpose, but that can be used in combination in a once through process, or so it is hoped. The use of TODGA with various phase modifiers, has been suggested in a DIAMEX style process which includes the extraction of the lanthanides in conjunction with the actinides. The phase modifiers, such as TBP or 1-octanol, have been proposed in combination with TODGA as they aid third phase prevention in these systems. Consequently, a further stripping stage is required to isolate the actinides.

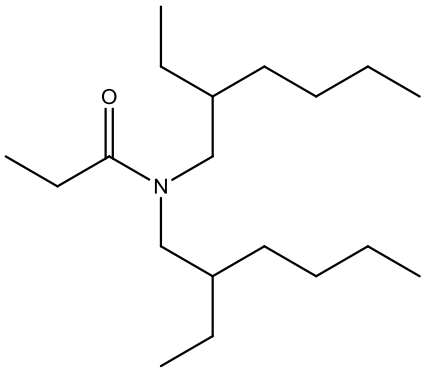

Figure 14: Structure of DEHiBA.

In addition, the synthesis of TODGA and the suggested phase modifiers have been shown to be relatively low cost and reproducible on a large scale. They have also been demonstrated to resist constant radiation effects and degradation in highly acidic surroundings.

The proposed EURO-GANEX solvent has been designed to cope with extracting all transuranic (TRU) ions in oxidation states III, IV, VI and possibly V, as well as high plutonium loading.[48] Previous reprocessing techniques have not been deemed to work effectively for the separation of all the aforementioned transuranic oxidation states, in combination with high plutonium loading, without the occurrence of precipitation or third phase formation. The preliminary step of the EURO-GANEX

process uses a monoamide (e.g. N, N-di(2-ethylhexyl)isobutyramide (DEHiBA; Figure 14)) to remove the bulk of the uranium. After the selective removal of U(VI) in the primary step, the TRU and trivalent lanthanides are separated during the second cycle. A mixture of TODGA and DMDOHEMA in dodecane has been found to work effectively for the extraction of III, IV and VI actinides as well as the co-extraction of trivalent lanthanides. The TODGA/DMDOHEMA system was found to be capable of extracting up to 40 g L^{-1} Pu(IV) without precipitation or third phase formation.[49] Suppression of fission product extraction has been successful within this solvent system with the use of 1, 2-cyclohexanediaminetetraacetic acid (CDTA) as a masking agent. The separation of actinides from lanthanides utilises hydrophilic ligands, such as SO_3-Ph-BTP (Figure 12), also proposed for use in the *i*-SANEX process, and AHA which is used in the UREX process. The ligand SO_3-Ph-BTP strips the minor actinides while AHA reduces and therefore strips, the neptunium and plutonium in to the aqueous phase.

In these systems, the use of SO_3-Ph-BTP for the selective stripping of actinides gave high separation factors and was accomplished efficiently using low HNO_3 concentrations, when tested using centrifugal contactors at high flow rates.

1.7 Molten Salts Technology

Molten salt reactors are a proposed high temperature reactor that utilise fluorides and chlorides of fissile isotopes (such a plutonium, uranium and sometimes thorium) in combination with a carrier salt that is in liquid form and also acts as a coolant. In thermal molten salt reactors, fluoride salts are the preferred fuel type whilst for fast molten salt reactors, chloride compounds are favoured.[50] The fuel takes the form of molten chloride compounds such as $PuCl_3$ and UCl_3 in a NaCl diluent.[50] LiCl-KCl has been selected as the main candidate for the carrier salt and is the main candidate for pyrochemical recovery of the actinides used in the reactor fuel.[51]

Due to the nature of these systems, it is necessary to investigate the potential for chloride contamination in relevant spent nuclear fuel reprocessing processes for the eventual final core residuals.

1.8 Orphan Fuels and Residues

Due to the earlier activities of the nuclear industry, it is now known that there is a legacy of nuclear material that requires decommissioning. This legacy waste includes what are known as 'orphan fuels' and 'residues',[52] which in some cases have been deemed inappropriate for generic disposal methods, such as the THORP and MAGNOX reprocessing plants. A large arsenal of chloride contaminated plutonium residues have been quantified which, due to third phase concerns and therefore subsequent criticality issues, are potentially unsuitable for standard reprocessing techniques.[52] The implications concerning the presence of chloride during nitric acid dissolution during any proposed solvent extraction methods, also needs to be considered. It is therefore necessary to investigate the potential effects of the presence of chloride on the separation of heavy metals under current and proposed reprocessing techniques, with a view to aid the cleanup of legacy wastes.

1.9 Heavy Metal Behaviour Relevant to Current and Proposed Solvent Extraction Processes

1.9.1 Zirconium (Zr)

Zirconium, a naturally occurring metal in the earth's crust, has become a primary construction material in nuclear engineering due to its corrosion resistance, structural strength and low neutron absorption.[53] Zirconium is the main constituent of the cladding used to house the fuel assemblies in reactor cores and can therefore be dissolved into the waste raffinate upon dissolution by nitric acid. Zirconium has a low neutron absorption cross section, a high melting point and high corrosion resistance which makes it a suitable material for use in fuel cladding.

REDOX chemistry surrounding Zr is relatively simple as the 4+ oxidation state generally presides in solution and solid form. However, zirconium can undergo extensive hydrolysis depending on the surrounding pH, due to its high charge density. Hydrolysis of Zr^{4+} can occur in some acidic media. Within solvent extraction in the nuclear industry, hydrolysis is highly undesirable. It has been

suggested that hydrolysed zirconium species will be the solubility limiting solid phase in a GDF for spent nuclear fuel.[54] Several isotopes of zirconium contribute to the overall fission product (FP) composition, with ^{93}Zr considered a long lived FP with a half life of over a million years.

Previous literature has detailed the successful ability of TBP to selectively remove zirconium from solutions in the reprocessing of SNF but the process is complex and dependent on several factors. For zirconium extractions with TBP, it was found that the hydroxy solvate[55] as well as the acidic solvates, $[Zr(NO_3)_4(HNO_3)_2.TBP]$ and $[Zr(NO_3)_4(HNO_3)_4.TBP]$ were formed under PUREX conditions of 30 % TBP by volume in the organic solvent with aqueous phase HNO_3 concentrations from 1 to 6 M.[56] The zirconium was sourced by the dissolution of zirconyl nitrate into 10 M HNO_3, where the Zr cation exists in its 4+ state. The resultant solution was diluted to various concentrations of nitric acid to analyse speciation whilst simulating reaction conditions analogous to the PUREX process.

In conjunction with the variance in HNO_3 concentrations, it can be said that at elevated acidity, more anhydrous complexes are formed preferentially over hydrated Zr-TBP type complexes. With respect to high zirconium concentrations and elevated nitric acid acidity, not only is hydrolysis hindered but anhydrous Zr-NO_3-TBP complexes form throughout the organic phase.[57] IR data suggests that at aqueous phase acid concentrations below 3 M, hydrolysed zirconium complexes are formed whereas additional species are formed at increased acidity.[55]

Sinegribova *et al*. aimed to investigate the solubility of TBP within aqueous phases (H_2O and HNO_3) as a function of zirconium speciation. The formation of metal hydroxides at lower pH levels can lead to inaccurate values for the amount of TBP dissolved in to the aqueous phase due to TBP sorption to the hydroxide surface. Evidence of this was observed when the concentration of TBP in the aqueous phase was almost always determined to be lower in the Zr-HNO_3-TBP system when compared to TBP-HNO_3 systems. Additionally, at low acidities, almost no zirconium was extracted but the general occurrence of zirconium in the aqueous phase lead to a change in concentration of TBP in this phase with respect to a purely HNO_3 and TBP systems in the absence of metal species.[58]

Alternative extractants for the removal of Zr from aqueous media include Cyanex 925 (a mixture of branched chain alkylated phosphine oxides) which gave extraction percentages of up to 61 %,[59] and Cyanex 272 (bis(2,4,4-trimethylpentyl) phosphinicacid)[60] which gave optimum extraction percentages of around 70 %.

The suppression of zirconium extraction in future reprocessing techniques, such as the proposed GANEX process, can be achieved using complexing agents such as cyclohexanediaminetetraacetic acid (CDTA). Previous studies have shown that zirconium distribution ratios of < 0.01 have been achieved using this complexing agent, resulting in almost all the zirconium being retained within the feed solution.[61]

1.9.2 Uranium (U)

Uranium is a naturally occurring metal, found throughout the earth's crust, and is found in various oxidation states throughout the environment. The natural concentration of uranium depends on several factors such as environmental pH, redox potential, temperature and microbial activity.[62] Once separated from its natural ore, the uranium metal is converted in to fuel for use in a reactor core. The enrichment process allows for a higher concentration of fissionable ^{235}U to be found in the fuel pellets *c.f.* the naturally occurring composition. The dominant isotope of naturally occurring uranium is ^{238}U with a small amount of ^{235}U. Radioactive decay of these uranium isotopes is dominated by alpha emission where serious hazards with regard to radiotoxicity are more concerned with inhalation and ingestion which can lead to lung irradiation and pulmonary toxicity.

Uranium has several oxidation states, all of which are considered highly radiotoxic. In reducing conditions, the U(IV) ion dominates which is essentially insoluble. However, under oxidising (and therefore reprocessing) conditions, several accessible oxidation states of uranium exist, most prominent of which is the U(VI) state. U(IV) is more readily found in reducing conditions, such as underground or in areas of low oxygen. U(V) species can be obtained but generally under synthetic conditions will readily undergo disproportionation to the more stable U(IV) and U(VI) states. In acidic media, U(VI) ions exist as the uranyl moiety, UO_2^{2+}, but at pH values higher than 2.5, the uranyl moiety undergoes hydrolysis which considerably hinders its

extraction with organic ligands.[63] It is therefore necessary to retain an acidic nature of the aqueous fraction during the reprocessing of spent nuclear fuel.

Under aqueous-oxic conditions the linear cation UO_2^{2+} is favourable and co-ordinates with hard donor ligands in the plane orthogonal to the O=U=O axis. UO_2^{2+} in particular, is an exceptionally stable molecular species.[64] The oxo-groups in hexavalent uranyl are generally thermodynamically and kinetically inert. Uranium aqueous chemistry deals with the metal speciation and hydrolysis behaviour in acidic solutions. Around pH 2, the species $[U(IV).nH_2O]^{4+}$, $[U(VI)OH.nH_2O]^{3+}$, $[U(IV)O.nH_2O]^{2+}$ and $[U(VI)O_2.nH_2O]^{2+}$ can exist in equilibrium collectively.[65] Acidic solutions usually enhance the stability of lower oxidation state metals whilst more alkaline environments favour higher oxidation states.

For uranium reprocessing within the nuclear industry, the most important species is $U(VI)O_2^{2+}$ (or uranyl).[66] For extraction of uranyl from nitric acid solutions, the most common equilibrium reaction is as follows:

$$[UO_2]^{2+}{}_{(aq)} + 2NO_3^-{}_{(aq)} + nX \rightleftharpoons UO_2(NO_3)_2 \,.\, nX \qquad (5)^2$$

Where X = extractant.

Within the PUREX process, the organic phase $[UO_2(NO_3)_2(TBP)_2]$ complex is thought to be relatively stable. It is thought this complex is formed at the aqueous-organic interface. However formation of which is dependent on a number of factors: initial acidity of the aqueous phase, equilibrium concentration of species within the aqueous phase (such as nitrate concentration, uranyl concentration and dissolved aqueous TBP concentration), temperature etc.[67] Once separated into the organic fraction using TBP, the UO_2^{2+} is treated for conversion to solid UO_2 or gaseous UF_6 for further use as reactor fuel. Distribution ratios are thought to be at an optimum for uranyl at around 7 M HNO_3, above which third phase formation may become an issue. However at 7 M HNO_3 and room temperature, U(VI) has the least propensity for third phase formation when compared to Np(VI) and Pu(VI), which has the strongest propensity for third phase formation under the same conditions.[68]

It is now clear that to facilitate proliferation resistance and reduce the overall radiotoxicity of the HLW produced from SNF reprocessing, a more adaptable reprocessing process is required over PUREX. The current line of thought is that the initial bulk removal of the reusable uranium from the acidic liquor is recovered using a monoamide such as DEHiBA. Previous tests have shown that more than 99.999 % uranium recovery was observed under GANEX style conditions using this ligand.[69] The remaining useful metals will be removed using a number of ligands each with a specific role, in a once through process.

1.9.3 Plutonium (Pu)

Plutonium was known to have been created when stars explode but is now primarily synthesised during the fission of uranium within a nuclear reactor core. ^{239}Pu is produced in a reactor through neutron capture of ^{238}U. It is a fissile material so can therefore sustain a fission chain reaction.

Plutonium can exist in several oxidation states in solution, including Pu(III), Pu(IV), Pu(V) and Pu(VI).[70] Solubility, complexation ability and mobility behaviour are all determined by the specific oxidation state of plutonium so it is therefore necessary to understand the REDOX chemistry of each plutonium oxidation state under particular reprocessing conditions.

Plutonium REDOX chemistry and speciation shows a wide range of behavioural aspects in acidic to alkaline conditions. Previously reported UV/vis/nIR spectra were considerably different for species found in low and high concentration aqueous nitric acid solutions. At higher nitrate concentrations, it was found that the following species are formed: $[Pu(NO_3).nH_2O]^{3+}$, $[Pu(NO_3)_2.nH_2O]^{2+}$, $[Pu(NO_3)_4.nH_2O]$ and $[Pu(NO_3)_6.nH_2O]^{2-}$.[71] Plutonium ions generally exhibit a high charge density and therefore show a high propensity to undergo hydrolysis. Hydrolysis of plutonium in the reprocessing of spent nuclear fuel is undesirable due to its highly fissionable nature. Previously determined, the Pu(IV) ion shows the most extensive hydrolysis[72] *c.f.* remaining Pu oxidation states. As the Pu(IV) ion is most commonly found in nuclear reprocessing, it is important to understand the hydrolytic nature under these conditions. The solubility product of the fully hydrolysed $Pu(OH)_4$ species has been

calculated to be 7 x 10^{-56} mol L^{-1},[72] and therefore would be highly insoluble in aqueous media. It is therefore a necessity to prevent plutonium hydrolysis during nuclear reprocessing.

Much work has focussed on the speciation of plutonium in both the aqueous and organic media especially with regard to the aforementioned PUREX and UREX reprocessing techniques. Irradiated nuclear fuel is dissolved into a nitric acid solution during PUREX reprocessing. The plutonium is in the Pu(IV) state and is easily extracted into the organic fraction using TBP, as is the uranyl species, UO_2^{2+}. Further partitioning of the Pu(IV) is necessary for separation of the Pu(IV) species from the UO_2^{2+} moiety. This is achieved using ferrous sulfamate, which reduces the Pu(IV) to Pu(III), where it is subsequently stripped into the aqueous fraction; the UO_2^{2+} remains soluble in the organic fraction. The Pu(III) within the aqueous fraction is precipitated as plutonium nitrate and is consequently converted to PuO_2 by evaporation and further precipitation with oxalate, followed by calcination to produce a powder.[4]

The extraction of plutonium by TBP in the UREX process however, at HNO_3 concentrations of around 0.1 M, is governed mainly by the disproportionation (see Equation 7) reaction of tetravalent plutonium.[73] Disproportionation can be defined as a species being both oxidised and reduced simultaneously to form two different products. This disproportionation increases the amount of inextractable trivalent plutonium in the aqueous feed within UREX which has negative implications for plutonium distribution ratios.

Plutonium disproportionation at low aqueous nitric acid concentrations (~ 1 M) has previously been represented by the following equation:

$$3Pu^{4+} + 2H_2O \rightarrow 2Pu^{3+} + PuO_2^{2+} + 4H^+ \qquad (6)^{74}$$

However, additions of nitrate and/or acid restrain the hydrolysis and disproportionation of Pu(IV) significantly, providing a maximum Pu separation at 6-8 M HNO_3. Conversely, an increase in nitric acid concentration above 8 M leads to a decrease in extracted plutonium. The mechanism by which plutonium is extracted by

TBP is thought to be similar to that of hexavalent uranium, with transfer of the complex $[Pu(NO_3)_4.(TBP)_2]$ into the organic phase being the rate determining step.[75] This complex fits the expected stoichiometry for a tetravalent plutonium species and has been further confirmed by Small Angle Neutron Scattering (SANS) techniques.[76]

The extraction of the transuranic elements (TRU), such as plutonium, has been shown to be effective using the proposed EURO-GANEX solvent system. The intended EURO-GANEX process provides a more proliferation resistant and simpler route for the separation of highly radiotoxic actinide isotopes. Using a solvent system of 0.2 M TODGA with 0.5 M DMDOHEMA in kerosene, plutonium distribution ratios for the extraction step were observed to be above 100. Further stripping to recover the plutonium gave distribution ratios around 0.02.[77] This stripping step also proved effective in separating the TRU from the trivalent lanthanides. Separation of TRU from lanthanides in the stripping steps was achieved successfully using a combination of SO_3-Ph-BTP and AHA.[77] Provided effective fission product suppression is achieved in the extraction step, the EURO-GANEX route shows much promise for an improved future reprocessing technique.

1.9.4 Neptunium (Np)

Neptunium is a by-product of uranium fission within nuclear reactors. The ^{237}Np isotope has a long lived half-life of around 2.16×10^6 years, which is of particular importance when considering the reprocessing and disposal of nuclear waste. Synthesis of ^{237}Np is significant as it is produced from the neutron capture of ^{235}U within a reactor core.

Neptunium can exist in several oxidation states in aqueous solutions, including Np(III), Np(IV), Np(V), Np(VI) and Np(VII). However, the most mobile (and stable) of which is Np(V) which, in the environment, can lead to serious toxicology problems. Hydrolysis of cations is of particular importance in the reprocessing of SNF. The most susceptible Np oxidation state to undergo hydrolysis is the Np(IV) ion but the most common form of neptunium is the NpO_2^+ species which has been found to have the least tendency to undergo hydrolysis.[78] Pentavalent neptunium, usually found to exist as neptunyl, NpO_2^+ can readily disproportionate, under certain

conditions to Np(IV) and Np(VI). Sjoblom and Hindman reported the disproportionation of Np(V) in > 5 mol L^{-1} $HClO_4$ to occur via the following mechanism:

$$2NpO_2^+ + 4H^+ \rightleftharpoons NpO_2^{2+} + Np^{4+} + 2H_2O \quad (7)$$

Additionally, NpO_2^{2+} and NpO_2^+ ions were found to coexist in 8-10 mol L^{-1} $HClO_4$.[79] Susceptibility for disproportionation is often dependent on the nature of the solvent; it has been illustrated that, in non-aqueous media, there is a significant enhancement in the disproportionation rate of Np(V) as compared to behaviour in aqueous solutions.[80]

Further, pentavalent actinide ions (An(V)) undergo different disproportionation mechanisms with respect to acid dependency. For U(V) and Pu(V) a single protonation step is required, whereas for Np(V), it is thought a double protonation step is involved.[81] Stability of some pentavalent actinide ions follows the order Np(V) > Pu(V) > U(V), where disproportionation of Np(V) is slow compared to Np(IV)-Np(VI) reproportionation. It is only the Np(V) ion that undergoes disproportionation.

In solution, Np(V) readily coordinates with other cations, including Np(VI) to form cation-cation interactions (CCI). CCIs have been defined as the coordination of an actinyl "yl" oxygen to the metal centre of another actinyl fragment (see Figure 15). NpO_2^+ CCIs are relatively common and easily formed in solution where as UO_2^{2+} CCIs are rarely observed.[64]

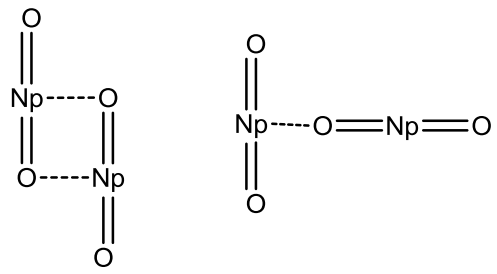

Figure 15: Neptunyl cation-cation interactions, side on (left) and end-on (right).[82]

Upon the dissolution of spent fuel in nitric acid during the PUREX process, neptunium REDOX speciation is dominated by Np(V). However, higher acid concentrations, and therefore increasing ionic strength effects, are effective in achieving an equilibrium state where the oxidation reaction of Np(V) to Np(VI) is dominant. Oxidation of Np(V) to Np(VI) by nitric acid is important in solvent extraction processes, as Np(VI) is easily extractable by TBP. This oxidation reaction, in addition, involves the participation of nitrous acid which serves as a catalyst to Np(V) oxidation.[83] The somewhat unpredictable nature of nitrous acid formation, either from radiolysis of nitric acid or through the dissolution of fuel elements, and with additional extraction by TBP into the organic phase, makes predicting the REDOX behaviour of neptunium within these systems difficult.[84] Generally in the dissolver solution in PUREX reprocessing, the following reaction occurs:

$$2NpO_2^+ + 3H^+ + NO_3^- \rightleftharpoons 2NpO_2^{2+} + HNO_2 + H_2O \quad (8)$$

Sarsfield *et al*. have reported the instability of Np(V) in TBP/OK (30 % TBP by volume)[85] and its disproportionation to Np(IV) and Np(VI). The rate of disproportionation of Np(V) to Np(IV) and Np(VI) was measured to be some 500 times faster and consequently, more thermodynamically favourable than previously observed in aqueous solutions where comproportionation is more favourable.[82]

Previously, Np(V) extracted into TBP/OK (30 % TBP by volume) can be further reduced to Np(IV), by the addition of *p*-hydroquinone. This circumvents the issue of a low distribution coefficient for Np(V) in some systems.[86] Electronic absorption spectroscopy[87] has been employed to detect the period of stability of Np(V) post reduction by *p*-hydroquinone and was found to be in the region of 2 hours. The gradual appearance of additional peaks in the electronic absorption spectra suggest the disproportionation of Np(V) to Np(IV) and Np(VI). Spectra also suggest the formation of CCIs between Np(V) and Np(VI) which have been scarcely reported in organic media.

Furthermore, the distribution ratio, D, of extracted Np(VI) during the PUREX process increases with increasing nitric acid concentration similar to the effective extraction of both Pu(IV) and U(VI).[24] Therefore, increasing the nitric acid

concentration of the high activity raffinate further, should serve as an effective method for the complete removal of neptunium in this system. Conversely, studies have been conducted using hydrochloric acid in the aqueous phase in nuclear fuel reprocessing. The advantages of which seem to indicate a better separation of neptunium from plutonium and uranium by enhanced control of the actinide oxidation states.[88]

As previously mentioned, the GANEX and EURO-GANEX extraction processes have been proposed as possible future reprocessing techniques. The main premise is to separate the MA, neptunium, americium and curium, for transmutation or for usable purposes. As the REDOX chemistry of neptunium under reprocessing conditions is complex and therefore poorly understood, an extraction system which does not require oxidation state control is favourable. Several solvent systems have shown much promise in the separation of neptunium from dissolved spent fuel. The $CyMe_4$-BTBP with TBP/DEHiBA solvent systems proposed by Chalmers gave effective results for the separation of neptunium as well as additional TRU isotopes. The $CyMe_4$-BTBP/TBP solvent system gave improved neptunium distribution ratios *c.f.* the $CyMe_4$-BTBP/DEHiBA solvent system, but does however, carry disadvantageous properties such as non-compliance with the CHON principle.[89]

In addition, literature has suggested a TODGA/DMDOHEMA solvent system for the collective separation of the TRU elements. Using this proposed solvent, it was observed that neptunium was rapidly extracted from the aqueous liquor under reprocessing type conditions. However, the extent of Np back extraction depended on the nitric acid concentration across the flowsheet analysed. The neptunium here, was however, effectively and rapidly stripped using the proposed stripping solution, AHA/SO_3-Ph-BTP.[49]

1.9.5 Americium (Am)

Americium is a transuranic (TRU) element produced during fission processes within a nuclear reactor core. The initial reactor fuel containing mostly ^{238}U, undergoes neutron capture to produce ^{239}Pu. The ^{239}Pu undergoes further neutron capture to

produce ^{241}Pu which beta decays to form ^{241}Am, the half life of which is relatively short at 432 years. Both transmutation sequences are detailed below:

$$^{238}_{92}U + {}^{1}_{0}n \rightarrow {}^{239}_{92}U \xrightarrow{\beta} {}^{239}_{93}Np \xrightarrow{\beta} {}^{239}_{94}Pu \quad (9)$$

$$^{239}_{94}Pu \xrightarrow{\gamma,n} {}^{240}_{94}Pu \xrightarrow{\gamma,n} {}^{241}_{94}Pu \xrightarrow{\beta} {}^{241}_{95}Am \ (\xrightarrow{\alpha} {}^{237}_{93}Np) \quad (10)$$

In aqueous media americium predominantly exists as a trivalent ion. However, under strongly oxidising conditions, it has been found that the penta and hexavalent americium ions exist.[90] Within the dissolution of spent nuclear fuel under PUREX conditions, americium predominantly exists in the Am(III) state.

The properties of some trivalent actinides, specifically Am(III) and Cm(III), both physical and chemical are relatively similar to the trivalent lanthanides, Ln(III). Both Am(III) (and Cm(III)) and Ln(III) are strongly hydrated in solution with comparable ionic radii.[91] In acidic conditions, as in reprocessing, Am(III) does not readily undergo hydrolysis, and is therefore usually a mobile ion in solution. In higher pH solutions (as in the environment), there is a higher propensity for Am(III) hydrolysis. The formation of hydrolysed Am(III) usually occurs via the following reaction:

$$Am^{3+} + 3H_2O \rightleftharpoons Am(OH)_3 + 3H^+ \quad (11)^{92}$$

Am(III) is not easily extracted under standard PUREX conditions and therefore remains in the high activity raffinate. Americium has not, to date, been separated from the reusable isotopes (U, Pu) as a lone product but exists in the high level waste stream with the other minor actinides and fission products. However, due to its relatively long term radiotoxicity and heat load within nuclear waste, it is necessary to partition and transmutate americium to give a more efficient and safe nuclear waste repository.

Currently, there is much research in to advanced reprocessing techniques that not only recycle the reusable uranium, but also the long-lived, highly radiotoxic actinide isotopes for further use or transmutation. As previously mentioned, the preferred route for reprocessing now leads to the group extraction of both actinides and lanthanides, with no prior REDOX control. This is followed by the separation of the

actinides from the non-reusable lanthanides. The BTP type ligands, proposed for use in SANEX and GANEX processes (see previous) have given the most promising results for the selective extraction of trivalent actinides over trivalent lanthanides. Americium extraction via *n*-Pr-BTP has previously been found to increased as a function of BTP concentration. However, radiolytic degradation of the BTP ligands at high absorbed doses lead to a decrease in the distribution ratios of the Am(III).[93] The radiolytic stability of the latest class of extractants is a necessary factor in selecting the most effective ligand for a once through nuclear waste reprocessing process.

Nilsson *et al.* have previously reported a separation factor between americium and europium ($SF_{Am/Eu}$) of around 150 using an organic phase containing 6,6'-bis-(5,6-dipentyl-[1,2,4]triazin-3-yl)-[2,2']bipyridinyl (C5-BTBP) (Figure 16) in cyclohexanone. However, C5-BTBP has been found to be susceptible to hydrolysis causing a decrease in the distribution ratios with increased contact time.[94]

Further, exploiting the affinity of the soft donor ligands to actinides, Panak *et al.* have demonstrated efficient separation factors using the sulfonated BTP type ligands (Figure 14) in order to suppress the extraction of Am(III) thus retaining it within the aqueous fraction and allowing the trivalent lanthanides to be extracted in to the organic fraction. The $SF_{Am/Eu}$ reported are in the range of 250-1000 *c.f.* $SF_{Am/Eu}$ of around 7 in the absence of a sulfonated BTP (when using TODGA as the organic phase extractant).[93]

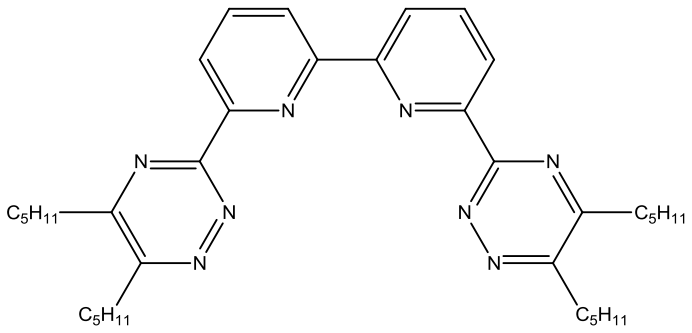

Figure 16: C5-BTBP

1.9.6 Technetium (Tc)

Although technetium is a transition metal, it is produced in appreciable quantities during the operation of nuclear reactors. Technetium poses significant environmental and biological threats due to its long half life and enhanced mobility in solution. For every ton of uranium burned, 1 kg of ^{99}Tc is produced, so its behaviour in both the waste and environment is of particular importance.[95] With the exception of neutron capture of molybdenum, all ^{99}Tc is formed in the fission of ^{235}U and ^{239}Pu.[96] The ^{99}Tc isotope has a half life of around 200000 years; it consequently contributes considerably to the overall radiotoxicity of the nuclear waste. Therefore, with the continued use of nuclear fission as a stable form of energy, comes the need to develop vital control methods for the prolonged management of ^{99}Tc.

In solution Tc exists predominantly as the pertechnetate ion, TcO_4^- where the Tc is in the +7 oxidation state.[97] It is this species that is of most concern to the environment. Most natural organic matter (NOM) exists with a negatively charged surface and hence repels the pertechnetate ion enhancing it mobility in solution. The reduction of the TcO_4^- to its (insoluble) Tc(IV) form facilitates its immobilisation and therefore its containment.[98] During the UREX process, acetohydroxamic acid (AHA) is employed to reduce the plutonium and neptunium, allowing the recovery of a separate uranium stream using TBP, and thus retaining the plutonium within the aqueous fraction, appeasing proliferation concerns surrounding an isolated plutonium stream. Previous studies suggested that the use of AHA did not however reduce the TcO_4^- in solution, to the extractable Tc^{4+} cation.

During the dissolution of SNF, some technetium produced in the fission processes remains as an insoluble residue but the majority dissolves in to the nitric acid solution as TcO_4^- which is extracted by TBP. The separated technetium can be scrubbed and disposed of appropriately. However, previously reported is the use of uranium to enhance the extraction of technetium from aqueous media. The coextraction of Tc in PUREX based systems is as follows:

$$TcO_4^- + UO_2(NO_3)_2.2TBP \rightarrow UO_2NO_3TcO_4.2TBP + NO_3^- \quad (12)$$

The above reaction is most effective below 0.5 M and above 3 M aqueous nitric acid and is facilitated by increasing aqueous uranium concentration in combination with increasing temperature.[99] Takeuchi *et al.* reported a larger distribution of Tc in the presence of uranium when using the extractant CMPO (Figure 7) as CMPO has a higher affinity for uranium. However this relationship was best observed below 1 M nitric acid; above 1 M, the Tc distribution was independent of uranium concentration.[100]

Further, the proposed complexation of the pertechnetate moiety to additional actinide species in PUREX type raffinate has little conclusive supporting evidence. Some literature has suggested that there is almost no complexation of the pertechnetate ion to neptunyl and plutonyl in aqueous solution.[101] However, solid complexes of pertechnetate with actinyl ions have been reported, such as the $[(NpO_2)_2(TcO_4)_4.3H_2O]$ and $[(PuO_2)_2(TcO_4)_4.3H_2O]$ species, the crystallographic data of which implies that the pertechnetate ion enters the coordination sphere of the actinide ion, allowing complex formation.[101] Solution state behaviour of the pertechnetate ion in nuclear reprocessing is complex due to its anionic nature, and therefore further solution state analysis is necessary to understand its relationship with the remaining species under reprocess conditions, in current and proposed methodologies.

It is known that the pertechnetate species is better separated from aqueous chloride containing media *c.f.* nitrate based media; the pertechnetate moiety is, over time, reduced to the more extractable Tc^{4+} ion in acidic media by halides.[102] High temperature alkali metal chloride-based melts are potential reaction media for pyrochemical processing of spent nuclear fuels,[103] so in theory, hybrid reprocessing schemes chloride may carry through and be present in dissolved fuel aqueous phases within solvent extraction processes. Therefore understanding the behaviour of technetium, inevitably produced during the fission of uranium, is of paramount importance. It is therefore necessary to consider the ease of recovery of more problematic isotopes in SNF reprocessing when designing prospective processes throughout the nuclear industry.

2 Aims

The aim of this work is to build on the information currently reported surrounding solvent extraction in the nuclear industry. This work will build on the principles of the presently utilised PUREX reprocessing process as well as investigate proposed solvent extraction techniques, such as the GANEX process, for the extraction of lanthanides and actinides from aqueous acid media, such as nitric and hydrochloric acid.

This work will utilise several organic extractants including, tributyl phosphate (TBP), N,N,N′,N′-tetraoctyl diglycolamide (TODGA) and 2-[2-(hexyloxy)ethyl]-N,N’-dimethyl-N,N’-dioctyl-propanediamide (DMDOHEMA). It is hoped that using these ligands, distribution ratios under various conditions can be calculated as well as solution state speciation, with particular emphasis on organic phase speciation post extraction. The relationship between extraction efficiency and organic phase speciation of extracted metal ions will be explored.

The systems analysed will undergo analysis via numerous spectroscopic techniques including 1 and 2D NMR spectroscopy, liquid scintillation counting (LSC), near Infra Red (nIR), Ultra Violet/visible (UV/vis) and Extended X-ray Absorption Fine Structure (EXAFS) spectroscopies.

With a wider knowledge of current and proposed solvent extraction processes surrounding the nuclear industry, it is hoped that this work will contribute to a conclusive "all purpose" reprocessing methodology which reduces the radiotoxicity of the nuclear waste and promotes proliferation resistance.

3 Experimental

3.1 Phase Preparation

All chemicals used were used as received, unless otherwise stated.

3.1.1 PUREX Solvent Preparation

Odourless kerosene (OK), used as the diluent, was reagent grade and low odour. Tributyl phosphate (TBP) (> 99 %) was used as the extractant. Both were obtained from Sigma Aldrich and used as received. A TBP-OK (30 % TBP by volume) solvent system was prepared. Before each extraction the TBP solvent was washed with HNO_3 (1 M); Na_2CO_3 (1 M); NaOH (1 M); HNO_3 (1 M) and used within 14 days, although no noticeable degradation was observed by NMR spectroscopy after 14 days. Preparation of hydrochloric acid (HCl) washed organic phases were prepared as above but omitting HNO_3 for HCl.

3.1.2 GANEX Solvent Preparation

Stock solvent solutions consisting of TODGA (0.2 M) with various phase modifiers (TBP, DMDOHEMA (0.5 M) or octanol (5 % by volume)) in a dodecane diluent were formulated. Both TODGA and DMDOHEMA were obtained from Technocomm and used as received. The ^1H NMR spectra of these compounds indicate the lack of any protic impurities.

3.1.3 Preparation of Zirconium Solutions

Both $ZrO(NO_3)_2.xH_2O$ and $ZrCl_4$ were obtained from Sigma Aldrich and used as received. Stock solutions (100 mL, 0.043 M) of zirconium nitrate were prepared by dissolution of $ZrO(NO_3)_2.xH_2O$ (1 g) in aqueous nitric acid (2-16 M). This stock solution (100 mL, 0.043 M) preparation was replicated using zirconium chloride ($ZrCl_4$) dissolved in various concentrations of hydrochloric acid (2 - 12 M).

3.1.4 Preparation of Uranyl Nitrate Solutions

Stock solutions (100 mL, 0.04 M) of uranyl nitrate were prepared by dissolution of $UO_2(NO_3)_2.6H_2O$ (^{238}U(VI), 2 g, ~ 25 kBq) in aqueous nitric acid (2-16 M).

3.1.5 Synthesis of Uranyl Chloride, UO_2Cl_2, and Preparation of UO_2Cl_2 Solutions

Solid UO_2Cl_2 was synthesised by dissolving UO_3 (^{238}U, 10 g, 124 kBq) in aqueous hydrochloric acid (40 mL, 12 M) and evaporating the solution to *near* dryness using a Schlenk line. Assuming 100 % UO_3 was converted to UO_2Cl_2, small aliquots, equivalent to 2 g UO_2Cl_2, of the resultant solution were taken and made up to separate stock solutions (100 mL, 0.06 M) using aqueous hydrochloric acid (2 - 12 M).

3.1.6 Preparation of Plutonium Solutions

From the primary plutonium stock solution (^{239}Pu(IV) in HNO_3, 41.17 MBq, 0.75 mL, 100 mM), aliquots (4.12 MBq, ~10 mM Pu(IV)) were taken and heated to dryness. The resultant solid was redissolved into aqueous nitric and hydrochloric acid solutions of various acid concentration or mixtures thereof (0.75 mL). These Pu containing aqueous fractions were contacted with relevant organic fractions and the phases analysed as detailed below.

3.1.7 Preparation of Lanthanide Solutions

Lanthanide (La, Pr, Nd, Sm, Eu, Gd, Tb, Dy, Ho, Er, Tm, Yb, Lu) nitrates were used as received from Sigma Aldrich and stored within a vacuum desiccator when not in use. The lanthanide nitrates (~ 0.5 g) were dissolved in aqueous nitric acid solutions (100 mL) of various concentration (1-16 M) giving stock solutions with a Ln(III) concentration of ~ 0.010 M.

3.1.8 Preparation of Neptunium Nitrate/Chloride, $NpO_2(NO_3)_2$ / NpO_2Cl_2, Solutions

The neptunium stock solution (3 mL max.; 5 mg Np-237 / mL in 4 M HNO_3) was pipetted in to a vial and the vial placed in to an aluminium heating vessel. The nitric acid solution was evaporated using a heat lamp and hot plate until no liquid remained. The resultant residue was redissolved in 60 % $HClO_4$ (max. 4 mL) to give a pale pink solution which was further heated to produce white fumes. At this stage the conversion to Np(VI) should be complete which was confirmed by taking a portion of the solution for analysis by UV/vis/nIR spectroscopy. The solution was evaporated to near dryness and the residual solid was dissolved in deionised water (~ 2 mL) and the solution separated evenly between four vials. To each vial, NaOH (6 M, max. 4 mL) was added drop wise to give a brown precipitate of $NpO_2(OH)_2$. The vials were sealed and centrifuged for approx. 5 minutes. The supernatant was removed and the remaining solid washed with deionised water (1 mL), vials sealed and centrifuged again for approx. 5 minutes. This washing process was repeated three times. The brown precipitate was dissolved in to various concentration nitric or hydrochloric acid solutions (1 - 10 M) or deionised water.

3.2 Separation Technique

Batch-wise separation was implemented throughout this work. Each experiment was repeated in triplicate, where possible. Equal volumes (0.5 - 5 mL) of each phase, aqueous and organic, were contacted using a Labinco L45 vortex shaker for approx. 10 minutes. Once contacted, phase separation was achieved centrifugally at 4000 rpm for up to 5 minutes. Each phase was analysed separately. For actinide analysis, an aliquot of the resultant organic phase post extraction was removed and back extracted using aqueous HNO_3 (0.01 M). For lanthanide and lanthanide/actinide separation, back extraction was achieved using an aqueous HNO_3 (0.01 M) and glycolic acid (0.5 M) solution. Separation of the aqueous and back extracted organic phases was implemented as above and the resultant aqueous phase analysed as detailed below.

Both organic (via back extraction) and aqueous phase samples were analysed, isotope dependent, via Inductively Charged Plasma - Optical Emission Spectroscopy or Mass Spectrometry (ICP-OES/MS), Liquid Scintillation Counting (LSC), QUANTULUS (ultra low level background LSC) and Ultra Violet/visible/near Infra Red (UV/vis/nIR) spectroscopy techniques. Multi-nuclear Nuclear Magnetic Resonance (NMR) spectroscopy was utilised for direct organic phase analysis, as detailed below.

For mixed HNO_3-HCl systems, it is necessary to work in a well ventilated area at all times due to the formation of aqua-regia. Mixed acid solutions were stored in loosely sealed vials if necessary but preferably disposed of as quickly as possible, once fully characterised.

3.3 Instrumentation

3.3.1 Nuclear Magnetic Resonance (NMR) Spectroscopy

NMR spectra were recorded on a Bruker Avance Ultrashield-400 instrument at 161.91 (^{31}P), 100.602 (^{13}C) and 400.052 (^{1}H) MHz using a BBFO probe, at the Centre for Radiochemistry Research (CRR), The University of Manchester. The variable temperature unit was set to 298 K unless otherwise stated. The lowest temperature setting for the variable temperature (VT) experiments performed was 248 K using chloroform-*d* for deuterium lock. For VT NMR, a liquid nitrogen Dewar was used with a fitted copper heat exchange coil between the incoming cooling gas and the point of cooling to the probe. Samples were run after temperature equilibration was reached. The temperature was controlled remotely using Bruker Topspin 3.2. Spectra were processed using Topspin 3.2 software.

For neptunium paramagnetic samples, the following parameters were altered from the standard Bruker experiment list: SW = 500; RG = 2050; NS = 75k; d1 = 0.5

3.3.2 NMR Sample Preparation

An aliquot (0.2 mL) of the desired sample was pipetted into a PTFE NMR tube insert to avoid unwanted mixing of the sample and deuterated solvent. The deuterated solvent (0.2 mL) was pipetted into a 5 mm, 8" length glass NMR tube. The PTFE tube was inserted into the glass NMR tube and the cap sealed using parafilm. This, in addition, created a secondary containment barrier for active samples.

3.3.3 Elemental analysis

ICP-OES analysis were performed at the School of Chemistry Micro-Analysis Department, The University of Manchester, using a Fisons Horizon Elemental Analysis ICP-OES spectrometer, for zirconium and uranium analysis only. Lanthanide analysis was done in the School of Atmospheric and Earth Science on an Agilent 7500cx ICPMS, in a class 1000 clean room. Actinide analysis was done on a variety of instruments all housed in the School of Chemistry.

3.3.4 ICP Sample Preparation

Liquid samples for ICP analysis were of aqueous nature and particulate free. The total dissolved elemental content should not reach over 1000 parts per million (ppm), per sample. Samples were prepared in plastic vials and acidified (typically 2 - 8 percentage HCl/HNO_3). An aliquot (usually 0.1 mL) of each aqueous phase (direct or post back extraction) was added to water (9.9 mL) giving 100 times dilution and ensuring metal content was below the required 1000 ppm limit.

3.3.5 Liquid Scintillation Counting (LSC)

Liquid scintillation measurements were taken using a Packard tri-carb 1900 liquid scintillation analyser. The scintillation cocktail (ScintiSafe 3^{TM}) contains phosphors (most commonly 2,5-diphenyloxazole and 1,4-bis(2-methylstyryl)benzene) that will fluoresce upon the interaction with a particle emitted by a radioactive decay process, in a diluent, usually toluene. The scintillation counter quantifies the resultant flashes of light. Consequently, this method does not distinguish between alpha, beta or gamma decay, but provides the overall activity of the sample. For alpha beta

discrimination, the QUANTULUS was used. QUANTULUS measurements were taken using a Wallac Quantulus 1220 ultra-low level LS spectrometer.

3.3.5.1 LSC Sample Preparation

An aliquot (0.1 mL) of each sample to be analysed was placed into a scintillation vial and the scintillation cocktail (10 mL) added. Each scintillation vial was shaken on the Labinco L45 vortex shaker for approx. 10 seconds. Each vial was wiped with a Kimwipe before being placed into the LSC and the samples run immediately. Samples which were not analysed immediately were stored in a fridge at around 4^{o}C and collected as soon as possible.

3.3.6 Sample Preparation for X-Ray Absorption Spectroscopy

For uranium and zirconium samples analysed by X-ray absorption spectroscopy, a small aliquot (0.4 mL) of each organic fraction, post extraction, was isolated into a plastic 650 uL Eppendorf vial. Each plastic lid was sealed with Araldite Rapide and further sealed with Parafilm. For active samples, the sealed vial was additionally contained via a heat sealed bag. Each containment layer was swabbed and scintillation counted for contamination before transportation.

Solution state neptunium samples, were prepared at the KIT-INE (Karlsruhe, Germany) using neptunium provided in house. The original neptunium solution (0.5 mL max.; 4 mg Np-237/ mL in 5 M $HClO_4$) was separated evenly between seven vials and each was evaporated to dryness. To the remaining solid, 10 M HNO_3 was added in order to oxidise the neptunium solid to Np(VI). These solutions were taken to near dryness and the residual solid was further dissolved into a various concentration nitric acid. Conversion to Np(VI) was assessed using UV/vis/nIR spectroscopy. The resultant Np(VI) aqueous fractions were contacted with various GANEX solvent systems for 15 minutes and centrifuged for full phase separation. An aliquot (300 uL) of the resultant organic fraction was isolated into a plastic 350 uL Eppendorf vial and sealed using Araldite Rapide. The lids were further sealed using parafilm.

3.3.7 X-Ray Absorption Spectroscopy (XAS)

Uranium and zirconium L_{III}-edge and K-edge spectra, respectively, were collected on station B18 (2-35 keV) at the Diamond Light Source, unless otherwise stated, using a 9 element solid-state Ge detector, focusing optics (beam size 0.5 mm^2), and a Si-111 double crystal monochromator. Between 8 and 20 Quick EXAFS (QEXAFS) scans were collected per sample and averaged in order to increase the signal to noise ratio.

Neptunium L_{III}-edge XAS data for extracted organic fractions were recorded in fluorescence mode at the KIT-INE-Beamline for actinide research at ANKA, Karlsruhe, Germany.[104] The spectra presented were measured using a Canberra LEGe detector; 5 to 8 scans were averaged to reduce the noise level. Neptunium spectra were calibrated against the first inflection point in the XANES spectrum using a foil of yttrium. This inflection point was defined as the first derivative maximum set to the K-edge of yttrium: 17038 eV.

The XANES spectra were isolated from XAS scans following subtraction of the pre-edge background absorption. For all XAS measurements, EXAFS data analysis was based on standard data reduction and least squares fit techniques, parameters (coordination numbers (CN), distance to neighbour atoms (R) and EXAFS Debye–Waller factors ($\sigma 2$)) were determined. Background processing was performed using Athena, and EXAFS modelling was carried out using Artemis.[105]

3.3.8 Ultra Violet/ visible/ near Infra Red Spectroscopy (UV/vis/nIR)

Absorption spectra were recorded for solution state neptunium samples for analysis of aqueous and organic phases, on a T60U spectrometer (PG Instruments Ltd.) using fused quartz cells with a path length of 1 cm or on a Shimadzu UV-2600. Approximately 0.8 mL of each phase was used for samples measurements.

4 Modified PUREX Systems Relevant to Fission Product Separation

4.1 Metal Free Systems

Nuclear Magnetic Resonance (NMR) studies on solvent systems and non-metal containing acid extractions were examined as a comparative to the metal containing systems studied in order to observe possible differences in extractant related speciation within systems of a PUREX nature. Experiments used the extractant TriButyl Phosphate (TBP) throughout, where a constant TBP concentration (30 % by volume) was retained throughout the organic phase. The TBP was diluted in odourless kerosene (OK) as this is the solvent system used in PUREX reprocessing. All ^{31}P NMR spectra are collected with proton decoupled to avoid interference from the diluent.

The ^{31}P NMR spectra detailed below (Figure 17) show the signal from the TBP moiety in both neat TBP and TBP diluted in OK (30 % by volume), in which a small shift downfield from -0.2 to -0.05 ppm from the former to the latter is observed. The two samples analysed were solvent only as a comparative tool, and had not been acidified.

In these HCl/HNO_3-TBP-OK systems, it is thought that in the presence of acid, the TBP separates some acid through contact of aqueous and organic phases. The resultant species are thought to be the HCl-TBP and HNO_3-TBP adducts. It is likely that these adducts are formed through hydrogen bonding of the phosphate oxygen and the acidic hydrogens.[106]

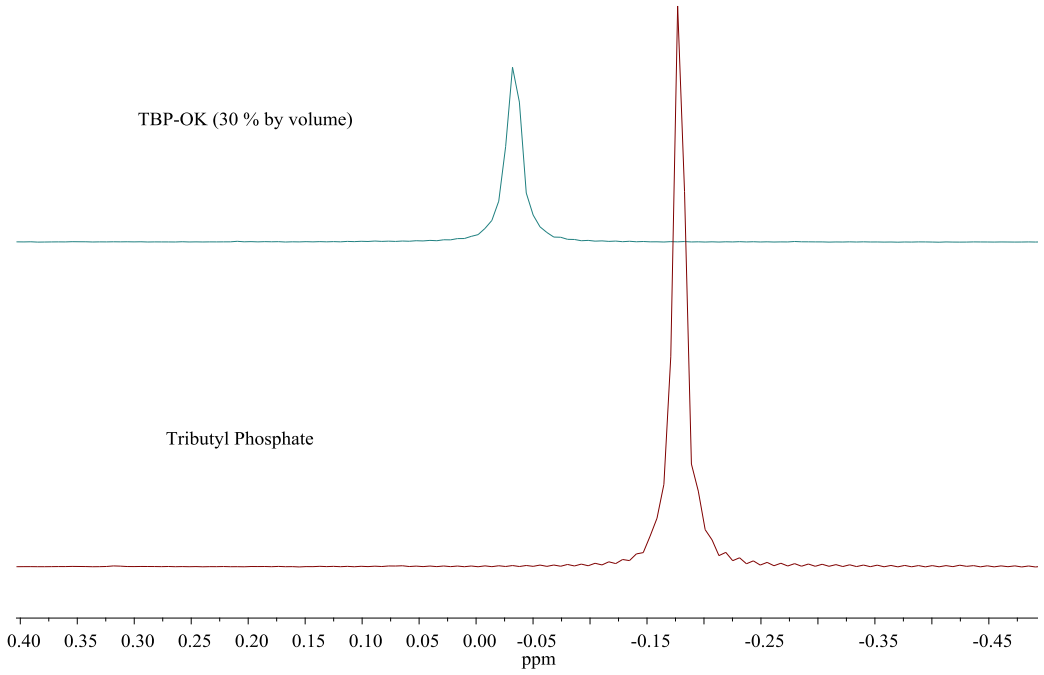

Figure 17: ^{31}P NMR spectra of pure TBP and TBP-OK (30 % TBP by volume).

A number of aqueous nitric acid (HNO_3) and hydrochloric acid (HCl) phases were prepared from concentrations of 2-16 M and 2-12 M respectively. These aqueous phases were contacted with the TBP-OK (30 % TBP by volume) solvent, mechanically agitated for approx. 10 minutes, and centrifuged for full phase equilibrium. A small aliquot (enough for a distinct ^{31}P NMR signal) was taken from each organic phase post extraction and the ^{31}P NMR spectra collected using identical acquisition parameters.

The ^{31}P NMR signals observed in the organic phase post extraction for aqueous nitric acid phases contacted with TBP-OK are detailed in Figure 18. The signal shifts to around -2 ppm as the aqueous HNO_3 concentration increases from 2 to 10 M. Above 10 M HNO_3, the ^{31}P NMR signal shifts downfield to around -1.6 ppm. This shift to further downfield regions was not observed in the HCl-TBP-OK systems. Table 1 outlines the initial aqueous phase composition for the samples analysed in Figure 18. Generally, for initial aqueous phase concentrations between 0 and 14 M HNO_3, it is thought that the following species exist in solution: TBP-HNO_3, $(TBP)_2$-HNO_3 and TBP-$(HNO_3)_2$.[107] At medium acid concentrations, it is known that the TBP-HNO_3 predominates. In systems of low acid concentration and high TBP concentration,

hydrated species are known to exist, most prolific of which are TBP-H_2O and $(TBP)_2$-HNO_3-H_2O.[108]

The presence of one phosphorus signal in the ^{31}P NMR for the HNO_3-TBP-OK systems indicates the HNO_3-TBP adduct dominates the organic phase speciation. However, changes in the chemical shift of this signal are observed in Figure 18 with changes in the nitric acid concentration and with respect to the unacidified solvent (Figure 17). Thereby, indicating the formation of other species over the various solution conditions which are in exchange with one another to give a single signal that is averaged over the species that are present. The HNO_3-TBP adduct could be hydrated to a certain degree, more so at lower aqueous acid concentrations.[109] Over the aqueous acid concentration range studied, the suggested hydrated species formed within the organic fraction post separation could be TBP-H_2O and $(TBP)_2$-HNO_3-H_2O to the TBP-HNO_3 species as the concentration of HNO_3 increases, up to 10 M. For aqueous HNO_3 concentrations above 10 M, less hydrated organic phase species are observed to form, due to the greater nitric acid content in the initial aqueous fraction, potentially forming the HNO_3-$(TBP)_2$ and $(HNO_3)_2$-TBP species. For HNO_3-TBP-OK systems, previous data suggest the nature of the adduct formed is dependent on the volume percent of TBP used.

It is thought that HNO_3 is extracted most effectively by TBP and its extraction in to the organic phase is accompanied by little transfer of water.[110] Extraction of HCl by TBP is much lower comparatively and is accompanied by a higher transfer of water in to the organic phase.[111] It is thought that extraction of inorganic acids occurs via the formation on reverse micelles by the TBP.[112] The presence of large amounts of water in the polar core of the reverse micelles should make the micellar core more polar and therefore, should increase the strength of the intermicellar attraction, thus facilitating third phase formation.[113] Micellar formation is thought to be facilitated by the relatively strong amphiphilic character brought about by the hydrogen bonding of water and nitric/hydrochloric acid molecules to the P=O group of the TBP molecule. This hydrogen bonding within the amphiphilic core of the reverse micelle may be stronger between HCl molecules and the P=O group due to its higher electronegativity *c.f.* the electronegativity within the HNO_3 species. The hydrogen bonding attraction of the HCl to the P=O may also facilitate the hydrogen bonding,

and therefore higher extraction, of water molecules. The increased water concentration in the core of the reverse micelle will make the core more polar. It is thought that this increased polarity increases the intermicellar attraction.[110] This may postulate as to why third phase is observed in HCl containing systems of much lower aqueous acidity over analogous HNO_3 containing systems. Whereas, within HNO_3-TBP-OK systems, it has previously been reported that third phase formation is unattainable with initial aqueous HNO_3 concentrations as high as 16 M.[114] Of the nitric acid systems analysed, there were no third phases observed even at aqueous nitric acid concentrations of 16 M.

Sample	N2	N4	N6	N8	N10	N12	N14	N16
$[HNO_3]$ / M	2.00	4.00	6.00	8.00	10.00	12.00	14.00	16.00

Table 1: Initial aqueous phase HNO_3 concentrations for samples N2 – N16.

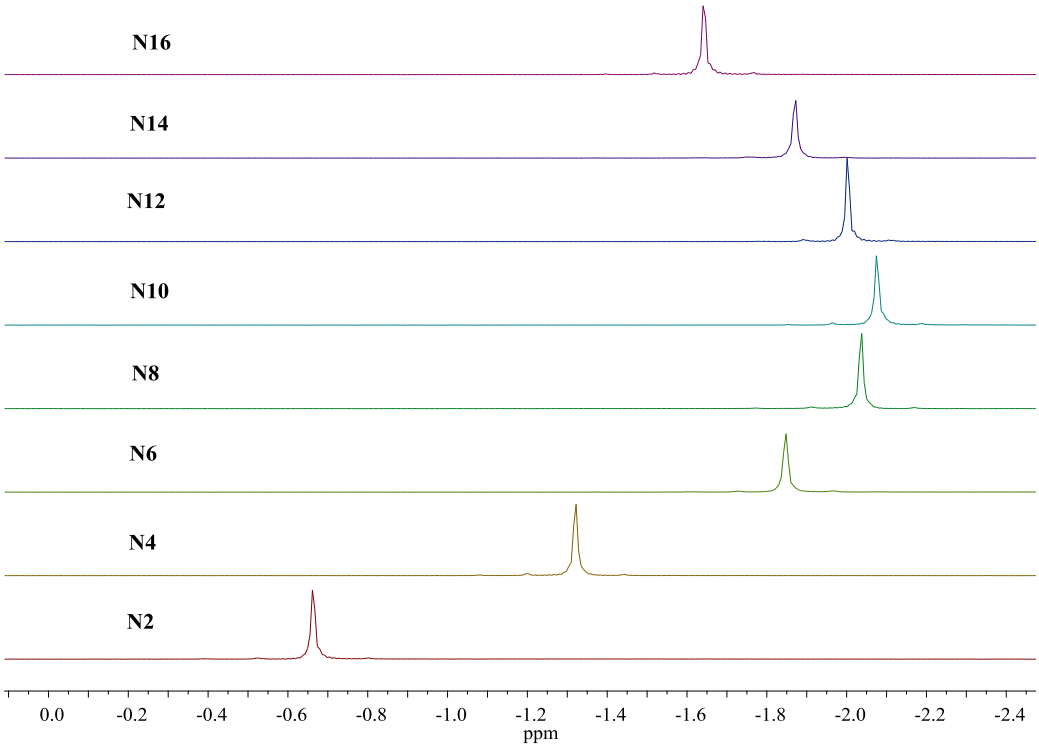

Figure 18: ^{31}P NMR spectra showing the organic phase post extraction for samples N2 – N16.

With respect to the ^{31}P NMR spectra for neat TBP and TBP in OK (30 % by volume), the NMR data presented in Figure 19 illustrates the NMR signals for samples containing initial HCl aqueous phases where at low HCl concentrations a signal is observed at around -0.10 ppm for the organic phase post extraction, which shifts slightly upfield and diminishes with respect to background, with increasing HCl concentration in the initial aqueous fraction. This upfield shift is thought to correspond to the change in TBP coordination by acid at various concentrations *i.e.* at low acid concentration, relatively more water is present, and therefore hydrated species are thought to be more prolific. It was noted in two phase systems using an aqueous HCl phase above 6 M HCl a third phase was observed.

As Figure 19 shows the NMR data for the organic fraction only, the loss of signal above background at higher initial aqueous phase HCl concentrations may corroborate the observation of a third phase, which contains the majority of the TBP leaving the light organic phase containing predominantly OK.

The third phase observed to form in samples containing initial aqueous phase concentrations of 8, 10 and 12 M HCl was absent in samples where an aqueous phase concentration of 2 and 4 M HCl was present. ^{31}P NMR spectra were recorded of the third phase post extraction, the results of which are presented in Figure 20. Clear signals were observed at -1.25 ppm for third phase samples containing aqueous 8 M HCl, shifting upfield to around -2 ppm for samples containing aqueous 12 M HCl. It is thought that in systems containing HCl, water molecules are also extracted by TBP, more so than in systems containing HNO_3 or H_2SO_4, for example. Therefore, this apparent upfield shift may be indicative of various levels of hydration of the extracted species within the third phase. The upfield shift is observed as a function of increasing aqueous phase HCl concentration. The composition of the initial aqueous fractions for the samples analysed are detailed in Table 2. Those samples where a third phase was observed are shown in red.

The tabulated initial aqueous phase compositions used throughout this section use the nomenclature "C" or "N" which refer to the presence of chloride or nitrate, and its subsequent aqueous phase molar concentration. This nomenclature is not referring to the elements carbon or nitrogen.

Sample	C2	C4	C6	C8	C10	C12
[HCl] / M	2.00	4.00	6.00	8.00	10.00	12.00

Table 2: Initial aqueous phase HCl concentrations for samples C2 - C12. Red indicates samples in which a third phase was observed.

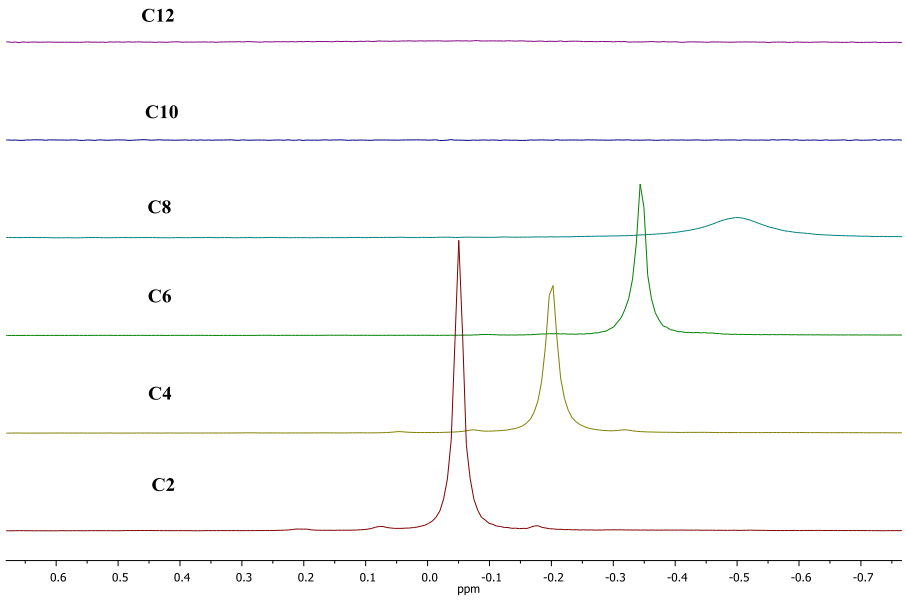

Figure 19: ^{31}P NMR spectra showing the organic phase post extraction for samples C2 – C12.

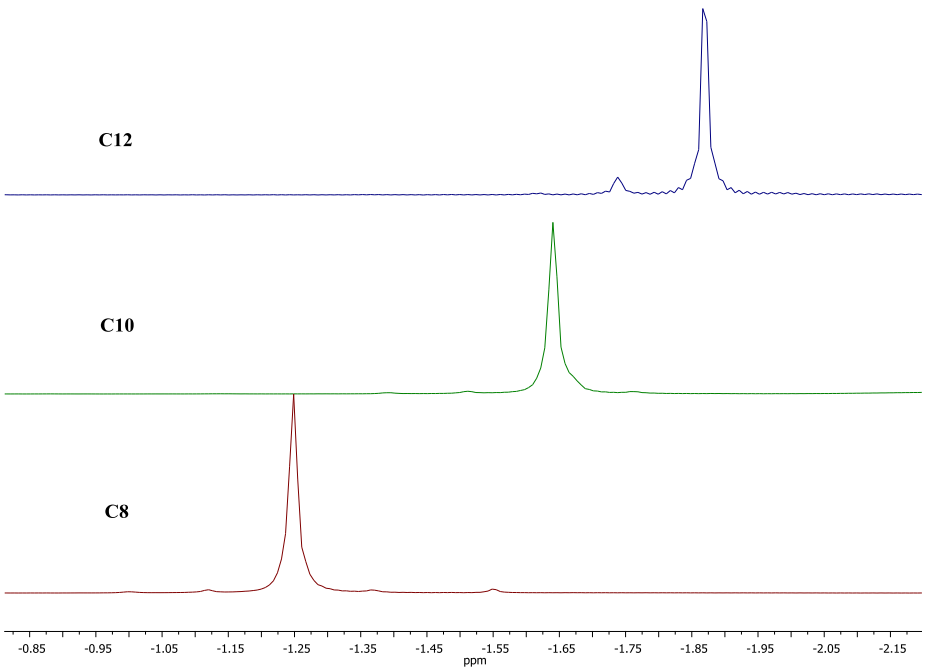

Figure 20: ^{31}P NMR spectra for the third phase, post extraction for samples C6 – C12.

The phenomena of third phase formation in solvent extraction systems has been studied heavily, especially throughout the nuclear industry.[115] It is normally observed at high metal loading concentrations where the organic phase splits to form a heavy and a light phase which contain most, if not all of the metal species and mostly organic diluent respectively. For HCl-TBP-OK systems, the HCl-TBP adduct is not formed as readily (with respect to the HNO_3-TBP adduct) in solvent systems of TBP-OK. In these HCl/HNO_3-TBP-OK systems, the concentration of acid increases throughout the organic fraction with increasing initial aqueous acid concentrations and therefore third phase is more likely to occur at higher initial aqueous acid concentrations. It is thought that the HCl-TBP adduct is surrounded by large amounts of water, which is said to facilitate third phase formation.[114] Although, a third phase in the systems detailed in Table 1 was observed at initial aqueous HCl concentrations of 6 M, third phase formation has been found to form using a TBP-OK (30 % TBP by volume) organic phase composition at initial aqueous phase HCl concentration of 7.6 M.[114] The surrounding temperature has however, been known to effect the propensity of third phase formation in general, and although every effort was made to maintain a constant temperature, this may explain the differences in results.

Systems were analysed where aqueous fractions consisted of variable concentrations of both chloride and nitrate. The aqueous fractions, compositional details of which are detailed in Table 3, were contacted with TBP-OK (30 % by volume), mechanically agitated and centrifuged for full phase separation. The resultant organic phase was analysed by ^{31}P NMR, the results of which are presented in Figure 21.

For samples C9:N1 – C1:N9, the ^{31}P NMR spectra indicates that one phosphorus species is present as the initial aqueous phase chloride concentration is increased and the initial nitrate concentration decreased. The phosphorus signal is observed at -2 ppm, similar to some signals observed in the individual acid systems. There is little shift up or downfield in these chloride and nitrate containing systems indicating the mixture of acids gives one acid-TBP species. The signal observed in Figure 21 is likely attributed to the TBP-HNO_3 or TBP-HCl adduct but it is thought the TBP-HNO_3 adduct is more likely as formation of which is favoured over the formation of the TBP-HCl adduct.[116]

No third phases were observed in any of these non metal containing mixed acid systems analysed. All sample analysis was conducted at room temperature.

Sample	C9:N1	C8:N2	C7:N3	C6:N4	C5:N5	C4:N6	C3:N7	C2:N8	C1:N9
$[H^+]$ / M	10.00	10.00	10.00	10.00	10.00	10.00	10.00	10.00	10.00
$[Cl^-]$ / M	9.00	8.00	7.00	6.00	5.00	4.00	3.00	2.00	1.00
$[NO_3^-]$ / M	1.00	2.00	3.00	4.00	5.00	6.00	7.00	8.00	9.00

Table 3: Initial aqueous phase H^+, Cl^- and NO_3^- concentrations for samples C9:N1 – C1:N9.

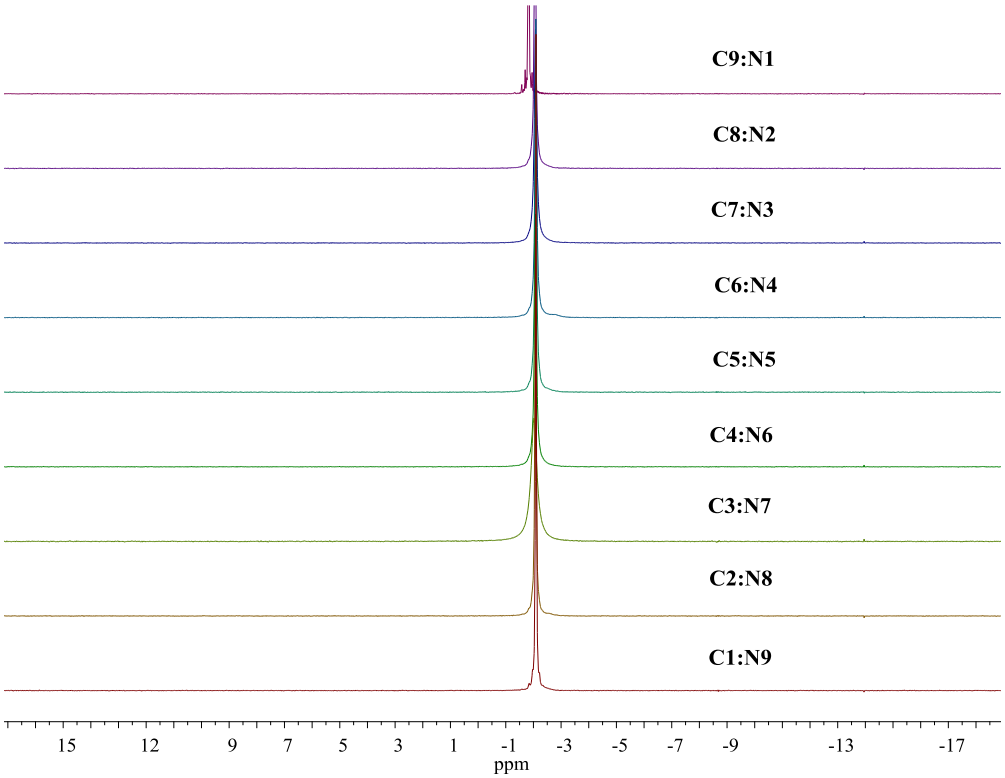

Figure 21: ^{31}P NMR spectra of the organic phase post extraction for samples C9:N1 - C1:N9.

A number of other aqueous chloride and nitrate combinations were analysed via the same methodologies, *i.e.* retaining nitrate at one concentrations and varying the chloride concentration, and *vice versa*. As observed in Figure 21, there is little shift in the ^{31}P organic phase NMR spectra of these mixed chloride/nitrate containing systems.

4.2 Zirconium Separated from Aqueous Nitric Acid

Zirconium was studied as it is the main component of zircalloy cladding used in nuclear fuel assemblies. It is also a fission product produced during nuclear fission and therefore the extraction of which under reprocess conditions has been investigated.

$ZrO(NO_3)_2$ (0.086 M) was dissolved over a range of aqueous nitric acid concentrations (2-16 M) and the resultant aqueous phases contacted with TBP-OK (30 % TBP by volume), mechanically agitated for approx. 10 minutes and

centrifuged for full phase separation. The nitrated zirconium species was used at it retained anionic consistency with the aqueous nitric acid. The organic phases were analysed by proton decoupled ^{31}P NMR spectroscopy. Distribution ratios were calculated with data received from ICP-OES analysis.

Post extraction, an aliquot of the resultant aqueous and organic phases was taken for ICP-OES analysis. The aqueous aliquot was diluted 100 fold with deionised water and submitted, whilst the organic aliquot was contacted with nitric acid (0.1 M) and the zirconium back extracted. Of this resultant aqueous phase, a further aliquot was taken and diluted 100 fold and submitted for analysis. Both ICP-OES results were compared in order to calculate the distribution ratio of zirconium at each aqueous nitric acid concentration. Distribution ratio (D_{Zr}) data for separated zirconium is presented in Table 4. The data shows that an initial aqueous HNO_3 concentration of 16 M gives a D_{Zr} of ~ 50. This equates to almost 100 % zirconium separation. The D_{Zr} increases as a function of aqueous nitrate concentration.

Sample	N2.Zr	N4.Zr	N6.Zr	N8.Zr	N10.Zr	N12.Zr	N14.Zr	N16.Zr
[HNO_3] / M	2.00	4.00	6.00	8.00	10.00	12.00	14.00	16.00
Distribution Ratio (D)	0.25	0.72	2.33	7.33	15.66	19.00	19.00	49.00
Log D	-0.60	-0.14	0.37	0.87	1.19	1.28	1.28	1.69

Table 4: Initial aqueous phase concentration and distribution ratios for samples N2:Zr - N16.Zr.

Figure 22 illustrates the distribution ratio of zirconium in samples N2.Zr - N16.Zr as a function of nitric acid concentration. The plot shows a clear increase in the distribution ratio of zirconium extracted from HNO_3 as a function of ascending acid concentration.

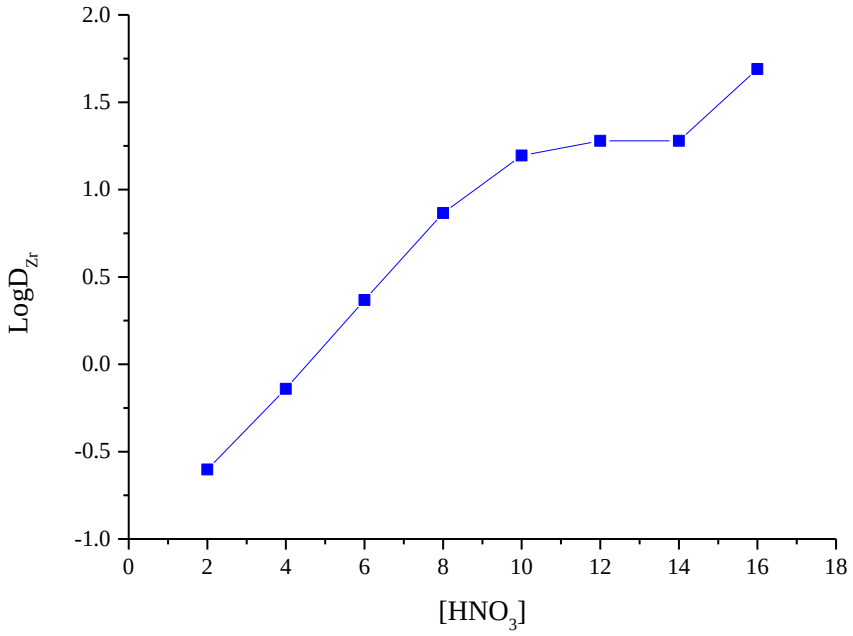

Figure 22: The logarithmic distribution ratio for zirconium as a function of HNO_3 concentration.

The ^{31}P NMR spectra recorded of the organic phase post extraction for the samples detailed in Table 4 and presented in Figure 23, shows a small shift in the resonance corresponding to what is thought to be the HNO_3-TBP adduct at around -1.6 ppm. The signal observed at -9 ppm for initial aqueous phase HNO_3 concentrations of 8 M and above, is thought to be an extracted Zr-NO_3-TBP type complex. The observed signal becomes less broad with ascending HNO_3 concentration, indicating a lack of exchange processes at higher nitrate concentrations, which could further indicate possible zirconium saturation in the organic fraction. At lower aqueous nitrate concentrations (6 and 4 M HNO_3), there is no signal observed at -9 ppm indicating low separation of zirconium and therefore too little of the Zr-NO_3-TBP type complex formation to give a signal in the NMR spectrum.

Previous studies have shown that systems where the initial aqueous phase concentration is above 8 M HNO_3, the resultant organic phase does not contain hydrolysed zirconium with speciation dominated by the $Zr(NO_3)_4$.2TBP solvate.[117] The NMR data presented in Figure 23 indicates the possible presence of this species

from the signals observed at around -9 ppm. The lack of signal observed in samples N4.Zr and N6.Zr may indicate that a hydrated species is not as easily separated compared with those anhydrous species.

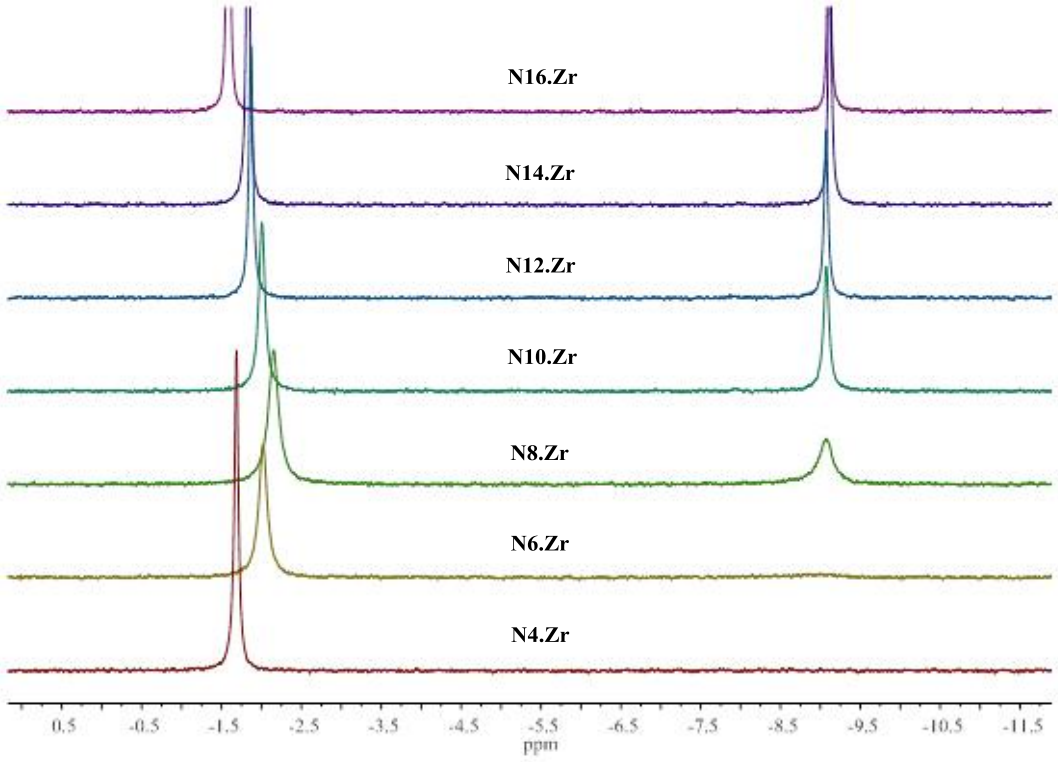

Figure 23: ^{31}P NMR spectra for the organic phase post extraction for samples N4:Zr - N16.Zr.

Extended X-ray Absorption Fine Structure (EXAFS) spectra were collected at the DIAMOND light source, Oxford, for the organic phase post extraction for sample N8.Zr. The fitted spectra and numerical parameters are detailed in Figure 24 and Table 5, respectively. The fit is in good agreement with the $[Zr(NO_3)_4(TBP)_4]$ species demonstrating that this complex dominates the organic phase speciation in this system. This is a best fit analysis, however. The fit is modelled using 4 nitrate groups with the oxygen and phosphorus of the phosphate group. Both nitrate group oxygen and phosphate group oxygen atoms are within the primary coordination shell with the phosphorus of the phosphate group held in the secondary shell, as is the nitrogen of the nitrate group.

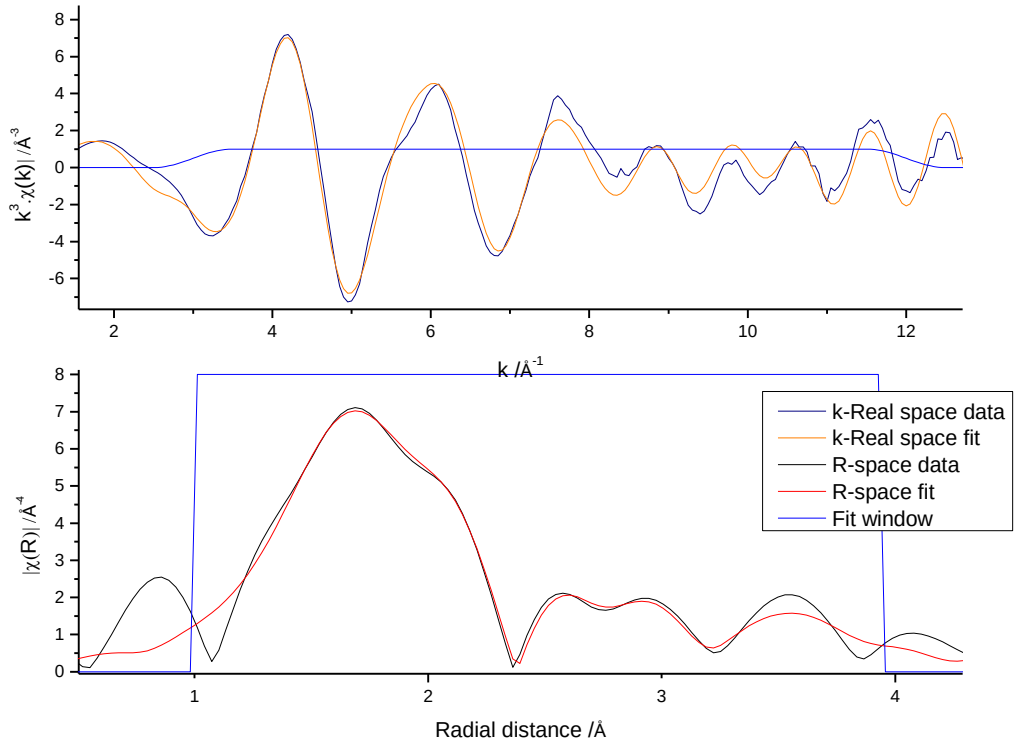

Figure 24: k^3-weighted χ(k)-function (top) and Fourier transform (bottom) of Zr K-edge EXAFS data for the organic phase post extraction from an initial aqueous phase consisting pure $ZrO(NO_3)_2$ in 8 M HNO_3. The data are fitted to $[Zr(NO_3)_4(TBP)_4]$.

Sample	Shell	Occupancy	σ^2	E_0 (eV)	R_i (Å)	R_f (Å)	ΔR (Å)
Zr^{4+} extracted from 8 M $HNO_{3(aq)}$ into 30 % TBP-OK, fitted as $[Zr(NO_3)_4(TBP)_4]$	O (nit)	8	0.0056		2.2792	2.2865	-0.0074
	N (nit)	4	0.0032		2.7520	2.7347	0.0173
	O (nit)	4	0.1995		3.9529	3.9356	0.0173
	N/O (MS)	8	0.0040	-2.332	3.9533	3.9360	0.0173
	O(phos)	4	0.0039		2.1262	2.1162	0.0100
Amp = 0.995 R factor = 0.01 χ^2 = 1526.48	P(phos)	4	0.00436		3.5150	3.5444	-0.0294
	O/P (MS)	8	0.0033		3.6167	3.5888	0.0289

Table 5: Parameters obtained from EXAFS fits in k^3-space of Zr^{4+}, extracted into TBP-OK (30 % TBP by volume) from an initial aqueous phases composition of 8 M HNO_3. E_0 is the relative shift in ionization energy, R_i is the initial distance of the shell (Å) and R_f is the refined distance of the shell (Å). Statistics of fit (χ^2 and r-factor) and amplitude factor (Amp) provided

4.3 Zirconium Separated from Aqueous Hydrochloric Acid

$ZrCl_4$ (0.086 M) was dissolved over a range of aqueous hydrochloric acid concentrations (2-12 M) and the resultant aqueous phases contacted with TBP-OK (30 % TBP by volume), mechanically agitated for approx. 10 minutes and centrifuged for full phase separation. The chlorinated zirconium species was used at it retained anionic consistency with the aqueous hydrochloric acid. The organic phases were analysed by proton decoupled ^{31}P NMR spectroscopy. Distribution ratios were calculated with data received from ICP-OES analysis.

For analysis, an aliquot of the post-extracted aqueous phase was diluted 100 fold with deionised water, whilst the organic aliquot was contacted with hydrochloric acid (0.1 M) and the zirconium back extracted. Of this resultant aqueous phase, a further aliquot was taken and diluted 100 fold for analysis. Table 6 outlines the distribution

ratio data for these samples. Samples where a third phase was observed are shown in red. Although a third phase was observed in samples C8.Zr - C12.Zr, both heavy and light organic phases were treated as one phase when considering the overall distribution ratio as the volume of the third phase was immeasurable. The data shows that an initial aqueous chloride concentration of 12 M gives a D_{Zr} of ~ 100. This equates to almost 100 % zirconium separation. The D_{Zr} increases as a function of aqueous chloride concentration as displayed in Figure 25. This trend is much the same as the data obtained for nitrate systems. However, D_{Zr} for sample C12.Zr is around 2 times greater than the distribution ratio observed for sample N12.Zr. Aqueous chloride concentrations of 8 M and above, gave significantly higher D_{Zr} than below 8 M.

Sample	C2.Zr	C4.Zr	C6.Zr	C8.Zr	C10.Zr	C12.Zr
[HCl] / M	2.00	4.00	6.00	8.00	10.00	12.00
Distribution Ratio (D)	0.11	0.23	1.08	5.66	49.00	99.00
Log D	-0.95	-0.63	0.03	0.75	0.69	1.99

Table 6: Initial aqueous phase concentrations and distribution ratios for samples C2:Zr - C12.Zr. Red indicated the observation of a third phase.

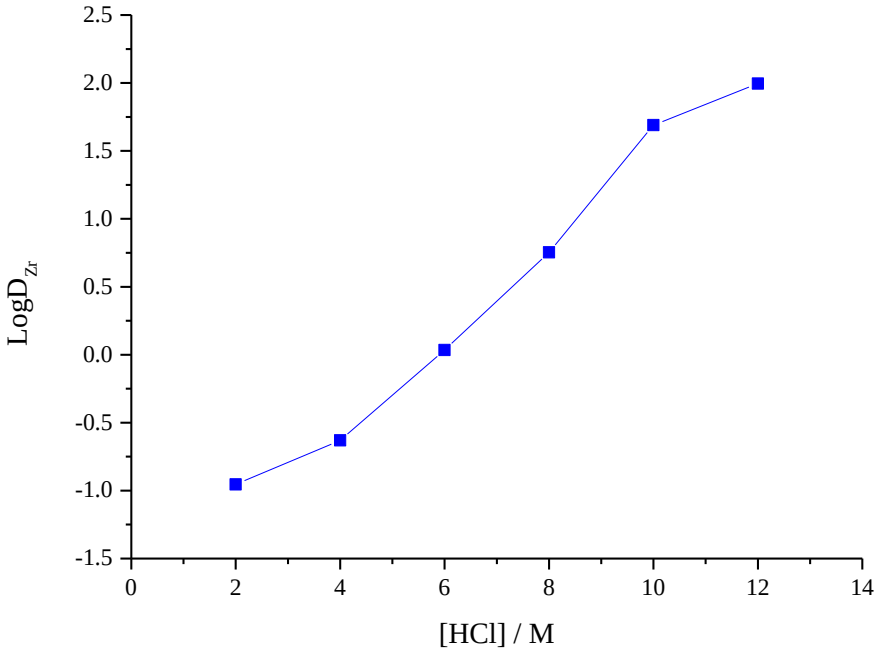

Figure 25: The logarithmic distribution ratio for zirconium as a function of HCl concentration.

Organic aliquots were taken post extraction and the ^{31}P NMR data collected, as detailed in Figure 26. There is one phosphorus signal seen at around 0 ppm which shifts slightly upfield with ascending aqueous chloride concentration. The lack of complexation signal could in part be due to the complexed metal species being retained in the third phase from low aqueous chloride concentration and therefore it is likely that the observed signal is due to the HCl-TBP adduct.

The subsequent ^{31}P NMR spectra for the analysed third phases, presented in Figure 27, show several species in solution in addition to what is thought to be the TBP-HCl adduct signal, seen at around -2 ppm. Using TBP as the extractant, it has been previously suggested that ZrX_4 (where X is a halide) forms the complex ZrX_4.2TBP in the organic phase post extraction.[118] Other complexation could occur via the formation of the $ZrCl_4$.4TBP species. Due to the hydrolytic nature of Zr^{4+} in these systems, as previously mentioned, additional species shown in Figure 27 may be the result of hydrolysed Zr-TBP complexes.

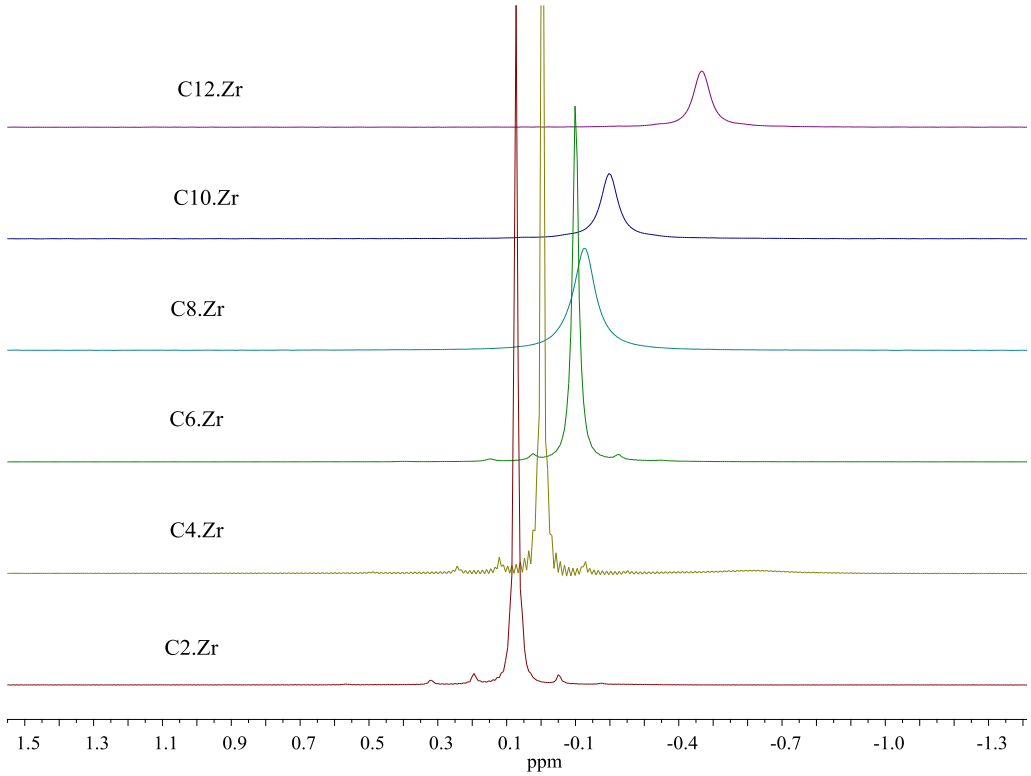

Figure 26: ^{31}P NMR spectra of the post extracted organic phase for samples C2:Zr - C12.Zr.

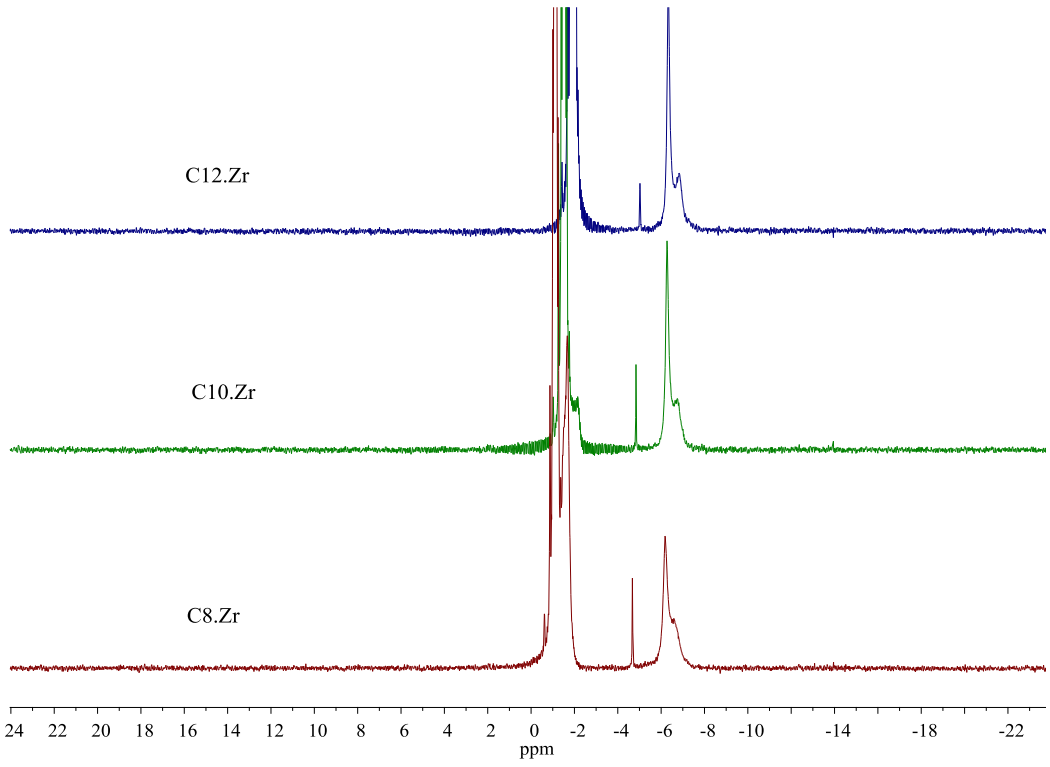

Figure 27: ^{31}P NMR spectra of the third phase post extraction for samples C2:Zr - C12.Zr.

Extended X-ray Absorption Fine Structure (EXAFS) spectra were collected at the DIAMOND light source, Oxford, for the organic phase post extraction for sample C5.Zr. The fitted spectra and numerical parameters are detailed in Figure 28 and Table 7, respectively. The fit is in good agreement with the $[ZrCl_4.(TBP)_4]$ species showing that this complex dominates the organic phase speciation in this system. This is a best fit agreement, however. The fit is modelled using 4 chloride atoms with the oxygen and phosphorus of the phosphate group. Both chloride and phosphate oxygen atoms are within the primary coordination shell with the phosphorus of the phosphate group held in the secondary shell. A multiple scattering shell was used for this fit as its scattering path was ranked of high importance in the feff calculation and improved the quality of the fit compared to when this shell was not included.

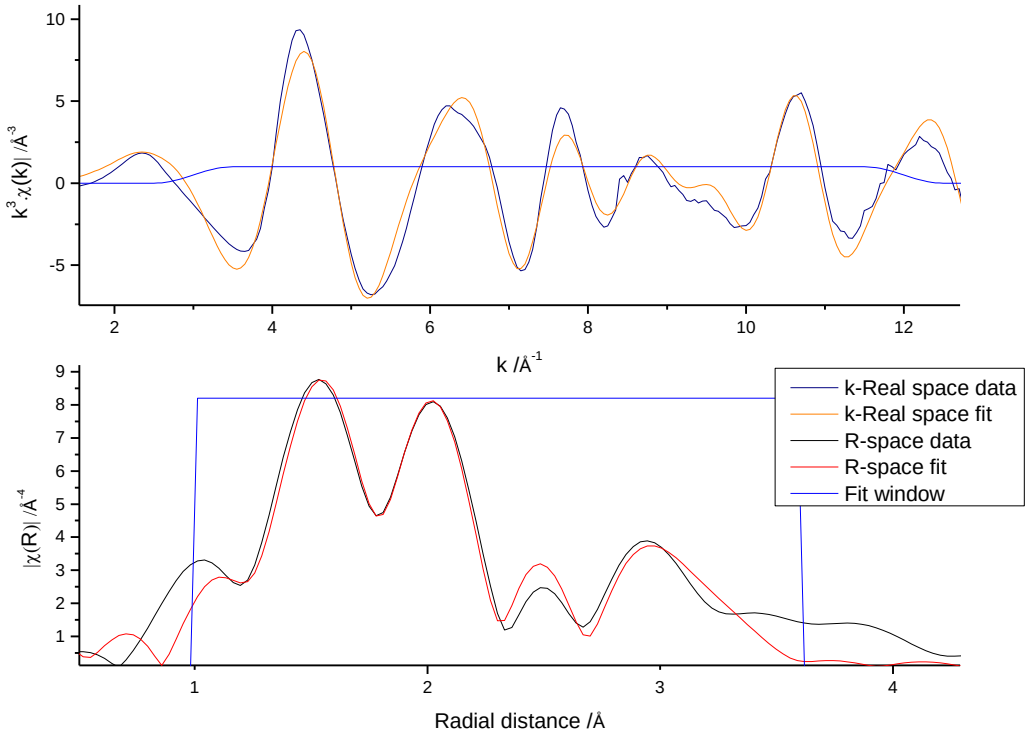

Figure 28: k^3-weighted χ(k)-function (top) and Fourier transform (bottom) of Zr K-edge EXAFS data for the organic phase post extraction from an initial aqueous phase consisting pure $ZrCl_4$ in 5 M HCl. The data is fitted to $[ZrCl_4(TBP)_4]$.

Sample	Shell	Occupancy	σ^2	E_0 (eV)	R_i (Å)	R_f (Å)	ΔR (Å)
Zr^{4+} extracted from 5 M HCl into 30 % TBP-OK, fitted as $[ZrCl_4(TBP)_4]$	Cl_4	4.00	0.00537	-2.428	2.4331	2.4871	-0.0540
	O(phos)	4.00	0.00236		2.0865	2.1162	-0.0297
	P(phos)	4.00	0.00322		3.6527	3.5444	0.1083
Amp = 0.925 R factor = 0.015 χ^2 = 2526.38	O(phos)P(phos) (MS)	8.00	0.01624		3.6503	3.5880	0.0623

Table 7: Parameters obtained from EXAFS fits in k^3-space for Zr^{4+} extracted into TBP-OK (30 % TBP by volume) from an initial aqueous phases composition of 5 M HCl. E_0 is the relative shift in ionization energy, R_i is the initial distance of the shell (Å) and R_f is the refined distance of the shell (Å). Statistics of fit (χ^2 and r-factor) and amplitude factor (Amp) provided.

4.4 Zirconium Separated from Mixed Aqueous Nitric and Hydrochloric Acid

For the purpose of this work, various concentrations of aqueous zirconium nitrate and aqueous zirconium chloride mixed solutions were prepared. The overall concentration of zirconium in each solution was 0.086 M throughout. These aqueous phases were contacted with TBP-OK (30 % by volume) by mechanical agitation for approx. 10 minutes and centrifuged for full phase separation. The organic phase was analysed via proton decoupled ^{31}P NMR spectroscopy. Distribution ratio data was calculated using data obtained from ICP-OES.

Separation of zirconium was achieved from aqueous mixtures 1-9 M aqueous HCl and aqueous 9-1 M HNO_3 (samples C1:N9.Zr - C9:N1.Zr; Table 10). An aliquot of both aqueous and organic phases was taken post extraction. The aqueous phase was

diluted for analysis. Two separate aliquots were taken from the organic fraction; one underwent back extraction using HNO_3 (0.1 M) and the other using HCl (0.1 M). Each result was compared and the distribution ratios calculated. Figure 29 and Table 8 both show an increase in the zirconium separation as a function of increasing aqueous chloride concentration. Sample C5:N5.Zr gave a distribution ratio of ~ 50 which equated to around a 98 % separation of zirconium in to the organic phase.

Figure 29 illustrates the distribution ratio data for the samples C1:N9.Zr - C9:N1.Zr. The distribution ratio increases as a function of ascending aqueous chloride concentration. This implies that the presence of chloride enhanced the separation of zirconium in these systems. A number of other aqueous chloride and nitrate combinations were analysed for their effectiveness of zirconium separation via the same methodologies, *i.e.* retaining aqueous nitrate at one concentration and varying the aqueous chloride concentration, and *vice versa*. The ^{31}P NMR spectra gave almost identical results to those outlined in Figure 30. This could indicate that for zirconium extracted into TBP-OK from various mixtures of HNO_3 and HCl, similar species are formed giving indistinguishable ^{31}P NMR spectra. The distribution data was also remarkably similar with improved separation of zirconium observed in systems tending towards higher aqueous chloride concentrations.

Sample	C1:N9 .Zr	C2:N8 .Zr	C3:N7 .Zr	C4:N6 .Zr	C5:N5 .Zr	C6:N4 .Zr	C7:N3 .Zr	C8:N2 .Zr	C9:N1 .Zr
$[H^+]$ / M	10.00	10.00	10.00	10.00	10.00	10.00	10.00	10.00	10.00
$[Cl^-]$ / M	1.00	2.00	3.00	4.00	5.00	6.00	7.00	8.00	9.00
$[NO_3^-]$ / M	9.00	8.00	7.00	6.00	5.00	4.00	3.00	2.00	1.00
Distribution Ratio (D)	24.00	32.33	32.33	49.00	49.00	99.00	99.00	99.00	99.00
Log D	1.38	1.51	1.51	1.69	1.69	1.99	1.99	1.99	1.99

Table 8: Initial aqueous phase concentrations and distribution ratios for samples C1:N9.Zr - C9:N1.Zr.

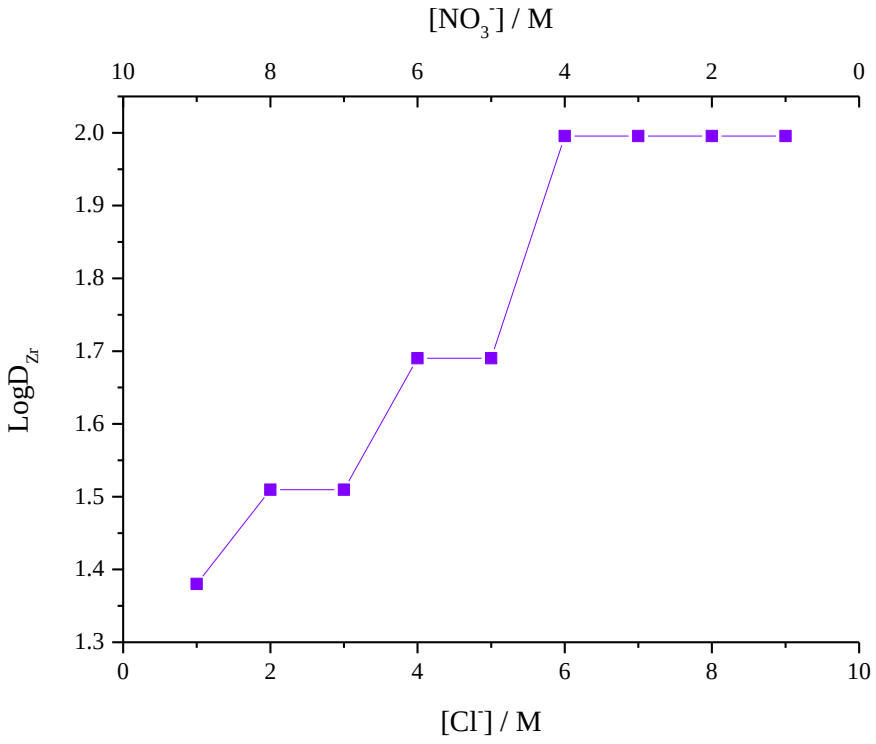

Figure 29: Distribution data for samples C1:N9.Zr - C9:N1.Zr as a function of initial aqueous anion concentration (initial $[H^+]$ = 10 M).

The ^{31}P NMR spectra presented in Figure 30 illustrate the organic phase post extraction for the samples detailed in Table 8. A prominent species is observed at around -9 ppm for sample C9:N1.Zr. This signal decreases with a decrease in the initial aqueous phase chloride concentration. Figure 30, in addition, shows the formation of a species, seen prominently at -8 ppm for sample C3:N7.Zr, which increases and subsequently decreases in intensity with increasing aqueous chloride concentration in the initial aqueous phase. The signal intensity is observed at its maxima, with reference to the other signals observed, in sample C5:N5.Zr. Further species are observed at -6.5 and -7.5 ppm in samples C1:N9.Zr and C2:N8.Zr. The species observed at -6.5 ppm decreases in intensity (relative to the remaining signals) with decreasing aqueous nitrate concentration and is most prominently seen in samples of higher aqueous nitrate concentration. The signal observed at -7.5 ppm decreases in intensity with decreasing aqueous nitrate concentration. For all these spectra, no two signals within the expected region of ^{31}P NMR resonances for TBP coordinated to Zr(IV) exhibit the same relative intensity across the various solution conditions studies so it can be assumed that each signal obtained represents a distinct Zr(IV)-TBP complex.

The NMR data presented in Figure 30 for these systems is different to that observed for the analogous single acid systems. For chloride containing systems, the zirconium complexation signal in the ^{31}P NMR spectra was observed at - 7 ppm which is not observed in the spectra presented in Figure 30. The signal at - 7.5 ppm seen in the spectra of Figure 30 is observed to decrease with ascending aqueous chloride concentration, which implies it is not due to Zr-Cl type complexation. The main complexation signal for zirconium separated from nitrate only systems was observed at - 8.75 ppm which does not correspond to the signals observed in Figure 30. The prominent signals observed in Figure 30 at - 8 and - 9 ppm are more significant for zirconium separated from higher aqueous chloride concentrations. This implies that they are not the result of Zr-NO_3 type complexation. There are also additional signals observed in Figure 30 that are not seen in the analogous single acid NMR spectra, which implies that there are several phosphorus environments in the post-separated organic fraction. Further analysis, in addition to EXAFS spectroscopy would aid speciation determination.

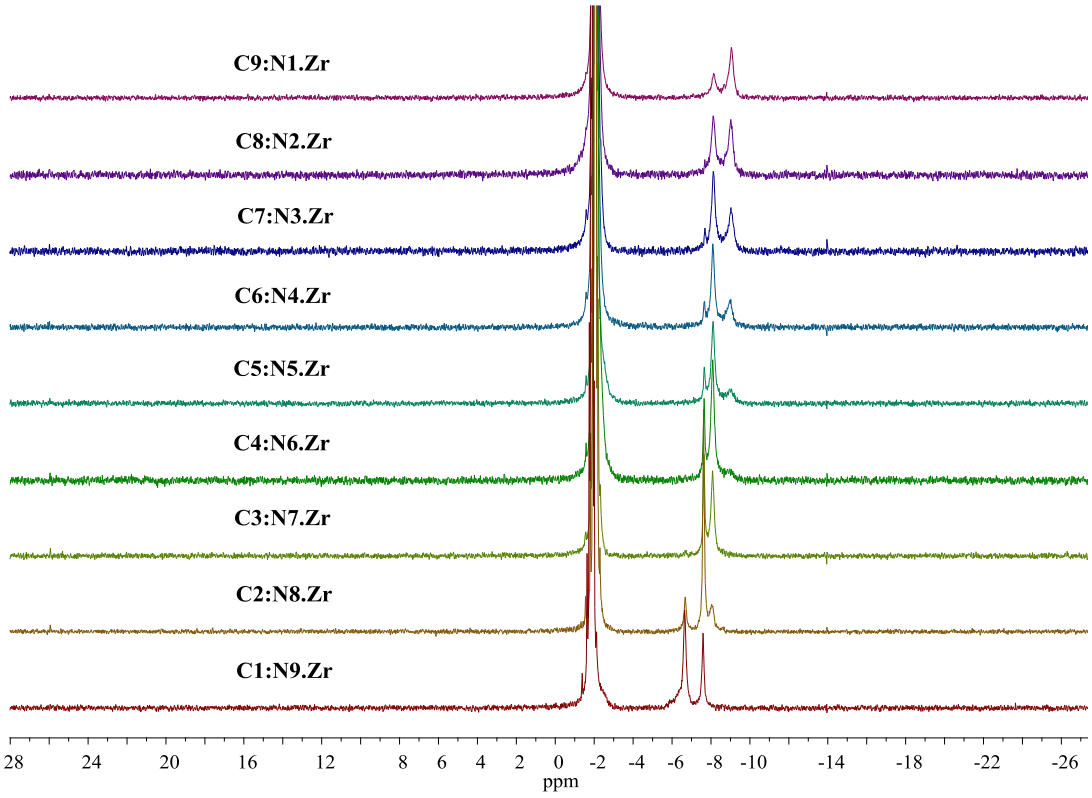

Figure 30: ^{31}P NMR spectra for the third phase, post extraction for samples C1:N9.Zr - C9:N1.Zr.

Extended X-ray Absorption Fine Structure (EXAFS) spectra were collected for a selection of the mixed acid systems with zirconium at the DIAMOND light source, Oxford. The sample with an initial aqueous phase of 2 M Cl^- and 10 M NO_3^- was studied as it contained a significantly higher aqueous nitrate concentration compared to the aqueous chloride concentration. As expected the organic phase speciation was dominated by the $[Zr(NO_3)_4(TBP)_4]$ moiety, according to the fitted spectra shown in Figure 31. This is a best fit analysis, however. Table 9 details the numerical parameters associated with this fit. Various fit parameters were exhausted using a pure chloride primary coordination shell as well as a mixed nitrate/chloride shell, but this was clearly the best fit of the data collected for this sample. This model uses the nitrate group oxygen atoms as well as the phosphate oxygen in its primary coordination shell and the phosphorus atoms of the phosphate group as well as the nitrogen atoms in the nitrate group in the second coordination shell.

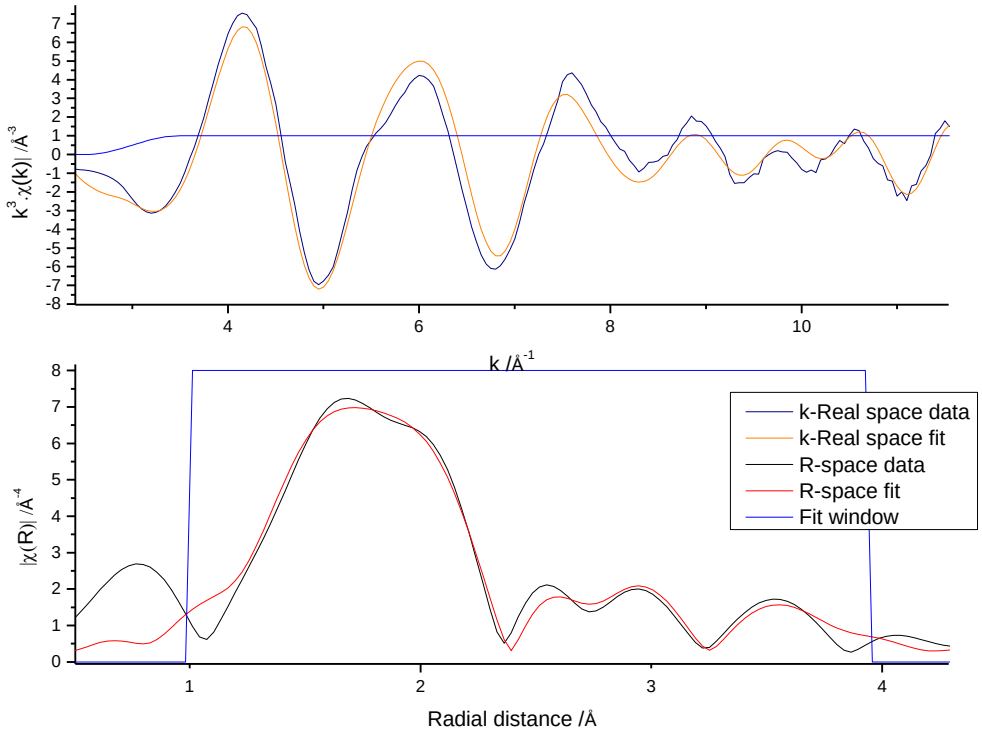

Figure 31: k^3-weighted $\chi(k)$-function (top) and Fourier transform (bottom) of Zr K-edge EXAFS data for the organic phase post extraction from an initial aqueous phase consisting of 10 M nitrate and 2 M chloride. The data is fitted to $[Zr(NO_3)_4(TBP)_4]$.

Sample	Shell	Occupancy	σ^2	E_0 (eV)	R_i (Å)	R_f (Å)	ΔR (Å)
Zr^{4+} extracted from 2 M Cl^-/10 M NO_3^-/12 M H^+ into 30 % TBP-OK, fitted to $[Zr(NO_3)_4(TBP)_4]$	O (nit)	8	0.11339	2.412	2.3296	2.3205	0.0091
	N (nit)	4	0.00570		2.7678	2.7347	0.0331
	O (nit)	4	0.01125		3.9687	3.9356	0.0331
	N/O (MS)	8	0.01696		3.9691	3.9360	0.0331
Amp = 0.961 R factor = 0.016 χ^2 = 1874.04	O(phos)	4	0.00115		2.1718	2.1162	0.0556
	P(phos)	4	0.01785		3.3539	3.5444	-0.1905

Table 9: Parameters obtained from EXAFS fits in k^3-space for Zr^{4+} extracted into TBP-OK (30 % by volume) from an initial aqueous phase composition of 10 M nitrate and 2 M chloride (12 M H^+). E_0 is the relative shift in ionization energy, R_i is the initial distance of the shell (Å) and R_f is the refined distance of the shell (Å). Statistics of fit (χ^2 and r-factor) and amplitude factor (Amp) provided.

The C6:N6.Zr sample was chosen as it contained equal concentrations of aqueous nitrate and chloride to ascertain any preferential binding of NO_3^- over Cl^- to Zr(IV) (or *vice versa*) speciation within the organic fraction post extraction. From the EXAFS data collected, the organic phase speciation was dominated by the $[ZrCl_4(TBP)_4]$ moiety, as the fitted spectra shows in Figure 32. This is a best fit analysis, however. Table 10 details the numerical parameters associated with this fit. Various fit parameters were exhausted using a pure nitrate coordination shell as well as a mixed nitrate/chloride shell, but the pure chloride species was clearly the best fit of the data collected for this sample. This model uses four chloride groups as well as the phosphate oxygen in its primary coordination shell and the phosphorus atoms of the phosphate group in the second coordination shell.

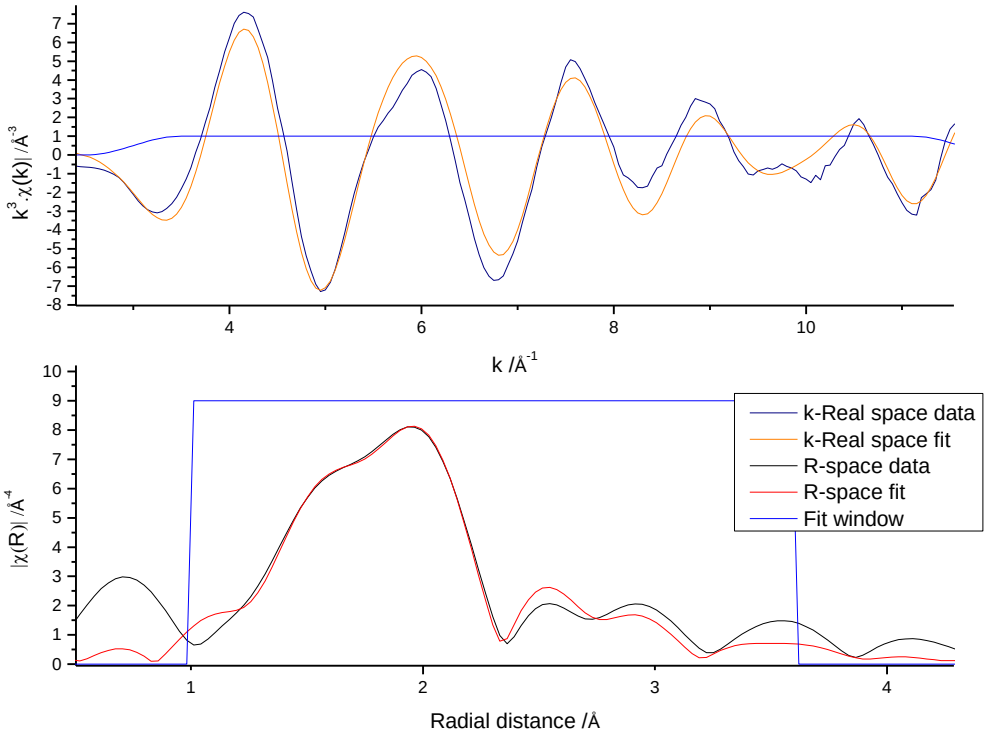

Figure 32: k^3-weighted χ(k)-function (top) and Fourier transform (bottom) of Zr K-edge EXAFS data for Zr^{4+} extracted into a 30 % TBP-OK organic phase from an initial aqueous phase consisting of 6 M nitrate and 6 M chloride (12 M H^+). The data is fitted to $[ZrCl_4(TBP)_4]$.

Sample	Shell	Occupancy	σ^2	E_0 (eV)	R_i (Å)	R_f (Å)	ΔR (Å)
Zr^{4+} extracted from 6 M Cl^-/ 6 M NO_3^-/ 12 M H^+ into 30 % TBP-OK, fitted to $[ZrCl_4(TBP)_4]$	Cl_4	4.00	0.00487		2.4857	2.4871	-0.0014
	O(phos)	4.00	0.00418		2.1796	2.1162	0.0634
	P(phos)	4.00	0.00885		3.8865	3.5444	0.3423
				-4.838			
Amp = 0.909 R factor = 0.008 χ^2 = 2075.57	O(phos)P(phos) (MS)	8.00	0.01135		3.5942	3.5880	0.0062

Table 10: Parameters obtained from EXAFS fits in k^3-space for Zr^{4+} extracted into TBP-OK (30 % by volume) from an initial aqueous phase composition of 6 M nitrate and 6 M chloride (12 M H^+). E_0 is the relative shift in ionization energy, R_i is the initial distance of the shell (Å) and R_f is the refined distance of the shell (Å). Statistics of fit (χ^2 and r-factor) and amplitude factor (Amp) provided.

The C10:N2.Zr sample was selected as it contained a significantly higher aqueous chloride concentration compared to the aqueous nitrate concentration. As expected the organic phase speciation was dominated by the $[ZrCl_4(TBP)_4]$ moiety, according to the fitted spectra shown in Figure 33. This is a best fit analysis, however. Table 11 details the numerical parameters associated with this fit. Various fit parameters were exhausted using a pure nitrate primary coordination shell as well as a mixed nitrate/chloride shell, but this was clearly the best fit of the data collected for this sample. This model is the same as used to fit the data for Zr^{4+} extracted from a chloride-only containing aqueous phase.

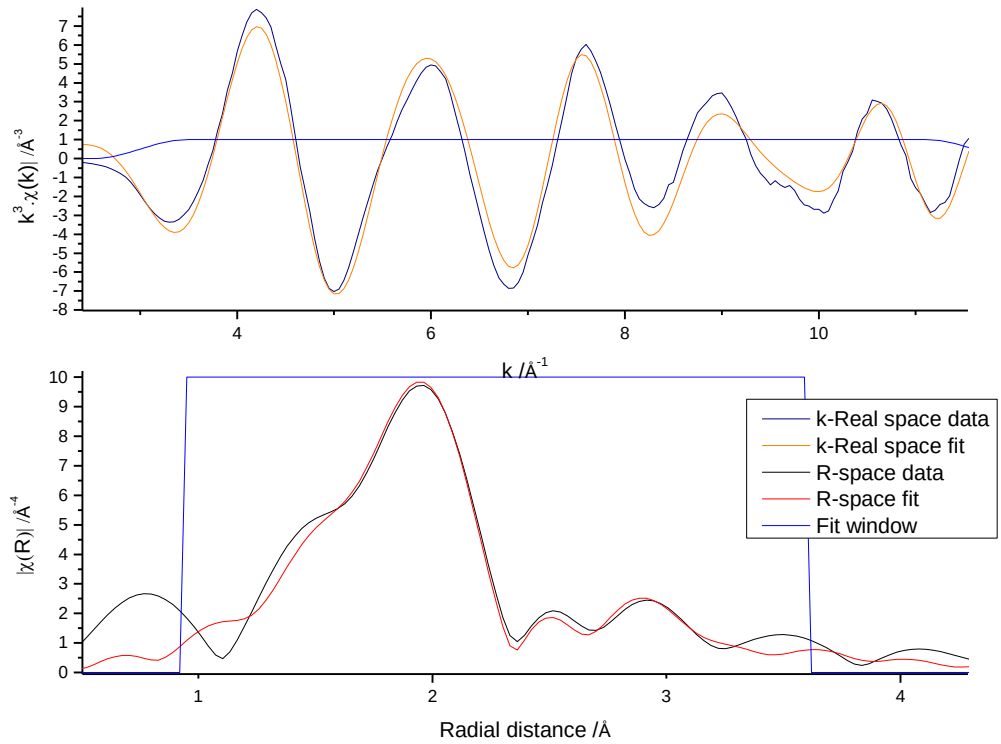

Figure 33: k^3-weighted χ(k)-function (top) and Fourier transform (bottom) of Zr K-edge EXAFS data for Zr4+ extracted into a 30 % TBP-OK organic phase from an initial aqueous phase consisting of 2 M nitrate and 10 M chloride (12 M H^+). The data are fitted to $[ZrCl_4(TBP)_4]$.

Sample	Shell	Occupancy	σ^2	E_0 (eV)	R_i (Å)	R_f (Å)	ΔR (Å)
Zr^{4+} extracted from 10 M Cl^- / 10 M NO_3^- / 12 M H^+ into 30 % TBP-OK, fitted to $[ZrCl_4(TBP)_4]$	Cl_4	4.00	0.00639	-3.715	2.4870	2.4871	-0.0001
	O(phos)	4.00	0.01002		2.2042	2.1162	0.0880
	P(phos)	4.00	0.00124		3.6185	3.5444	0.0741
Amp = 1.00 R factor = 0.009 χ^2 = 2140.81	O(phos)P(phos) (MS)	8.00	0.00572		3.7017	3.5888	0.1137

Table 11: Parameters obtained from EXAFS fits in k^3-space for Zr^{4+} extracted into TBP-OK (30 % by volume) from an initial aqueous phases composition of 2 M nitrate and 10 M chloride (12 M H^+). E_0 is the relative shift in ionization energy, R_i is the initial distance of the shell (Å) and R_f is the refined distance of the shell (Å). Statistics of fit (χ^2 and r-factor) and amplitude factor (Amp) provided.

4.5 Summary of Zirconium Extraction Behaviour in Modified PUREX

Zirconium demonstrated high distribution ratios when separated from both aqueous HCl and HNO_3, but showed slightly higher distribution ratios when separated from aqueous mixtures of both chloride and nitrate. The ^{31}P NMR spectra illustrated the presence of several post-separated zirconium complexes in the organic fraction, some of which were confirmed via EXAFS spectroscopy. As expected, $[Zr(NO_3)(TBP)_4]$ and $[ZrCl_4(TBP)_4]$ dominated speciation in the post-extracted organic phases for nitrate and hydrochloric acid systems, respectively. Speciation in the post-separated organic phase for mixed acid systems of equal chloride and nitrate, as shown by EXAFS, was dominated by $[ZrCl_4(TBP)_4]$, over the analogous nitrate complex. The presence of several phosphorus species in the post-separated organic fraction as shown by the ^{31}P NMR data were not confirmed through EXAFS. However the averaging techniques utilised by EXAFS modelling may explain the apparent

presence of one post-separated zirconium species. It must also be made apparent that the "complex" notations are not chemically sound, but merely represent the presence of the TBP species by, what is thought to be, hydrogen bonding of the phosphate oxygen atom with the metal centre.

4.6 Technetium Separated from Aqueous Nitric Acid

Technetium (Tc) exists predominantly as the pertechnetate ion, TcO_4^-, in solution which is highly mobile throughout the environment due to its anionic nature.[119] The pertechnetate ion is the most common form of Tc found in the nuclear fuel cycle and the most frequently encountered ^{99}Tc isotope has a long lived half life of 2.3×10^5 years, meaning it is a major contributor to the long term radioactivity of spent nuclear fuel. A trace level study was conducted to assess the effectiveness of technetium separation using aqueous nitric over a range of concentrations. The aqueous nitric acid range was chosen around the concentrations elected for current nuclear waste reprocessing conditions.

Aqueous nitric acid (6-10 M, 1.9 mL) was spiked with ^{99}Tc (287 Bq, 100 uL, 46 uM) and the resultant aqueous fraction (2.3 uM ^{99}Tc) contacted with TBP-OK (30 % TBP by volume), mechanically agitated and centrifuged for full phase separation. Both aqueous and organic fractions, post-separation were analysed using by LSC in order to determine the effectiveness of technetium separation under these conditions. An aliquot of both aqueous and organic phases was taken and scintillation fluid (ScintSafe3, 10 mL) added. These samples were analysed for 30 minutes each.

Table 12 details the technetium distribution ratio (D_{Tc}) data for samples N6.Tc - N10.Tc. The D_{Tc} decreases with an increase in the concentration of HNO_3. This is contrary to the previous systems detailed in this work, where generally metal extraction increases as a function of acid concentration. Those systems, however, revolve around metals in their cationic forms whereas technetium here, exists predominantly as an anionic species and therefore it is thought to have limited separation under typical reprocessing conditions. The D_{Tc} for sample N10.Tc correspond to ~ 2 % technetium separation in to the organic fraction. The D_{Tc} for sample N6.Tc was ~ 0.2 which corresponds to ~ 15 % technetium separation. Figure

34 illustrates the decrease in the distribution ratio for samples N6.Tc - N10.Tc as a function of aqueous nitric acid concentration.

These results are consistent with previous findings which suggest that the optimum aqueous HNO_3 concentration for the extraction of Tc, in the absence of any additional co-extractable metals, is 1 M.[99] Above initial aqueous nitric acid concentrations of 1 - 2 M, it is thought that separation of technetium is improbable, as the data presented here demonstrates.

Sample	N6.Tc	N6.5.Tc	N7.Tc	N7.5.Tc	N8.Tc	N8.5.Tc	N9.Tc	N9.5.Tc	N10.Tc
$[HNO_3]$ / M	6.00	6.50	7.00	7.50	8.00	8.50	9.00	9.50	10.00
Distribution Ratio D	0.18	0.12	0.09	0.08	0.06	0.06	0.05	0.04	0.02
Log D	-0.75	-0.91	-1.06	-1.12	-1.19	-1.19	-1.28	-1.38	-1.69

Table 12: Initial aqueous phase concentrations and distribution ratio data for samples N6.Tc - N10.Tc.

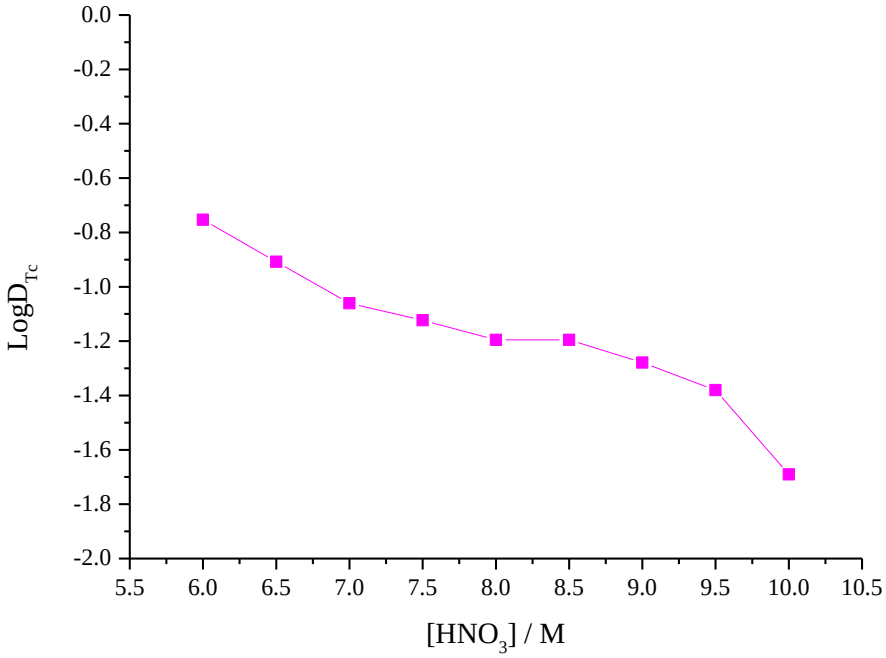

Figure 34: Distribution ratio data as a function of aqueous acid concentration for samples N6.Tc - N10.Tc.

4.7 Technetium Separated from Aqueous Nitric Acid in the Presence of Zirconium

The stability of the pertechnetate anion in nitric acid solutions usually means the extraction of Tc from aqueous fractions is minimal. However, it has been suggested that in the presence of co-extractable metals, the extraction of pertechnetate moiety from aqueous solutions is greatly increased.[99] The co-extraction of pertechnetate and zirconium has been studied as zirconium is present as a fission product in spent nuclear fuel. It is thought that under acidic PUREX type conditions, co-extraction occurs by the following mechanism:

$$Zr(IV) + 3NO_3^- + TcO_4^- + 2TBP \rightarrow [Zr(NO_3)_3(TcO_4)(TBP)_2]$$ [120]

The pertechnetate anion is co-extracted as TcO_4^- by coordination with Zr(IV). For this work, the distribution ratio of technetium was calculated over a range of aqueous nitric acid concentrations using zirconium as a co-extractable metal.

Technetium was separated from aqueous nitric acid (6-10 M, 2 mL total) containing zirconium, using TBP-OK (30 % TBP by volume). Samples N6.Tc.Zr - N10.Tc.Zr were spiked with Tc (^{99}Tc, 364 Bq, 100 uL, 58 uM) and Zr(IV) (100 uL, 0.023 M) and the resultant aqueous fraction (2.9 uM ^{99}Tc) contacted with TBP-OK as described in Section 4.6. Both aqueous and organic fractions, post-separation were analysed as described in Section 4.6. The data presented in Table 13 details the distribution ratio data for samples N6.Tc.Zr - N10.Tc.Zr as a function of aqueous nitric acid concentration; Figure 35 illustrates the trend in technetium separation as a function of increasing aqueous nitric acid concentration.

For these systems containing Zr, the amount of Tc extracted in to the organic phase increases as a function of increasing HNO_3 concentration, as Figure 35 illustrates. In analogous systems in the absence of Zr, the opposite trend is observed, the distribution of Tc decreases as a function of aqueous HNO_3 concentration. However, the amount of technetium separated overall is significantly lower in systems where there is no co-extraction than in systems containing Zr. For example, sample N6.Tc gave a D_{Tc} of 0.18, whereas the analogous system in the presence of the co-extractable metal, Zr (sample N6.Tc.Zr) gave a D_{Tc} of 1.63.

Thus providing evidence that the pertechnetate ion is coordinating to Zr^{4+} as part of an extractable complex, such as $[Zr(NO_3)_3(TcO_4)(TBP)_2]$. This work is consistent with the work of Garraway and Wilson, where it was reported that under PUREX style conditions (similar to this work), the distribution ratio of Tc increased in the presence of zirconium. However, their work reported pertechnetate distribution data for aqueous nitrate concentrations of up to 3 M only.[121]

Sample	N6. Tc.Zr	N6.5. Tc.Zr	N7. Tc.Zr	N7.5. Tc.Zr	N8. Tc.Zr	N8.5. Tc.Zr	N9. Tc.Zr	N9.5. Tc.Zr	N10. Tc.Zr
$[HNO_3]$ / M	6.00	6.50	7.00	7.50	8.00	8.50	9.00	9.50	10.00
Distribution Ratio D	1.63	1.70	1.86	2.33	2.57	2.57	2.70	2.85	3.35
Log D	0.21	0.23	0.26	0.39	0.41	0.41	0.43	0.45	0.52

Table 13: Initial aqueous phase concentration and distribution ratio data for samples N6.Tc.Zr - N10.Tc.Zr.

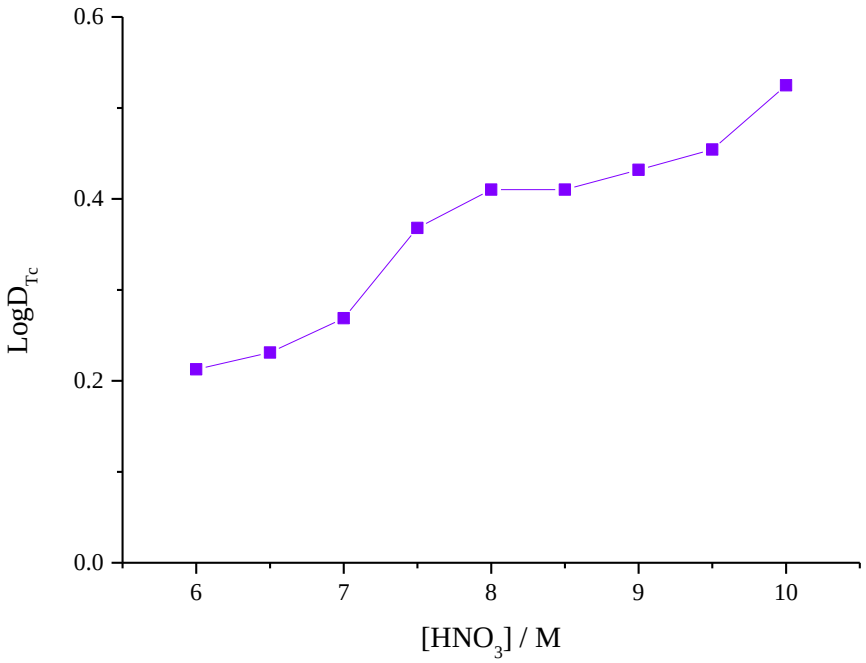

Figure 35: Distribution ratio data as a function of aqueous acid concentration for samples N6.Tc.Zr - N10.Tc.Zr.

4.8 Technetium Separated from Aqueous Nitric Acid in the Presence of Uranium

With the majority of SNF containing uranyl, it is necessary to investigate the propensity for the coextraction of pertechnetate with the uranyl moiety. The solvent extraction process in SNF reprocessing is done from aqueous nitric acid, in which uranyl is known to separate well.[122] Previously reported data suggests that at low HNO_3 concentration (< 0.7 M), and in the presence of uranium, the distribution ratio of technetium separated from aqueous nitric acid, increases with increasing aqueous nitrate concentration. Therefore the effectiveness of technetium separation is examined under these conditions. In solution, separation of technetium from aqueous nitric acid in the presence of uranium, occurs via the following mechanism:

$$UO_2^{2+} + TcO_4^- + NO_3^- + 2TBP \rightleftharpoons [UO_2(NO_3)(TcO_4)(TBP)_2] \quad ^{123}$$

Technetium was separated from aqueous nitric acid (6-10 M, 2 mL total) using TBP-OK (30 % TBP by volume). Samples N6.Tc.U - N10.Tc.U were spiked with Tc (^{99}Tc, 11.77 kBq, 100 uL, 1.88 mM) and U(VI) (100 uL, 0.17 M) and the resultant aqueous fraction (93.20 uM ^{99}Tc) contacted with TBP-OK, mechanically agitated and centrifuged for full phase separation. Both aqueous and organic fractions, post-separation were analysed using LSC as described in Section 4.6. The data presented in Table 14 details the distribution ratio data for samples N6.Tc.U - N10.Tc.U as a function of aqueous nitric acid concentration. Figure 36 illustrates the trend in technetium separation as a function of increasing aqueous nitric acid concentration.

The data presented in Table 14 shows that there is an increase in the distribution ratio for technetium as the aqueous nitric acid concentration is increased. The opposite of which is observed in samples N6.Tc - N10.Tc where there was no co-extractable metal present in the initial aqueous fraction. The distribution ratio for sample N6.Tc.U is 0.44 which is approximately double of the distribution ratio of 0.18 observed for sample N6.Tc. Comparatively, the data presented in Table 14 for samples N6.Tc.U - N10.Tc.U reiterates the implication that technetium separation is enhanced in the presence of uranium, where distribution ratios observed for the

separation of technetium in the presence of uranium were observed to be, sometimes an order of magnitude higher than those systems without co-extraction. The distribution ratio observed for sample N10.Tc.U is around 0.6 which corresponded to ~ 40 % technetium separation in to the organic fraction. Whereas the distribution ratio for sample N10.Tc was 0.02 which corresponded to an overall % separation of only 2 %. The coordination of technetium with uranium, which itself is known to readily occur, from aqueous nitric acid solutions which can then be extracted by TBP is the most likely reason for the relatively high Tc distribution ratios observed in these uranium containing systems resulting in technetium being a problematic species under reprocessing conditions.

Sample	N6. Tc.U	N6.5. Tc.U	N7. Tc.U	N7.5. Tc.U	N8. Tc.U	N8.5. Tc.U	N9. Tc.U	N9.5. Tc.U	N10. Tc.U
$[HNO_3]$ / M	6.00	6.50	7.00	7.50	8.00	8.50	9.00	9.50	10.00
Distribution Ratio D	0.44	0.46	0.48	0.48	0.50	0.53	0.53	0.55	0.60
Log D	-0.36	-0.34	-0.32	-0.32	-0.30	-0.27	-0.27	-0.26	-0.22

Table 14: Initial aqueous phase concentration and distribution ratio data for samples N6.Tc.U - N10.Tc.U.

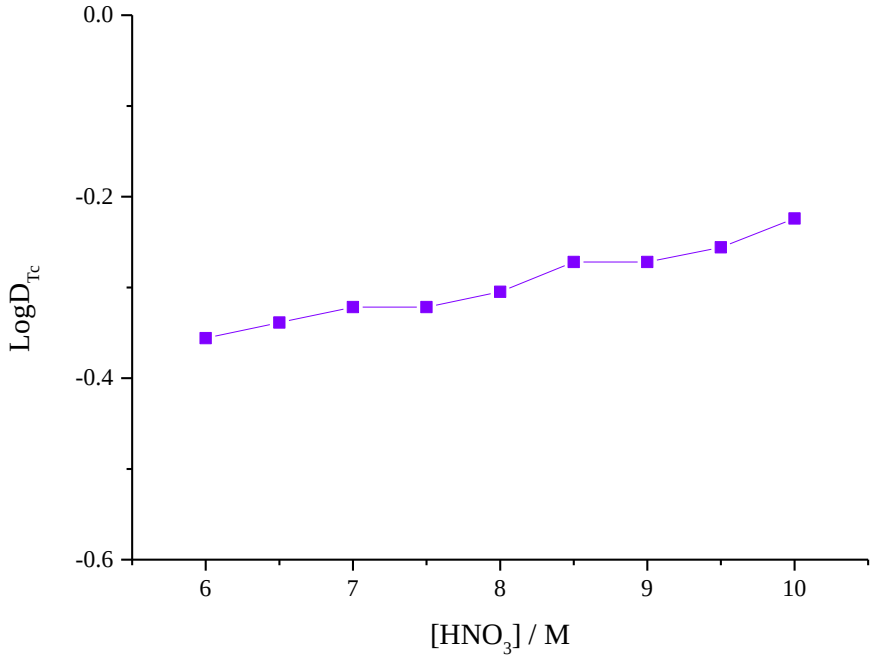

Figure 36: Distribution data as a function of acid concentration for samples N6.Tc.U - N10.Tc.U.

4.9 Technetium Separated from Aqueous Hydrochloric Acid

Previous literature has suggested that the separation of Tc from aqueous, chloride containing media is more effective that analogous nitrate containing systems.[124] It is thought that this preference for Tc separation in chloride containing media is due to the reduction of the TcO_4^- moiety to its cationic form, Tc(IV), with oxidation of the aqueous chloride.[125] Tc(IV) is more easily extracted than the TcO_4^- anion as it exists as a 4+ cation; the efficiency of TBP to extract 4+ metal cations has been previously demonstrated.[126] It has also been suggested that in relatively concentrated hydrochloric acid TcO_4^- reduces to $TcCl_6$, where the Tc exists in its 6+ state.[127]

Aqueous hydrochloric acid (6-10 M, 1.9 mL) was spiked with ^{99}Tc, extracted and analysed by the same methodology used for analogous ^{99}Tc studies from nitric acid aqueous solutions (Section 4.6). Above concentrations of 7 M aqueous HCl, a third phase was observed, as shown in red in Table 15. The volume of the third phase, when obtained, was immeasurable in terms of the desired accuracy and therefore the distribution ratios are calculated as a comparison of the resultant aqueous and overall

organic fractions. Whilst it is assumed from established data that the majority of the separated metal-extractant complex will be contained within the third phase, the methodologies used were not appropriate enough to determine with certainty the exact metal concentration in each of the split organic fractions.

The distribution ratio (D_{Tc}) data for the separation of technetium for samples C6.Tc - C10.Tc are presented in Table 15. For technetium separated from aqueous hydrochloric acid, it is clear that there is a significantly higher separation observed *c.f.* analogous aqueous nitric acid systems. The optimum conditions for the distribution ratio of technetium in samples C6.Tc - C10.Tc was observed for sample C10.Tc, giving a D_{Tc} of 32.30. This corresponds to ~ 97 % technetium separation into the organic fraction. The D_{Tc} calculated for the separation of Tc from the aqueous to the overall organic fraction, increased as a function of aqueous HCl concentration. The lowest D_{Tc} was observed for sample C6.Tc, as illustrated in Figure 37. The anionic nature of the pertechnetate moiety may contribute to the increased extraction at higher aqueous acid concentrations in much the same way as the mechanisms thought to be responsible for the extraction of water in to the organic (and subsequently the third) phase. Anionic species possess high mobility in aqueous media; this has lead to the belief that negatively charged species, such as Cl^- are extracted into the organic fraction via the formation of reverse micelles.

Sample	C6.Tc	C6.5.Tc	C7.Tc	C7.5.Tc	C8.Tc	C8.5.Tc	C9.Tc	C9.5.Tc	C10.Tc
[HCl] / M	6.00	6.50	7.00	7.50	8.00	8.50	9.00	9.50	10.00
Distribution Ratio D	3.76	4.26	4.88	5.25	5.67	6.14	9.00	19.00	32.30
Log D	0.58	0.63	0.69	0.72	0.75	0.79	0.95	1.28	1.51

Table 15: Initial aqueous phase concentrations and distribution ratio data for samples C6.Tc - C10.Tc.

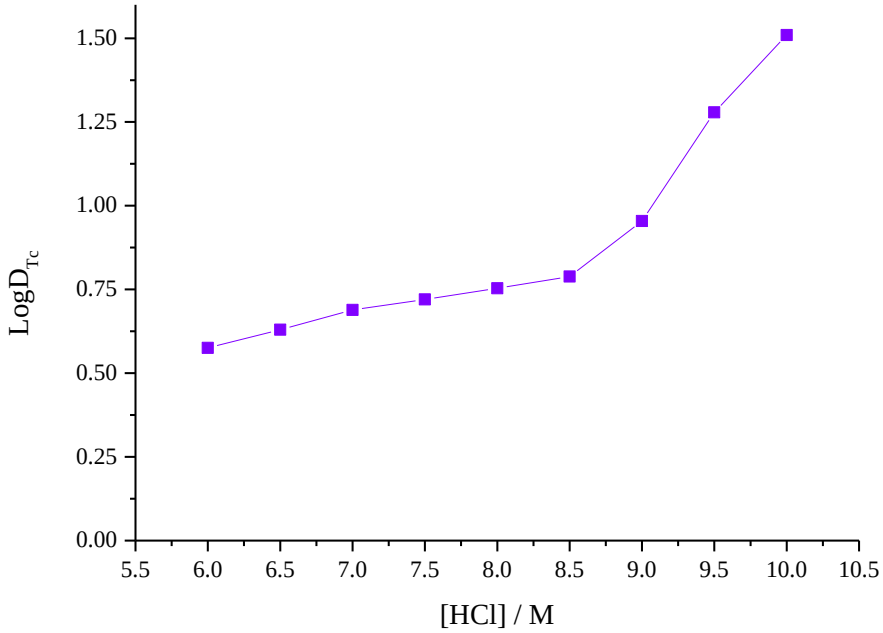

Figure 37: Distribution ratio data as a function of aqueous acid concentration for samples C6.Tc - C10.Tc.

4.10 Technetium Separated from Aqueous Hydrochloric Acid in the Presence of Zirconium

Technetium was separated from aqueous hydrochloric acid (6-10 M, 2 mL total) using TBP-OK (30 % TBP by volume). Samples C6.Tc.Zr - C10.Tc.Zr were spiked with ^{99}Tc and Zr(IV), contacted with TBP-OK and analysed as described in Section 4.6. Above concentrations of 7 M aqueous HCl, a third phase was observed, as shown in red in Table 16. The data presented in Table 16 details the distribution ratio data for samples C6.Tc.Zr - C10.Tc.Zr as a function of aqueous hydrochloric acid concentration. Figure 38 illustrates the trend in technetium separation as a function of increasing aqueous hydrochloric acid concentration. The volume of the third phase, when obtained, was immeasurable in terms of the desired accuracy so distribution ratio calculations and relevant assumptions were made as described in Section 4.6.

The data presented in Table 16 and Figure 38 shows an increase in the amount of technetium separated as a function of aqueous hydrochloric acid concentration.

Sample C10.Tc.Zr gave what was determined to be the optimum condition for the co-extraction of technetium with zirconium, under these conditions, with an overall distribution ratio of 4.56. The separation of technetium using the co-extractable metal zirconium, was most effective at higher aqueous hydrochloric acid concentrations, with sample C10.Tc.Zr corresponding to ~ 82 % separation of technetium in to the overall organic fraction.

Generally, the distribution ratios observed for technetium separated from aqueous hydrochloric acid in the absence of zirconium were higher over the range of aqueous HCl concentrations analysed relative to the equivalent zirconium containing systems. It is thought that the presence of chloride in the aqueous fraction effectively reduces the TcO_4^- anion into the Tc(IV) cation which is efficiently extracted by the TBP; the TBP moiety favours the separation of M(IV) species (where M is a metal). This reduction could inhibit the co-extraction route for the pertechnetate and subsequently, lower distribution ratios are observed than analogous systems in the absence of co-extraction. It is also possible that there is competitive coordination of both the Tc^{4+} (reduced from TcO_4^-) and the Zr^{4+} to the TBP moiety as the Zr^{4+} is in excess, thus reducing the overall distribution of Tc observed.

Sample	C6.Tc.Zr	C6.5Tc.Zr	C7.Tc.Zr	C7.5.Tc.Zr	C8.Tc.Zr	C8.5.Tc.Zr	C9.Tc.Zr	C9.5.Tc.Zr	C10.Tc.Zr
[HCl] / M	6.00	6.50	7.00	7.50	8.00	8.50	9.00	9.50	10.00
Distribut-ion Ratio D	0.92	1.08	1.33	1.38	1.44	1.63	2.33	3.00	4.56
Log D	-0.03	0.03	0.12	0.14	0.16	0.21	0.37	0.48	0.66

Table 16: Initial aqueous phase concentration and distribution ratio data for samples C6.Tc.Zr - C10.Tc.Zr.

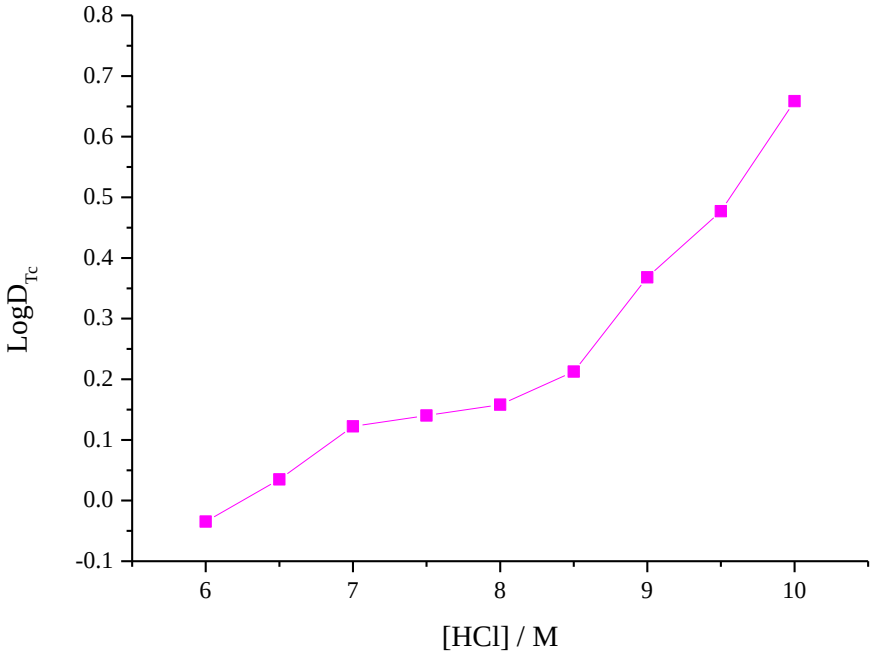

Figure 38: Distribution ratio as a function of acid concentration for samples N6.Tc.Zr - N10.Tc.Zr and C6.Tc.Zr - C10.Tc.Zr.

4.11 Technetium Separated from Aqueous Hydrochloric Acid in the Presence of Uranium

Technetium separations were performed and analysed as described in Section 4.6, but omitting aqueous nitric acid for aqueous hydrochloric acid (6 - 10 M). Above concentrations of 7 M aqueous HCl, a third phase was observed, as shown in red in Table 17. The volume of the third phase, when obtained, was immeasurable in terms of the desired accuracy, therefore the distribution ratio calculations and relevant assumptions were made as described in Section 4.6. The data presented in Table 17 details the distribution ratio data for samples C6.Tc.U - C10.Tc.U as a function of aqueous hydrochloric acid concentration. Figure 39 illustrates the trend in technetium separation as a function of increasing aqueous hydrochloric acid concentration.

The distribution ratio data presented in Table 17 shows that optimum separation of technetium is observed at 10 M aqueous hydrochloric acid. Figure 39 illustrates the trend in technetium separation in the presence of uranium, where an increase in

distribution ratio from 0.58 - 3.97 is observed over samples C6.Tc.U - C10.Tc.U, i.e. the distribution ratio increases as a function of aqueous hydrochloric acid concentration. The highest distribution ratio was observed for sample C10.Tc.U in these systems analysed which corresponded to around 80 % technetium separation in to the overall organic fraction.

Comparatively, the amount of technetium separated in the presence of uranium is lower over the whole concentration range analysed, than both technetium separated from pure HCl and technetium separated in the presence of zirconium. This could be due to the high distribution ratios observed for uranium separated from aqueous hydrochloric acid, implying there may be preferential complexation of the TBP with the uranium over the uranium-pertechnetate species. The presence of chloride may also inhibit the formation of an analogous extractable complex, such as $[UO_2(NO_3)(TcO_4)(TBP)_2]$, thought to aid pertechnetate separation in uranyl-nitrate systems.

Sample	C6. Tc.U	C6.5. Tc.U	C7. Tc.U	C7.5. Tc.U	C8. Tc.U	C8.5. Tc.U	C9. Tc.U	C9.5. Tc.U	C10. Tc.U
[HCl] / M	6.00	6.50	7.00	7.50	8.00	8.50	9.00	9.50	10.00
Distribution Ratio D	0.58	0.98	1.08	1.23	1.63	1.82	2.30	2.83	3.97
Log D	-0.07	-0.01	0.03	0.09	0.21	0.26	0.36	0.45	0.60

Table 17: Initial aqueous phase concentration and distribution ratio data for samples C6.Tc.U - C10.Tc.U.

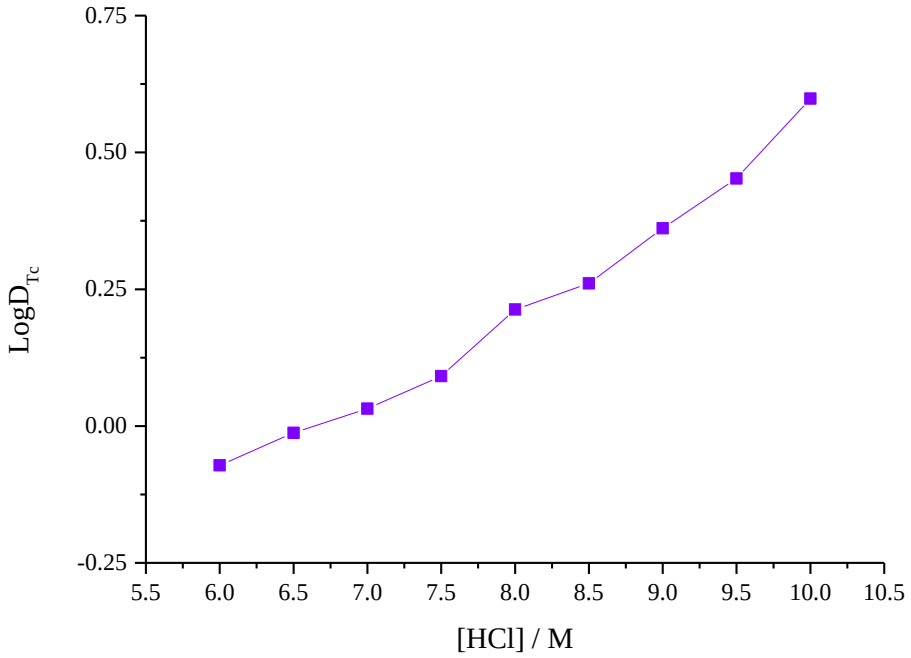

Figure 39: Distribution data as a function of acid concentration for samples C6.Tc.U - C10.Tc.U.

4.12 Technetium Separated from Aqueous Nitric and Hydrochloric Acid

Technetium was separated from aqueous mixtures of nitric and hydrochloric acid (1-9 and 9-1 M, respectively, 2 mL total) using TBP-OK (30 % TBP by volume). Samples C9:N1.Tc - C1:N9.Tc were spiked with ^{99}Tc (^{99}Tc, 287 Bq, 100 uL, 46 uM) and the resultant aqueous fraction (2.3 uM ^{99}Tc) contacted with TBP-OK, using the same procedures as described in Section 4.6. Both aqueous and organic fractions, post-separation were analysed as described in Section 4.6. No third phases were observed in these samples.

The data presented in Table 18 indicates that a higher distribution of technetium was observed in samples containing a higher aqueous chloride concentration. Sample C1:N9.Tc showed a D_{Tc} of 0.25 which corresponds to ~ 20 % technetium separation in to the organic fraction. Sample C9:N1.Tc gave a D_{Tc} of around 6.14 where ~ 86 % technetium separation was observed. These distribution ratios are slightly lower overall than those observed for the pure HCl system. Conversely, the distribution

ratios are higher than those observed for pure HNO_3 systems, implying that the mixed acid aspect gives better distribution ratios overall. However, although the distribution of technetium is improved by the mixed acid aspect *c.f.* pure HNO_3 systems, the pure HCl systems gave significantly better distribution ratios overall than any other system analysed. Figure 40 shows a clear relationship between the distribution ratio of technetium and the concentration of aqueous chloride present. This preference of technetium separation in the presence of chloride is due to the reduction of the TcO_4^- moiety to its cationic form, Tc(IV), which is easily extracted by TBP.[128]

The separation of Tc into the organic fraction is usually undesired in SNF reprocessing. However, if aspirations for the separation of Tc became apparent, then separation using a mixed HCl/ HNO_3 aqueous fraction could be considered.

Sample	C9:N1. Tc	C8:N2. Tc	C7:N3. Tc	C6:N4. Tc	C5:N5. Tc	C4:N6. Tc	C3:N7. Tc	C2:N8. Tc	C1:N9. Tc
$[H^+]$ / M	10.00	10.00	10.00	10.00	10.00	10.00	10.00	10.00	10.00
$[Cl^-]$ / M	9.0	8.0	7.0	6.0	5.0	4.0	3.0	2.0	1.0
$[NO_3^-]$ / M	1.0	2.0	3.0	4.0	5.0	6.0	7.0	8.0	9.0
Distribution Ratio D	6.14	3.00	1.38	1.04	0.72	0.70	0.54	0.39	0.25
Log D	0.79	0.48	0.14	0.02	-0.14	-0.16	-0.27	-0.41	-0.60

Table 18: Initial aqueous phase concentrations and distribution ratio data for samples C1:N9.Tc - C9:N1.Tc.

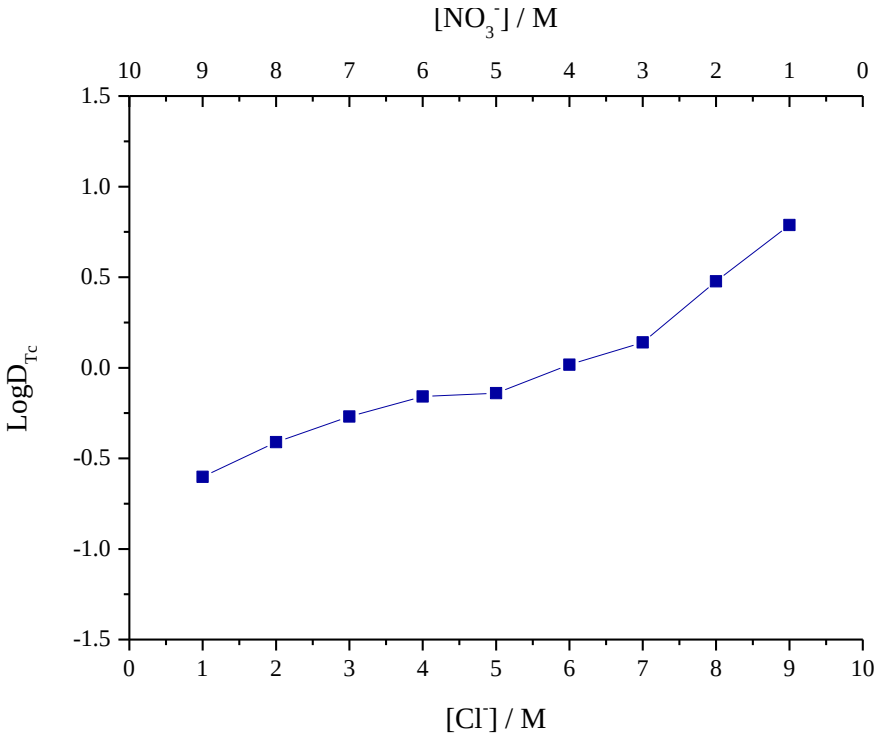

Figure 40: Distribution ratio data as a function of aqueous acid concentration for samples C1:N9.Tc - C9:N1.Tc.

4.13 Technetium Separated from Aqueous Nitric and Hydrochloric Acid in the Presence of Zirconium

Technetium was separated from aqueous mixtures of nitric and hydrochloric acid (1-9 and 9-1 M, respectively, 2 mL total) using TBP-OK (30 % TBP by volume). Samples C9:N1.Tc.Zr - C1:N9.Tc.Zr were spiked with Tc (^{99}Tc, 364 Bq, 100 uL, 58 uM) and Zr(IV) (100 uL, 0.023 M) and the resultant aqueous fraction (2.9 uM ^{99}Tc) contacted with TBP-OK, as previously described in Section 4.6. Both aqueous and organic fractions, post-separation were analysed as detailed in Section 4.6. No third phases were observed in these samples.

The data presented in Table 19 outlines the distribution ratios obtained for technetium as a function of aqueous acid concentration, for samples C1:N9.Tc.Zr to C9:N1.Tc.Zr. The distribution ratio of technetium is seen to increase from 0.22 to 3.55 for samples C1:N9.Tc.Zr and C9:N1.Tc.Zr, respectively, therefore indicating the separation of technetium is enhanced by the presence of aqueous chloride. Figure

41 illustrates the relationship between the D_{Tc} and the initial aqueous phase acid concentration.

Comparatively, analogous systems in the absence of the co-extractable metal zirconium for all acid combinations and concentrations, give higher distribution ratios for technetium separation overall. This implies that reduction of the TcO_4^- to Tc^{4+} is a dominating factor in the amount of technetium sequestered into the overall organic fraction, rather than co-extraction factors.

Sample	C1:N9. Tc.Zr	C2:N8. Tc.Zr	C3:N7. Tc.Zr	C4:N6. Tc.Zr	C5:N5. Tc.Zr	C6:N4. Tc.Zr	C7:N3. Tc.Zr	C8:N2. Tc.Zr	C9:N1. Tc.Zr
$[H^+]$ / M	10.00	10.00	10.00	10.00	10.00	10.00	10.00	10.00	10.00
$[Cl^-]$ / M	1.00	2.00	3.00	4.0	5.0	6.00	7.0	8.00	9.0
$[NO_3^-]$ / M	9.00	8.00	7.00	6.00	5.00	4.00	3.00	2.00	1.00
Distribution Ratio D	0.22	0.33	0.47	0.61	0.82	1.38	1.78	2.57	3.55
Log D	-0.66	-0.48	-0.33	-0.21	-0.09	0.14	0.25	0.41	0.55

Table 19: Initial aqueous phase concentrations, and distribution ratio data for samples C1.N9.Tc.Zr - C9.N1.Tc.Zr.

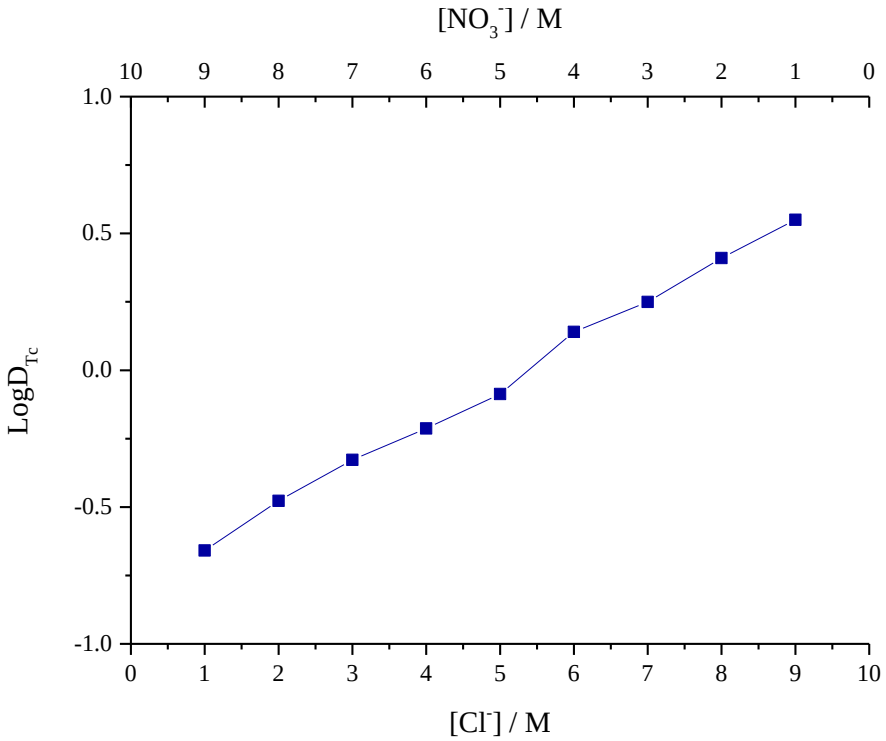

Figure 41: Distribution data as a function of acid concentration for samples C1:N9.Tc.Zr - C9:N1.Tc.Zr.

4.14 Technetium Separated from Aqueous Nitric and Hydrochloric Acid in the Presence of Uranium

Technetium was separated from aqueous mixtures of nitric and hydrochloric acid (1-9 and 9-1 M, respectively, 2 mL total) using TBP-OK (30 % TBP by volume). Samples C9:N1.Tc.U - C1:N9.Tc.U were spiked with Tc (^{99}Tc, 364 Bq, 100 uL, 58 uM) and U(VI) (100 uL, 0.17 M) and the resultant aqueous fraction (2.9 uM ^{99}Tc) contacted with TBP-OK, as described previously in Section 4.6. Both aqueous and organic fractions, post-separation were analysed as detailed in Section 4.6. No third phases were observed in these samples.

The data presented in Table 20 and Figure 42 shows the distribution ratios for samples C9:N1.Tc.U - C1:N9.Tc.U over the mixed aqueous acid concentrations analysed. As previously observed in these mixed acid aqueous samples in the absence of a co-extractable metal and in the presence of the co-extractable metal zirconium, the technetium separation using the co-extractable metal uranium,

increases as a function of increasing aqueous chloride concentration. Sample C9:N1.Tc.U gave a distribution ratio of 3.25 which corresponds to ~ 75 % technetium separation in to the organic fraction. Conversely, sample C1.N9.Tc.U gave a distribution ratio of 0.10 which corresponds to ~ 10 % technetium separation. The preference of technetium separation from aqueous hydrochloric acid media is thought to be due to the reduction of the heptavalent technetium to Tc(IV), which is easily extracted using TBP. Further, the distribution ratio data obtained for samples C9:N1.Tc - C1:N9.Tc and C9:N1.Tc.Zr - C1:N9.Tc.Zr demonstrated a higher separation of technetium overall, than that obtained for samples C1:N9.Tc.U - C9:N1.Tc.U. This suggests that separation of technetium from mixed acid aqueous fractions in the presence of uranium is inhibited *c.f.* in the absence of a co-extractable metal and in the presence of zirconium.

Sample	C1:N9.Tc.U	C2:N8.Tc.U	C3:N7.Tc.U	C4:N6.Tc.U	C5:N5.Tc.U	C6:N4.Tc.U	C7:N3.Tc.U	C8:N2.Tc.U	C9:N1.Tc.U
$[H^+]$ / M	10.00	10.00	10.00	10.00	10.00	10.00	10.00	10.00	10.00
$[Cl^-]$ / M	1.00	2.00	3.00	4.00	5.00	6.00	7.00	8.00	9.00
$[NO_3^-]$ / M	9.00	8.00	7.00	6.00	5.00	4.00	3.00	2.00	1.00
Distribution Ratio D	0.10	0.19	0.37	0.60	1.23	1.58	2.21	2.60	3.25
Log D	-1.00	-0.72	-0.43	-0.22	0.09	0.20	0.34	0.41	0.52

Table 20: Initial aqueous phase concentrations and distribution ratio data for samples C1:N9.Tc.U - C9:N1.Tc.U.

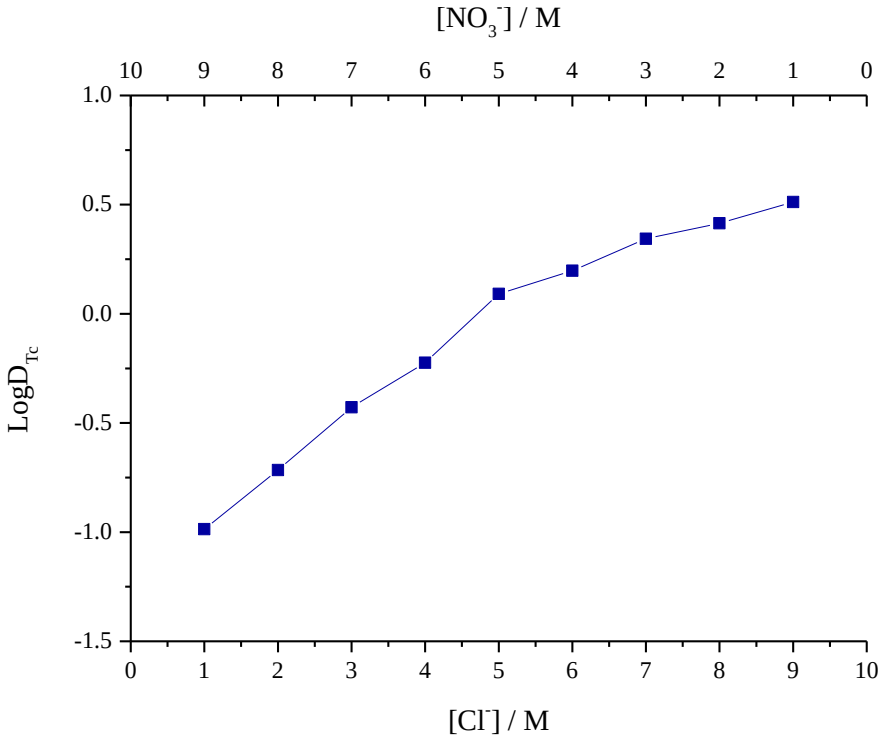

Figure 42: Distribution data as a function of acid concentration for samples C1:N9.Tc.U - C9:N1.Tc.U.

4.15 Summary of Technetium Extraction Behaviour in Modified PUREX Systems

Overall, technetium separated from aqueous nitric acid was enhanced in the presence of co-extractable metals, especially in the presence of zirconium. The distribution ratios observed for technetium separated from aqueous hydrochloric acid were significantly higher than those observed for analogous nitrate containing systems. The presence of co-extractable metals did not enhance the separation of technetium from HCl. A higher separation was observed in HCl containing systems at higher aqueous acid concentrations. For mixed chloride and nitrate systems, increasing distribution ratios were observed with ascending aqueous chloride concentrations.

5 Modified PUREX Systems Relevant to Actinide Separation

5.1 Uranium Separated from Aqueous Nitric Acid

Much work over the last 50 years has focussed on the separation of uranium from nitric acid using TBP, so this work was not intended to compete with previous data, but was simply used as a direct point of comparison for additional studies. It was also helpful to develop methodologies and compare data to ensure good laboratory practice.

Uranyl nitrate [$(UO_2(NO_3)_2$].$6H_2O$ (0.04 M) was used as received and dissolved over a range of aqueous nitric acid concentrations (2-16 M) and the resultant aqueous phases contacted with TBP-OK (30 % TBP by volume), mechanically agitated for approx. 10 minutes and centrifuged for full phase separation. The nitrated uranium species was used at it retained anionic consistency with the aqueous nitric acid. The organic phases were analysed by proton decoupled ^{31}P NMR spectroscopy. Distribution ratios were calculated with data received from ICP-OES analysis from aliquots of the resultant aqueous and organic phases which were treated as described for similar analyses in Section 4.2.

Distribution ratio (D_U) data for separated uranium is presented in Table 21. The data shows that an initial aqueous HNO_3 concentration of 16 M gives a D_U of ~ 100. This equates to almost 100 % uranium separation. The D_U increases as a function of aqueous nitrate concentration. Uranium separated from aqueous nitric acid using TBP gave high distribution ratios across the whole aqueous nitric acid concentration range analysed. The distribution ratios as a function of aqueous nitric acid concentration are pictorially represented in Figure 43. Previous data has suggested that U(VI) separated from aqueous nitric acid using 1.1 M TBP in dodecane gave distribution ratios of ~ 20 at 8 M aqueous nitric acid.[129] This is lower than the value calculated here where a distribution ratio of ~ 50 was observed for U(VI) separated from 8 M aqueous nitric acid. Dietz *et al.* showed that the distribution ratio of U(VI) using 1.1 M TBP in dodecane at 10 M was ~ 40.[130] Further, Todd *et al.* have reported several uranium distribution ratios for these systems over nitric acid concentrations

of between 0 and 7 M aqueous nitric acid. Their studies suggest very similar data to those presented in Table 21; around 2, 4 and 6 M aqueous nitric acid concentration, the distribution ratios were calculated to be 20, 40 and 50, respectively.[131]

Sample	N2.U	N4.U	N6.U	N8.U	N10.U	N12.U	N14.U	N16.U
$[HNO_3]$ / M	2.00	4.00	6.00	8.00	10.00	12.00	14.00	16.00
Distribution Ratio (D)	19.00	24.00	32.33	49.00	49.00	49.00	99.00	99.00
Log D	1.28	1.38	1.51	1.69	1.69	1.69	1.99	1.99

Table 21: Initial aqueous phase composition and distribution ratios for samples N2.U - N16.U.

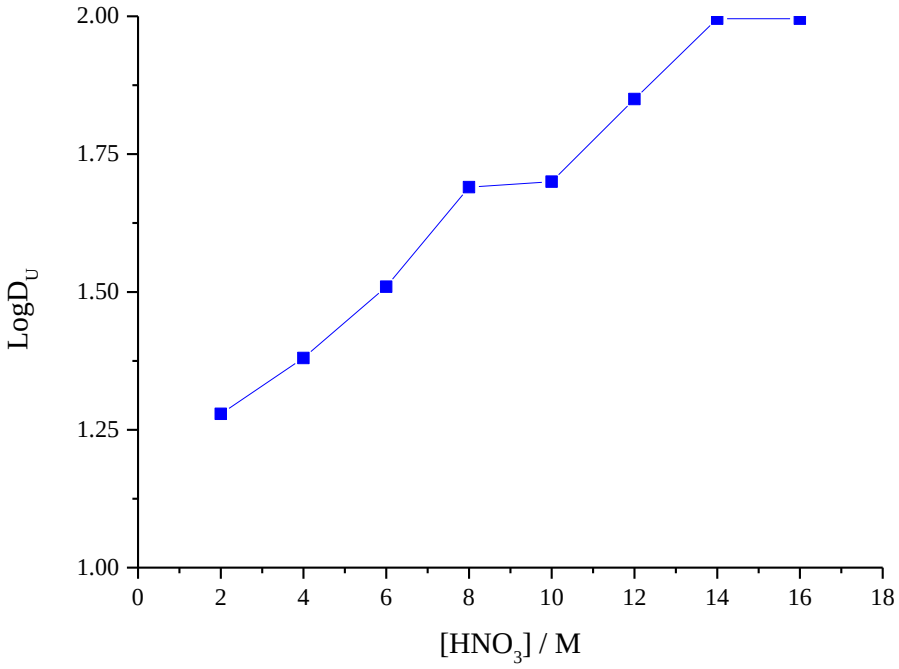

Figure 43: Distribution data as a function of acid concentration for samples N2.U - N12.U.

The ^{31}P NMR spectra recorded at - 50 ^{o}C of the organic phase post extraction for the samples detailed in Table 21 are presented in Figure 44. There is a small shift in the resonance corresponding to the HNO_3-TBP adduct at around -1.6 ppm, observed in the identical, metal free systems. The sharp signal observed at 1.5 ppm is thought to be the result of uranyl complexation with the TBP moiety, most likely $[UO_2(NO_3)_2(TBP)_2]$. For higher aqueous nitric acid samples, N12.U - N16.U, there is a further signal observed at 2 ppm. This could indicate the formation of a more nitrated species, such as $[UO_2(NO_3)_3.TBP]^{-1}$. Further analysis using EXAFS spectroscopy, for example, may indicate any alternative speciation at high acidities.

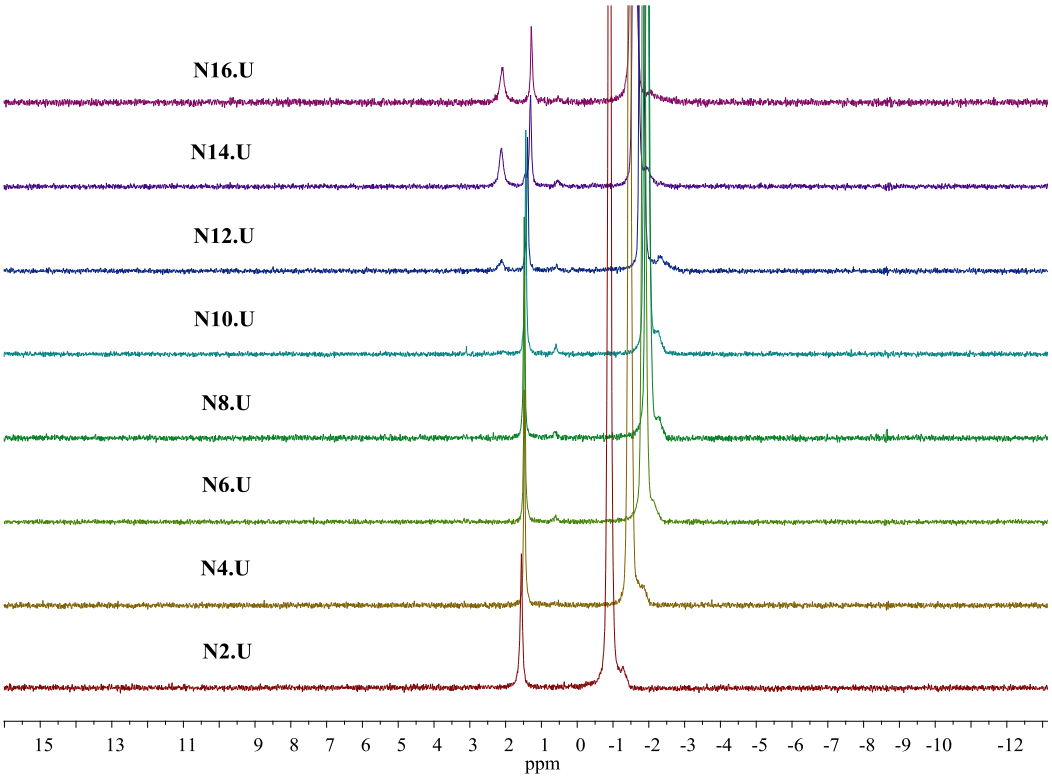

Figure 44: ^{31}P NMR spectra of the post extracted organic phase for samples N2.U - N16.U at -50 ^{o}C.

Extended X-ray Absorption Fine Structure (EXAFS) spectra were collected at the DIAMOND light source, Oxford, for the organic phase post extraction for sample N8.U. The fitted R-space and k^3-space spectra and numerical parameters are detailed in Figure 45 and Table 22, respectively. The fit is in good agreement with the $[UO_2(NO_3)_2(TBP)_2]$ species that is commonly considered the dominant organic phase species in PUREX systems.[132] This is a best fit analysis, however. The fit is modelled using 2 nitrate groups with the oxygen and phosphorus of the phosphate group. Both nitrate group oxygen and phosphate group oxygen atoms are within the primary coordination shell with the phosphorus of the phosphate group held in the secondary is the nitrogen of the nitrate group. This confirms that the signal observed in the corresponding ^{31}P NMR spectra at 2 ppm is due the phosphorous environment in $[UO_2(NO_3)_2(TBP)_2]$.

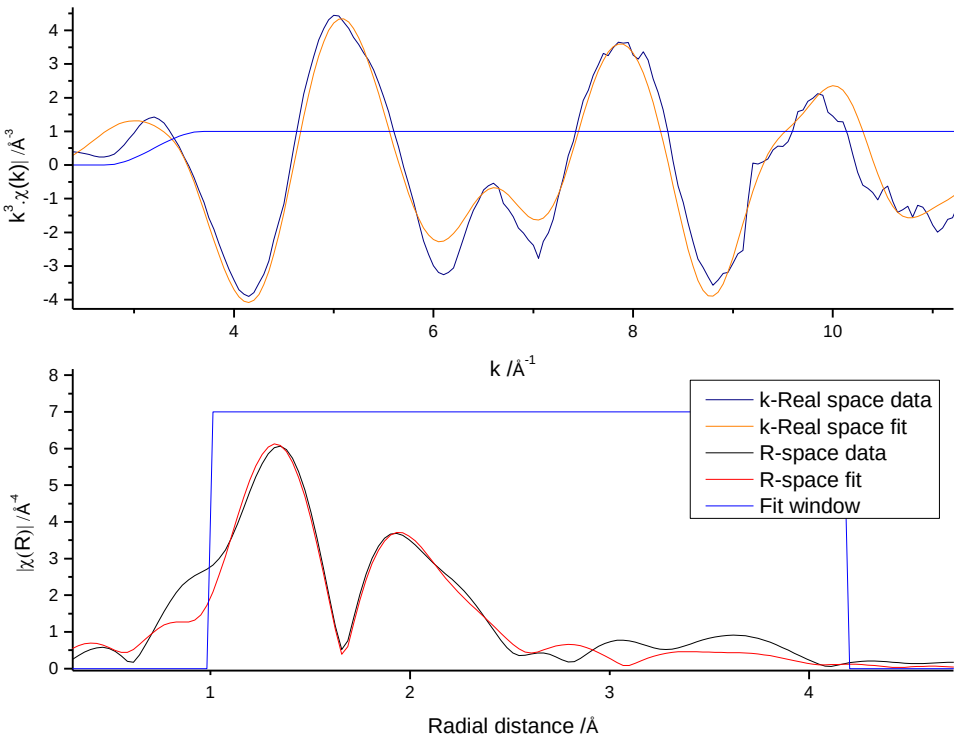

Figure 45: k^3-weighted χ(k)-function (top) and Fourier transform (bottom) of U L_{III} edge EXAFS data for $(UO_2)^{2+}$ extracted into 30 % TBP-OK from 8 M HNO_3 aqueous solution. The data are fitted to $[UO_2(NO_3)_2(TBP)_2]$.

Sample	Shell	Occupancy	σ^2	E_0 (eV)	R_i (Å)	R_f (Å)	ΔR (Å)
$(UO_2)^{2+}$ extracted into 30 % TBP-OK from 8 M HNO_3, fitted to $[UO_2(NO_3)_2(TBP)_2]$ Amp = 0.968 R factor = 0.019 χ^2 = 1267.67	Oyl	2	0.03331		1.9980	1.7525	0.2455
	N (nit)	2	0.00436		2.4572	2.5254	-0.0681
	O (nit)	4	0.00111	7.227	2.9460	2.9684	-0.0224
	N/O (MS)	8	0.00221		4.1401	4.1849	-0.0448
	O(phos)	2	0.00273		1.7675	1.7571	0.0104

Table 22: Parameters obtained from EXAFS fits in k^3-space for $(UO_2)^{2+}$ extracted into TBP-OK (30 % TBP by volume) from 8 M aqueous HNO_3. E_0 is the relative shift in ionization energy, Ri is the initial distance of the shell (Å) and R_f is the refined distance of the shell (Å). Statistics of fit (χ^2 and r-factor) and amplitude factor (Amp) provided.

5.2 Uranium Separated from Aqueous Hydrochloric Acid

Uranyl chloride $[UO_2Cl_2.xH_2O]$ (0.06 M) was synthesised in house by dissolution of UO_3 (10 g) into aqueous hydrochloric acid (HCl) (40 mL). It was assumed that all of the UO_3 was converted into $[UO_2Cl_2.xH_2O]$. UO_2Cl_2 (0.06 M) was subsequently dissolved over a range of HCl concentrations, samples C2.U - C12.U. Each resultant aqueous phase was contacted with TBP-OK (30 % TBP by volume), mechanically agitated for approx.10 minutes and centrifuged for full phase separation. The organic fraction post separation was analysed using proton decoupled ^{31}P NMR spectroscopy. Distribution ratio data was obtained through ICP-OES analysis. Solution preparations for ICP-OES analysis are described in Section 4.2 but using HCl for back extraction rather than HNO_3. The volume of the third phase, when obtained, was again immeasurable in terms of the desired accuracy and therefore the

distribution ratios calculations and relevant assumptions were undertaken as previously described in Section 4.2.

Distribution ratio (D_U) data for separated uranium is presented in Table 23, as well as initial aqueous HCl concentrations. The D_U increases as a function of aqueous HCl concentration. The data shows that an initial aqueous chloride concentration of 12 M gives a D_U of ~ 100. This equates to almost 100 % uranium separation. The D_U for sample C2.U is 0.35 which equates to a 25 % separation of uranium. Between samples C2.U and C6.U, there is a large increase in the D_U observed, reaching almost 100 % separation of uranium at aqueous HCl concentrations of 6 M. Above 8 M aqueous HCl concentration, a third phase was observed throughout the overall organic layer. Samples in which a third phase was observed are shown in red in Table 27. Figure 46 is a pictorial representation of the distribution ratios for samples C2.U - C12.U. Previous literature has suggested an increase in D_U with increasing aqueous HCl concentration up to a maximum D_U of 100 at ~ 8 M aqueous HCl. The D_U then decrease by an order of magnitude to ~ 10 at 13 M aqueous HCl.[133] This data was however, recorded using a pure TBP organic fraction without diluent.

Another study offered similar results, where a maximum D_U of 70 was observed at ~ 8 M aqueous HCl concentration. The D_U was then seem to decrease to ~ 50 at 12 M aqueous HCl concentration.[134] This previous study however, was carried out using benzene or carbon tetrachloride as diluents.

Sample	C2.U	C4.U	C6.U	C8.U	C10.U	C12.U
[HCl] / M	2.00	4.00	6.00	8.00	10.00	12.00
Distribution Ratio (D)	0.35	4.26	24.00	32.33	49.00	99.00
Log D	-0.45	0.63	1.38	1.51	1.69	1.99

Table 23: Initial aqueous phase concentrations and distribution ratios for samples C2.U - C12.U.

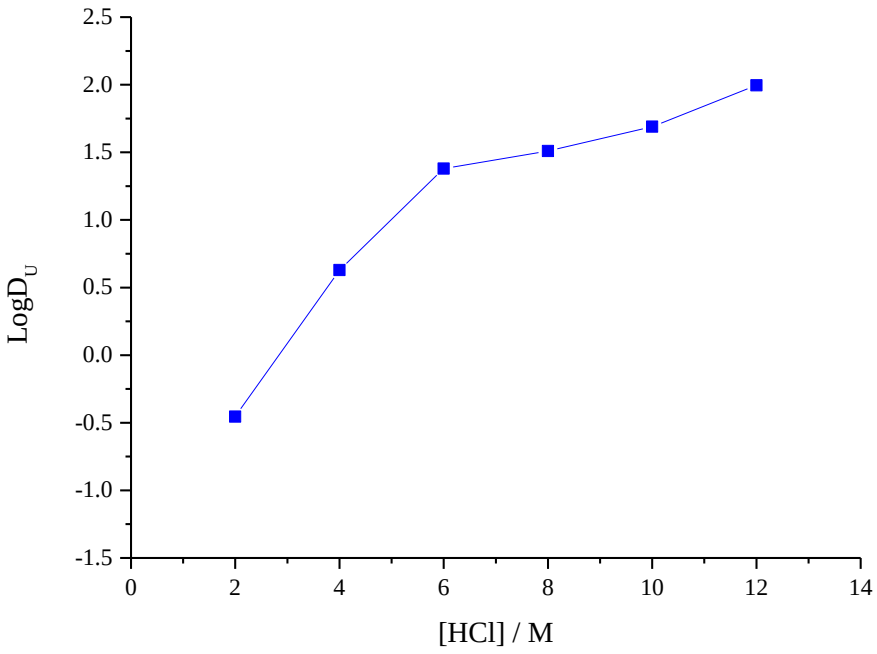

Figure 46: Distribution data as a function of acid concentration for samples C2.U - C12.U.

^{31}P NMR data of the post extracted organic phases were collected at -50 ^{o}C, as detailed in Figure 47. Conditions below room temperature were necessary to observe resolved signals within the NMR spectra for these samples, as ligand exchange processes did not allow acceptable signals to be observed at room temperature. There is one phosphorus signal seen at ~ 0 ppm which is not observed to deviate over the

aqueous HCl concentration range analysed. This trend is much the same as TBP contacted with HCl in the absence of any metal species. The lack of any signal that could be assigned to a U-TBP type complex in the organic phase NMR for samples C8.U - C12.U, could in part be due to the complexed metal species being predominantly retained in the third phase rather than the (light) organic phase. The high distribution values observed for samples C6.U - C12.U would corroborate this conclusion, as enough uranyl is separated to give a U-TBP type complexation signal. However, for samples in which a third phase was not observed visually, the lack of any observed complexation signal in the NMR spectra is not explained by third phase formation. It is possible though that third phase has formed but with such a low volume that it cannot be detected by the naked eye. The majority of the complexed uranyl may still be retained within the small volume of third phase present leaving only a small amount uranyl in the light organic fraction, and is not of a significant quantity for NMR detection with the parameters used.

The subsequent ^{31}P NMR spectra for the analysed third phases at - 50 ^{o}C, presented in Figure 48, show an additional phosphorus environment in solution in addition to what is thought to be the phosphorus signal due to the HCl-TBP adduct, seen at ~ -2 ppm. No resonance signals were observed at RT or several subsequent lower temperatures; at - 50 ^{o}C, a resonance signal was observed. This could imply that ligand exchange was too fast to observe a signal. The complexed species is thought to be $[UO_2Cl_2(TBP)_2]$. However, to confirm this species dominates the organic fraction, further analysis is required, such a solution state EXAFS spectroscopy. Although here, third phase samples were analysed via NMR, it was not possible to define an exact volume in which to calculate separate distribution ratios. Here, only 200 uL of each phase was needed, and therefore NMR analysis was possible. Exact separation of the phases was also challenging and could not be done with precise enough accuracy to report, with the equipment used.

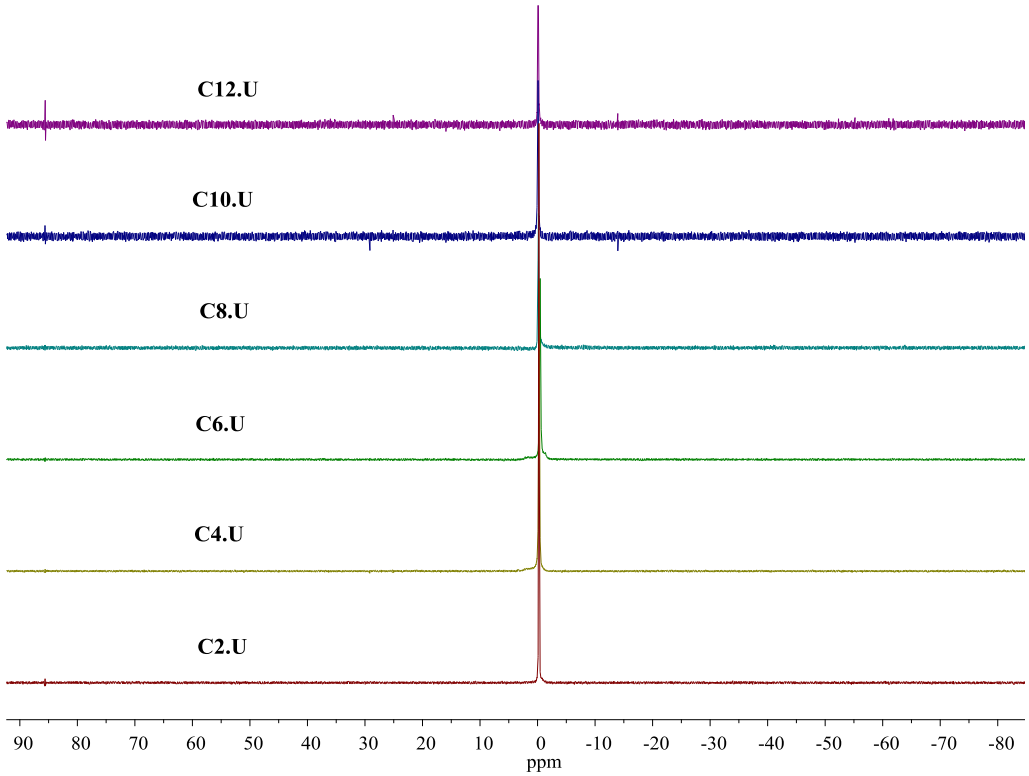

Figure 47: ^{31}P NMR spectra of the post extracted (light) organic phase for samples C2.U - C12.U at - 50 ^{o}C.

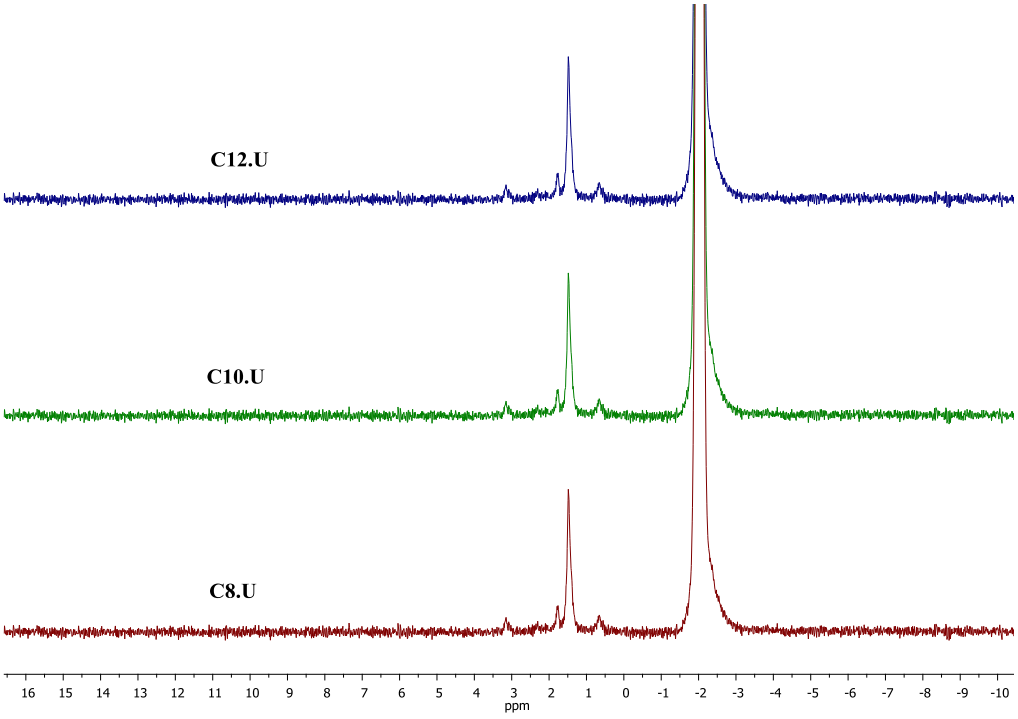

Figure 48: ^{31}P NMR spectra of the post extracted third phase for samples C2.U - C12.U at - 50 ^{o}C.

Extended X-ray Absorption Fine Structure (EXAFS) spectra were collected for the sample C5.U, using the ANKA beam line, Karlsruhe, Germany. Uranyl chloride was synthesised from uranyl nitrate at the INE site. The resultant uranyl chloride (1.72 mM) solid was dissolved in to 5 M HCl (0.5 mL) and the resultant aqueous phase contacted with TBP-OK (30 % TBP by volume). A lower initial aqueous phase HCl concentration was used here to avoid third phase formation and hence acquire a more realistic view of the speciation within the organic fraction. With more time, a separate third phase sample would also have been analysed.

EXAFS of the organic fraction is best fit to the complex $[UO_2Cl_2(TBP)_4]$. The data presented in Table 24 details the numerical fit parameters for the $[UO_2Cl_2(TBP)_4]$ species. This is a best fit analysis, however. All parameters are within the bounds of an excellent fit. Although this complex is not thought to be the most likely to be found in the organic fraction post separation, that being $[UO_2Cl_2(TBP)_2]$, it remains a charge neutral species. Although the coordination number of the fitted complex is high for typical uranyl complexes, but it is still feasible to have six coordination sites about the uranyl equatorial plane.

The R-space and k^3-space spectra are presented in Figure 49 and show the fit modelled on previously defined crystal structures.

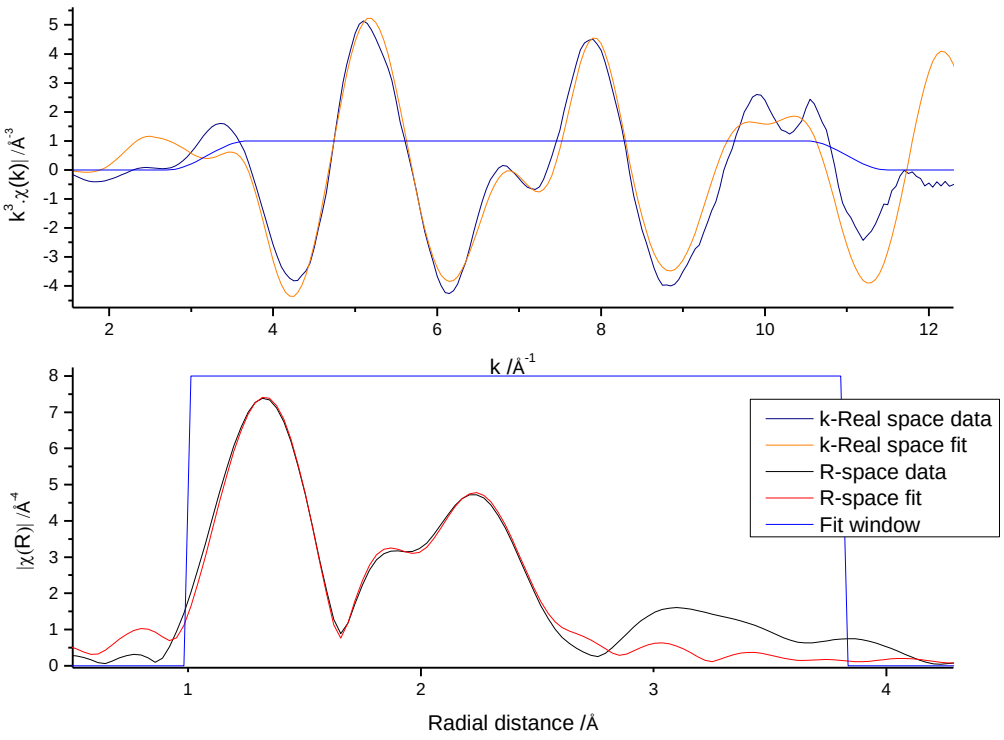

Figure 49: k^3-weighted $\chi(k)$-function (top) and Fourier transform (bottom) of U L_{III}-edge EXAFS data for $(UO_2)^{2+}$ species within an organic phase of 30 % TBP-OK post extraction, from an initial aqueous phase of 5 M HCl. The data are fitted to $[UO_2Cl_2(TBP)_4]$.

Sample	Shell	Occupancy	σ^2	E_0 (eV)	R_i (Å)	R_f (Å)	ΔR (Å)
$(UO_2)^{2+}$ extracted into 30 % TBP-OK from 5 M HCl, fitted to $[UO_2Cl_2(TBP)_4]$ Amp = 0.814 R factor = 0.020 χ^2 = 35.71	Oyl	2.00	0.00103		1.7708	1.7868	-0.0159
	Cl	2.00	0.00208		2.6970	2.7006	-0.0036
	Oyl (MS)	2.00	0.00207	9.939	3.5279	3.5733	-0.0454
	O(phos)	4.00	0.01139		2.3965	2.3719	0.0248
	P(phos)	4.00	0.00929		3.5623	3.8157	-0.2534

Table 24: Parameters obtained from EXAFS fits in k^3-space for $(UO_2)^{2+}$ extracted into TBP-OK (30 % TBP by volume) from an initial aqueous phases composition of 5 M HCl. E_0 is the relative shift in ionization energy, Ri is the initial distance of the shell (Å) and R_f is the refined distance of the shell (Å). Statistics of fit (χ^2 and r-factor) and amplitude factor (Amp) provided.

5.3 Uranium Separated from Mixed Aqueous Nitric and Hydrochloric Acid

Solutions with various concentrations of aqueous uranyl nitrate and aqueous uranyl chloride mixed solutions were used (1 - 9 M chloride and 9 - 1 M nitrate, respectively; samples C1:N9.U - C9:N1.U) where the overall concentration of uranium in each solution was 0.086 M throughout. The resultant uranium containing aqueous phases were contacted with TBP-OK (30 % by volume) as described previously in Section 4.2. The organic phase was directly analysed via proton decoupled ^{31}P NMR spectroscopy. Distribution ratios (Table 25) were calculated using data obtained from ICP-OES of the individual phases using the sample sampling procedure as described in Section 4.2. Third phases were not observed in any of these samples.

The data presented in Table 25 and Figure 50 shows an increase in the uranium separation as a function of increasing aqueous nitrate concentration. Sample C1:N9.U gives the highest D_U of 49.00 assumingly as it contains the highest aqueous concentration of nitrate. The D_U decreases to a minimum of 5.66 for sample C5:N5.U which has an equal aqueous concentration of both nitrate and chloride. Sample C9:N1.U, which contains the highest concentration of chloride gave a D_U of 24.00. It is clear that the D_U is improved in the presence of nitrate. It can be said that there is evidence for improved separation of uranium at higher aqueous acid concentrations, but a more significant improvement is observed with regard to higher aqueous nitrate concentrations. Overall however, the distribution ratios associated with uranyl separation from mixed acid aqueous phases does not enhance separation. Higher distribution ratios are observed in general in the corresponding individual acid systems *c.f.* the distribution ratios outlined in Table 25. It is feasible that the competing anionic presence of multiple anion types in solution is inhibiting the effective separation of the uranyl moiety by the TBP. This could explain why the lowest distribution ratio is observed at equal concentrations of nitrate and chloride in the initial aqueous fraction.

Sample	C1:N 9.U	C2:N 8.U	C3:N 7.U	C4:N 6.U	C5:N 5.U	C6:N 4.U	C7:N 3.U	C8:N 2.U	C9:N 1.U
$[H^+]$ / M	10.00	10.00	10.00	10.00	10.00	10.00	10.00	10.00	10.00
$[Cl^-]$ / M	1.00	2.00	3.00	4.00	5.00	6.00	7.00	8.00	9.00
$[NO_3^+]$ / M	9.00	8.00	7.00	6.00	5.00	4.00	3.00	2.00	1.00
Distribution Ratio (D)	49.00	24.00	13.29	9.00	5.66	7.33	5.66	11.50	24.00
Log D	1.69	1.38	1.12	0.95	0.75	0.87	0.75	1.06	1.38

Table 25: **:** Initial aqueous phase concentrations and distribution ratios for samples C1:N9.U - C9:N1.U.

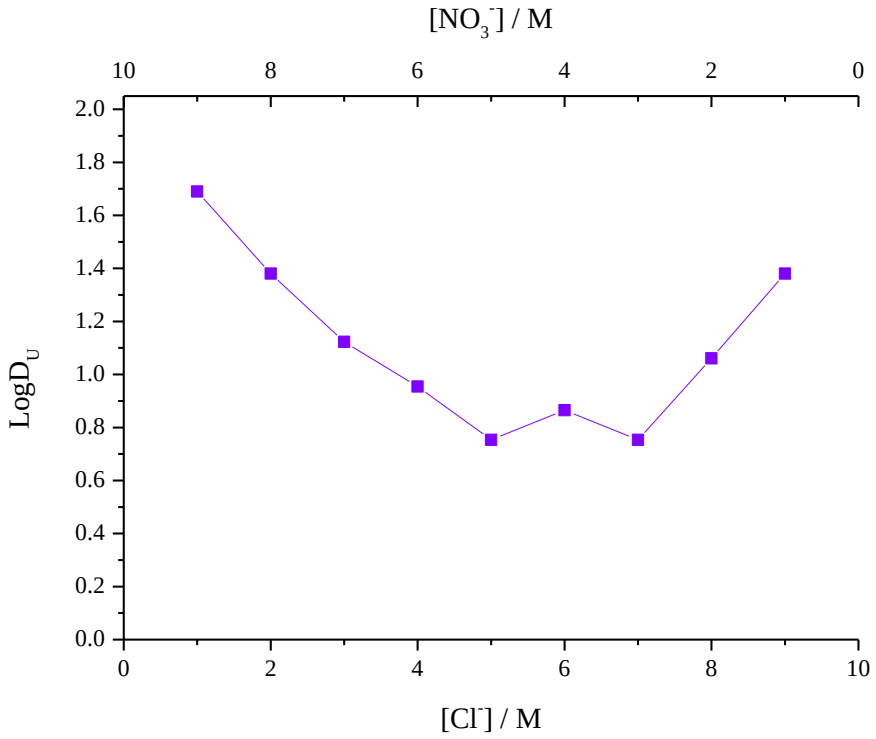

Figure 50: Distribution data as a function of acid concentration for samples C1:N9.U - C9:N1.U.

The ^{31}P NMR data for the samples detailed in Table 31, recorded at -50 ^{o}C, are presented in Figure 51. Based on previous data collected, the acid-TBP adduct is assigned to the signal at -2 ppm. In addition, a signal at 1.5 ppm is observed, decreasing in intensity with descending aqueous nitrate concentration. A chemical signal is observed at 3.5 ppm which increases in intensity with ascending chloride concentration.

The UO_2^{2+}-NO_3^--TBP-OK systems previously discussed, show a chemical signal recorded in the ^{31}P NMR spectra at around 1.5 ppm (Figure 44). It is therefore with good reason, that the signal observed at 1.5 ppm in Figure 51 is due to the complexed UO_2^{2+}-NO_3^--TBP type species. The additional signal observed at around 3.5 ppm in Figure 51 is not seen in the UO_2^{2+}-Cl^--TBP-OK systems (Figure 48) nor the UO_2^{2+}-NO_3^--TBP-OK systems, possibly implying the formation of a mixed chloride/nitrate uranyl complex.

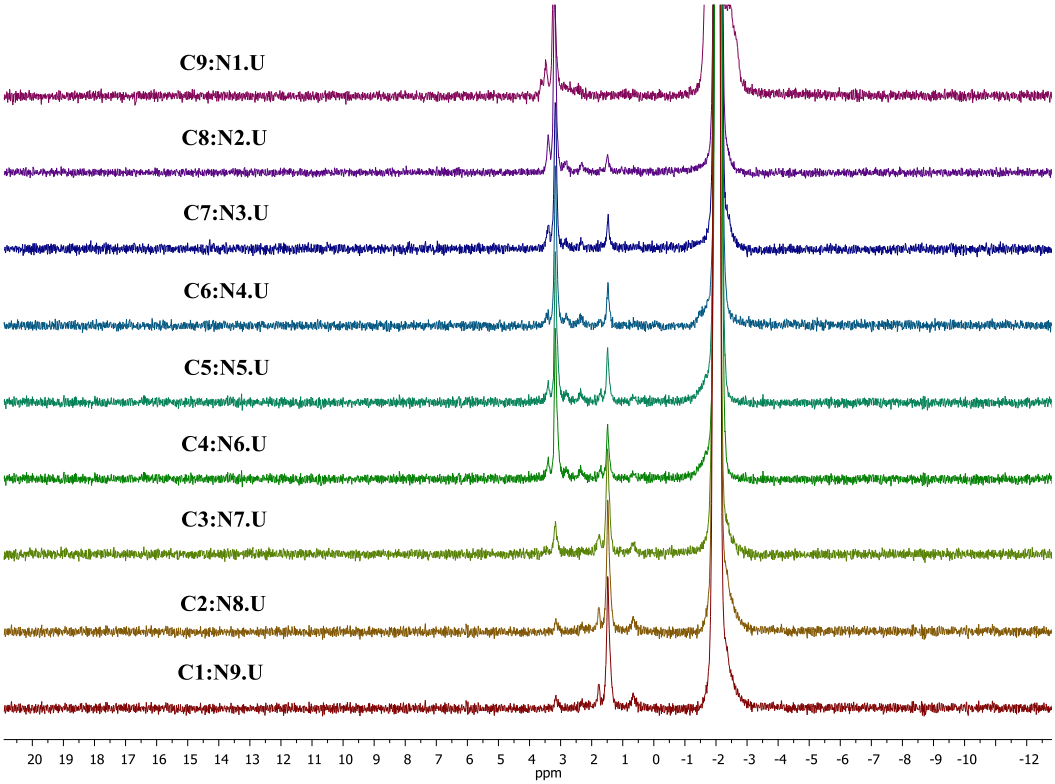

Figure 51: ^{31}P NMR spectra of organic phase post extraction for samples C1:N9.U - C9:N1.U.

A number of other aqueous chloride and nitrate uranium containing combinations were analysed for their effectiveness of uranium separation via the same methodologies, i.e. retaining aqueous nitrate at one concentration and varying the aqueous chloride concentration, and *vice versa*. The ^{31}P NMR spectra gave almost identical results to those outlined in Figure 51. Systems where the aqueous nitrate concentration was retained at 8 M saw the prominence of the signal observed at 1.5 ppm throughout the NMR spectra. This indicates that the UO_2-NO_3-TBP species dominates these systems. The distribution data were also remarkably similar with improved separation of uranium observed in systems tending towards higher aqueous nitrate concentrations.

Extended X-ray Absorption Fine Structure (EXAFS) spectra were collected for the sample C2:N10.U at the DIAMOND light source, Oxford. This initial aqueous phase was chosen as it contained a significantly higher aqueous nitrate concentration compared to the aqueous chloride concentration. Unexpectedly, the organic phase speciation was dominated by the $[UO_2Cl_2(TBP)_2]$ moiety, according to the fitted R-space and k^3-space spectra shown in Figure 52. Table 26 details the numerical parameters associated with this fit. Various fit parameters were exhausted using a pure nitrate primary coordination shell as well as a mixed nitrate/chloride shell, but this was clearly the best fit of the data collected for this sample. This model consists of two axial oxygen atoms, two chloride atoms as well as the phosphate oxygen in its primary coordination shell and the phosphorus atoms of the phosphate group in the second coordination shell. Similar fits were obtained for the EXAFS spectra from samples C6:N6.U (Figure 53 and Table 27) and C10:N2.U (Figure 54 and Table 28) obtained in the same manner as described here. It should be noted here, that the fits are a best fit average, however.

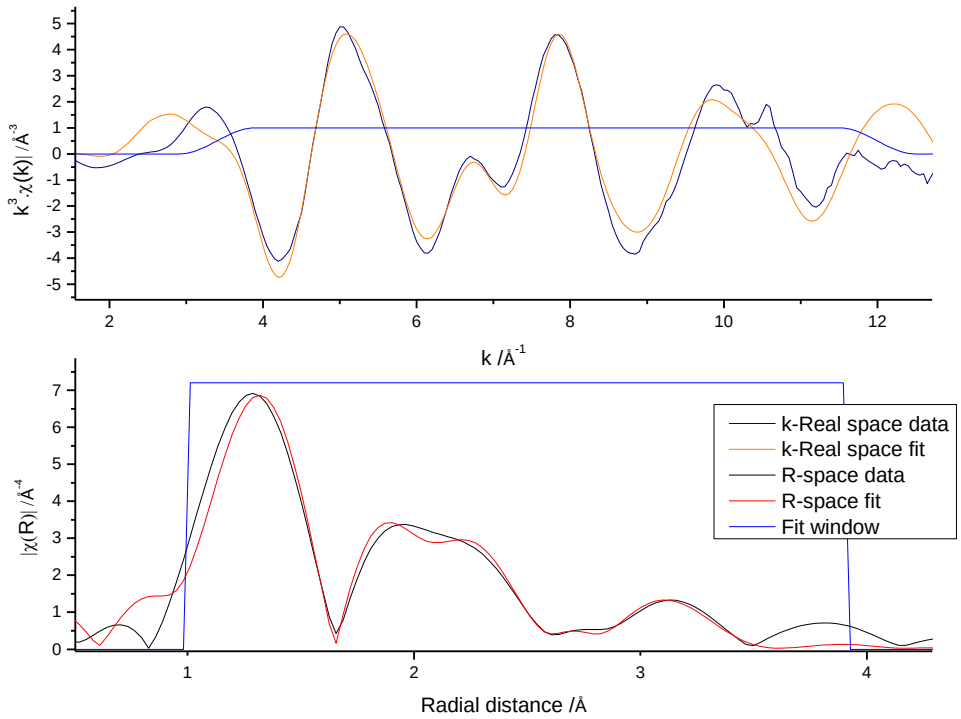

Figure 52: k^3-weighted $\chi(k)$-function (top) and Fourier transform (bottom) of U L_{III}-edge EXAFS data for $(UO_2)^{2+}$ extracted into 30 % TBP-OK, from an initial aqueous phase consisting of 10 M nitrate and 2 M chloride (12 M H^+). The data were fitted to $[UO_2Cl_2(TBP)_2]$.

Sample	Shell	Occupancy	σ^2	E_0 (eV)	R_i (Å)	R_f (Å)	ΔR (Å)
$(UO_2)^{2+}$ extracted into 30 % TBP-OK from 10 M NO_3^-/ 2 M Cl^-/ 12 M H^+ $[UO_2Cl_2(TBP)_2]$ Amp = 0.929 R factor = 0.0159 χ^2 = 4504.87	Oyl	2.00	0.00180		1.7545	1.7868	-0.0323
	Cl	2.00	0.00783		2.6944	2.7001	-0.0062
	Oyl (MS)	2.00	0.00361	4.408	3.5089	3.5736	-0.0647
	O(phos)	2.00	0.00627		2.4193	2.3717	0.0496
	P(phos)	2.00	0.01186		4.0928	3.8157	0.2771

Table 26: Parameters obtained from EXAFS fits in k^3-space for $(UO_2)^{2+}$ extracted into TBP-OK (30 % TBP by volume) from an initial aqueous phases composition of 10 M nitrate and 2 M chloride. E_0 is the relative shift in ionization energy, Ri is the initial distance of the shell (Å) and R_f is the refined distance of the shell (Å). Statistics of fit (χ^2 and r-factor) and amplitude factor (Amp) provided.

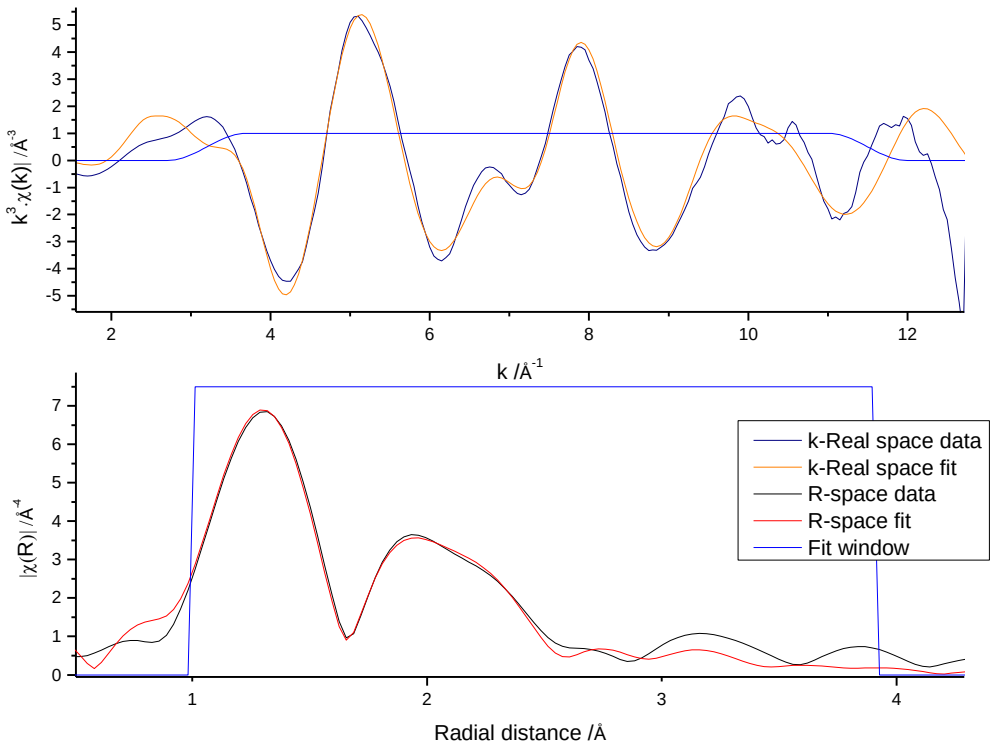

Figure 53: k^3-weighted $\chi(k)$-function (top) and Fourier transform (bottom) of U L_{III}-edge EXAFS data for $(UO_2)^{2+}$ extracted into 30 % TBP-OK, from an initial aqueous phase consisting of 6 M nitrate and 6 M chloride (12 M H^+). The data were fitted to $[UO_2Cl_2(TBP)_2]$.

Sample	Shell	Occupancy	σ^2	E_0 (eV)	R_i (Å)	R_f (Å)	ΔR (Å)
$(UO_2)^{2+}$ extracted into 30 % TBP-OK from 6 M NO_3^-/ 6 M Cl^-/ 12 M H^+, fitted to $[UO_2Cl_2(TBP)_2]$ Amp = 1.00 R factor = 0.0111 χ^2 = 3694.43	Oyl	2.00	0.00333		1.7555	1.7868	-0.0314
	Cl	2.00	0.00945		2.6787	2.7006	-0.0219
	Oyl (MS)	2.00	0.00666	4.637	3.5109	3.5736	-0.0627
	O(phos)	2.00	0.00936		2.4288	2.3717	0.0571
	P(phos)	2.00	0.01938		3.6445	3.8157	-0.01713

Table 27: Parameters obtained from EXAFS fits in k^3-space for $(UO_2)^{2+}$ extracted into TBP-OK (30 % TBP by volume) from an initial aqueous phases composition of 6 M nitrate and 6 M chloride. E_0 is the relative shift in ionization energy, Ri is the initial distance of the shell (Å) and R_f is the refined distance of the shell (Å). Statistics of fit (χ^2 and r-factor) and amplitude factor (Amp) provided.

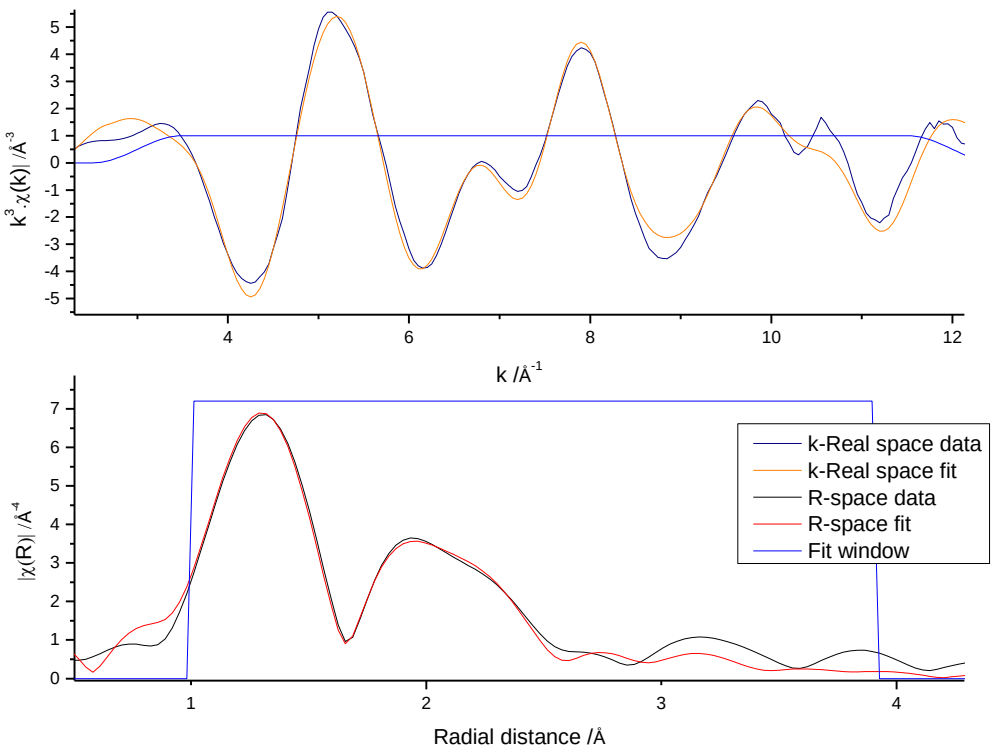

Figure 54: k^3-weighted χ(k)-function (top) and Fourier transform (bottom) of U L_{III}-edge EXAFS data for $(UO_2)^{2+}$ extracted into 30 % TBP-OK, from an initial aqueous phase consisting of 2 M nitrate and 10 M chloride.

Sample	Shell	Occupancy	σ^2	E_0 (eV)	R_i (Å)	R_f (Å)	ΔR (Å)
$(UO_2)^{2+}$ extracted into 30 % TBP-OK from 2 M NO_3^-/ 10 M Cl^-/ 12 M H^+, fitted to $[UO_2Cl_2(TBP)_2]$ Amp = 1.00 R factor = 0.0164 χ^2 = 6269.66	Oyl	2.00	0.00333		1.7576	1.7868	-0.0292
	Cl	2.00	0.00809		2.6799	2.7006	-0.0207
	Oyl (MS)	2.00	0.00665	5.882	3.5151	3.5736	-0.0585
	O(phos)	2.00	0.00806		2.4084	2.3717	0.0366
	P(phos)	2.00	0.02919		3.7836	3.8157	-0.0321

Table 28: Parameters obtained from EXAFS fits in k^3-space for $(UO_2)^{2+}$ extracted into TBP-OK (30 % TBP by volume) from an initial aqueous phases composition of 2 M nitrate and 10 M chloride. E_0 is the relative shift in ionization energy, Ri is the initial distance of the shell (Å) and R_f is the refined distance of the shell (Å). Statistics of fit (χ^2 and r-factor) and amplitude factor (Amp) provided.

In summary, uranyl separated from both aqueous HCl and HNO_3 yielded high distribution ratios, that showed an increase with ascending aqueous acid concentration. Uranyl separated from mixed chloride and nitrate aqueous fractions did not enhance the D_U over the concentrations ranges analysed and gave the lowest distribution ratio of uranyl in sample C5:N5.U, where equal chloride and nitrate concentrations were utilised in the initial aqueous fraction. There is however, a discrepancy between the NMR data presented and the fitted EXAFS data for the mixed acid systems. It was observed that the fitted complex in post separated organic phase for the mixed acid samples was $[UO_2Cl_2(TBP)_2]$, despite significantly higher nitrate concentrations in the initial aqueous fraction. One possible explanation is that EXAFS processing takes an average of the uranyl environments which may have been dominated by $[UO_2Cl_2(TBP)_2]$ scattering shells, in particular the Cl^- scattering shell over the possibly weaker NO_3^- scattering paths. This may result in the

$[UO_2Cl_2(TBP)_2]$ complex dominating the EXAFS profile even though the sample itself may consist of mainly $[UO_2(NO_3)_2(TBP)_2]$ as indicated in some samples by ^{31}P NMR spectroscopy. Further work is needed to confirm possible reasoning for this. It must also be made apparent that the "complex" notations are not chemically sound, but merely represent the presence of the TBP species by, what is thought to be, hydrogen bonding of the phosphate oxygen atom with the metal centre.

5.4 Trace Level Neptunium Separated from Aqueous Nitric Acid

Previous literature suggests that the neptunium oxidation state surrounding solvent extraction methods, is dependent on the aqueous acid concentration. The work of K. W. Kim *et al*. demonstrated that at aqueous nitric acid concentrations of 0.5 M, approximately 33 % of the neptunium will exist in the +5 state, where the remainder is Np(VI).[135] These tests were carried out under standard PUREX conditions (30 % TBP in OK), using electrochemistry to control the oxidation states. It has been shown, that under PUREX style reprocessing conditions, Np(V) is essentially inextractable where as Np(VI) is easily extractable.[135] It is thought that Np(VI) organic phase speciation is dominated, in systems analogous to PUREX, by the $[NpO_2(NO_3)_2(TBP)_2]$ species. Here, Np separation behaviour will be related to Np speciation in the organic phase determined by NMR spectroscopy and EXAFS analysis. Further, it has been suggested that the relationship for the oxidation of Np(V) to Np(VI) is thought to occur via the following route:

$$[NpO_2]^+ + 1/2\ NO_3^- + 3/2\ H^+ \rightleftharpoons [NpO_2]^{2+} + 1/2\ HNO_2 + 1/2\ H_2O \qquad ^{136}$$

Aqueous nitric acid (6 - 10 M, 1.9 mL) was spiked with Np (^{237}Np(V), 50 Bq, 100 uL, 81 uM) and the resultant aqueous fraction (4.05 uM ^{237}Np) contacted with TBP-OK (30 % TBP by volume), as described in Section 4.6. The neptunium was not manipulated in any way for these batch experiments, hence it can be assumed that the neptunium oxidation state composition is predominantly Np(V). Both aqueous and organic fractions, post-separation were analysed as described in Section 4.6. It is clear from the distribution data presented in Table 29 and the pictorial representation of the distribution ratio of neptunium as a function of aqueous nitric acid (Figure 55),

that Np separation in these systems is low. This is due to the dominance of the inextractable +5 Np oxidation state in each aqueous fraction studied.

The distribution ratios as detailed in Table 29, show a small increase in the separation of neptunium into the organic fraction as a function of increasing aqueous nitric acid concentration, for each sample analysed. Sample N10.Np, which gave a neptunium distribution ratio of 0.43 corresponded to less than 30 % neptunium separation. Under these conditions, neptunium REDOX chemistry is complex.

It is likely that the Np(V) contained within the aqueous fraction is oxidised to Np(VI), which is effectively separated under PUREX type conditions. This oxidation of Np(V) to Np(VI) is facilitated by higher aqueous nitric acid concentrations. Therefore, the calculated 30 % separation observed for sample N10.Np may be the result of separated Np(VI) from the oxidation of Np(V) to Np(VI), leaving any unoxidised Np(V) within the aqueous fraction. The use of UV/vis/nIR spectroscopy to confirm the Np oxidation state composition of these samples was not possible with the Np concentrations used with the standard spectroscopic techniques available (*i.e.* 1 cm path length cells).

Sample	N6.Np	N6.5.Np	N7.Np	N7.5.Np	N8.Np	N8.5.Np	N9.Np	N9.5.Np	N10.Np
$[HNO_3]$ / M	6.00	6.50	7.00	7.50	8.00	8.50	9.00	9.50	10.00
Distribution Ratio D	0.09	0.15	0.16	0.18	0.22	0.25	0.33	0.41	0.43
Log D	-1.10	-0.83	-0.79	-0.75	-0.65	-0.60	-0.48	-0.39	-0.37

Table 29: Initial aqueous phase concentration and distribution ratio data for samples N6.Np - N10.Np.

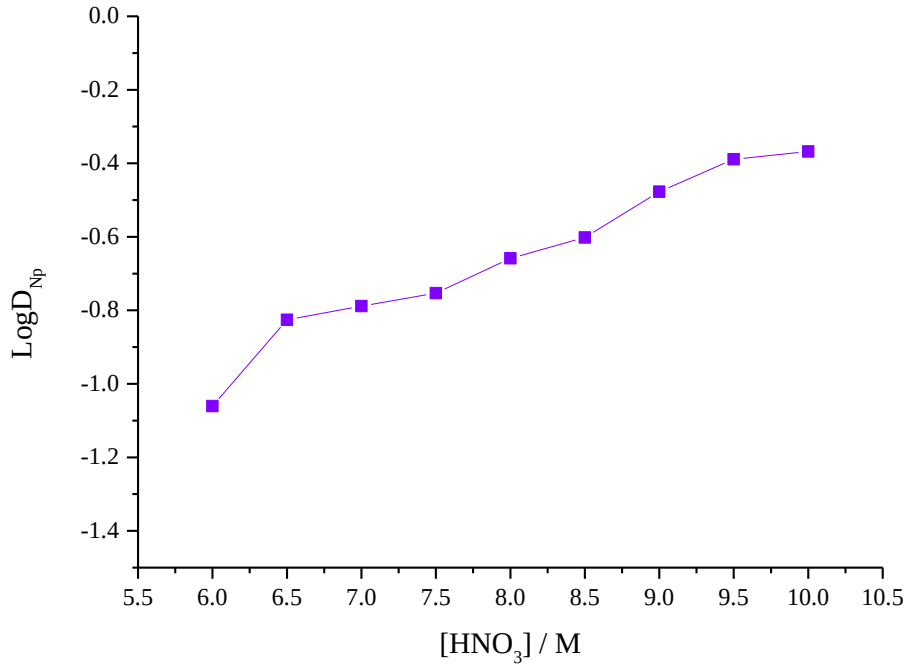

Figure 55: Distribution data as a function of acid concentration for samples N6.Np - N10.Np.

5.5 Neptunium (Np(VI)) Separated from Aqueous Nitric Acid

Higher concentrations of Np were subsequently used in contact studies to allow the determination of the Np oxidation state composition in the various phases obtained and apply other characterisation techniques such as NMR and EXAFS spectroscopies.

Neptunium(VI) hydroxide solid was synthesized in house via oxidation with perchloric acid (11.6 M). The resultant solid was dissolved into various concentration aqueous nitric acid (1-10 M) solutions (^{237}Np(VI), ~ 41 kBq, 2 mL, ~ 3.33 mM) (samples N1.Np - N10.Np) and those solutions were further contacted with TBP-OK (30 % TBP by volume). Each sample was mechanically agitated for approx. 15 minutes and centrifuged for full phase separation. The organic phases were directly analysed by proton decoupled ^{31}P NMR spectroscopy. Parameters (as previously described in Section 4.6) were altered to account for the paramagnetism of the Np(VI) ions (as detailed in Section 3.3.1).

Pre aqueous-organic phase contact, an aliquot of each aqueous phase was analysed using liquid scintillation counting (LSC), applying protactinium daughter activity subtraction. Post extraction, an aliquot (50 uL) of the resultant aqueous and organic phases was taken for LSC analysis. To each aliquot, scintillation fluid (ScintSafe 3, 10 mL) was added and the samples counted for 30 minutes each. From the given activities, the distribution ratio data for the separation of neptunium in these systems were calculated. Analysis via NMR spectroscopy and LSC was performed immediately after phase contact. Some samples were designated for EXAFS analysis at the KIT-INE beamline at the ANKA synchrotron (Karlsruhe, Germany).

Distribution ratio (D_{Np}) data for neptunium separated from aqueous nitric acid is presented in Table 30. The D_{Np} increases as a function of aqueous nitrate concentration. Neptunium extracted from aqueous nitric acid with an initial concentration of 1 M, ~ 60 % separation of the neptunium in to the organic fraction. The distribution ratios increase more significantly for samples N1.Np to N4.Np and stabilise for samples N4.Np to N10.Np, as Figure 56 details. for an initial aqueous nitric acid concentration of 10 M, D_{Np} was found to be ~ 5 equating to ~ 80 % neptunium separation. Figure 61 illustrates the change in D_{Np} as a function of aqueous HNO_3 concentration.

Sample	N1.Np*	N2.Np*	N4.Np*	N6.Np*	N8.Np*	N10.Np*
[HNO_3] / M	1.00	2.00	4.00	6.00	8.00	10.00
Distribution Ratio (D)	1.70	2.40	4.17	4.45	4.44	4.92
Log D	0.23	0.38	0.62	0.65	0.65	0.70

Table 30: Initial aqueous phase concentrations and distribution ratios for samples N1.Np - N10.Np. Here, the asterisk defines non-trace level neptunium samples.

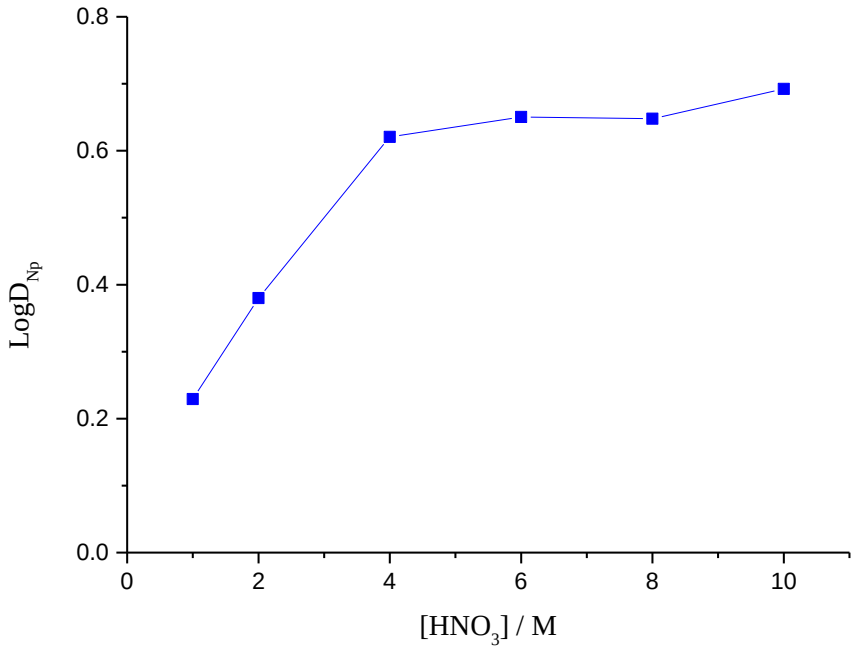

Figure 56: Distribution ratio data for samples N1.Np - N10.Np as a function of aqueous HNO_3 concentration.

The nIR spectra were obtained throughout experimentation in order to assess the oxidation state of the neptunium including post contact. Figure 57 illustrates the vis/nIR spectra of the aqueous phase post extraction for samples N1.Np - N10.Np. The signal observed at around 980 nm is indicative of Np(V). Lower aqueous nitric acid concentrations indicate a greater presence of the Np(V) compared to that at higher aqueous nitric acid concentrations. The nIR signal observed at 1200 nm for the organic fractions for all samples, post separation (Figure 58) show that when extracted, Np is only present in the organic phase as Np(VI). It is well established that Np(V) is difficult to extract whereas Np(VI) readily extracts into organic phases, particularly those containing TBP.[137] The amount Np extracted is observed to increase as a function of aqueous HNO_3 concentration. Therefore, it is most likely that at high aqueous HNO_3 concentrations Np(VI) is readily stabilised and extracted into the organic phase, whereas at low aqueous HNO_3 concentrations Np(VI) can reduce to Np(V). It should be noted however, that the validity of directly comparing aqueous neptunium behaviour before organic phase contact (as previously illustrated in literature), with the resultant aqueous phase behaviour post organic phase contact, is somewhat sceptical.

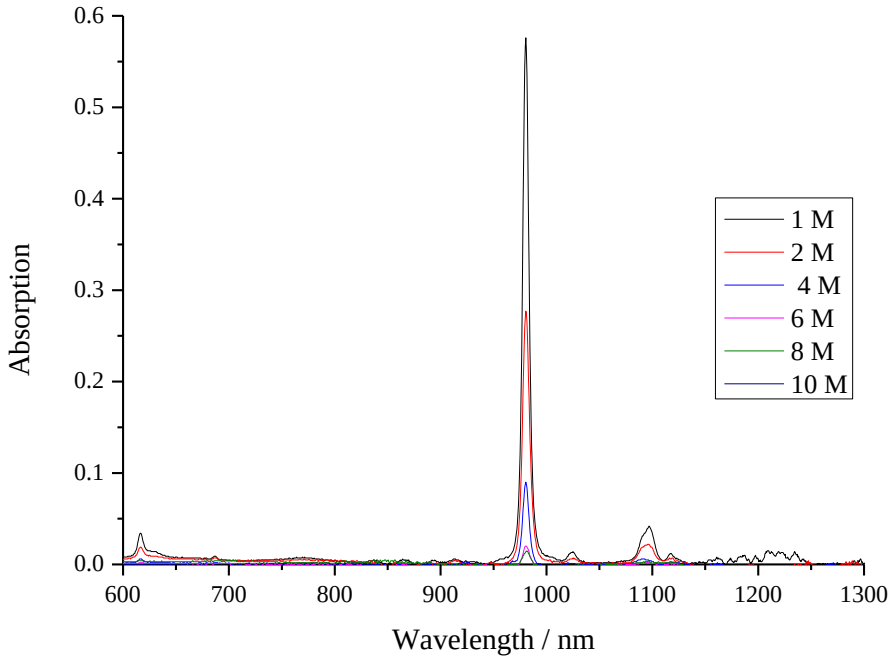

Figure 57: Vis/nIR spectra for resultant *aqueous* phases post extraction, for samples N1.Np - N10.Np.

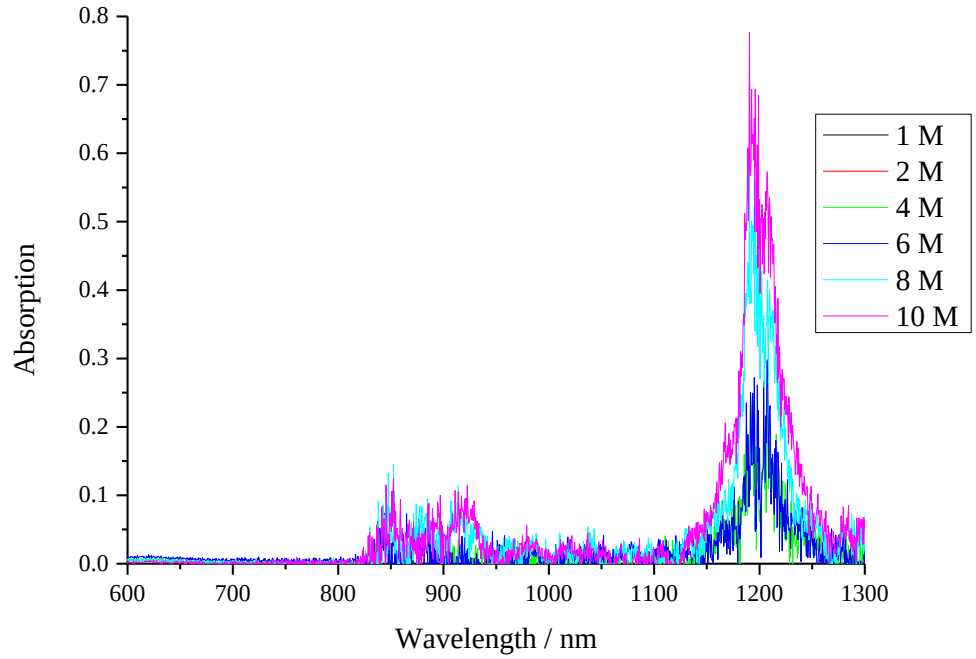

Figure 58: Vis/nIR spectra for resultant *organic* phases post extraction, for samples N1.Np - N10.Np.

An aliquot (200 uL) of the resultant, post-separation organic fraction was taken for ^{31}P proton decoupled NMR analysis. Each sample was run using identical, paramagnetic acquisition parameters for 20 hours. The spectra of samples N1.Np - N10.Np are presented in Figure 59. For each sample analysed, the TBP-acid adduct, as seen previously, is observed at around -2 ppm. Due to the paramagnetic nature of the neptunium species, it might be expected that broad resonances are observed in the NMR spectra. However, what may be the Np-TBP type complexation signal, observed around 28 ppm, is quite sharp. This signal however, is speculative, and due to the paramagnetic broadening, the signal observed at around -25 ppm for samples N6.Np - N10.Np could also be the result of Np-TBP complexation. There is little literature on the speciation of neptunyl TBP complexes via NMR so it is difficult to compare.

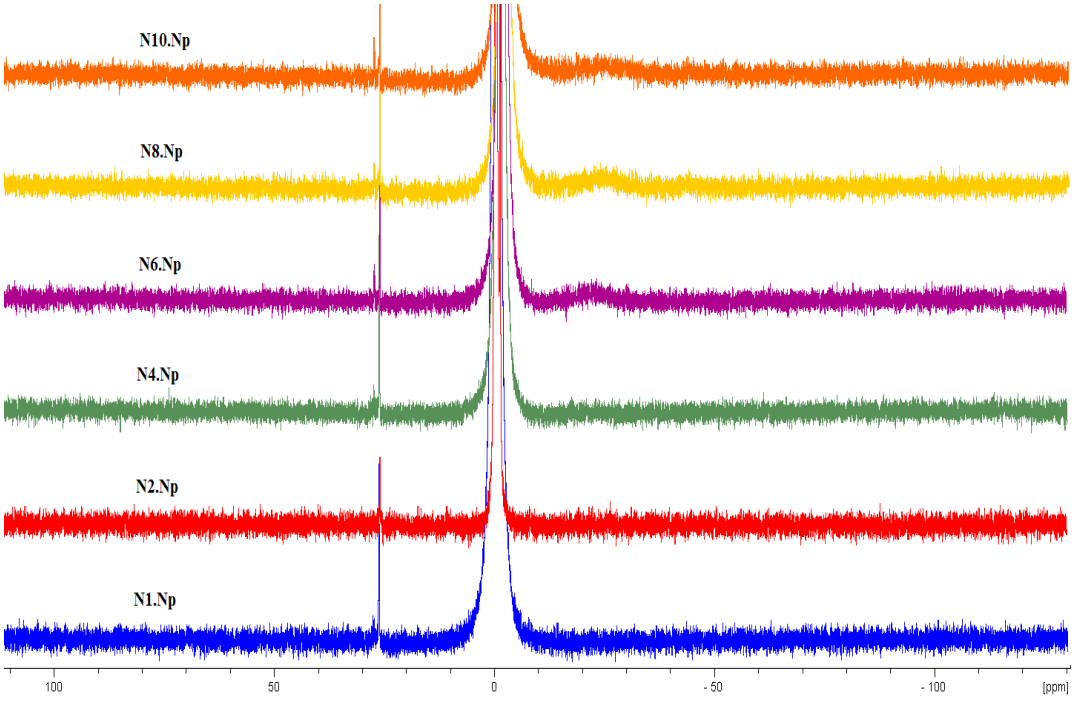

Figure 59: ^{31}P NMR of the organic phase post extraction from samples N1.Np - N10.Np.

EXAFS spectra were collected for pure NpO_2^{2+} ($^{237}Np(VI)$, ~ 5.86 kBq, 0.5 mL, ~ 1.9 mM) in 7.2 M HNO_3 extracted in to TBP-OK (30 % TBP by volume). The fitted R-space and k^3-space spectra, presented in Figure 60 are in good agreement with the $[NpO_2(NO_3)_2(TBP)_2]$ complex. The spectra were fitted using the axial oxygen atoms of the $(NpO_2)^{2+}$ species and the nitrogen and oxygen atoms of the nitrate anion group. The oxygen and phosphorus of the TBP moiety were also fitted. Table 31 outlines the parameters obtained from the fit. From the EXAFS data obtained, it is implied that the complexed species observed in the NMR spectra (Figure 64) is due to the $[NpO_2(NO_3)_2(TBP)_2]$ moiety. This is a best fit analysis, however.

Sample	Shell	Occupancy	σ^2	R_i (Å)	R_f (Å)	ΔR (Å)
$(NpO_2)^{2+}$ extracted into 30 % TBP-OK from 7.2 M HNO_3, fitted to, $[NpO_2(NO_3)_2(TBP)_2]$	O (yl)	2	0.00131	1.7629	1.7400	0.0229
	N (nit)	2	0.00119	2.9909	2.9741	0.0168
	O (nit)	4	0.00094	2.5033	2.5251	-0.0218
	O (nit)	2	0.00221	4.1855	4.1687	0.0168
Amp = 0.743 E_0 (eV) = 8.896 R factor = 0.018 χ^2 = 5.715	N/O (MS)	4	0.00340	4.1856	4.1688	0.0168
	O(phos)	2	0.00292	2.3538	2.1991	0.1547
	P(Phos)	2	0.00278	3.5770	3.5928	-0.0058

Table 31: Parameters obtained from EXAFS fits in k^3 space for $(NpO_2)^{2+}$ extracted into TBP-OK (30 % TBP by volume), from 7.2 M HNO_3. E_0 is the relative shift in ionization energy, Ri is the initial distance of the shell (Å) and R_f is the refined distance of the shell (Å). Statistics of fit (χ^2 and r-factor) and amplitude factor (Amp) provided.

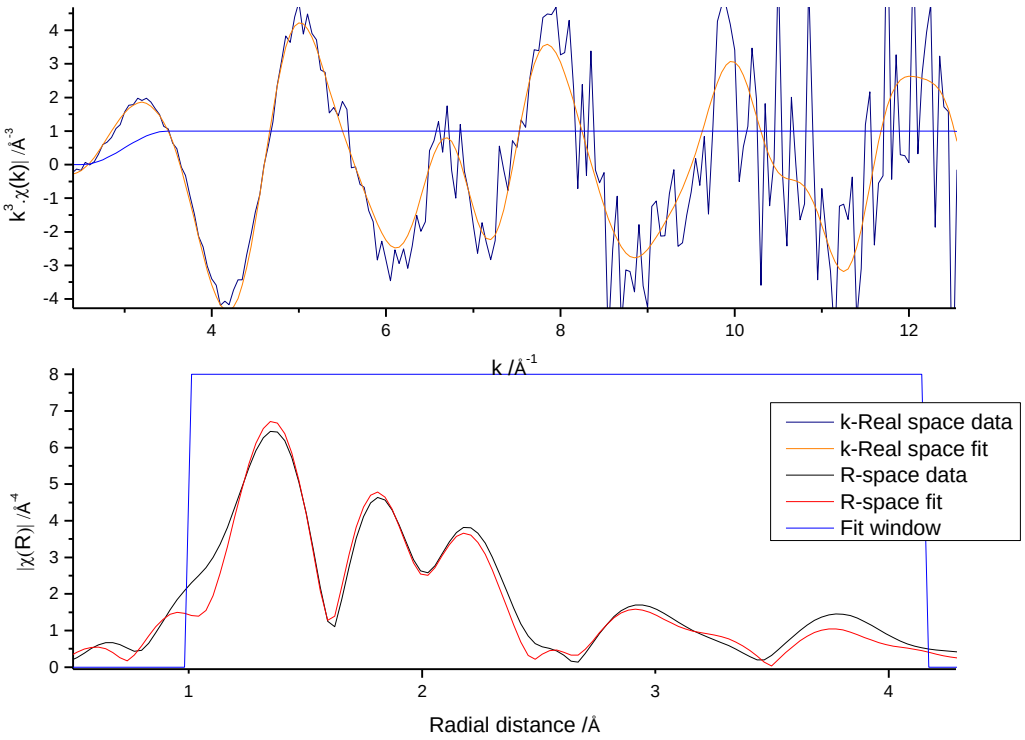

Figure 60: k^3-weighted χ(k)-function (top) and Fourier transform (bottom) of Np L_{III}-edge EXAFS data for the $(NpO_2)^{2+}$ extracted into 30 % TBP-OK, from an initial aqueous phase consisting of 7.2 M HNO_3. Date were fitted to $[NpO_2(NO_3)_2(TBP)_2]$.

5.6 Trace Level Neptunium Separated from Aqueous Hydrochloric Acid

The separation of neptunium from aqueous hydrochloric acid media has not been well documented, therefore investigations were undertaken to determine the optimum conditions for neptunium separation from aqueous hydrochloric acid.

Aqueous hydrochloric acid (6 - 10 M, 1.9 mL) was spiked with Np (^{237}Np(V), 271 Bq, 100 uL, 81 uM) and the resultant aqueous fraction (4.05 uM ^{237}Np) contacted with TBP-OK (30 % TBP by volume), as described in Section 4.6. Both aqueous and organic fractions, post-separation were analysed using the approach described in Section 4.6. A third phase was observed in samples C7.Np - C10.Np.

The volume of the third phase, when obtained, was again immeasurable in terms of the desired accuracy and therefore the distribution ratios are calculated as a comparison of the resultant aqueous and overall organic fractions as previously described in Section 4.7.

The data for the separation of neptunium from aqueous hydrochloric acid is presented in Table 32. The calculated distribution ratios for samples C6.Np - C10.Np increase with increasing aqueous hydrochloric acid concentration (Figure 61). The distribution ratios for samples C6.Np - C10.Np are significantly higher than those observed for samples N6.Np - N10.Np. This implies that the presence of chloride in the initial aqueous phase enhances the separation of neptunium under these conditions. Samples C10.Np gave a distribution ratio of ~ 100 which corresponds to almost 100 % separation. The distribution ratio calculated for sample C6.Np was indicative of ~ 50 % neptunium separation into the organic fraction. There is little evidence in the current work that reflects the ability of chloride to manipulate the neptunium oxidation state to aid separation but it is most likely that the chloride reduces the Np(V) to Np(IV) which is efficiently extracted by the TBP moiety.

Sample	C6.Np	C6.5.Np	C7.Np	C7.5.Np	C8.Np	C8.5.Np	C9.Np	C9.5.Np	C10.Np
$[HNO_3]$ / M	6.00	6.50	7.00	7.50	8.00	8.50	9.00	9.50	10.00
Distribution Ratio D	1.22	1.44	1.56	2.13	2.58	3.00	4.56	9.00	99.00
Log D	0.09	0.16	0.19	0.33	0.41	0.48	0.66	0.95	1.99

Table 32: Initial aqueous phase composition data and distribution ratio data for samples C6.Np - C10.Np.

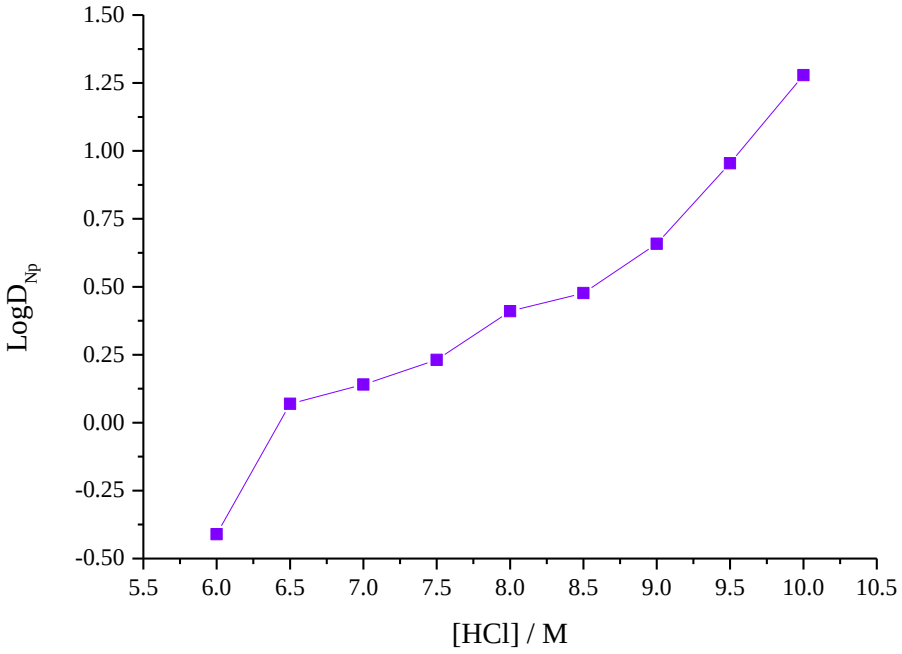

Figure 61: Distribution data as a function of acid concentration for samples C6.Np - C10.Np.

5.7 Neptunium (Np(VI)) Separated from Aqueous Hydrochloric Acid

In order to determine whether Np organic phase speciation can be linked to general Np extraction behavior in the presence of chloride, pure Np(VI) samples at concentrations required for NMR spectroscopic and EXAFS studies were used for the following Np speciation studies. Neptunium(VI)hydroxide solid was synthesized in house via oxidation with perchloric acid (11.6 M). The resultant solid was dissolved into solutions with various aqueous hydrochloric acid concentrations (1-10 M) (^{237}Np(VI), ~ 41 kBq, 2 mL, ~ 3.33 mM; samples C1.Np - C10.Np) and those solutions were further contacted with a TBP-OK (30 % TBP by volume). Each sample was mechanically agitated for approx. 15 minutes and centrifuged for full phase separation. The organic phases were analysed by proton decoupled ^{31}P NMR spectroscopy, using the acquisition parameters as described in Section 3.3.1.

Distribution ratios were calculated with data collected from liquid scintillation counting. Some samples were designated for EXAFS analysis at the KIT-INE beamline at the ANKA synchrotron (Karlsruhe, Germany).

For neptunium separated from aqueous hydrochloric acid, samples C1.Np - C10.Np, an aliquot of each aqueous fraction was analysed pre-extraction to determine the initial aqueous phase activity. Some samples (shown in red in Table 33) formed a third phase. Analysis via NMR spectroscopy and LSC was done immediately after phase contact.

Distribution ratio (D_{Np}) data for neptunium separated from aqueous hydrochloric acid are presented in Table 33. The D_{Np} increases as a function of aqueous chloride concentration. Neptunium was not extracted effectively from aqueous phases of initial aqueous HCl concentrations below 4 M with D_{Np} values as low as 0.01 obtained which is significantly lower than those of the analogous aqueous HNO_3 systems. The distribution ratios increase more significantly for samples C6.Np to C10.Np, with a large increase in D_{Np} to 5.47 observed for sample C8.Np corresponding to over 80 % neptunium separation for this sample. An initial aqueous HCl concentration of 10 M gives a D_{Np} of ~ 30 equating to over 90 % neptunium separation. Although a third phase was observed in samples C8.Np and C10.Np, the distribution ratios were calculated as a direct separation of the neptunium from the aqueous to the organic phase as a whole. This method was adopted due to the observed volume of the third phase being almost negligible, and therefore it was considered more accurate to measure the activity of the resultant aqueous phase for these samples. Figure 62 illustrates the change in D_{Np} as a function of aqueous HCl concentration. It is clear that a higher distribution of neptunium is observed in systems containing aqueous HCl *c.f.* aqueous HNO_3.

However, in systems of a lower aqueous HCl concentration, neptunium extraction is much less effective than those observed in systems of a lower HNO_3 concentration.

Sample	C1.Np*	C2.Np*	C4. Np*	C6. Np*	C8. Np*	C10. Np*
[HCl] / M	1.00	2.00	4.00	6.00	8.00	10.00
Distribution Ratio (D)	0.01	0.03	0.21	1.23	5.47	27.00
Log D	-1.97	-1.58	-0.68	0.09	0.74	1.43

Table 33: Initial aqueous phase composition and distribution ratios for samples C1.Np - C10.Np. Here, the asterisk defines non-trace level neptunium samples.

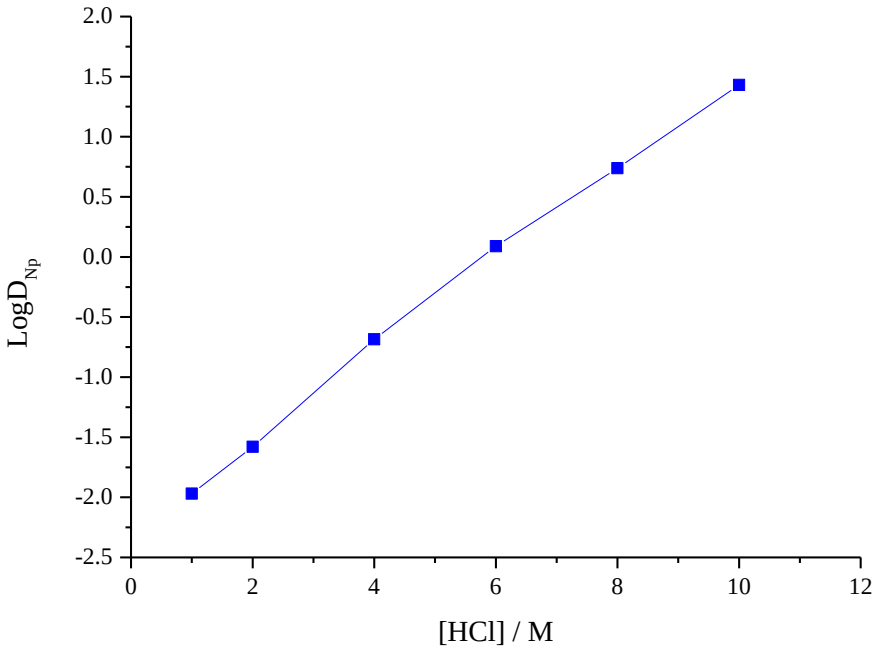

Figure 62: Distribution ratio data for samples C1.Np - C10.Np as a function of aqueous HCl concentration.

The vis/nIR spectra were obtained throughout experimentation in order to assess the oxidation state of the neptunium.

The aqueous fractions analysed post extraction, similar to the aqueous HNO_3 systems, show that the Np remaining exists as Np(V) with little or no Np(VI) species observed, as Figure 63 illustrates. The significant signal observed at 980 nm in the nIR data presented in Figure 63 is indicative of Np(V) , whereas there is no Np(VI) observed due to the absence of a signal at 1200 nm. It indicates that more Np(V) is present in lower aqueous HCl concentrations post extraction *c.f.* higher aqueous HCl concentrations, which is due to an increase in the extraction of neptunium at higher aqueous acid concentrations

The organic fractions for samples C1.Np - C10.Np were analysed via vis/nIR spectroscopy. The organic fractions for samples C1.Np and C2.Np gave no significant UV/vis/nIR data due to very little neptunium extraction at these low aqueous HCl concentrations. For samples C4.Np – C10.Np a signal is observed at around 1200 nm (Figure 64) which is indicative of Np(VI); there are no additional signals observed showing Np(VI) dominance in the organic fractions of the samples analysed. This data also confirms the LSC measurements which showed that greater neptunium extraction is obtained at higher aqueous HCl concentration , compared to that obtained at low HCl concentrations. It should be noted however, that the validity of directly comparing aqueous neptunium behaviour before organic phase contact (as previously illustrated in literature), with the resultant aqueous phase behaviour post organic phase contact, is somewhat sceptical.

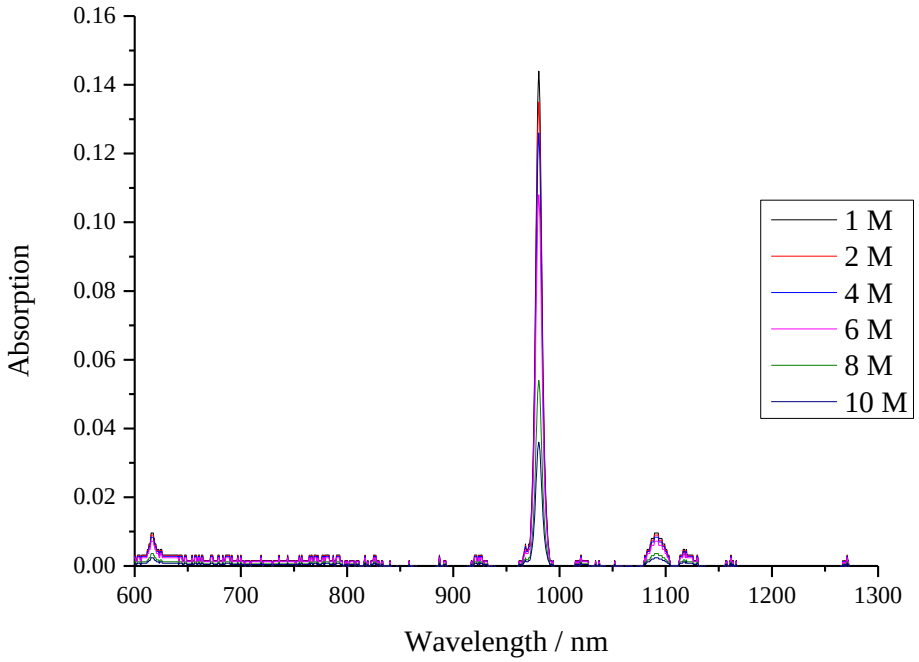

Figure 63: Vis/nIR spectra for resultant *aqueous* phases post extraction, for samples C1.Np - C10.Np.

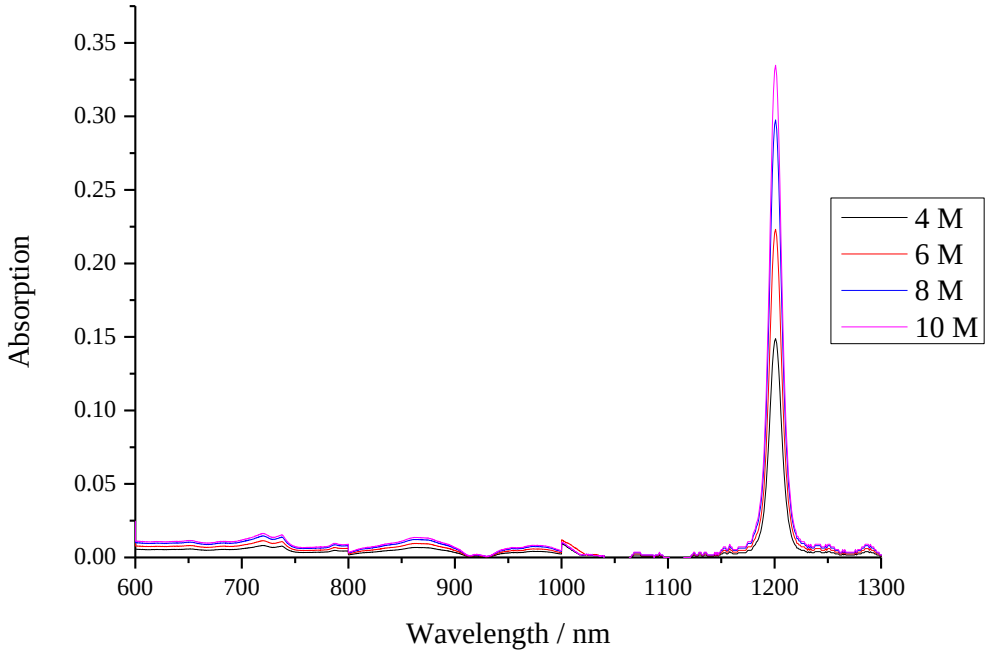

Figure 64: Vis/nIR spectra for resultant *organic* phases post extraction, for samples C4.Np - C10.Np.

An aliquot (200 uL) of each resultant, post-separation organic fraction from samples C1.Np – C10.Np was taken for ^{31}P proton decoupled NMR analysis. Each sample was run using identical, paramagnetic acquisition parameters for 20 hours and the spectra obtained are presented in Figure 65. For each sample analysed, the TBP-acid adduct, as seen previously, is observed at around -2 ppm. As previously mentioned with analogous Np-NO_3-TBP systems, due to the paramagnetic nature of the neptunium species, it might be expected that broad resonances are observed in the NMR spectra. However, what may be the Np-NO_3-TBP type complexation signal, observed around 28 ppm, is quite sharp. However, the broad resonance observed at around -25 ppm may also be the result of Np-NO_3-TBP type complexation. Despite minimal neptunium separation at lower aqueous HCl concentrations, what is thought to be the Np-Cl-TBP complexation signal (~ 28 ppm) is still observed, in both C1.Np and C2.Np samples. Previously reported is the ^{31}P NMR spectrum for the $[NpO_2Cl_2(Ph_3PO)_2]$ species where the complexation signal was observed at 15 ppm.[138] This signal was sharp and did not exhibit the characteristic broadening of a paramagnetic species.

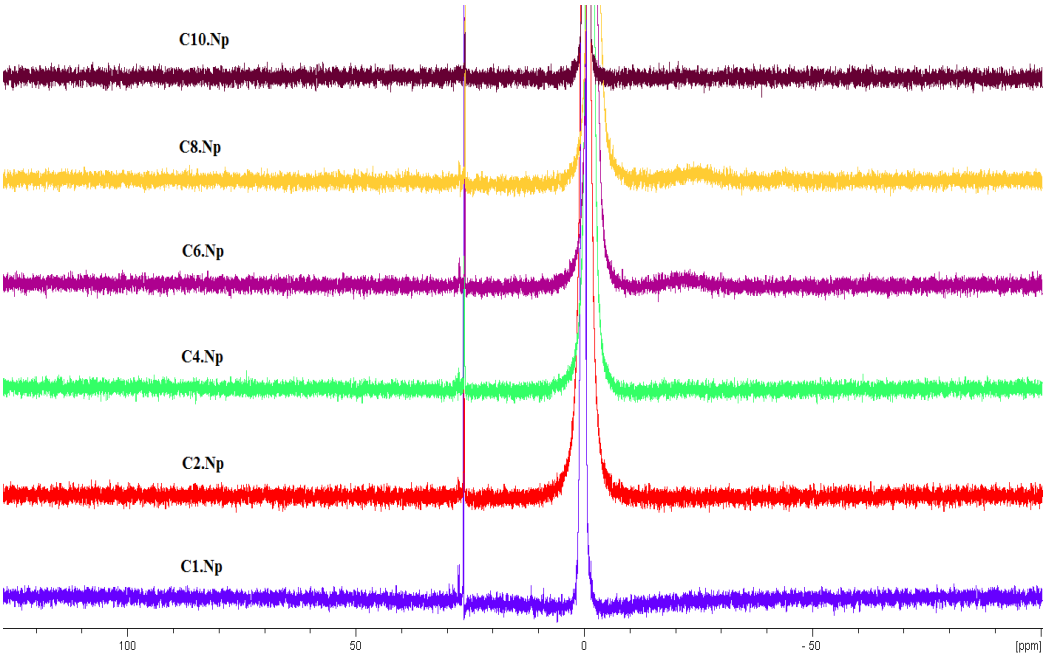

Figure 65: ^{31}P NMR spectra for the post extracted organic phases from samples C1.Np - C10.Np.

The NMR data presented here is notably similar to those data presented for samples N1.Np - N10.Np implying that the phosphorus signals due to Np-NO_3-TBP type complexation could be very similar chemical shifts. However, it is more reasonable to suggest that because of the prominence and broadness of the Cl-TBP (and NO_3-TBP) adduct signals, the Np-Cl-TBP signal may be shielded, and therefore is not able to be observed here.

EXAFS spectra were collected for pure (NpO_2^{2+}) (^{237}Np(VI), ~ 5.86 kBq, 0.5 mL, ~ 1.9 mM) in 5 M HCl extracted in to TBP-OK (30 % TBP by volume). The fitted R-space and k^3-space spectra, presented in Figure 66 are in good agreement with the $[NpO_2Cl_2(TBP)_2]$ moiety. The spectra were fitted using the axial oxygen atoms of the $(NpO_2)^{2+}$ species and two chloride atoms. The oxygen and phosphorus of the TBP moiety were also fitted, with the oxygen atoms of the phosphate group sat in the primary coordination shell. Table 34 outlines the parameters obtained from the fit.

Sample	Shell	Occupancy	σ^2	E_0 (eV)	R_i (Å)	R_f (Å)	ΔR (Å)
$(NpO_2)^{2+}$ extracted into 30 % TBP-OK from 5 M HCl. Fitted to $[NpO_2Cl_2(TBP)_2]$	Oyl	2.00	0.00118	7.378	1.7781	1.7207	0.0574
	Cl	2.00	0.00236		2.6986	2.6326	0.0660
	O(phos)	2.00	0.00168		2.4306	2.2745	0.1561
Amp = 0.863 R factor = 0.018 χ^2 = 16.723	P(phos)	2.00	0.00311		3.5250	3.7052	-0.1802

Table 34: Parameters obtained from EXAFS fits in k^3-space for $(NpO_2)^{2+}$ extracted into TBP-OK (30 % TBP by volume), from 5 M HCl. E_0 is the relative shift in ionization energy, Ri is the initial distance of the shell (Å) and R_f is the refined distance of the shell (Å). Statistics of fit (χ^2 and r-factor) and amplitude factor (Amp) provided.

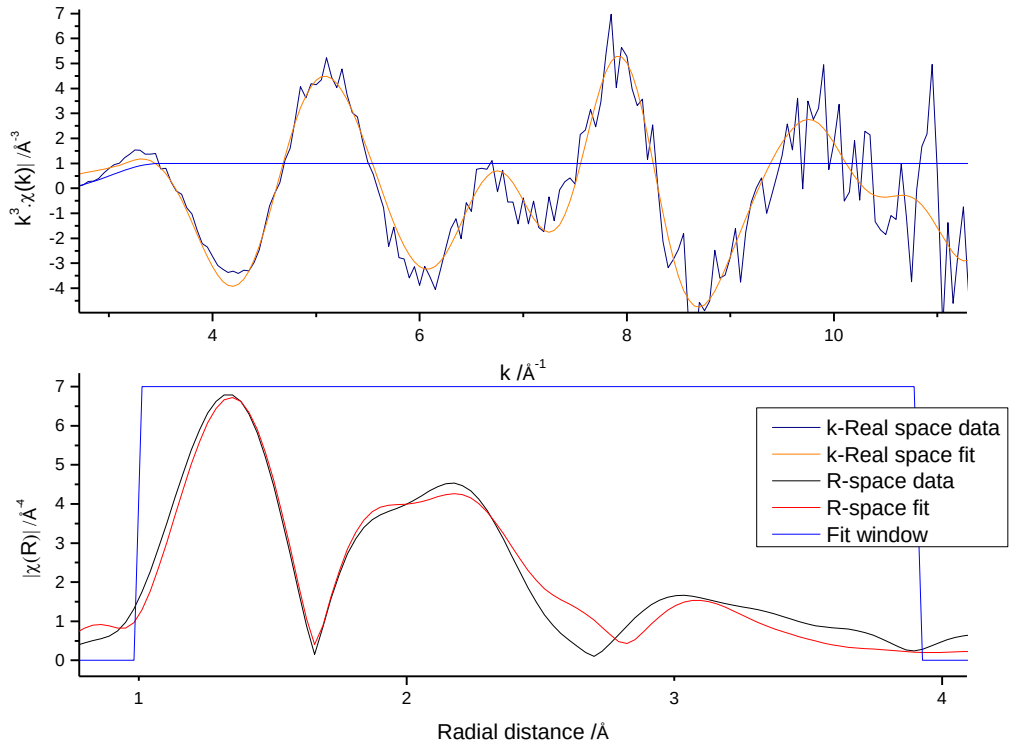

Figure 66: k^3-weighted χ(k)-function (top) and Fourier transform (bottom) of Np L_{III}-edge EXAFS data for $(NpO_2)^{2+}$ extracted into 30 % TBP-OK, from an initial aqueous phase consisting of 5 M HCl. Data were fitted to $[NpO_2Cl_2(TBP)_2]$.

5.8 Trace Level Neptunium Separated from Aqueous Nitric and Hydrochloric Acid

Neptunium was separated from aqueous mixtures of nitric and hydrochloric acid (1-9 and 9-1 M, respectively, 2 mL total) using TBP-OK (30 % TBP by volume). Samples C9:N1.Np - C1:N9.Np were spiked with Np (^{237}Np, Bq, 100 uL, 0.46 mM) and the resultant aqueous fraction (23.03 uM ^{237}Np) contacted with TBP-OK, as described in Section 4.6. Both aqueous and organic fractions, post-separation were analysed as detailed in Section 4.6. No third phases were observed in these samples.

The data presented in Table 35 and Figure 67 illustrate the distribution data for samples C9:N1.Np - C1:N9.Np. From the data presented, it is clear that the lowest distribution ratio for this data was observed for neptunium separated from equal concentrations of aqueous nitrate and chloride. Here, the highest distribution of

neptunium into the organic fraction, was observed for neptunium separated from aqueous fractions with a higher aqueous chloride concentration. The distribution data shown here is however, overall much lower than for neptunium separated from aqueous chloride systems only. Comparatively, neptunium separated from aqueous nitric acid in the absence of chloride ions was significantly lower than the data presented in Table 35 and Figure 67, indicating the presence of chloride in the aqueous fraction enhances the separation of neptunium under these conditions.

Sample	C9:N1 .Np	C8:N2 .Np	C7:N3 .Np	C6:N4 .Np	C5:N5 .Np	C4:N6 .Np	C3:N7 .Np	C2:N8 .Np	C1:N9 .Np
$[H^+]$ / M	10.00	10.00	10.00	10.00	10.00	10.00	10.00	10.00	10.00
$[Cl^-]$ / M	1.00	2.00	3.00	4.0	5.0	6.00	7.0	8.00	9.0
$[NO_3^-]$ / M	9.00	8.00	7.00	6.00	5.00	4.00	3.00	2.00	1.00
Distribution Ratio D	2.00	1.37	1.17	1.08	1.04	1.08	1.18	1.42	1.51
Log D	0.30	0.14	0.07	0.03	0.02	0.03	0.07	0.15	0.18

Table 35: Initial aqueous phase concentration and distribution ratio data for samples C1:N9.Np - C9:N1.Np.

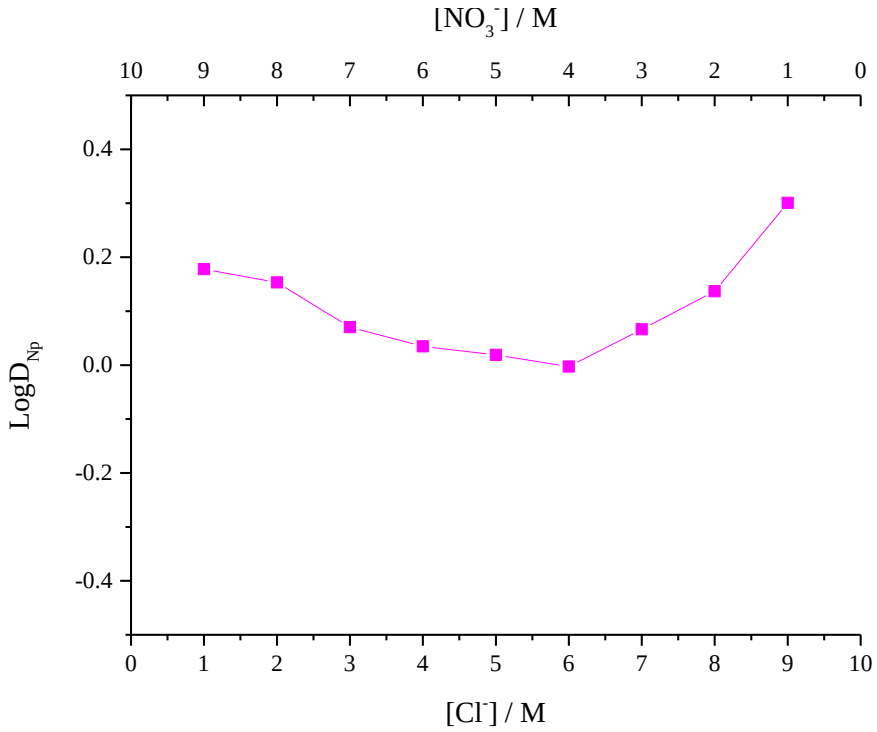

Figure 67: Distribution data as a function of acid concentration for samples C1:N9.Np - C9:N1.Np.

5.9 Neptunium (Np(VI)) Separated from Aqueous Nitric and Hydrochloric Acid

Neptunium(VI) hydroxide solid was synthesized in house via oxidation with perchloric acid (11.6 M). The resultant solid was dissolved into a mixed acid aqueous fraction (5 M HCl : 5 M HNO_3) (^{237}Np(VI), ~ 41 kBq, 2 mL, ~ 3.33 mM). The resultant aqueous fraction was further contacted with TBP-OK (30 % TBP by volume), mechanically agitated for approx. 15 minutes and centrifuged for full phase separation. Post extraction, an aliquot of each phase was taken for LSC analysis. The distribution ratio for neptunium separation in this system was calculated from LSC data obtained, as Section 4.6 describes.

An immediate UV/vis/nIR spectrum was taken of the resultant aqueous and organic fractions. The UV/vis/nIR data for the resultant organic fraction are presented in Figure 68. There is a large absorption at around 1200 nm indicative of Np(VI). There

is little Np(V) observed at around 980 nm indicating the dominance of Np(VI) in the organic fraction post-separation.

The distribution ratio for sample C5:N5.Np was calculated to be 30 which corresponded to ~ 95 % separation of the neptunium into the organic fraction. The mixed aqueous phase indicates that a higher neptunium separation is achieved than those observed for individual aqueous fractions of analogous concentration. A spectrum of the resultant aqueous fraction was obtained but did not show any significant peaks due to the high neptunium separation.

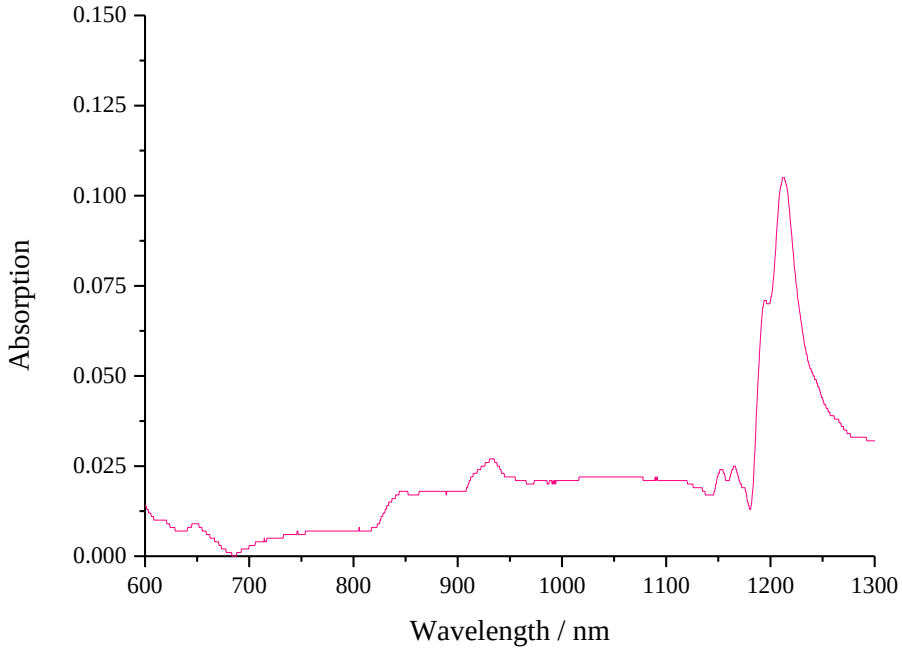

Figure 68: Vis/nIR spectra for resultant *organic* phases post extraction, for sample C5:N5.Np.

EXAFS spectra were collected at the ANKA beamline, Germany, for pure $(NpO_2)^{2+}$ (^{237}Np(VI), ~ 5.86 kBq, 0.5 mL, ~ 1.9 mM) separated from a 5 M HCl and 5 M HNO_3 aqueous mixture extracted in to TBP-OK (30 % TBP by volume). Although the organic phase for sample C5:N5.Np was observed to be predominantly Np(VI) before beam line analysis, both at Manchester and in Germany, once on the beam, this sample was seen to reduce immediately to Np(IV). Attempts to fit the EXAFS were not successful. Figure 69 illustrates the XANES plot for the organic phase post-

separation for sample C5:N5.Np, indicating the presence of Np(IV) through the absence of the shoulder in the XANES region. In contrast, the XANES spectrum obtained from the organic phase from sample C5.Np (Figure 70) clearly illustrates a shoulder in the XANES region, indicating the presence of the axial oxygens in the neptunyl species of either $[Np(V)O_2]^+$ or $[Np(VI)O_2]^{2+}$. The XANES spectrum presented in Figure 70 is similar to that obtained for the organic phases from both N7.2.Np and C5.Np samples where Np(VI) is the dominant Np oxidation state in this phase and both these spectra also display the characteristic shoulder due to the neptunyl moiety.

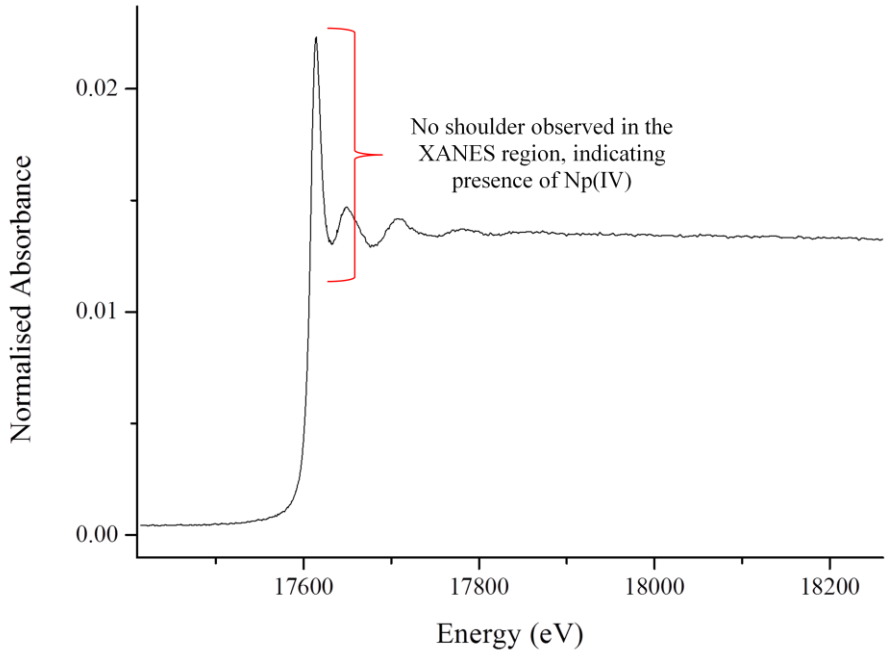

Figure 69: Normalised XANES spectra of the organic phase post extraction for sample C5:N5.Np.

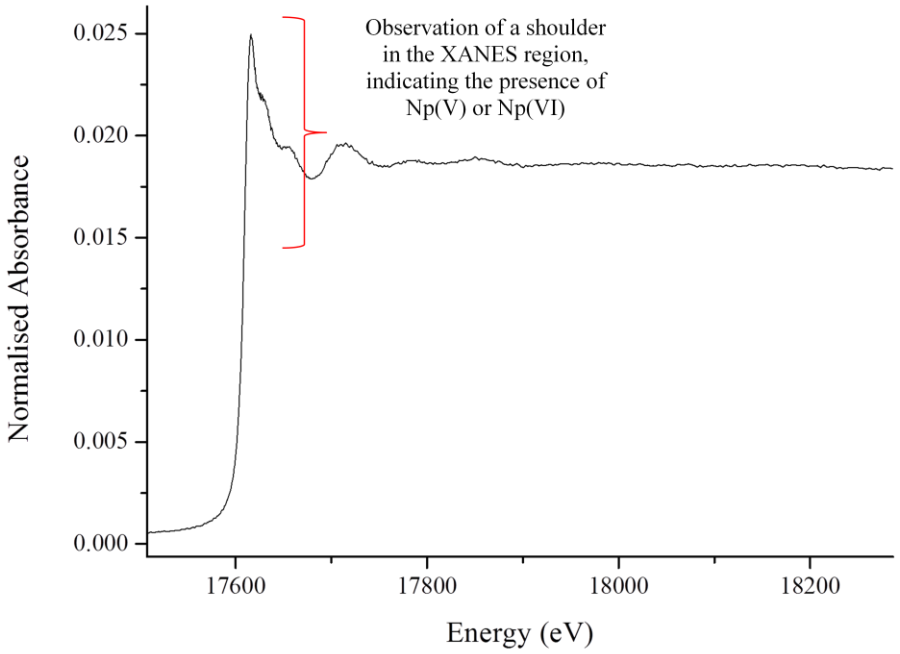

Figure 70: Normalised XANES spectra of the organic phase post extraction for sample C5.Np.

5.10 Trace Level Plutonium Separated from Aqueous Nitric Acid

It is well known that Pu is readily extracted in its 4+ state by TBP.[139] Pu extraction occurs via the following two complexes: $[Pu(NO_3)_4(TBP)_2]$ and $[Pu(OH)_2(NO_3)_2(TBP)_2]$.[140] For comparative purposes, the plutonium distribution ratios at different aqueous nitric acid concentrations, using standard PUREX methods were determined even though a substantial body of work on the extraction behaviour of these systems exists. Reports have suggested that an aqueous nitric acid concentration of around 8 M is required to separate the majority of plutonium before competition of the nitric acid for TBP moiety outweighs competition between the TBP and plutonium.[141] The concentration range for this work was therefore 6 - 10 M aqueous nitric acid concentration, namely samples N6.Pu - N10.Pu.

Aqueous nitric acid (6 - 10 M, 1.9 mL) was spiked with Pu (^{239}Pu(IV), 271 Bq, 100 uL, 4.94 uM) and the resultant aqueous fraction (24.69 uM ^{239}Pu) contacted with TBP-OK (30 % TBP by volume), mechanically agitated and centrifuged for full

phase separation. Both aqueous and organic fractions, post-separation were analysed using a Liquid Scintillation Counter (LSC) in order to determine the effectiveness of plutonium separation under these conditions. An aliquot of both aqueous and organic phases was taken and scintillation fluid (ScintSafe3, 10 mL) added. These samples were analysed for 30 minutes each and the results compared. Distribution ratio data was calculated based on the obtained LSC data, as described in Section 4.6.

From the data presented in Table 36, it is clear that the separation of plutonium from nitric acid increases as a function of increasing aqueous nitric acid concentration. The plot illustrated in Figure 71 depicts this trend pictorially. The distribution ratio for sample N10.Pu was calculated to be ~ 85, corresponding to almost 100 % separation of plutonium in to the organic fraction, under these conditions. The distribution ratio for samples N6.Pu is ~ 2 which was indicative of ~ 70 % plutonium separation. This confirms the extent of Pu^{4+} extraction at high nitric acid concentrations that has been previously established.

Sample	N6.Pu	N6.5.Pu	N7.Pu	N7.5.Pu	N8.Pu	N8.5.Pu	N9.Pu	N9.5.Pu	N10.Pu
$[HNO_3]$ / M	6.00	6.50	7.00	7.50	8.00	8.50	9.00	9.50	10.00
Distribution Ratio D	2.26	2.56	4.10	5.29	7.44	10.24	19.65	25.77	85.62
Log D	0.35	0.41	0.61	0.72	0.87	1.01	1.29	1.41	1.93

Table 36: Initial aqueous phase concentration and distribution ratio data for samples N6.Pu - N10.Pu.

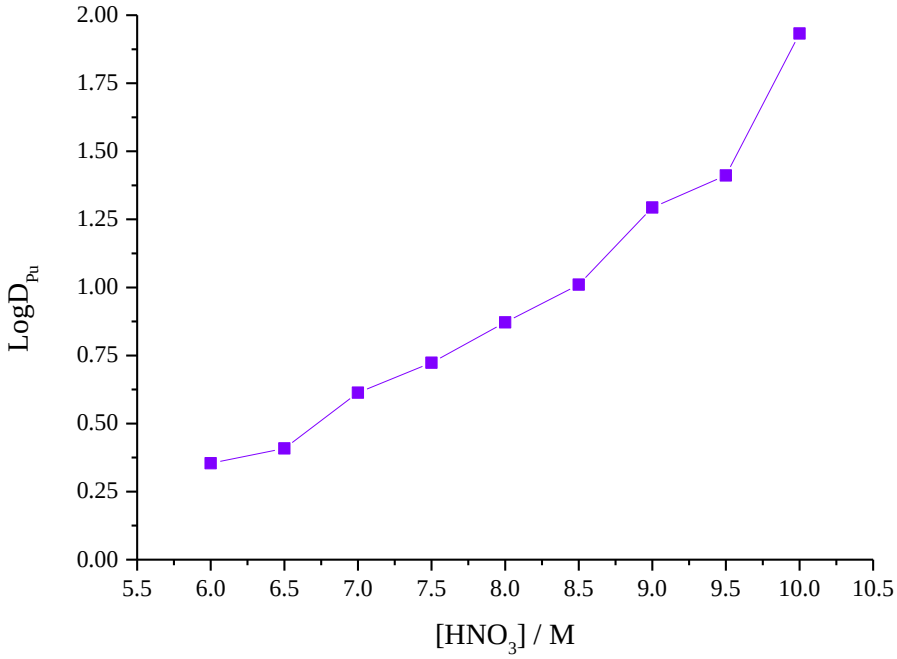

Figure 71: Distribution data as a function of acid concentration for samples N6.Pu - N10.Pu.

5.11 Trace Level Plutonium Separated from Aqueous Hydrochloric Acid

The extraction of Pu ions from HCl containing aqueous phases has not been well studied previously, however it has been suggested that complexes such as $[PuCl_4(TBP)_4]$, $[PuCl_4(TBP)_2]$ and $[PuCl_4(TBP)]$ may form on contact with Cl^- and TBP in solution.[142] It has been proposed that in HCl solutions, Pu(III) undergoes nearly complete α-particle induced oxidation to Pu(IV). Also, higher aqueous chloride concentrations will facilitate higher proportions of Pu(IV).[92] Previously reported data states that a distribution ratio of 10 is achieved using 5 M aqueous hydrochloric acid separated into TBP-OK (30 % by volume).[143] Work presented here provides a more comprehensive study of Pu^{4+} extraction behaviour by TBP from aqueous phases containing HCl than has been previously reported. NMR studies were performed to determine possible organic phase speciation of these systems, and whether it is related to extraction behaviour. EXAFS studies were not performed due to time constraints, but are necessary to corroborate any proposed organic phase plutonium speciation.

Aqueous hydrochloric acid (6 - 10 M, 1.9 mL) was spiked with Pu (^{239}Pu(IV), 271 Bq, 100 uL, 4.94 uM) and the resultant aqueous fraction (24.69 uM ^{239}Pu) contacted with TBP-OK (30 % TBP by volume), as described in Section 4.2. Both aqueous and organic fractions, post-separation were analysed as detailed in Section 4.6. A third phase was observed in samples C7.Pu - C10.Pu. The volume of the third phase, when obtained, was immeasurable in terms of the desired accuracy as was observed in other examples (e.g. Section 4.7) and therefore the distribution ratios are calculated as a comparison of the resultant aqueous and overall organic fractions. Analysis via LSC was done immediately after phase contact.

Plutonium separated from aqueous hydrochloric acid showed an overall increase in the distribution ratio as a function of increasing aqueous hydrochloric acid concentration. The data presented in Table 37 and Figure 72 illustrates the change in distribution ratio for samples C6.Pu - C10.Pu. Sample C10.Pu gave an overall distribution ratio of ~ 236 which corresponded to > 99 % separation of plutonium in to the overall organic fraction (both light and heavy). For sample C6.Pu, ~ 74 % of the plutonium was separated into the organic fraction. The distribution ratios observed here are overall significantly higher than those observed for analogous nitrate containing systems, implying that plutonium is effectively separated in the presence of chloride.

Sample	C6.Pu	C6.5.Pu	C7.Pu	C7.5.Pu	C8.Pu	C8.5.Pu	C9.Pu	C9.5.Pu	C10.Pu
[HCl] / M	6.00	6.50	7.00	7.50	8.00	8.50	9.00	9.5	10.00
Distribution Ratio D	2.76	3.92	4.70	6.69	8.80	11.33	27.03	128.51	235.54
Log D	0.44	0.59	0.67	0.83	0.94	1.05	1.43	2.11	2.37

Table 37: Initial aqueous phase concentration data and distribution ratio data for samples C6.Pu - C10.Pu.

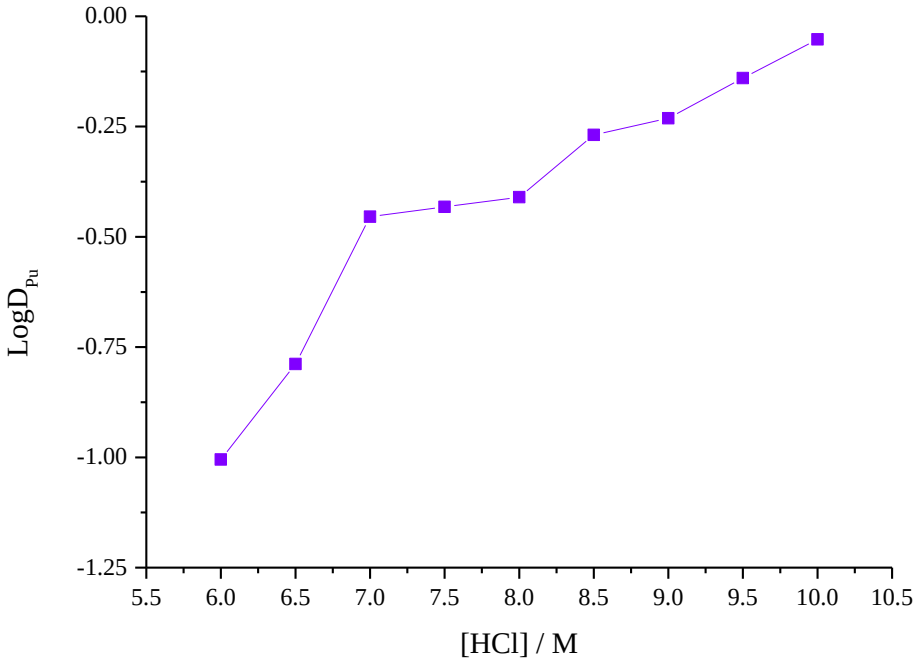

Figure 72: Distribution data as a function of acid concentration for samples C6.Pu - C10.Pu.

5.12 Trace Level Plutonium Separated from Aqueous Nitric and Hydrochloric Acid

Plutonium was separated from aqueous mixtures of nitric and hydrochloric acid (1-9 and 9-1 M, respectively, 2 mL total) using TBP-OK (30 % TBP by volume). Samples C9:N1.Pu - C1:N9.Pu were spiked with Pu (^{239}Pu, 272 Bq, 100 uL, 5 uM) and the resultant aqueous fraction (0.25 uM ^{239}Pu) contacted with TBP-OK, as described previously in Section 4.2. Both aqueous and organic fractions, post-separation were analysed by the same approach described in Section 4.6. No third phases were observed in these samples.

For plutonium separated from mixed nitrate and chloride aqueous fractions under these conditions, there is a preference for plutonium distribution into the organic fraction from higher aqueous nitrate concentrations. The data presented in Table 38 and Figure 73 indicates that plutonium is effectively separated under these conditions. The distribution ratios presented here correspond to over 90 % separation

of plutonium into the organic fraction for each samples analysed. The distribution ratios presented in Table 38 are overall lower than those observed for plutonium separated from the analogous single acid systems. A distribution ratio of 9.34 was observed for sample C9:N1.Pu, in comparison to a distribution ratio of 27.03 observed for sample C9.Pu. the distribution ratios observed for plutonium separated from aqueous nitric acid only, were also observed to be higher overall than the distribution ratio data calculated for the samples presented in Table 38.

Sample	C1:N9 .Pu	C2:N8 .Pu	C3:N7 .Pu	C4:N6 .Pu	C5:N5 .Pu	C6:N4 .Pu	C7:N3 .Pu	C8:N2 .Pu	C9:N1 .Pu
[H+] / M	10.00	10.00	10.00	10.00	10.00	10.00	10.00	10.00	10.00
$[Cl^-]$ / M	1.00	2.00	3.00	4.0	5.0	6.00	7.0	8.00	9.0
$[NO_3^-]$ / M	9.00	8.00	7.00	6.00	5.00	4.00	3.00	2.00	1.00
Distribution Ratio D	14.60	10.30	9.29	9.14	9.32	9.56	9.32	9.11	9.34
Log D	1.16	1.01	0.97	0.96	0.97	0.98	0.97	0.96	0.97

Table 38: Initial aqueous phase concentration and distribution ratio data for samples C1:N9.Pu - C9:N1.Pu.

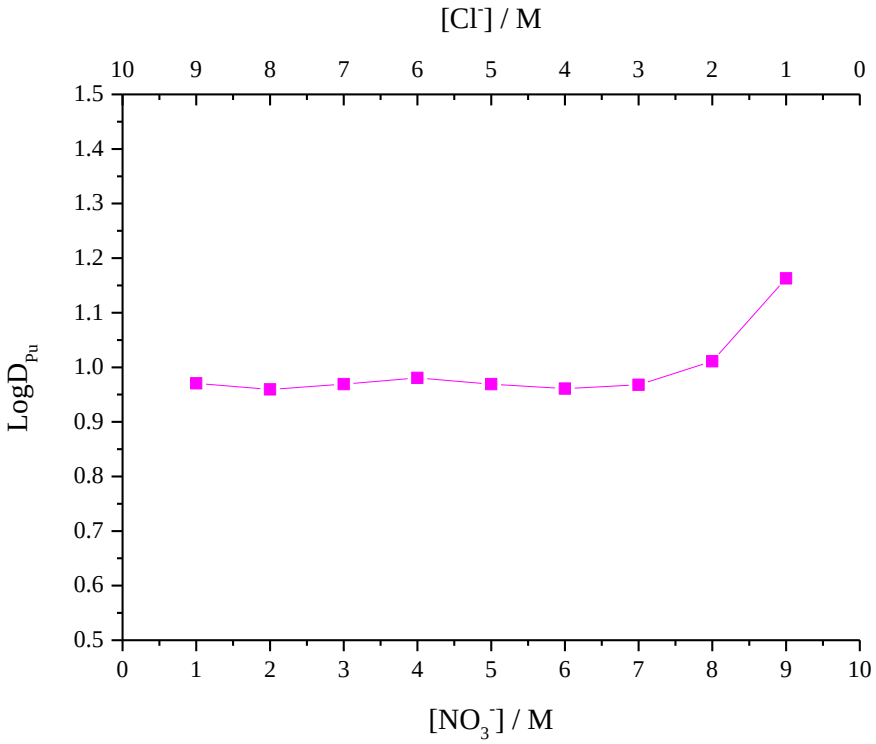

Figure 73: Distribution data as a function of acid concentration for samples C1:N9.Pu - C9:N1.Pu.

5.13 Plutonium Separated from Aqueous Nitric and/or Hydrochloric Acid - An NMR study

PUREX type plutonium separations were carried out at the INE-KIT, Karlsruhe, Germany. A plutonium solution (^{239}Pu(IV), 41.17 MBq, 0.75 mL, 100 mM), in aqueous nitric acid, was separated into 10 vials (4.12 MBq, ~ 10 mM Pu(IV)). Each vial was heated to dryness and the solid redissolved in to various concentrations of aqueous acid (nitric acid, hydrochloric acid and mixtures of both) (0.75 mL). Each aqueous fraction was contacted with TBP-OK (30 % TBP by volume), agitated and centrifuged for full phase separation. The organic fractions were analysed via ^{31}P proton decoupled NMR spectroscopy at various temperatures.

The ^{31}P NMR spectra recorded for the resultant organic phase, post-separation for sample N2.Pu is presented in Figure 74. The NMR spectra for sample N2.Pu at ~ 25 ^{o}C, show a broad chemical signal from approx. -25 to 25 ppm. This broad signal NMR spectrum recorded at room temperature (RT) could be the result of the

paramagnetism of the Pu(IV) species, as well as fast ligand exchange within the extracted species. As previously observed, this single signal is likely the HNO_3-TBP adduct. However, the Pu-HNO_3-TBP complexation signal may potentially be observed at a similar chemical shift to the HNO_3-TBP adduct, and could indicate the ligand exchange has been slowed within the extracted plutonium complex. At 25 ^{o}C, there are no additional signals observed in the ^{31}P NMR spectrum for sample N2.Pu. As the temperature is decreased further to -50 °C, the observed ^{31}P signal in the NMR spectrum presented in Figure 75, becomes sharper and two resonances emerge at approximately -1 and 0 ppm. It is likely that the observed broadened signals are representative of the TBP.HNO_3 solvate (~0 ppm) and a Pu(IV)-NO_3-TBP type complex (*i.e.* $[Pu(TBP)_2(NO_3)_4]$).

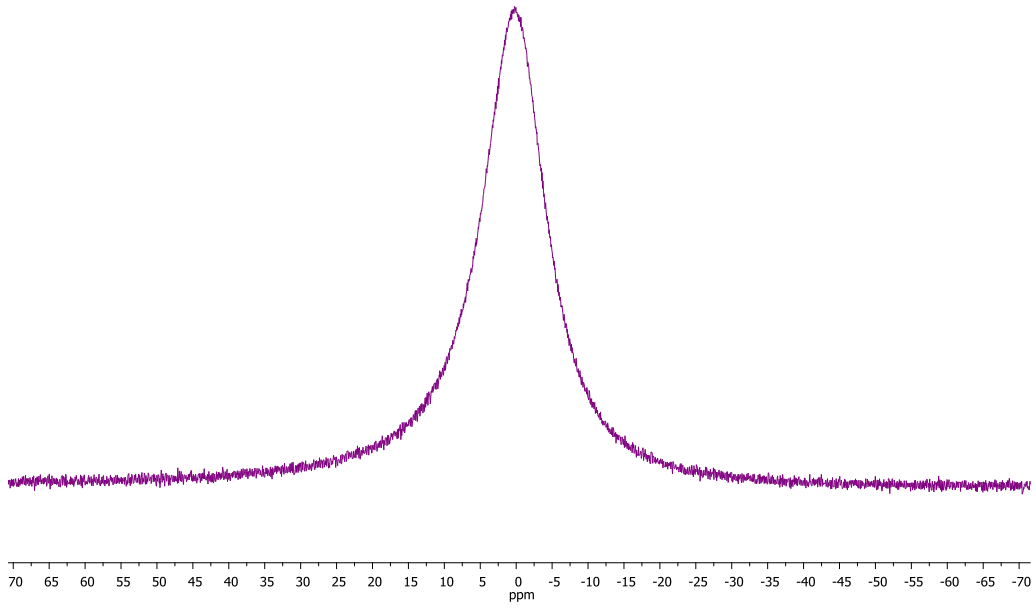

Figure 74: ^{31}P NMR spectrum of the post separated organic phase for sample N2.Pu at 25 ^{o}C.

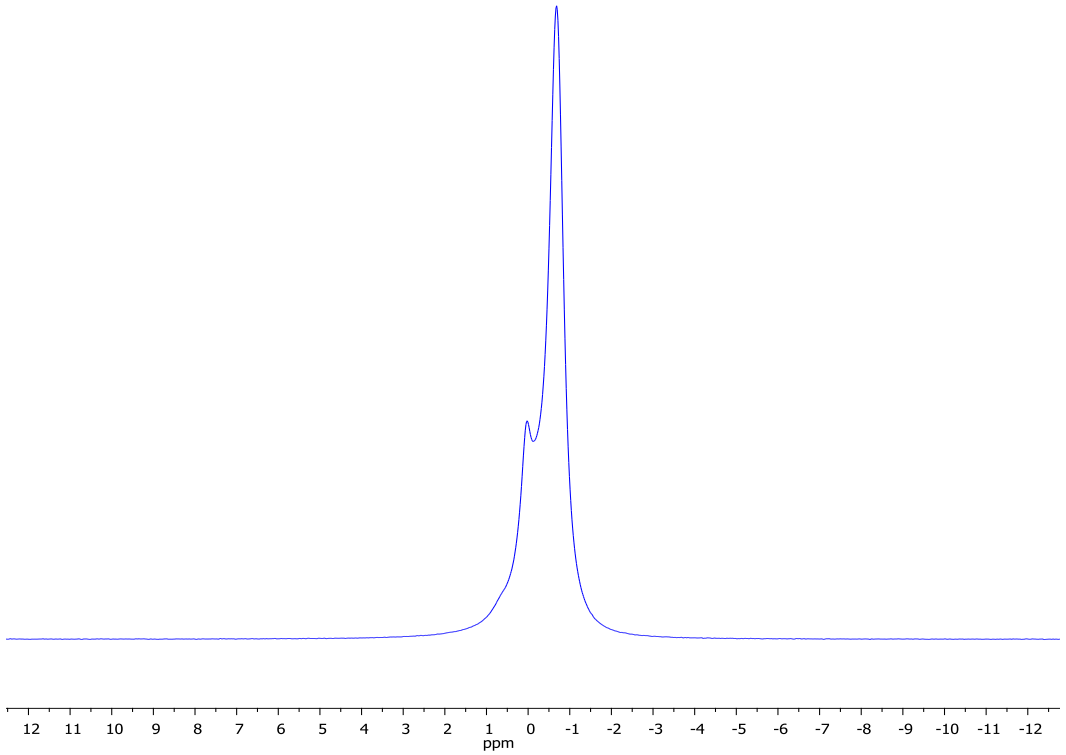

Figure 75: ^{31}P NMR spectrum of the post separated organic phase for sample N2.Pu at -50 ^{o}C.

The ^{31}P NMR spectrum recorded for a system with Pu(IV) ions in aqueous nitric acid (15 M) (sample N15.Pu), Figure 76, show a broadened resonance at ~ -0.5 ppm for the organic phase spectrum, recorded at 25 ^{o}C, post-separation. The spectrum recorded for the organic fraction for sample N15.Pu at -50^{o}C, Figure 77, has a sharper signal with an additional shoulder seen at ~ -1 ppm, possibly indicating the presence of a Pu(IV)-NO_3-TBP type complex. Similar to the NMR spectra recorded for sample N2.Pu as described previously, it is likely that both TBP.HNO_3 and Pu(IV)-NO_3-TBP complexes are formed in these systems, as Pu(IV) has shown to separate effectively in PUREX style systems. It is possible that the differences observed in the NMR spectra between the two different acid concentrations is due to varying quantities of HNO_3/NO_3 or Pu(IV) ions extracted in to the resultant organic fraction.

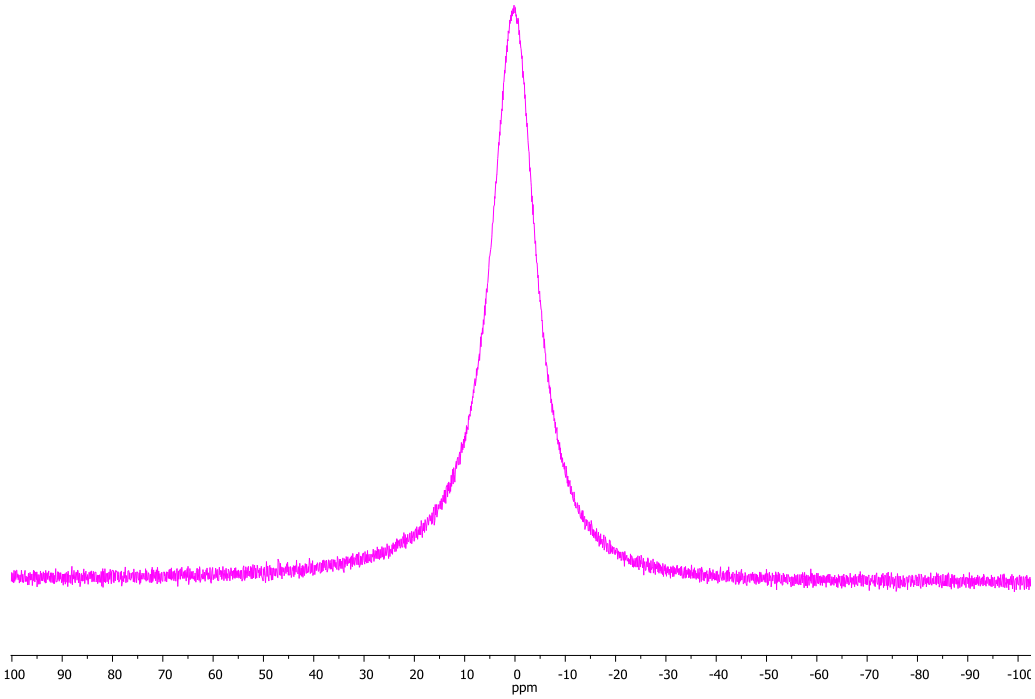

Figure 76: ^{31}P NMR spectrum of the post separated organic phase for sample N15.Pu at 25 ^{o}C.

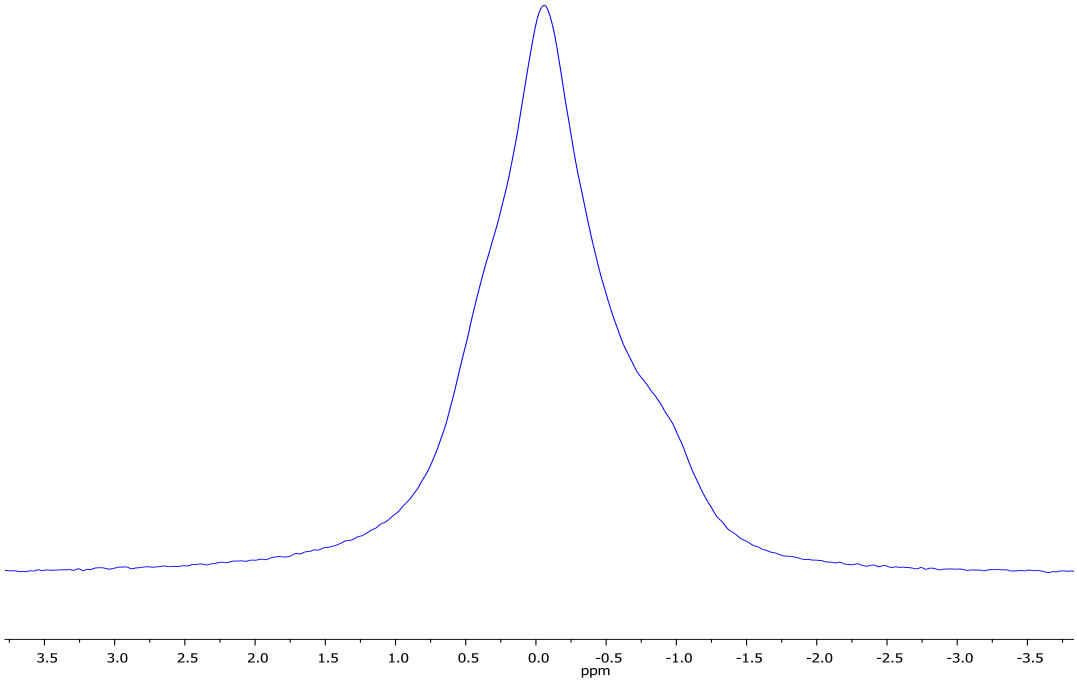

Figure 77: ^{31}P NMR spectrum of the post separated organic phase for sample N15.Pu at -50 ^{o}C.

The ^{31}P NMR spectra recorded for the resultant organic phase, post-separation for the sample C2.Pu at RT (25 ^{o}C) and - 50 ^{o}C are presented in Figures 78 and 79 respectively. The NMR data presented in Figure 78 show a single chemical signal from approx. 5 to 0 ppm. This is slightly broader than the signal previously observed for the HCl-TBP adduct at ~ -2 ppm. This broadened signal shown in the NMR spectrum recorded at room temperature (RT), could be the result of the paramagnetism from the Pu(IV) present, as well as potentially fast TBP exchange between the adduct and the Pu extracted species. The NMR spectrum recorded at - 50 ^{o}C displays a single signal which is broader compared to the room temperature spectrum, potentially implying TBP exchange has been slowed further. However, no discrete NMR signal is observed that can be assigned to an extracted Pu complex from sample C2.Pu.

The ^{31}P NMR spectrum of the organic phase from sample C11.Pu at room temperature, presented in Figure 80, shows again only one signal at ~ -1 ppm assigned to the HCl-TBP adduct. The corresponding NMR spectrum recorded at - 50 ^{o}C (Figure 81) shows two clear signals; one at ~ 0 ppm due to the HCl-TBP adduct which is sharper than the signal obtained at RT and a further signal observed at -1.8 ppm. This additional signal is most likely indicative of a Pu-Cl-TBP type species, such as $[PuCl_4(TBP)_2]$ or $[PuCl_4(TBP)_4]$ or other chemically feasible Pu-Cl-TBP type moieties. The observation of a ^{31}P NMR signal due to an extracted Pu complex from an aqueous phase with 11 M HCl but not from a 2 M HCl aqueous phase is most probably due to a higher concentration of extracted Pu in sample C2.Pu relative to that in sample C2.Pu. This is confirmed in the low concentration Pu studies where generally Pu extraction increases with increasing aqueous HCl concentration.

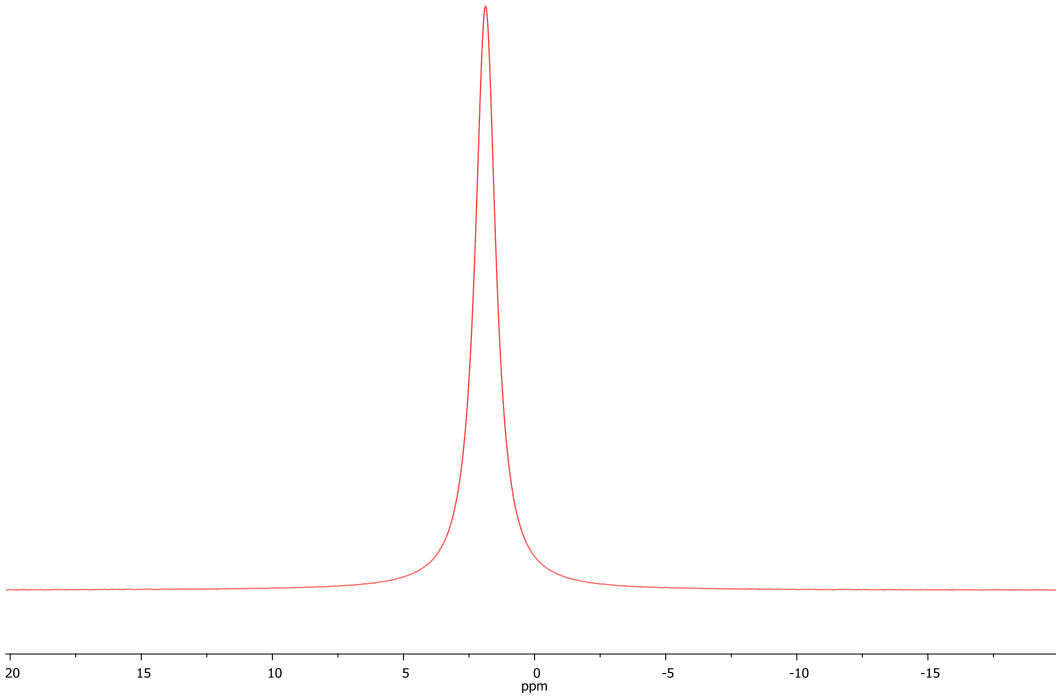

Figure 78: ^{31}P NMR spectrum of the post separated organic phase for sample C2.Pu at 25 ^{o}C.

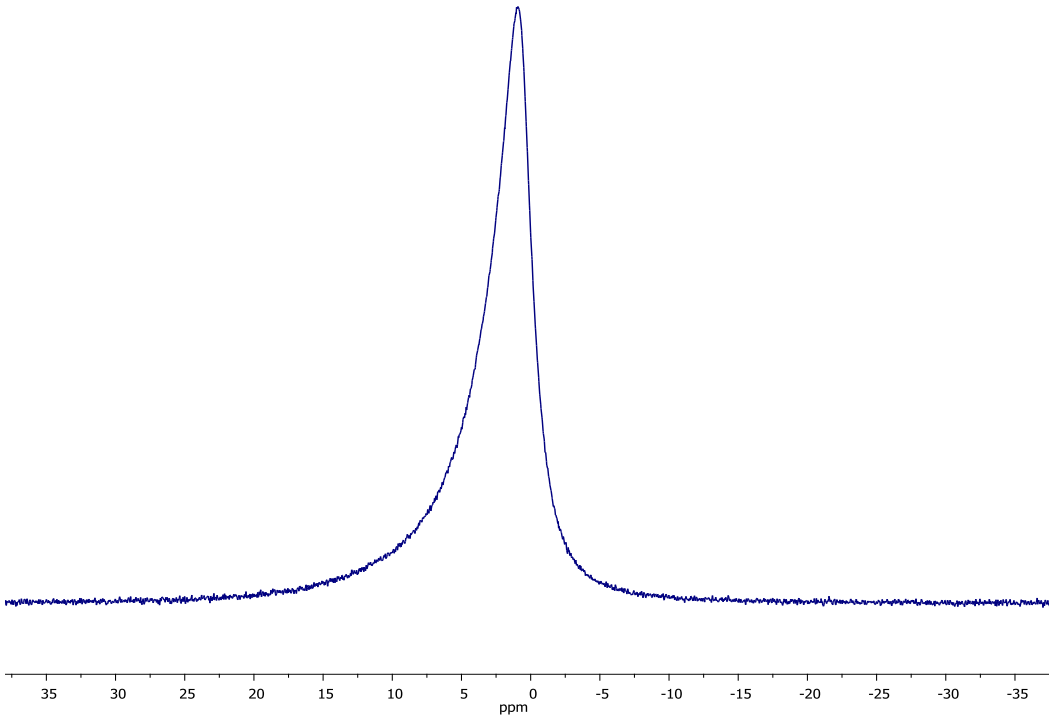

Figure 79: ^{31}P NMR spectrum of the post separated organic phase for sample C2.Pu at -50 ^{o}C.

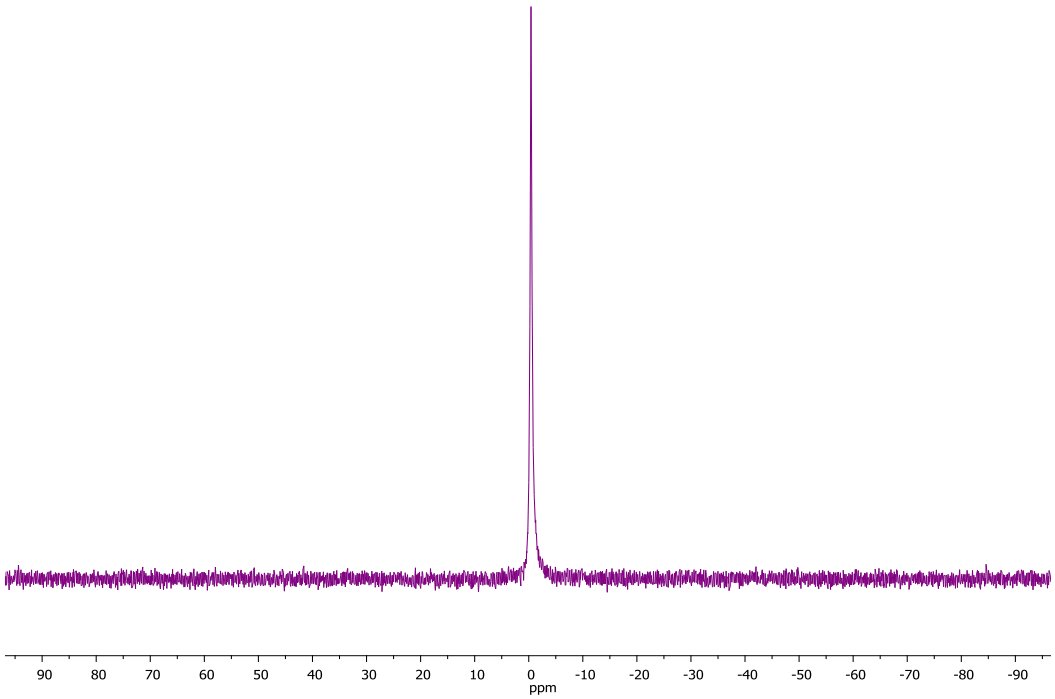

Figure 80: ^{31}P NMR spectrum of the post separated organic phase for sample C11.Pu at 25 ^{o}C.

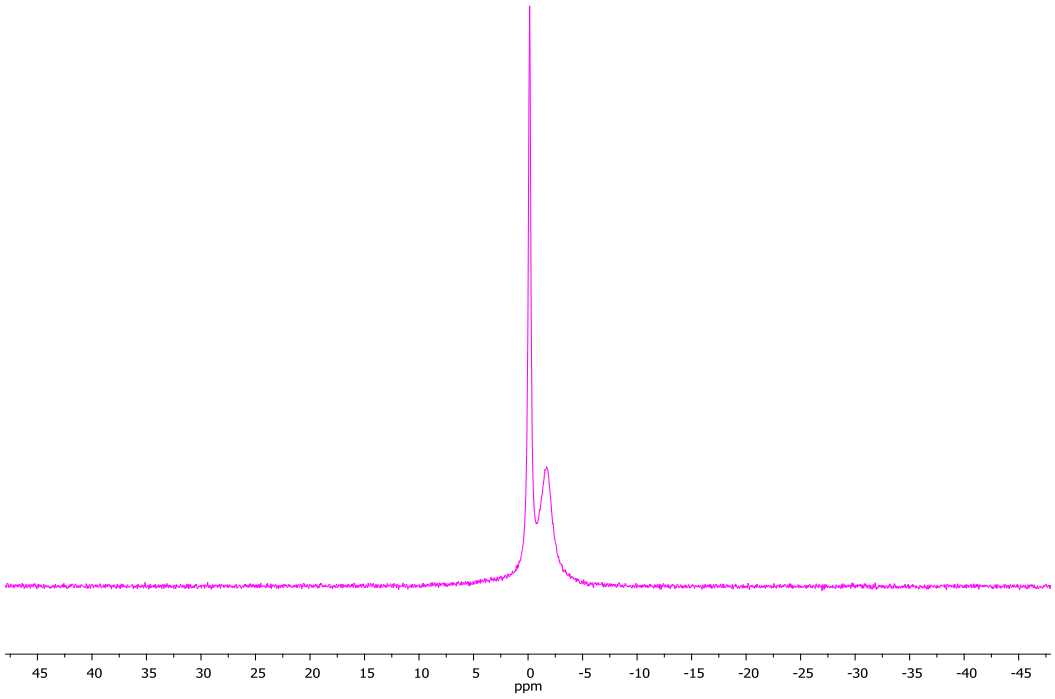

Figure 81: ^{31}P NMR spectrum of the post separated organic phase for sample C11.Pu at -50 ^{o}C.

The ^{31}P NMR spectra for plutonium separated from mixed nitric and hydrochloric acid aqueous phases were acquired. Each Pu(IV) (4.12 MBq, ~ 10 mM Pu(IV)) containing aqueous fraction was contacted with TBP-OK (30 % TBP by volume), agitated for approx. 15 minutes and centrifuged for full phase separation. The resultant organic fractions were used for NMR analysis.

The ^{31}P NMR spectrum measured for the separation of Pu(IV) ions from an aqueous mixed HNO_3 (2 M) and HCl (8 M) phase (sample C8:N2.Pu) shows a single signal at approximately 5 ppm for the spectrum recorded at 25 °C (Figure 82). This signal is shifted downfield when compared to both the hydrochloric and nitric single acid systems at room temperature, which may indicate that a different, dominant species is being formed in the solvent fraction. Although there may be a number of possible TBP species in solution, only a single signal is observed.

The most likely explanation of this is the paramagnetic nature of the Pu(IV) shielding the additional signals, in combination with the dominance of the TBP-acid adduct resonance which is vast excess. However, previous trace level studies indicate a lower distribution of Pu from aqueous chloride containing fractions which may indicate the absence of a signal in the NMR spectrum. The NMR spectrum recorded at - 50 ^{o}C for sample C8:N2.Pu, shows a relatively sharp resonance at -0.2 ppm and a resonance at -0.4 ppm that is resolved upon the intense signal at -0.02 ppm, as illustrated in Figure 83. The signal at -0.2 ppm may be representative of the $TBP.HNO_3$ or TBP.HCl solvate and the signal at -0.4 ppm is most likely due to a complexed Pu(IV)-X-TBP species (where X = NO_3^- or Cl^-). The decrease in the temperature of the system is likely to have caused the observed sharpening of the signal and the peak splitting into two resonances, due to the slowed ligand exchange at lower temperatures.

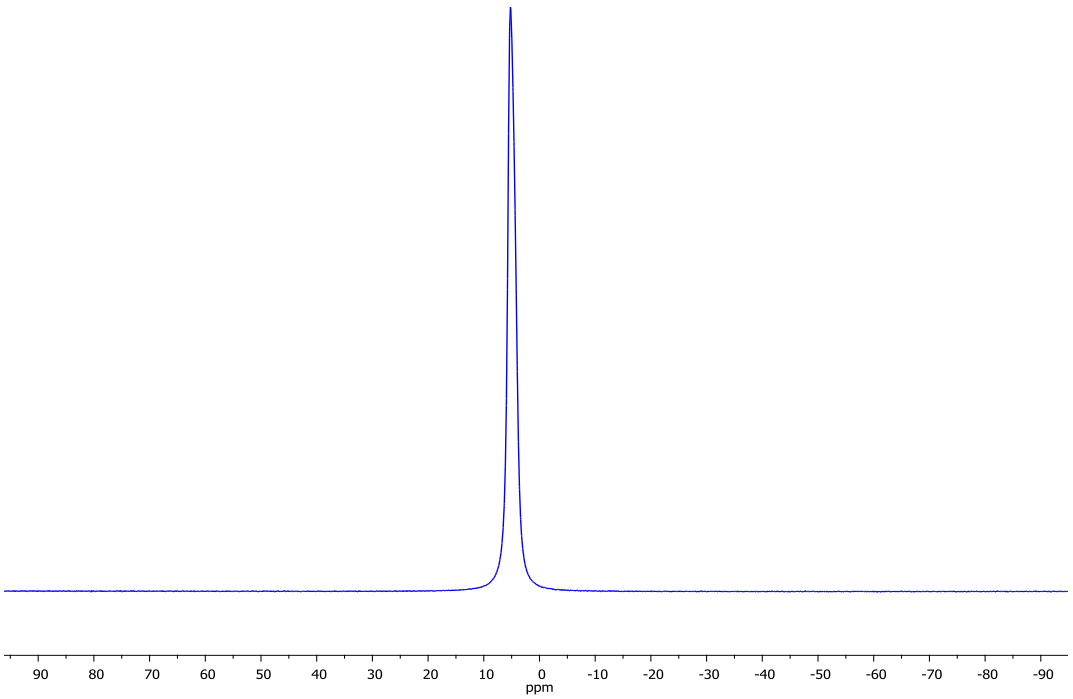

Figure 82: ^{31}P NMR spectrum of the post separated organic phase for sample C8:N2.Pu at 25 ^{o}C.

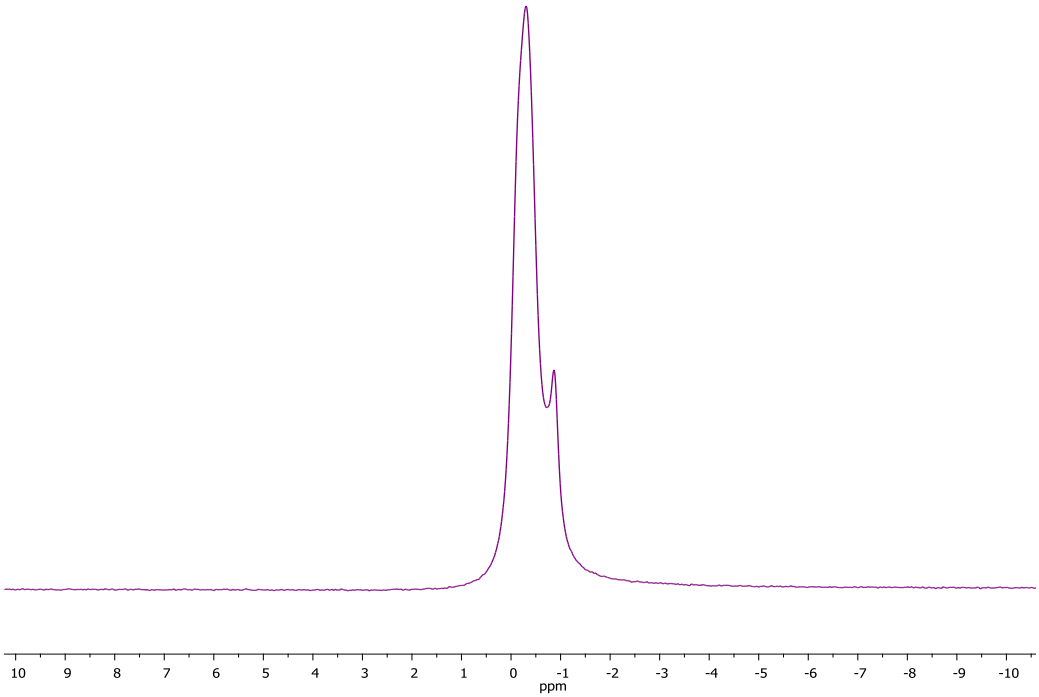

Figure 83: ^{31}P NMR spectrum of the post separated organic phase for sample C8.N2.Pu at -50 ^{o}C.

The ^{31}P NMR spectrum recorded of the organic phase at RT, post extraction from an aqueous phase containing Pu(IV) ions in 2 M HCl and 8 M HNO_3 shows a sharp signal at approximately - 2.5 ppm, which is overlapped by a broadened signal that is centred at -1 ppm, as detailed in Figure 84. The sharp signal is likely due to a TBP solvate, either TBP.HNO_3 or TBP.HCl (or a mixture of both) and the broadened signal may represent an extracted Pu(IV)-TBP containing complex. It is expected that the majority of the extracted complex will be a nitrate containing species (due to higher nitric acid concentration in the initial aqueous phase) but there may also be some extracted chloride containing complexes. The NMR spectrum recorded at - 50 °C for sample C2:N8.Pu, Figure 85, details a sharpened signal at -2.5 ppm, likely to be a TBP solvate (TBP.HNO_3/TBP.HCl); the additional chemical signal, at around -1 ppm, is likely to be an extracted Pu(IV) containing complex. There may be some mixed anion complexes formed in the organic phase *e.g.* Pu(IV)-TBP-NO_3-Cl, that undergo ligand exchange with all the Pu complexes present in this phase which is a possible reason for the obtained spectra being different from the single acid systems at both - 20 and - 50 °C.

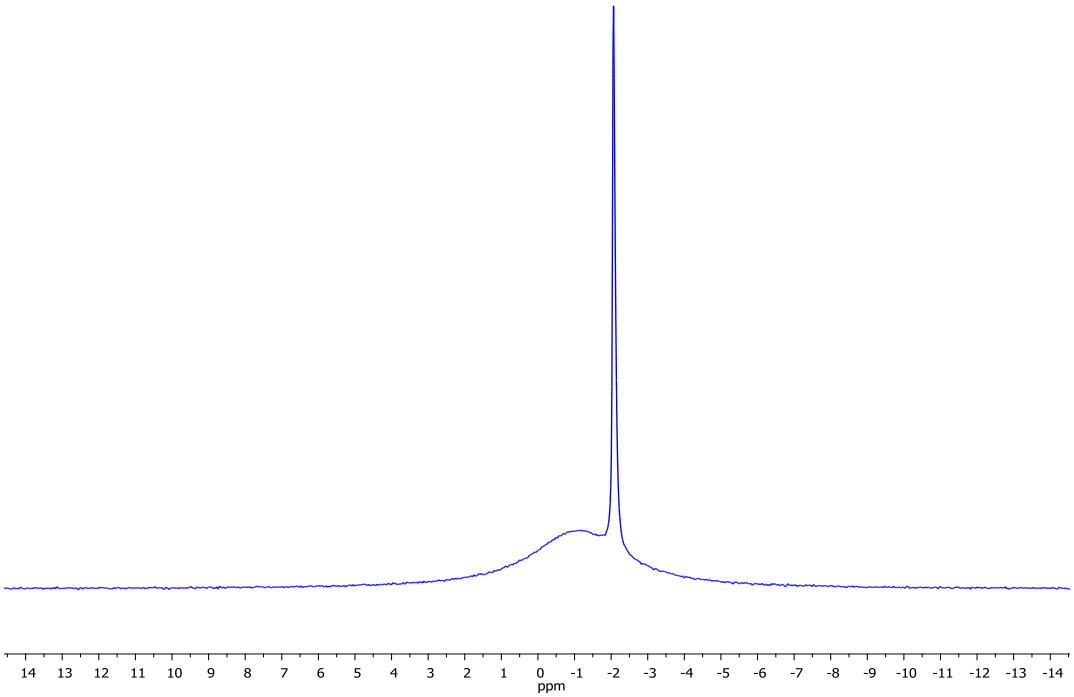

Figure 84: ^{31}P NMR spectrum of the post separated organic phase for sample C2:N8.Pu at RT.

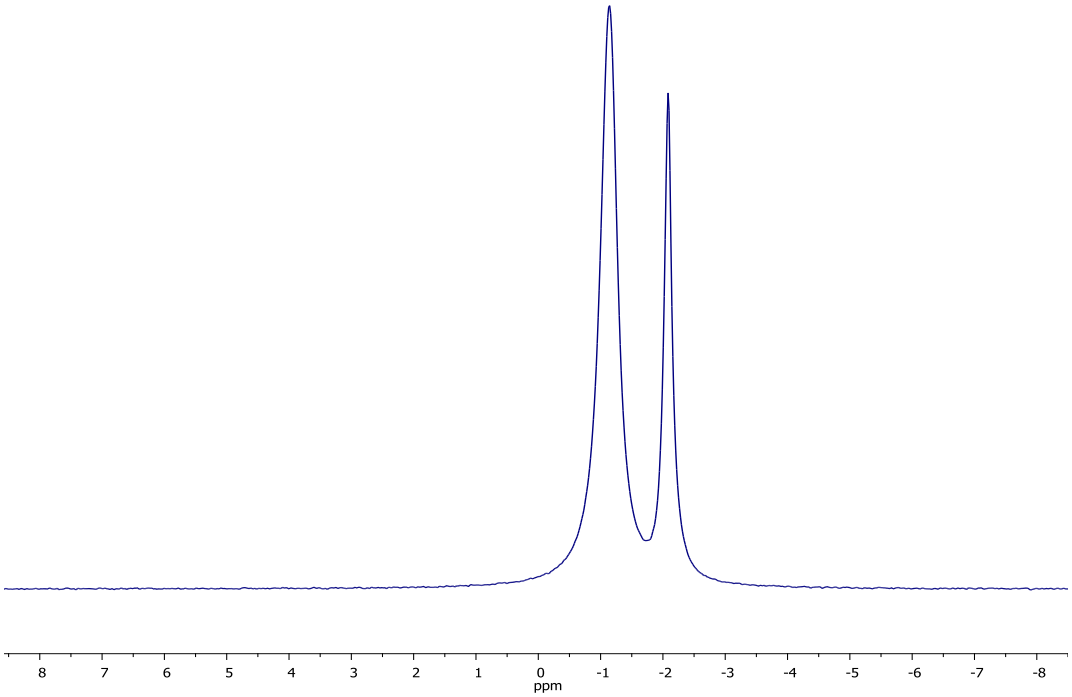

Figure 85: ^{31}P NMR spectrum of the post separated organic phase for sample C2:N8.Pu at -50 ^{o}C.

6 Investigating Aspects of the Proposed GANEX Concept

6.1 Introduction

Whilst the PUREX reprocessing systems has served the nuclear industry worldwide for many years, it is now favourable to develop new reprocessing systems that not only separate uranium and plutonium, but also the minor actinides. The Grouped ActiNide EXtraction (GANEX) process has been proposed in which the recycling of the actinides, uranium through curium occur in a homogenous procedure. The premise of the GANEX umbrella is to reduce the amount and radiotoxicity of the generated nuclear waste for improved and safer geological disposal. The recovery of actinides from spent nuclear fuel is also necessary for fuel fabrication for use in Generation IV (fast) reactors, or could be transmuted at dedicated facilities.[48]

In the "first cycle" the bulk uranium is removed using a monoamide type ligand. The "second cycle" extracts the remaining actinides and lanthanides into the organic fraction using a specific solvent system followed by selective back extraction of the actinides. Various solvent systems have been investigated by several institutions for use in this separation with differing outcomes. However for the purpose of this work, the use of N,N N',N' - tetraoctyl diglycolamide (TODGA) will be predominantly used as it has shown promise for the extraction of trivalent lanthanide and actinide ions as well as tetravalent actinide ions.[49] The use of TODGA alone however, leads to low metal loading capacities so it has therefore been suggested that the use of phase modifiers are employed to increase the metal loading capabilities and also to reduce the potential formation of a third phase. Tributyl phosphate (TBP), 1-octanol and N,N'-dimethyl-N,N'-dioctylhexylethoxymalonamide (DMDOHEMA) (Figure 102) have all been suggested as suitable phase modifiers by the European funded ACSEPT project.[49] The flow sheet associated with this work has been labelled "EURO-GANEX" (Figure 86) to differentiate between this particular flow sheet and others based on similar principals.

Figure 86 illustrates the proposed EURO-GANEX flow sheet after the "first cycle" has occurred in which the bulk uranium is removed by N,N-di(2-ethylhexyl)isobutyramide (DEHiBA) (Figure 87). The "second cycle" solvent fraction is treated to remove any separated fission products before undergoing a scrubbing to strip the transuranic actinides (TRU) using, in this flow sheet, a BTP type ligand. The BTP type ligands (see Section 1.6.2) are selective to trivalent actinides over trivalent lanthanides and can also strip Pu(IV). Neptunium speciation has been deemed complex in these systems and it is therefore necessary to add reducing agents (here, acetohydroxamic acid (AHA) is favoured) to force the reduction of Np(VI) to Np(IV) and Np(V).[49] The lanthanides are further stripped using glycolic acid. It is hoped that the solvent phase can be recycled.

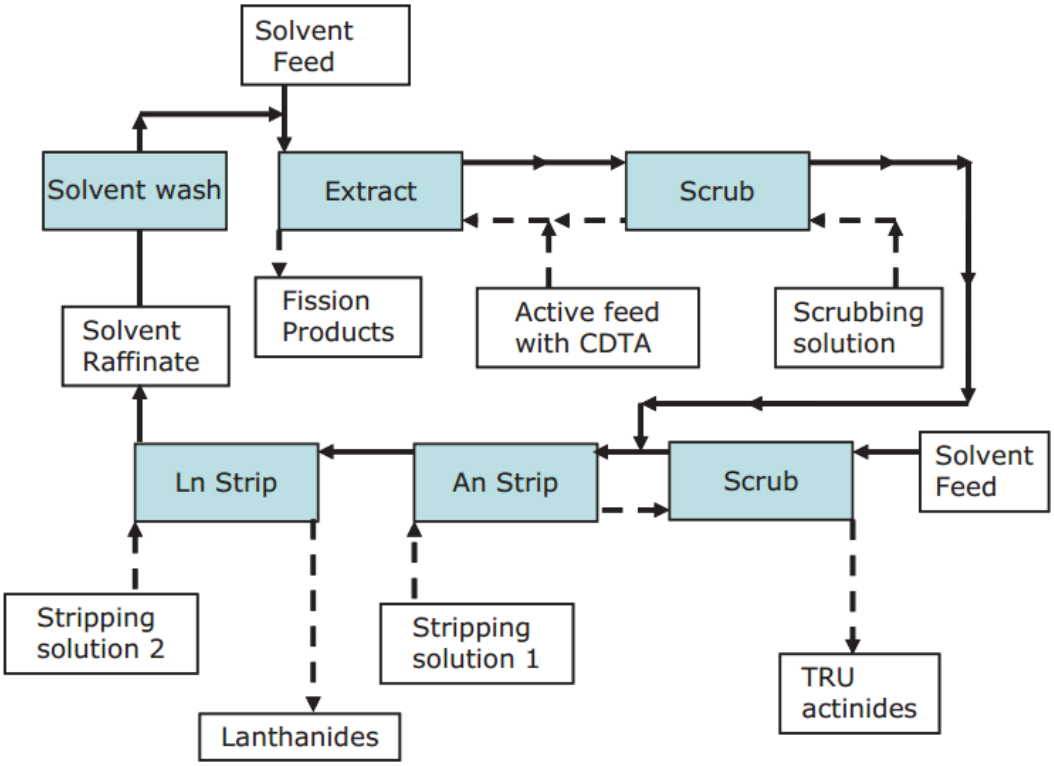

Figure 86: EURO-GANEX flow sheet after initial uranium separation cycle.[49]

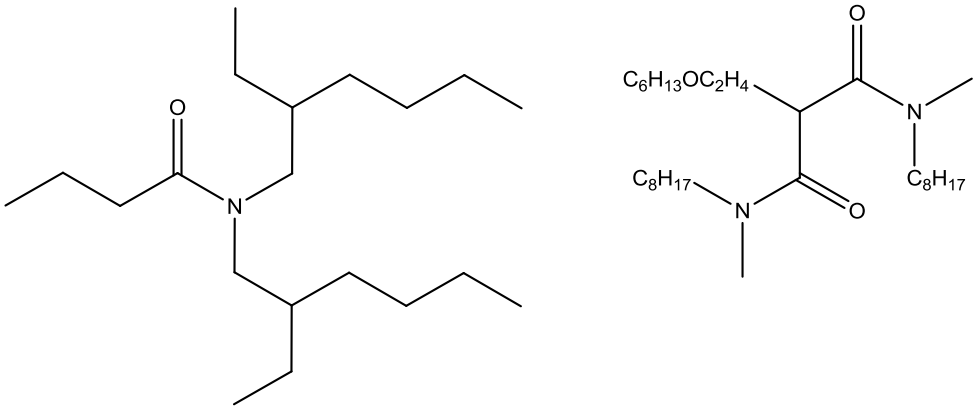

Figure 87: DEHiBA and DMDOHEMA.

Previous studies have shown that 0.2 M TODGA with 0.5 M TBP in an alkane diluent can successfully and completely extract minor actinides and trivalent lanthanides. The addition of 1-octanol (5 % by volume) in to the above solvent system has also shown improved distribution ratios for some actinides.[48] The following work will focus on the use of TODGA as a stand-alone extractant, or with the phase modifiers TBP, 1-octanol and with the ligand DMDOHEMA. Both TODGA and DMDOHEMA have shown much promise as extractants for both actinides and lanthanides and have shown good radiolytic stability under reprocessing conditions.[11] The GANEX type solvents for this work utilise a 0.2 M TODGA concentration throughout. When used in combination with either TBP and DMDOHEMA, those phase modifiers are present at 0.5 M concentrations. The TODGA/1-octanol solvent uses 0.2 M TODGA with 5 % 1-octanol by volume. The solvent system using DMDOHEMA as the only extractant utilise 0.5 M DMDOHEMA. All aforementioned GANEX solvents use a dodecane diluent. All experiments were carried out at room temperature (RT).

The lanthanide series was investigated as lanthanides are found throughout spent nuclear fuel as byproducts of fission. Rare earth elements which incorporate mostly lanthanides consist of around 40 % of the mass of fission products in spent nuclear fuel.[122] It is therefore necessary to understand their behaviour with respect to different reprocessing techniques.

6.2 Investigating the Effectiveness of TODGA with Various Phase Modifiers for the Separation of the Lanthanide Series

Batch experimentation was used to determine distribution ratio data for lanthanides and some actinides (D_{Lu} and D_{An} respectively). Aqueous nitric acid fractions of various concentration, containing lanthanides and/or actinides were contacted with the desired solvent system in a 1:1 volume ratio, unless otherwise stated. Samples were mechanically agitated using a vortex shaker for approx. 15 minutes and centrifuged for full phase separation. The Ln concentrations were determined by ICP-MS, with the active isotope concentrations determined by various counting methods in the Centre for Radiochemistry Research (CRR). A series of lanthanide (La, Pr, Nd, Sm, Gd, Tb, Dy, Ho, Er, Tb, Lu; ~ 0.05 M) solutions at a range of aqueous nitric acid concentrations (1-16 M) were contacted with a combination of GANEX style solvent systems in order to assess the effectiveness of each with respect to lanthanide separation, thereby determining the role and impact each extractant has in this process.

The data presented in Figure 88 shows the distribution ratio data for each lanthanide analysed as a function of HNO_3 concentration, extracted using 0.2 M TODGA in dodecane. Previously reported is the tendency of this solvent system to form a third phase above aqueous nitric acid concentrations of ~ 5 M.[144] Above 6 M nitric acid, a third phase was observed but further analysis on these samples was not performed. There is a notable trend in the lanthanides Sm to Lu which increase in distribution ratio as a function of nitric acid concentration. In contrast, the early lanthanides, La, Pr and Nd, decrease in their distribution ratios as a function of increasing nitric acid concentration. The absolute distribution ratios for the La, Pr and Nd fall below 1 for all the nitric acid concentration studied, whereas those ratios for the remaining latter lanthanides are all > 1.

The data presented in Figure 88 is somewhat different to that reported by Suzuki *et al.*, where the distribution ratios for the lanthanides examined were significantly higher in analogous conditions.[145] The contact time for these experiments however, was significantly longer, in the range of 1 hour, that the contact time used throughout these experiments. This implies that there is a kinetic effect surrounding the extraction of these metals in to the organic fraction and therefore thermodynamic equilibrium was not reached during the 15 minute contact time utilised for these batch experiments.

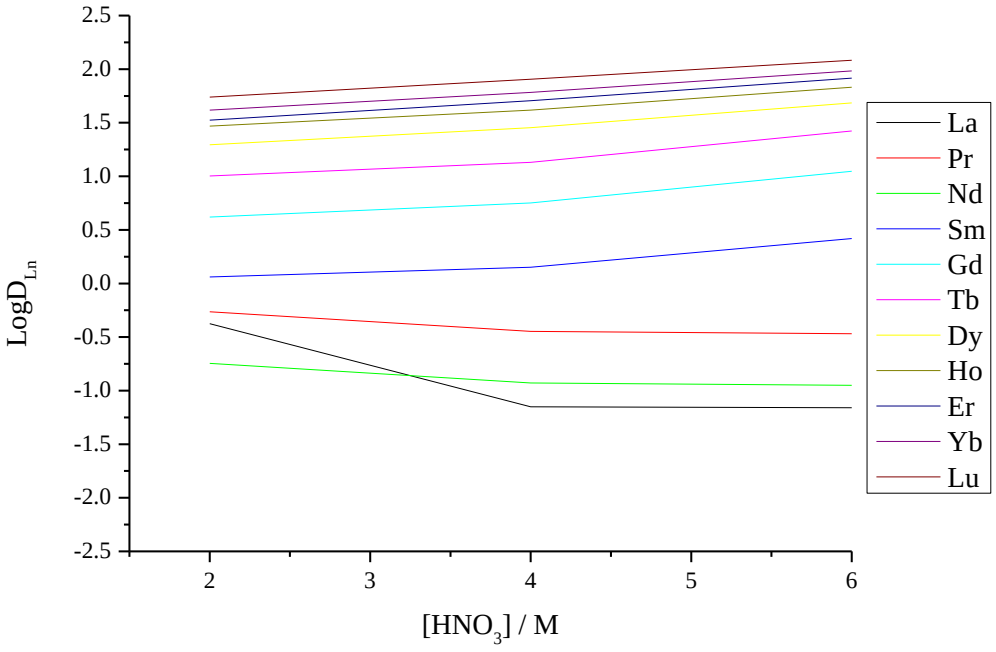

Figure 88: Distribution data for various lanthanides extracted using a 0.2 M TODGA in dodecane solvent as a function of HNO_3 concentration.

Figure 89 illustrates the lanthanide series distribution ratio data as a function of aqueous nitric acid concentration from 1-14 M using 0.2 M TODGA with 0.5 M TBP in dodecane as the organic solvent. No third phase was observed in these systems due to the presence of the TBP in the organic fraction. The distribution ratios across the lanthanides Sm to Lu are seen to generally increase as a function of increasing aqueous nitric acid concentration (Figure 89). The distribution ratios (plotted as $LogD_{Ln}$; Figure 89) associated with La, Pr and Nd again all fall below 1. It is clear

that the early lanthanides in the series separate less efficiently using these TODGA containing solvent systems, than those found later in the series.

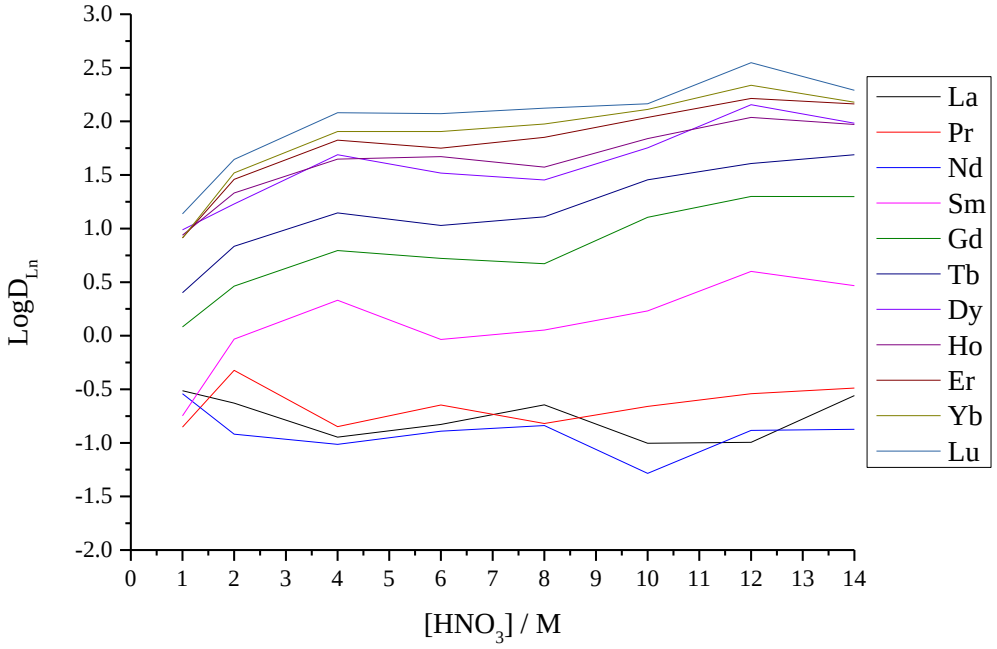

Figure 89: Distribution data for various lanthanides extracted using a 0.2 M TODGA, 0.5 M TBP solvent as a function of HNO_3 concentration.

The extractant DMDOHEMA has been developed at it showed particular promise in the separation of metal nitrates in acidic conditions. It has a low affinity for metal ions in dilute nitric acid aqueous solutions which allows for ease of back-extraction during the stripping steps. It also complies with the CHON principle and is therefore incinerable.[146] Recently proposed is the combination of TODGA and DMDOHEMA in an organic diluent for the separation of transuranics (TRU) and trivalent lanthanides from spent nuclear fuel. This solvent system has also shown to be effective in increased plutonium loading without precipitation.[147] The data presented in Figure 90 gives the distribution ratios over the lanthanide series as a function of aqueous nitric acid concentration using the solvent system 0.2 M TODGA and 0.5 M DMDOHEMA in dodecane. There is a clear trend from 1-2 M HNO_3, where the distribution ratio decreases with increasing aqueous HNO_3 concentration. From 2-6 M aqueous nitric acid concentration, the distribution ratio across the lanthanide series increases with increasing aqueous nitric acid concentration. From 6 M initial aqueous

nitric acid concentration there in a decrease in the distribution ratios to ~ 8 M, followed by a further increase to ~ 10 M aqueous nitric acid concentration.

From aqueous nitric acid concentrations of 10 to 16 M, a general decrease is observed in the distribution ratios for each lanthanide across the series. The data indicates optimum separation conditions for the entire Ln series are ~ 6 M aqueous nitric acid concentration for this solvent system.

Figures 88, 89 and 90 collectively display a general trend of improved distribution ratios with increasing atomic number across the lanthanide series. The early lanthanides La, Pr and Nd consistently exhibit lower distribution ratios in the previous three solvent systems detailed than the remaining lanthanides analysed. Generally, it could be said that higher atomic number lanthanides gave higher distribution ratios, in the solvent systems analysed.

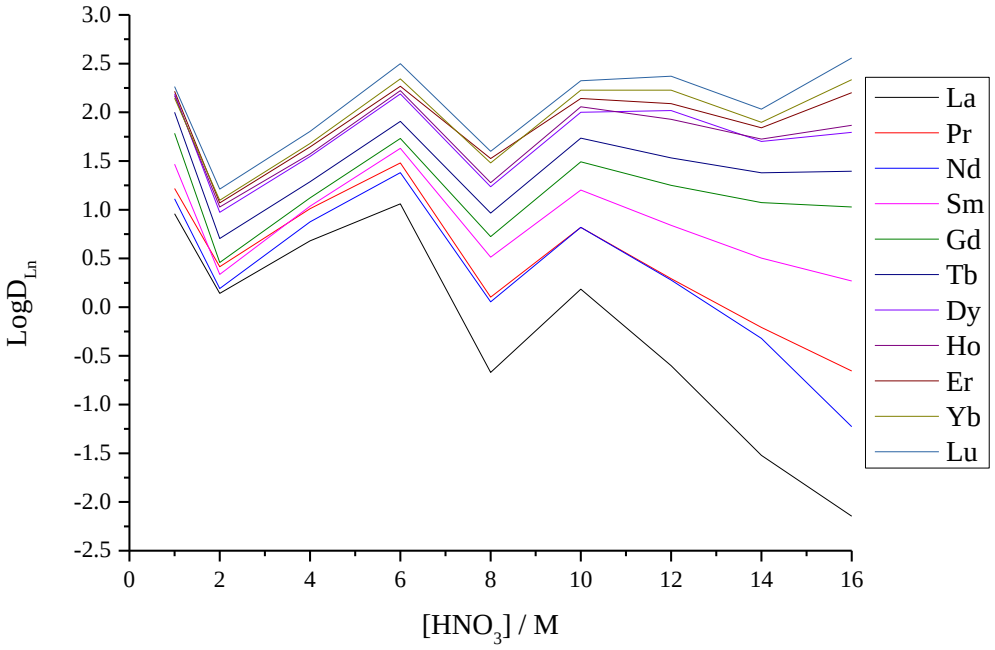

Figure 90: Distribution data for various lanthanides extracted using a 0.2 M TODGA, 0.5 M DMDOHEMA solvent as a function of HNO_3 concentration.

The addition of 1-octanol (5 % by volume) to 0.2 M TODGA in alkane diluents has been successfully tested for use as a GANEX style solvent. 1-octanol suppresses third phase formation, as does TBP, but 1-octanol does not extract excess aqueous nitric acid in to the organic fraction, as TBP does.[148] Figure 91 illustrates the distribution ratios of the lanthanide series as a function of aqueous nitric acid concentration using 0.2 M TODGA and 1-octanol in dodecane. The results present a general trend of increasing distribution ratio with increasing aqueous nitric acid concentration. Again, the initial lanthanides in the series, La, Pr and Nd, give the lowest distribution ratios of the metals analysed. The remaining lanthanides analysed show less of a general trend as observed in the previous three solvent systems analysed, but all still exhibit a higher distribution ratio than those of La, Pr and Nd, similar to the data presented in Figures 88, 89 and 90. Overall, the distribution ratios are higher than those previously described in this Chapter, indicating the combination of TODGA and 1-octanol gives the most effective separation of lanthanides from aqueous nitric acid solutions.

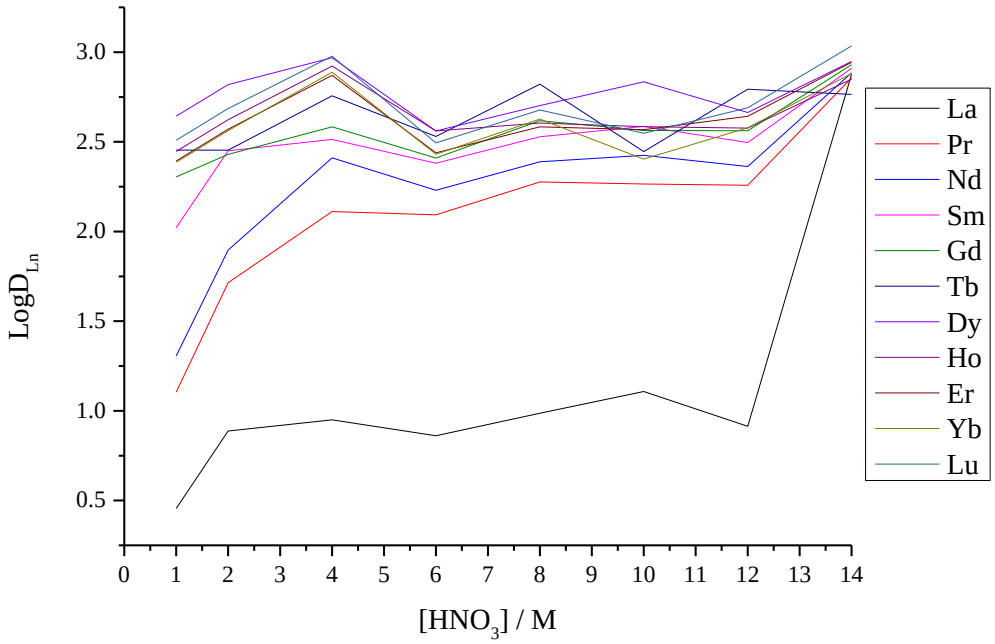

Figure 91: Distribution data for various lanthanides extracted using a 0.2 M TODGA with 1-octanol (5 % by volume) in dodecane as a function of HNO_3 concentration.

6.2.1 Lanthanides and Actinides Separated Using TODGA/ 1-Octanol

A number of lanthanides (La, Pr, Nd, Sm, Gd, Tb, Dy, Ho, Er, Tb, Lu; ~ 0.05 M) were dissolved in to aqueous nitric acid solutions of 2, 6, 10 and 14 M and contacted with organic fractions containing a range of TODGA concentrations (0.02, 0.05, 0.1, 0.2, 0.4 and 0.6 M) with 1-octanol (5 % by volume) in dodecane. Figure 92-95 display the distribution ratios obtained with respect to the concentration of TODGA for each of the aqueous nitric acid concentrations studies. Figure 92 presents the distribution ratio data obtained for lanthanides separated from a 2 M aqueous nitric acid fraction. The distribution ratio for each lanthanide analysed increased with increasing TODGA concentration in the organic fraction. At a 0.2 M TODGA concentration, commonplace for suggested GANEX style solvent systems, the Ln distribution ratios across the series were close to zero (in terms of $LogD_{Ln}$). Many studies have proven that metal separation is enhanced at higher aqueous acid concentrations; it is therefore likely that the lower separation can be attributed to the lower aqueous nitric acid concentration overall. A similar trend is observed here as in previous data presented on this work which illustrates a higher distribution ratio for metals in the latter part of the lanthanide series. Early lanthanides in the series have shown lower distribution ratios throughout the systems examined so far. This is also true of the data presented in Figures 92-95 where La, Pr and Nd exhibit lower distribution ratios that any other lanthanide analysed at each aqueous nitric acid concentration and TODGA concentration studied.

The data presented for in Figure 92 however, suggests that the contact time utilised here is not long enough for extraction equilibrium. Previous literature[44] presented by Wilden *et al.* surrounding lanthanide extraction under similar conditions (0.2 M TODGA/5 % volume 1-octanol in THP; aqueous phase 1 M HNO_3) gave considerable higher distribution ratios for the lanthanides analysed *c.f.* the lanthanide distribution ratios presented here. Further, Wilden *et al.* demonstrated that under analogous, ~ 2 M aqueous HNO_3, 0.1 M organic TODGA, the distribution ratios were between 40 and 110 across the lanthanide series reported. These are significantly higher than those reported in Figure 92 below, again suggesting a kinetic dependence of lanthanide extraction in these systems.

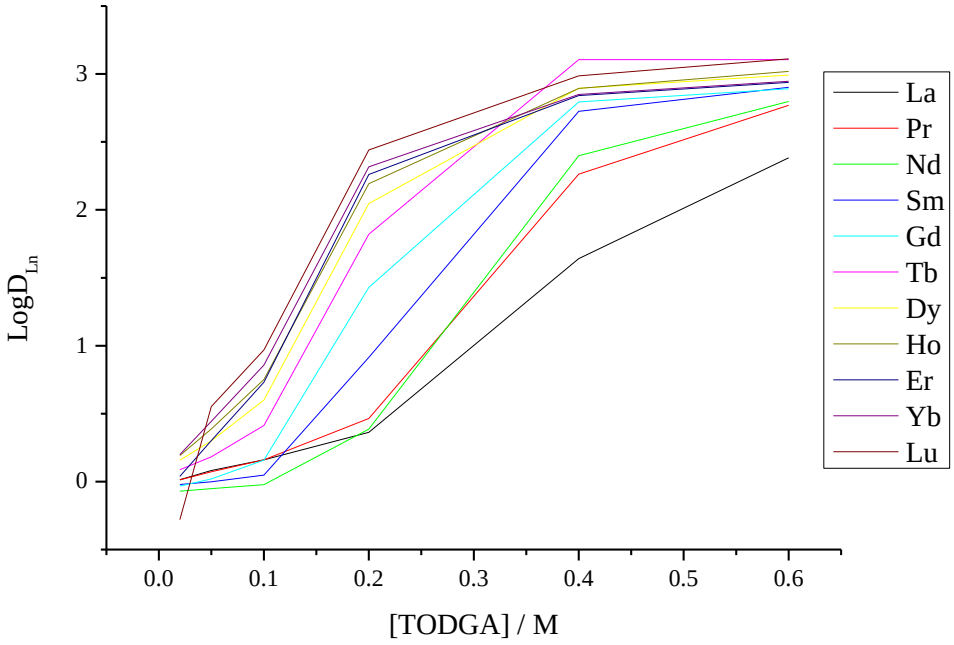

Figure 92: Distribution data for various lanthanides extracted from 2 M HNO_3, as a function of TODGA concentration.

Figure 93 presents the data for lanthanide distribution ratios over a range of TODGA concentrations separated from aqueous nitric acid fractions of 6 M. The general trend is similar to that of the data presented in Figure 92. At the lowest TODGA concentration (0.05 M) analysed however, there is a small decrease in the observed distribution ratios, in contrast to the initial trend seen in Figure 92. At 0.2 M TODGA the distribution ratios increase as a direct function of lanthanide atomic number. The distribution ratios observed for the metals Lu, Yb and Er at TODGA concentrations above 0.2 M remains constant, whilst a larger increase is observed for the remaining lanthanides in the series from 0.2 to 0.4 M TODGA. Analysis of systems containing between 0.4 and 0.6 M TODGA in the initial solvent phase showed that all lanthanide distribution ratios tended to ~ 3 at 6 M HNO_3. Indeed it is thought that optimum extraction conditions using the GANEX solvent systems are from aqueous nitric acid concentrations of ~ 5 M.[49]

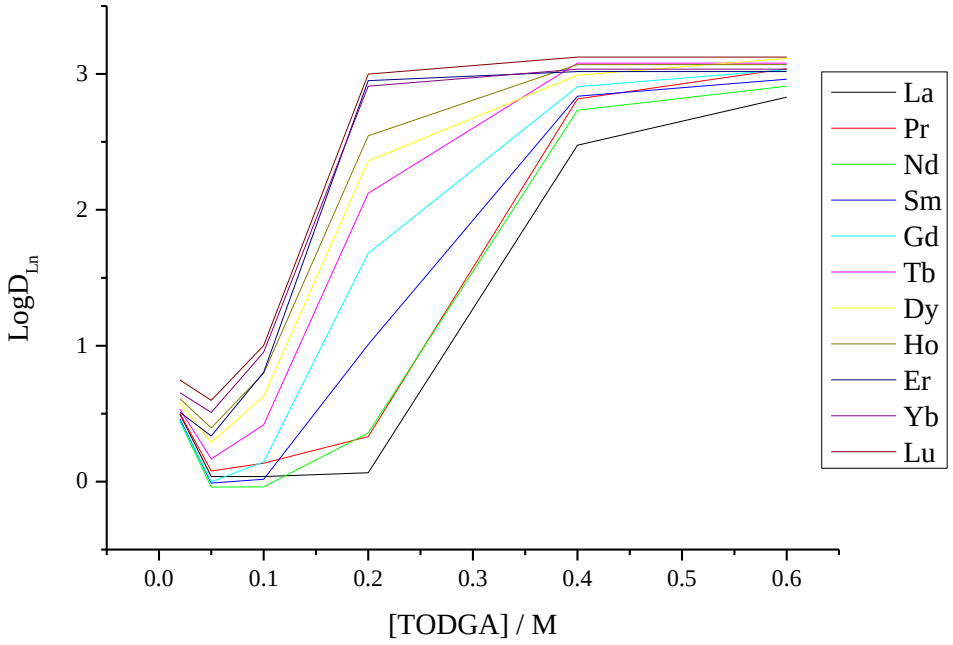

Figure 93: Distribution data for various lanthanides extracted from 6 M HNO_3, as a function of TODGA concentration.

The data presented in Figures 94 and 95 show the distribution ratio data for the lanthanide series over a range of TODGA concentrations separated from aqueous nitric acid concentrations of 10 and 14 M respectively. The general trends are similar to those detailed in Figures 92 and 93; there is an increase in the distribution ratios for each lanthanide analysed as a function of increasing TODGA concentration. At 0.4 M TODGA concentration at both 10 and 14 M aqueous nitric acid concentrations the distribution ratios for the majority of lanthanides in the series are ~ 3. Lanthanum is consistently less efficiently separated than the remaining lanthanides; this is clearly observed in Figure 95 where, at 0.4 M TODGA concentration, the D_{La} is an order of magnitude lower than the remaining lanthanides.

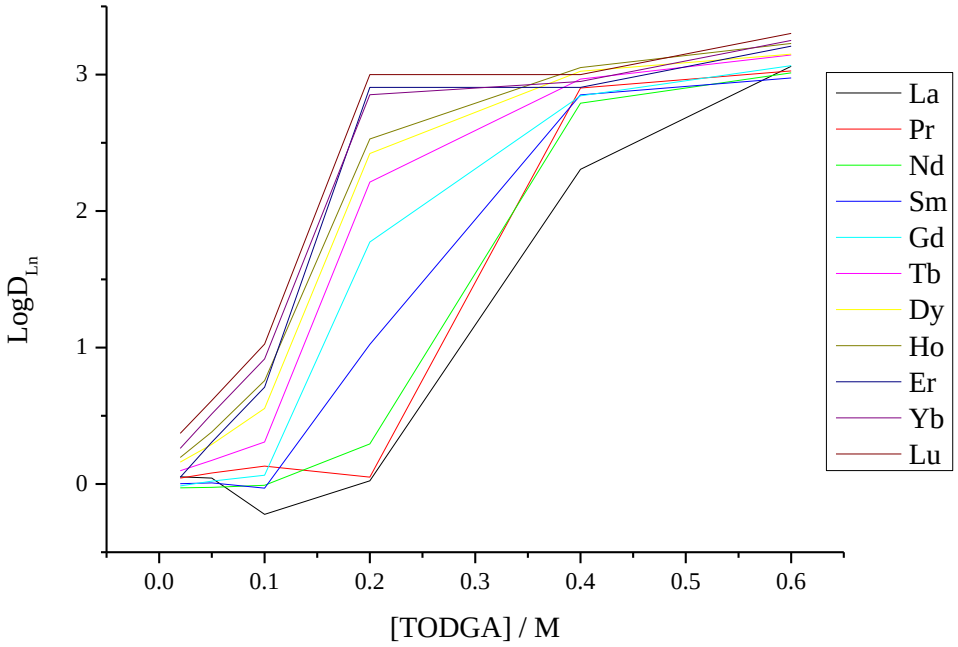

Figure 94: Distribution data for various lanthanides extracted from 10 M HNO_3, as a function of TODGA concentration.

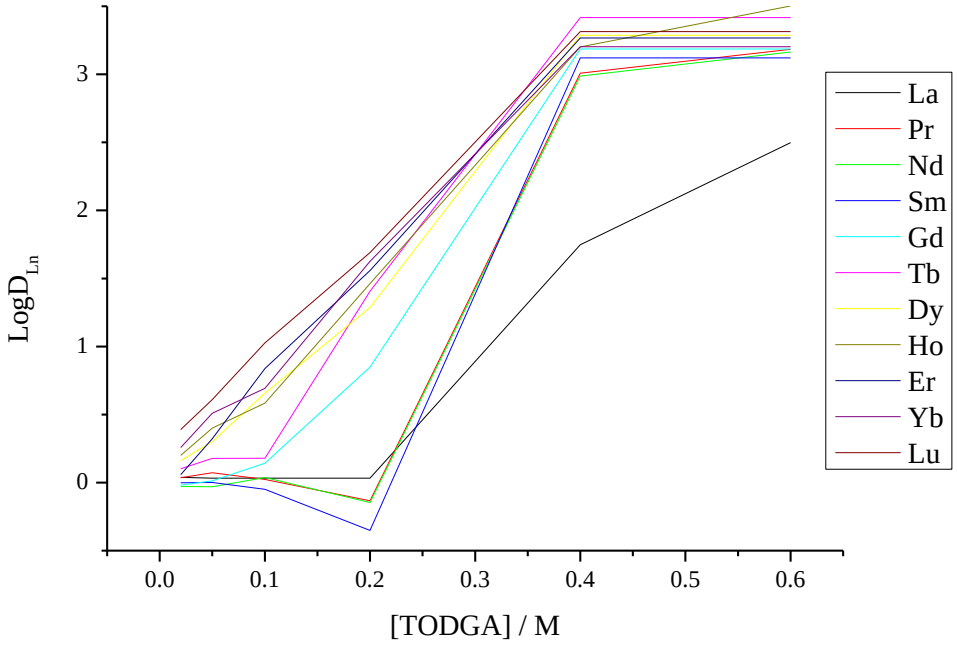

Figure 95: Distribution data for various lanthanides extracted from 14 M HNO_3, as a function of TODGA concentration.

The proposed Group ActiNide EXtraction (GANEX) process uses the TODGA molecule to extract trivalent actinides and lanthanides. It is therefore necessary to assess the effectiveness of the aforementioned ligand in the separation of transuranic elements from aqueous nitric acid. Technetium is a problematic element in nuclear reprocessing and is likely to be contained in the envisaged second step of the GANEX flow sheet. Here, Tc, Np, Am, Eu and Pu are separated from aqueous nitric acid over a range of organic TODGA and aqueous nitric acid concentrations, respectively. Each sample was mechanically agitated for approx. 15 minutes and centrifuged for full phase separation. Aliquots of each resultant aqueous and organic fraction were taken and analysed via LSC in order to establish the distribution ratios for each isotope under these conditions.

Aqueous nitric acid fractions (8 M) containing Tc, Np, Am, Eu and Pu (^{99}Tc(VII), 12 kBq, 13.66 mM; ^{237}Np(V), 182 Bq, 21.06 uM; ^{241}Am(III), 258 Bq, 6.03 nM; ^{152}Eu(III), 200 Bq, 0.15 nM; ^{239}Pu(IV), 275 Bq, 0.36 uL) were contacted with TODGA (0.02, 0.05, 0.1, 0.2, 0.4, 0.6 M) with octanol (5 % by volume) and the distribution ratio data calculated.

The distribution ratio data for the separation of Tc, Np, Am, Eu and Pu from aqueous nitric acid as a function of TODGA concentration is presented in Figure 96. It is clear from this data that the distribution ratio calculated for each metal under these conditions increases as a function of organic TODGA concentration. The distribution ratio for technetium at each TODGA concentration analysed however, is notably lower that those distribution ratios observed for Np, Am, Eu and Pu. The overall distribution ratios for plutonium are higher than those observed for each of the remaining isotopes analysed. TODGA has previously shown promise for the separation of M(IV) (where M is a metal), such as the plutonium used in these systems. Technetium does not separate well from aqueous nitric acid but does show improved separation at higher organic TODGA concentrations. Neptunium was observed to extract in these systems even though the typically inextractable Np(V) oxidation state was used in these studies. It has previously been shown that Np(V) disproportionates using GANEX type solvent systems.[149]

It is most likely that the Np is extractable in these studies by the formation of Np(IV) and Np(VI), which are readily extractable neptunium oxidation states in the aqueous phase through Np(V) disproportionation. The data recorded for these systems also showed high levels of extraction for americium and europium.

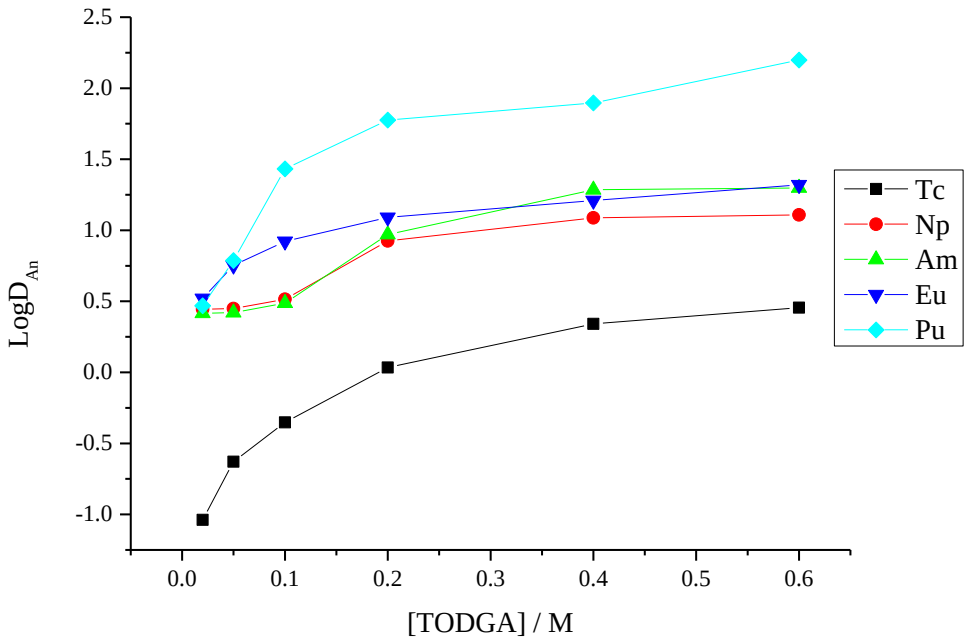

Figure 96: Distribution data for Tc, Np, Am, Eu and Pu separated from 8 M aqueous nitric acid, as a function of organic TODGA concentration.

Aqueous nitric acid fractions (1 - 14 M) containing Tc, Np, Am, Eu and Pu (^{99}Tc(VII), 12 kBq, 13.66 mM; ^{237}Np(V), 182 Bq, 21.06 uM; ^{241}Am(III), 258 Bq, 6.03 nM; ^{152}Eu(III), 200 Bq, 0.15 nM; ^{239}Pu(VI), 275 Bq, 0.36 uL) were contacted with TODGA (0.2 M) with octanol (5 % by volume) and the distribution ratio data calculated.

The distribution ratio data for Tc, Np, Am, Eu and Pu, presented in Figure 97, is given as a function of aqueous nitric acid concentration, where 0.2 M TODGA with octanol (5 % by volume) in dodecane was used as the organic fraction. With the exception of technetium, the distribution ratios increase as a function of aqueous nitric acid concentration. The distribution ratio for plutonium is observed to be higher than the remaining isotopes analysed over the aqueous nitric acid concentration range tested. The distribution ratio for technetium is seen to decrease as a function of aqueous nitric acid concentration. However at low initial aqueous nitric acid concentrations (1 and 2 M) it is observed to separate into the organic fraction.

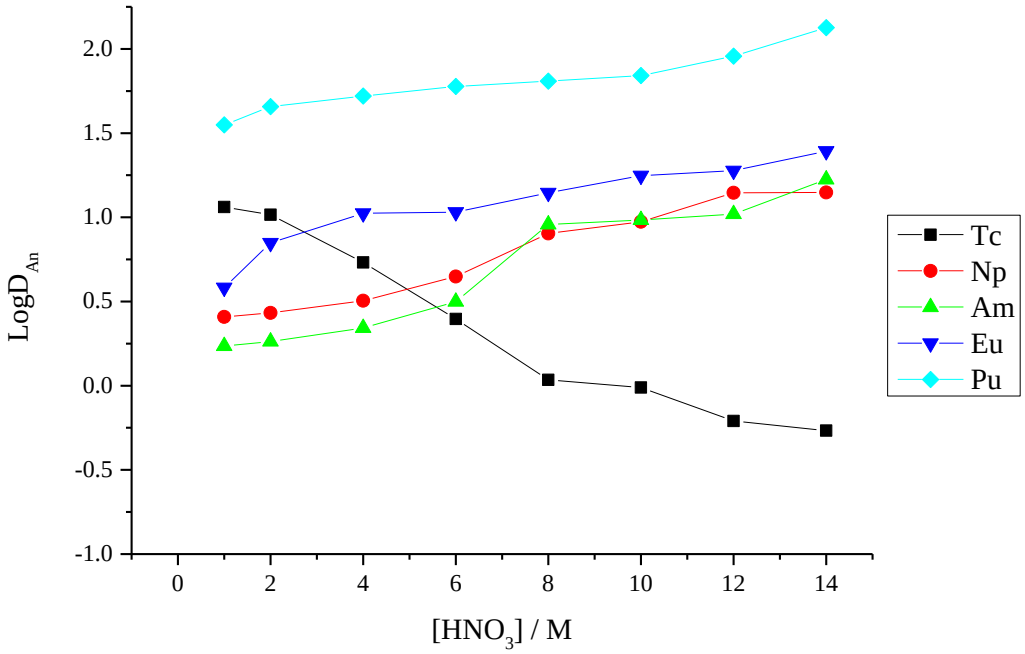

Figure 97: Distribution ratio data for Tc, Np, Am, Eu and Pu separated as a function of aqueous nitric acid concentration, using a 0.2 M TODGA in dodecane.

6.3 Lanthanides and Actinides Separated Using DMDOHEMA

As mentioned previously, the monoamide DMDOHEMA (Figure 87) has shown promise for the separation of trivalent lanthanides and actinides. Its ability as an effective extractant is enhanced further by its organophilicity which prevents third phase formation.[150]

The following data presents distribution ratio data for the lanthanide series separated from various aqueous nitric acid concentrations and over a range of DMDOHEMA concentrations to assess the effectiveness of each condition to separate metals relevant to the reprocessing of spent nuclear fuel. Figure 98 presents the distribution data for a number of lanthanides as a function of aqueous nitric acid concentration. Each aqueous fraction was contacted with 0.5 M DMDOHEMA in dodecane and the phases equilibrated for analysis. The distribution data for the lanthanides analysed follows a clear trend; at lower aqueous nitric acid concentrations, the distribution ratios increase with increasing acid concentration. This increase reaches a maximum distribution ratio of ~ 0.5 at initial aqueous phase nitric acid concentrations of 6 M. At aqueous nitric acid concentrations above 6 M, the distribution ratios for the lanthanide series decreases as a function of aqueous nitric acid concentration.

The decrease in lanthanide extraction at higher aqueous acid concentration, using DMDOHEMA, as shown in Figure 98, could possibly be explained by the higher concentration of protons at higher aqueous acid concentrations. This may imply that hydrogen bonding of the acidic protons to the oxygen atoms of the DMDOHEMA moiety is favoured over the complexation of the metal species in solution, at higher acid concentrations. However, this is a speculative suggestion and further analysis is necessary in order to ascertain the foundations of this trend.

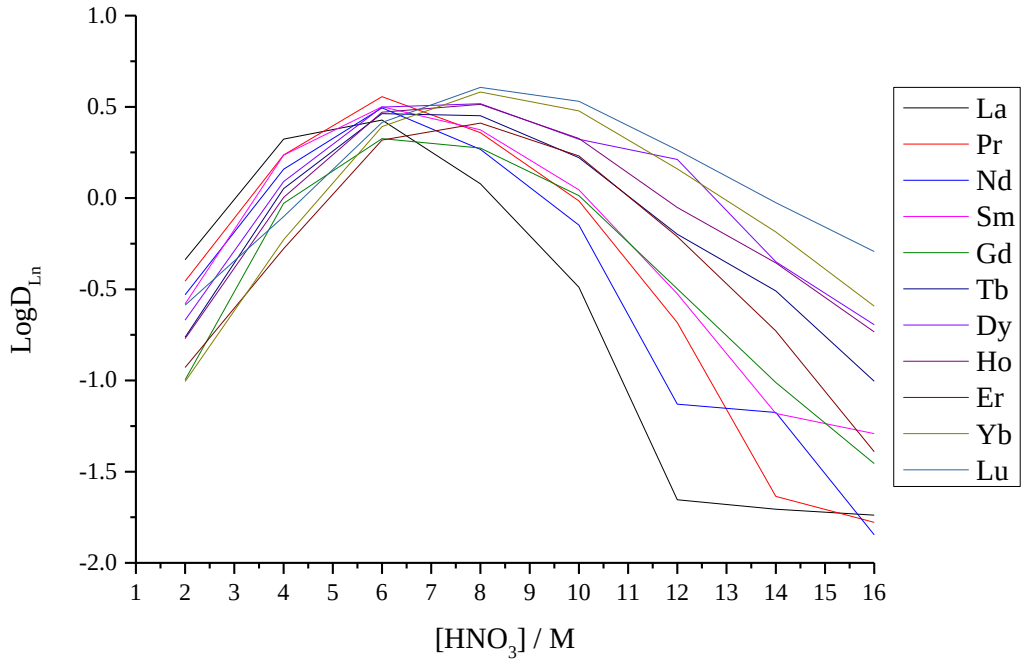

Figure 98: Distribution data for various lanthanides extracted using a 0.5 M DMDOHEMA in dodecane solvent as a function of HNO_3 concentration.

The effective separation of the lanthanide series was analysed over a range of DMDOHEMA concentrations at various aqueous nitric acid concentrations. Figures 99-102 present the distribution ratio data for lanthanides analysed at 2, 6, 10 and 14 M aqueous nitric acid concentration respectively, contacted with 0.2, 0.3, 0.4, 0.5, 0.6 and 0.8 M DMDOHEMA in dodecane. At the lowest nitric acid concentration analysed (Figure 99), there is a general trend illustrating an increase in distribution ratio with increasing DMDOHEMA concentration. However, this particular set of conditions gave distribution ratios below zero (plotted as $LogD_{Ln}$) and hence separation is unlikely to occur. It is known to be necessary to use a higher aqueous acidity to achieve optimum separation. At aqueous nitric acid concentrations of 6 M, lanthanide extraction was achieved. At DMDOHEMA concentrations of above 0.4 M, separation of all lanthanides was observed. At 6 M aqueous nitric acid, the trend is clearly linear and shows a distinct relationship between DMDOHEMA concentration and effectiveness of separation. In contrast to the TODGA containing systems, the lower atomic mass lanthanides show enhanced distribution ratios compared to those of the heavier lanthanides, at aqueous acid concentrations of 2 and 6 M.

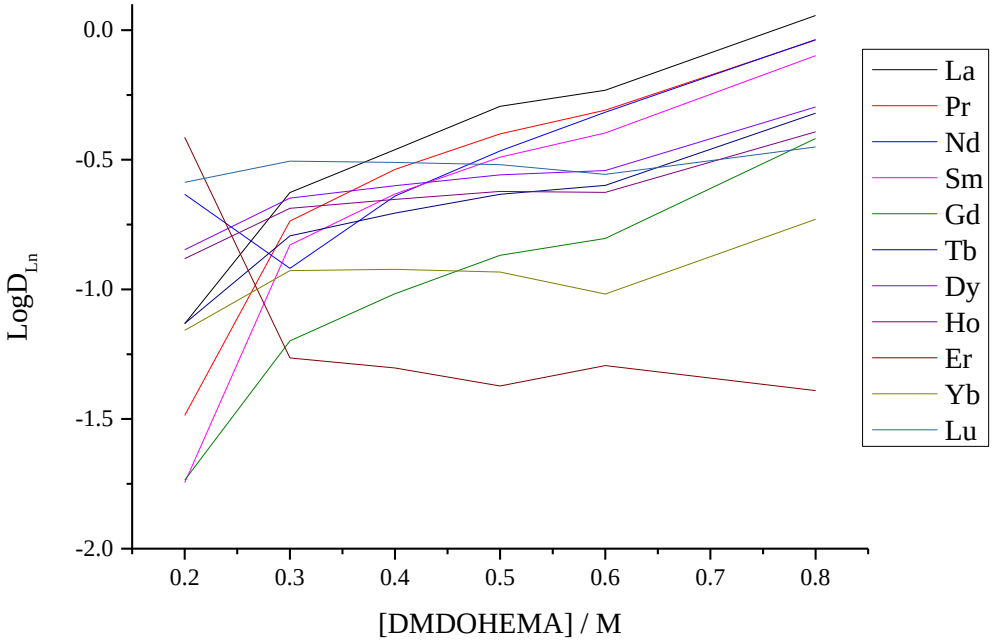

Figure 99: Distribution data for various lanthanides extracted from 2 M HNO_3, as a function of DMDOHEMA concentration.

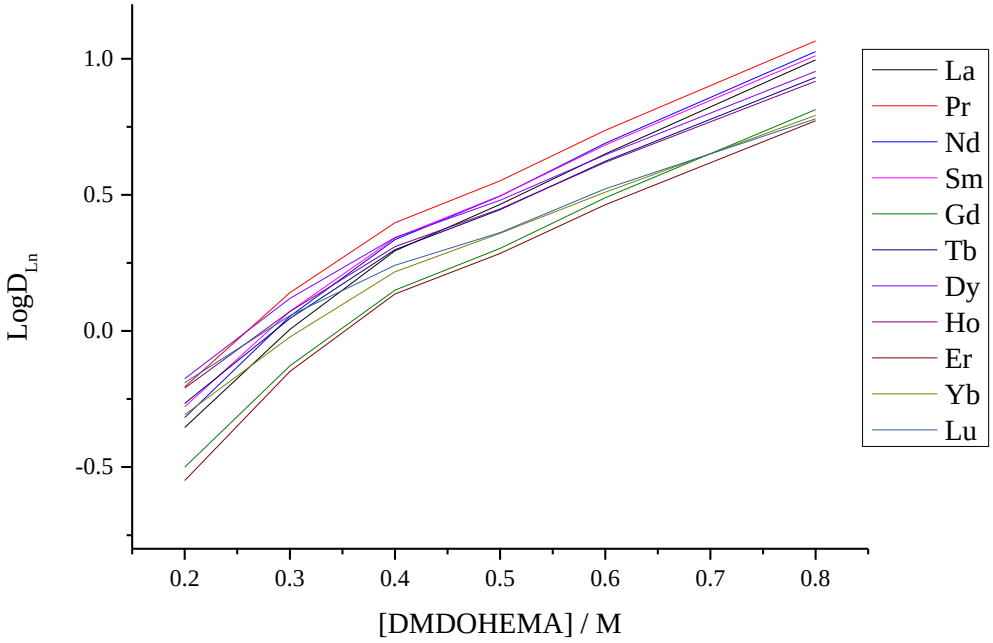

Figure 100: Distribution data for various lanthanides extracted from 6 M HNO_3, as a function of DMDOHEMA concentration.

The separation of lanthanides at higher aqueous nitric acid concentrations presented the opposite trend to those systems of lower acid concentration. Figures 101 and 102 illustrate the distribution ratio data for lanthanides separated from 10 and 14 M aqueous nitric acid concentration over a range of DMDOHEMA concentrations. The data in Figures 101 and 102 shows that lower atomic mass lanthanides gave lower distribution ratios under the conditions analysed. Lanthanides separated from 10 M aqueous nitric acid showed enhanced distribution ratios with higher DMDOHEMA concentrations. However, only at 0.7 M DMDOHEMA and above did all lanthanides give distribution ratios above zero. Lanthanides separated from 14 M aqueous nitric acid solutions gave distribution ratios below zero (plotted as $LogD_{Ln}$) for the majority of conditions analysed. This suggests that aqueous acid concentration is a dominating factor in the separation of lanthanides under these reprocessing conditions. DMDOHEMA concentration and lanthanide type factors have been observed to have little influence on the effectiveness of separation of the lanthanides analysed. Aqueous nitric acid concentrations of 6 M were shown to give the largest Ln distribution ratios of the lanthanide metals analysed.

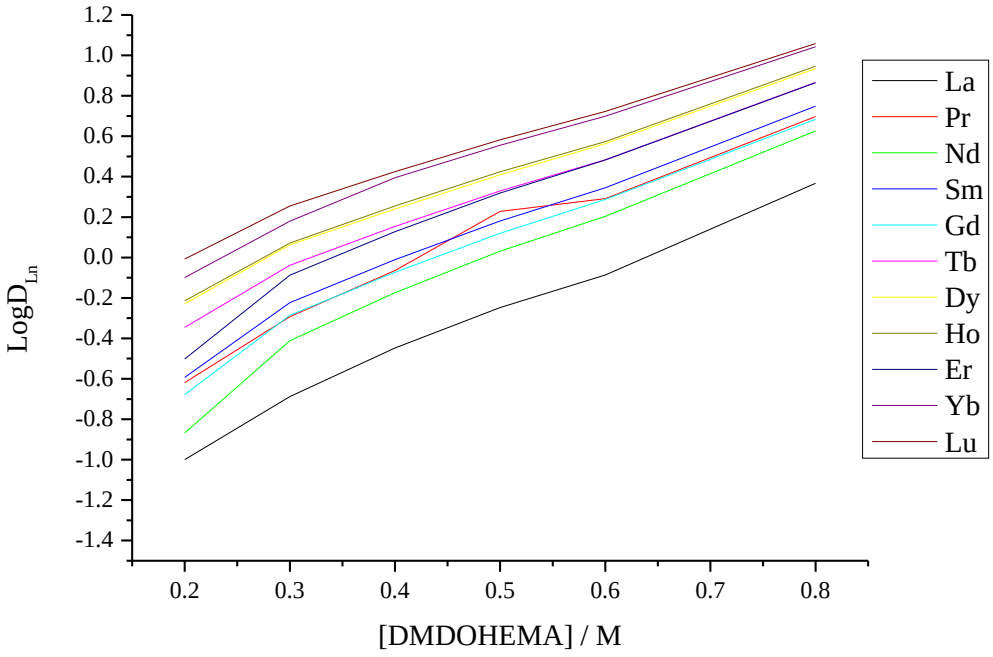

Figure 101: Distribution data for various lanthanides extracted from 10 M HNO_3, as a function of DMDOHEMA concentration.

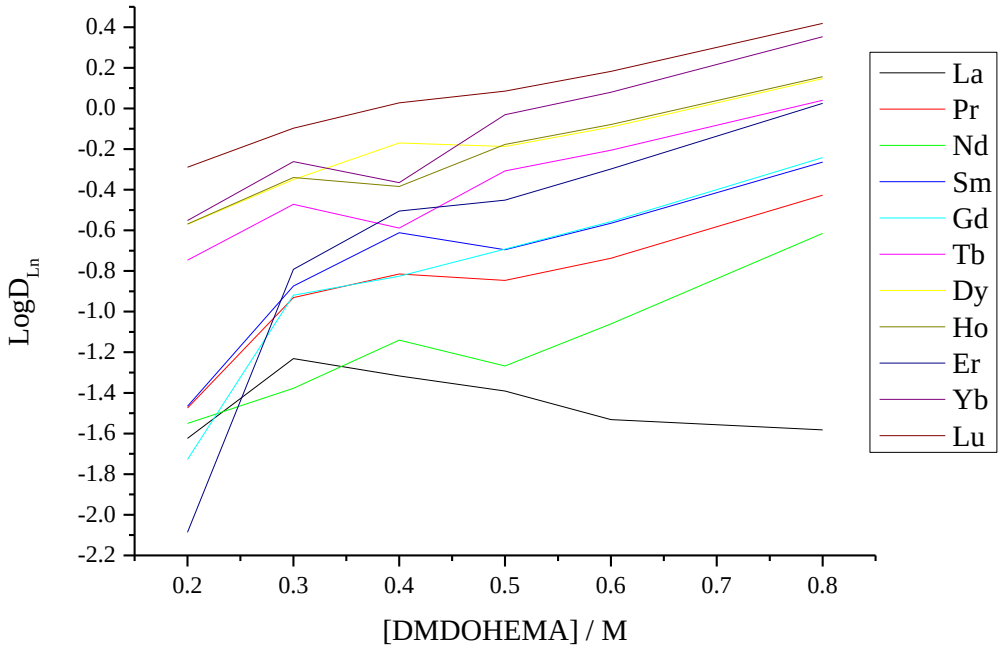

Figure 102: Distribution data for various lanthanides extracted from 14 M HNO_3, as a function of DMDOHEMA concentration.

Aqueous nitric acid fractions (8 M) containing Tc, Np, Am, Eu and Pu (^{99}Tc(VII), 12 kBq, 13.66 mM; ^{237}Np(V), 182 Bq, 21.06 uM; ^{241}Am(III), 258 Bq, 6.03 nM; ^{152}Eu(III), 200 Bq, 0.15 nM; ^{239}Pu(VI), 275 Bq, 0.36 uL) were contacted with DMDOHEMA (0.2, 0.3, 0.4, 0.5, 0.6, 0.8 M) in dodecane and mechanically agitated for approx. 15 minutes. The samples were prepared and analysed as previously described in this Section 6.2.1.

Distribution ratio data was calculated for Tc, Np, Am, Eu and Pu separated from aqueous nitric acid using various concentration organic DMDOHEMA fractions. The data presented in Figure 103 indicates that the highest separation was observed for plutonium in these systems. Technetium showed little separation over the DMDOHEMA concentration range analysed, but did exhibit an increased separation with increasing DMDOHEMA concentration in the organic fraction. Similar to the data presented in Figure 96, technetium separation was the lowest observed in comparison to the remaining isotopes analysed. The distribution ratios observed for the separation of Np, Am and Eu using DMDOHEMA showed an increase with increasing organic DMDOHEMA concentration.

Aqueous nitric acid fractions (1 - 14 M) containing Tc, Np, Am, Eu and Pu (^{99}Tc(VII), 12 kBq, 13.66 mM; ^{237}Np(V), 182 Bq, 21.06 uM; ^{241}Am(III), 258 Bq, 6.03 nM; ^{152}Eu(III), 200 Bq, 0.15 nM; ^{239}Pu(IV), 275 Bq, 0.36 uL) were contacted with DMDOHEMA (0.5 M) and the distribution ratio data calculated.

The distribution ratios for the separation of Tc, Np, Am, Eu and Pu as a function of aqueous nitric acid concentration are presented in Figure 104. The organic DMDOHEMA concentration was retained at 0.5 M. With the exception of technetium, the distribution ratios for Np. Am, Eu and Pu increase with increasing aqueous nitric acid concentration. As previously observed, technetium separation is inhibited at higher aqueous nitric acid concentrations. There was no technetium separation observed for aqueous nitric acid concentrations above 2 M. The distribution ratios for plutonium are observed to be higher than the remaining isotopes analysed, over the aqueous nitric acid concentration range.

The distribution ratio for europium, although increasing as a function of increasing aqueous nitric acid concentration, shows much higher distribution ratios above 10 M aqueous nitric acid concentration. Comparatively, the distribution ratios observed for Tc, Np, Am, Eu and Pu separated using DMDOHEMA were lower overall than those seen for Tc, Np, Am, Eu and Pu separated using TODGA.

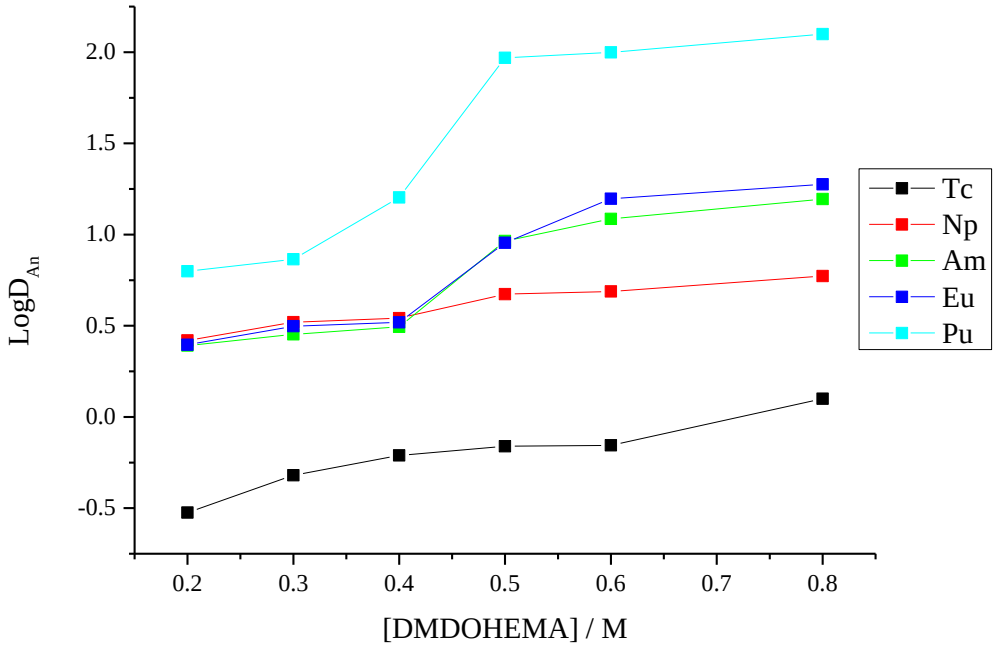

Figure 103: Distribution data for Tc, Np, Am, Eu and Pu separated from aqueous nitric acid, as a function of organic TODGA concentration.

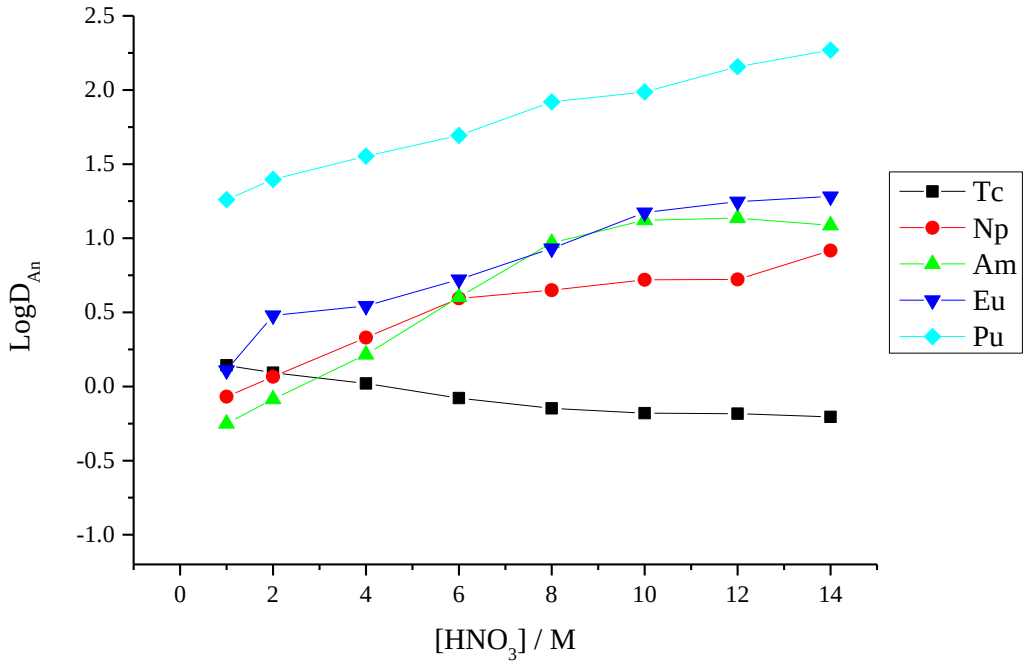

Figure 104: Distribution ratio data for Tc, Np, Am, Eu and Pu separated as a function of aqueous nitric acid concentration, using a 0.5 M DMDOHEMA in dodecane.

6.4 Neptunium Behaviour Under GANEX Style Conditions

Neptunium REDOX behaviour is not well understood under current reprocessing conditions and less understood in proposed reprocessing processes. Improved control of neptunium REDOX chemistry during the reprocessing of spent nuclear fuel can reduce the complexity, and hence cost of a process.[151] The following work saw the production of several Np(VI) containing samples for EXAFS analysis at the ANKA Beamline, Germany. Aqueous fractions were prepared (see Section 3.3.6) containing neptunium (0.5 mL max.; 0.22 mg Np-237 / sample, 2 mM) in nitric acid (6 M). Organic solvents were prepared as outlined in Table 39. Both aqueous and organic phases were contacted and mechanically agitated for approx. 15 minutes and centrifuged for full phase separation. The resultant organic phases were sent for analysis at the ANKA Beamline, Germany.

Solvent	[TODGA] / M	[DMDOHEMA] / M	[TBP] / M	1-Octanol	Diluent
1	0	0.5	0	0	Dodecane
2	0.2	0.5	0	0	Dodecane
3	0.2	0	0.5	0	Dodecane
4	0.2	0	0	5 % by volume	Dodecane

Table 39: Composition of each solvent system investigated by EXAFS at the ANKA Beamline, Germany.

From the initial XANES spectra recorded, it was clear that the four samples analysed reduced immediately on the beamline, from Np(VI) to Np(IV). This implies that the combination of these environments contributed to a change in oxidation state and therefore coordination number. The UV/vis/nIR spectra recorded for the solvent two system immediately prior to beamline analysis, is presented in Figure 105. It clearly shows the presence of a substantial amount of Np(VI) as indicated by the signal observed at 1200 nm. The XANES spectra presented in Figure 106 corresponds to solvent **2** containing systems and illustrates the absence of a shoulder in the XANES region, indicating the presence of Np(IV). Np(V) and Np(VI) exhibit a shoulder in their typical XANES region (Figure 73) which corresponds to the axial oxygens of the neptunyl moiety. Np(IV) does not exist as a neptunyl species and therefore does not display a shoulder in the XANES region. Neptunium in solvent systems **3** and **4** exhibited similar behaviour to one another as evidenced by UV/vis/nIR and XANES spectroscopy. This data implies that the beam in some way effects the REDOX chemistry of neptunium in these systems but the definitive source of this reduction is not clear. Of the four solvent systems analysed however, it was only possible to fit system **1** to a valid Np coordination complex.

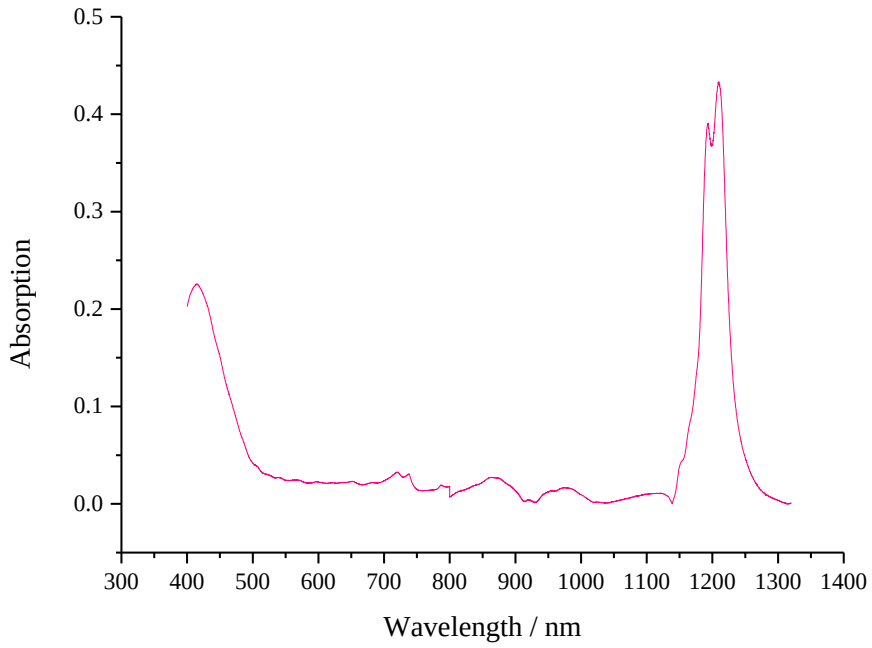

Figure 105: UV/vis/nIR for sample 2 immediately prior to beam line analysis.

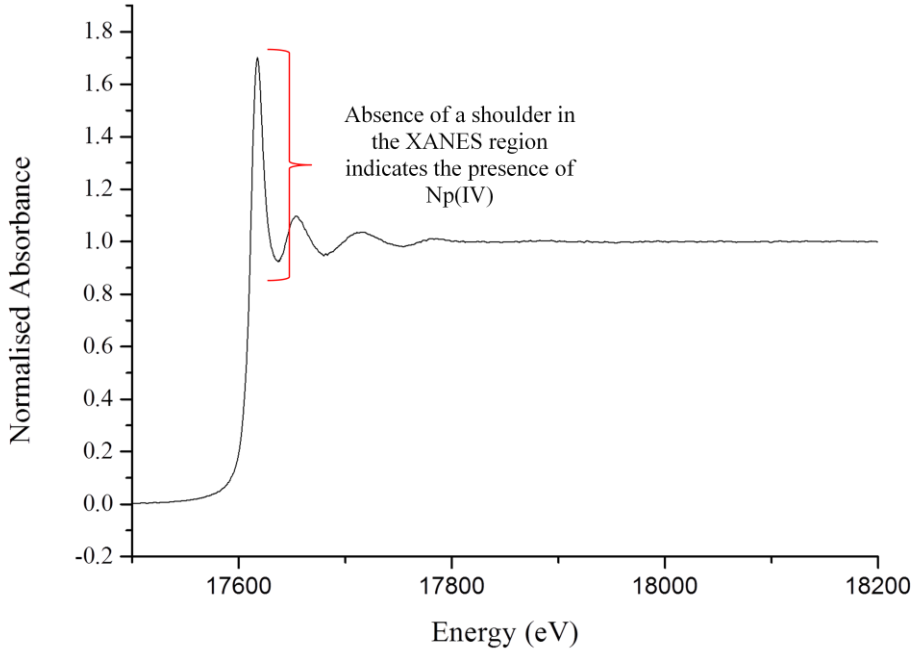

Figure 106: XANES spectrum for the organic phase, post separation for samples containing solvent 2.

The organic fraction post extraction for solvent system **1**, containing only the DMDOHEMA ligand modelled to within excellent agreement to the species $[Np(DMDOHEMA)_2(NO_3)_4]$. Table 40 outlines the parameters from the EXAFS fits for the pure $[Np(DMDOHEMA)_2(NO_3)_4]$ species, extracted from 6 M HNO_3 in to 0.5 M DMDOHEMA in dodecane. Figure 107 illustrates the k^3-weighted $\chi(k)$-function (top) and Fourier transform (bottom) of Np L_{III}-edge EXAFS data for the $[Np(DMDOHEMA)_2(NO_3)_2]$ species.

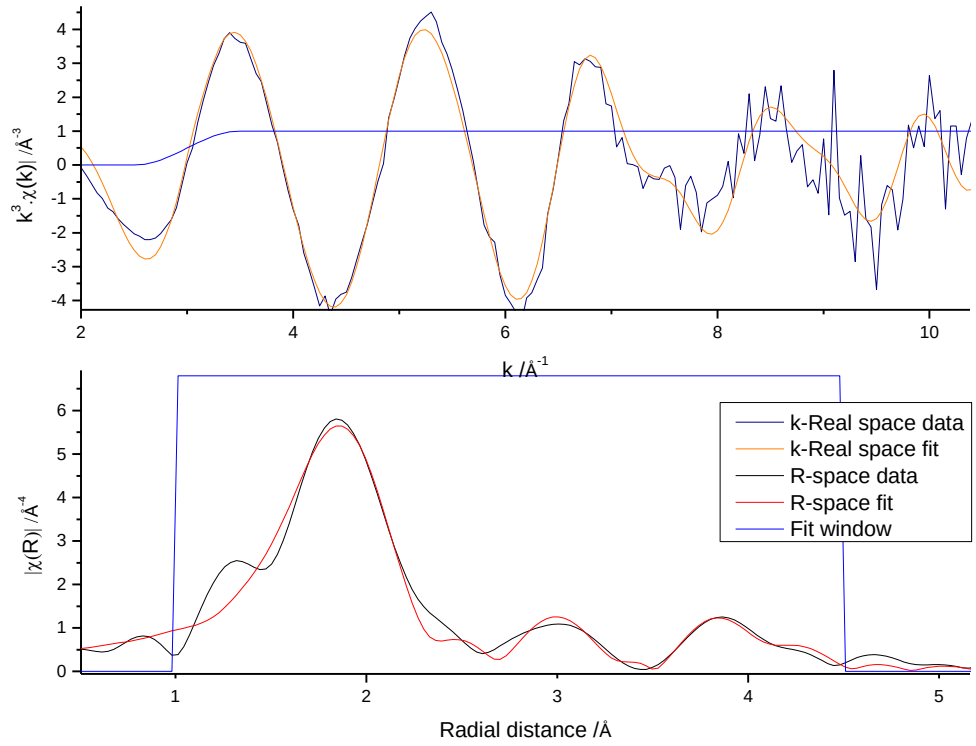

Figure 107: k^3-weighted $\chi(k)$-function (top) and Fourier transform (bottom) of Np L_{III}-edge EXAFS data for Np, extracted into 30 % TBP-OK from an initial aqueous phase consisting of 6 M HNO_3. The data is fitted to $[Np(DMDOHEMA)_2(NO_3)_4]$.

Sample	Shell	Occupancy	σ^2	R_i (Å)	R_f (Å)	ΔR (Å)
Np extracted into DMDOHEMA, 0.5 M from 6 M HNO_3, fitted to [Np(DMDOHEMA)$_2$ (NO_3)$_4$] Amp = 0.886 E_0 (eV) = 5.836 R factor = 0.019 χ^2 = 29.981	O (lig)	4	0.00702	2.2794	2.5203	-0.2409
	C (lig)	6	0.00544	3.4229	3.4132	0.0097
	N (lig)	4	0.00093	4.5993	4.5993	0.0002
	O (nit)	8	0.00837	2.4068	2.5791	-0.1723
	N (nit)	4	0.02860	3.0315	2.9919	0.0396
	O (nit)	4	0.00231	4.2571	4.2175	0.0396
	N/O (MS)	8	0.03091	4.2571	4.2180	0.0396

Table 40: Parameters obtained from EXAFS fits in k^3-space for Np extracted into a 0.5 M DMDOHEMA in dodecane solvent, from 6 M HNO_3. E_0 is the relative shift in ionization energy, Ri is the initial distance of the shell (Å) and R_f is the refined distance of the shell (Å). Statistics of fit (χ^2 and r-factor) and amplitude factor (Amp) provided.

Distribution ratio data was collected for neptunium containing samples extracted from aqueous nitric acid (5, 8 and 10 M) using the GANEX style solvent systems detailed in Table 39. The data presented in Figure 108 shows that the highest distribution ratio for neptunium separation in these systems was observed in solvent system **2**, a system containing TODGA and DMDOHEMA (red line). The lowest neptunium separation was observed in solvent system **4** containing TODGA and 1-octanol (blue line). Solvent system 1, only containing DMDOHEMA gave a good separation of neptunium as did solvent system 3, containing TODGA and TBP

(green line). There is an increase in the neptunium distribution ratio as a function of aqueous nitric acid concentration over all four solvent systems analysed.

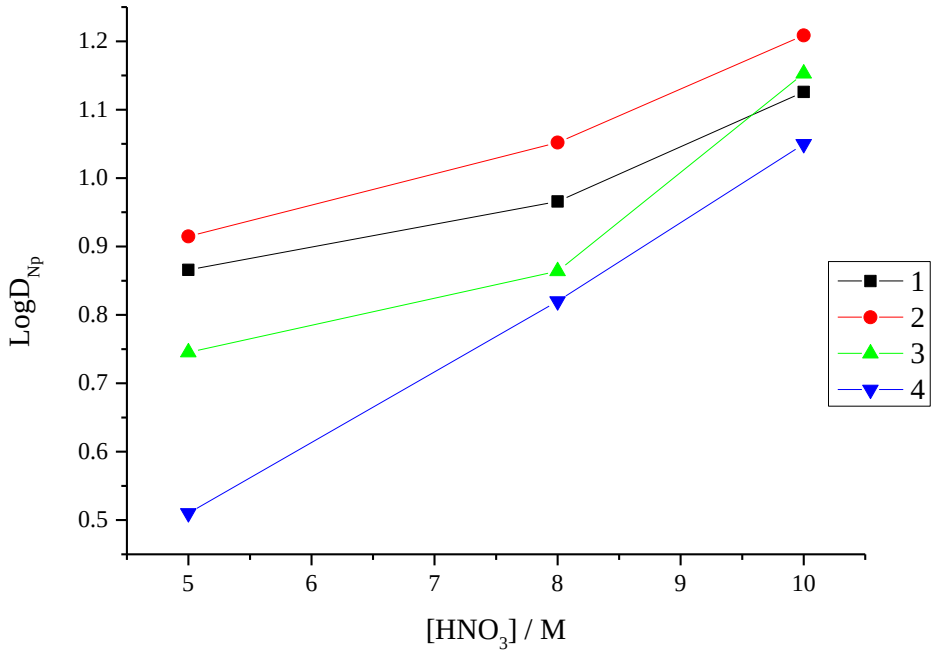

Figure 108: Distribution data for neptunium extracted from various concentration HNO_3 using four different GANEX style solvent systems.

7 Conclusion

Significant progress has been made over the last decade or so in improving the methodologies used to separate heavy metals in nuclear fuel reprocessing. This work served to enhance knowledge into the effectiveness of metal separation under current and proposed reprocessing conditions and to determine organic phase speciation, post separation.

The ^{31}P NMR data presented for zirconium separated from various aqueous nitric and hydrochloric acid mixtures using TBP, showed what are thought to be Zr-acid-TBP type complexation signals in addition to the TBP-acid adduct NMR signal. The EXAFS data collected for the organic phase post separation for a selection of these systems gave the $[Zr(NO_3)_4(TBP)_4]$ and $[ZrCl_4(TBP)_4]$ complexes for zirconium separated from 8 M nitric and 5 M hydrochloric acids, respectively. Zirconium separated from various aqueous mixtures of both nitric and hydrochloric acid seems to show preferential complexation to chloride over nitrate given by the dominance of the $[ZrCl_4(TBP)_4]$ species within the organic phase post separation according to EXAFS studies. The distribution ratios recorded for these systems increase as a function of increasing aqueous acid concentration. Zirconium separated from mixed nitric and hydrochloric acid aqueous phases showed higher distribution ratios in comparison to those recorded for singular acid systems, indicating that the presence of both anions has a cooperative effect for Zr extraction but with little evidence for the extensive formation of mixed anion complexes of Zr(IV) it is unlikely this increase in extraction is due to the formation of alternative Zr complex species in the bulk organic phase.

Technetium (pertechnetate (TcO_4^-)) separated from aqueous nitric acid using TBP was low over the nitric acid concentration range analysed, *c.f.* analogous chloride containing systems. Pertechnetate separated using TBP in the presence of zirconium illustrated similar trends in distribution ratio as a function of aqueous acid concentration, as observed in the absence of zirconium, but the presence of zirconium notably enhanced the pertechnetate separation overall. For pertechnetate separated from aqueous nitric acid in the presence of uranium, distribution ratios

were enhanced *c.f.* in the absence of uranium. Technetium separated from aqueous nitric acid in the presence of zirconium demonstrated the more efficient separation *c.f.* pure technetium and technetium co-extraction with uranium and demonstrates the difficulty in controlling Tc extraction when multiple metal ions are present in spent nuclear fuel.

Pertechnetate separated from aqueous hydrochloric acid using TBP gave much higher distribution ratios than analogous nitric acid containing systems, over the concentration range analysed and showed optimum separation at 10 M aqueous hydrochloric acid. Although here, technetium separated in the presence of co-extractable metals (zirconium and uranium) from hydrochloric acid did not enhance the separation efficiency *c.f.* pure Tc-HCl systems, the distribution ratios overall were higher than those for technetium separated with co-extractable metals (zirconium and uranium) from analogous nitric acid systems.

Technetium separated from systems where a mixed nitric-hydrochloric acid aqueous phase was utilised, demonstrated that distribution ratios increased as a function of increasing aqueous chloride concentration. The pure technetium-acid systems showed the greatest technetium separation efficiencies *c.f.* analogous systems containing co-extractable metals. This shows that Tc control in solvent extraction processes where chloride may be present will be highly problematic where both direct Tc extraction and co-extraction with other metals can occur and will require further study if such processes are to be implemented.

The ^{31}P NMR data presented for uranium separated from various aqueous nitric and hydrochloric acid mixtures using TBP showed what are thought to be U-acid-TBP type complexation signals in addition to the TBP-acid adduct NMR signal. The EXAFS data collected for the organic phase post separation for a selection of these systems modelled excellently to the $[UO_2(NO_3)_2(TBP)_2]$ and $[UO_2Cl_2(TBP)_4]$ complexes for uranium separated from 8 M nitric and 5 M hydrochloric acids respectively. Uranium separated from various aqueous mixtures of both nitric and hydrochloric acid show preferential complexation to chloride over nitrate given by the dominance of the $[UO_2Cl_2(TBP)_2]$ species within the organic phase post separation according to EXAFS studies. This observed dominance of chloride

containing species in these uranium systems was unexpectedly observed in samples of high aqueous nitrate concentration. In contrast, NMR studies indicate multiple species are present with differing dominant species at high nitrate and chloride concentrations, respectively. These contrasting results may be due to a specific issue with the chloride scattering paths in the EXAFS but without definitive assignments for each of the species observed by ^{31}P NMR spectroscopy it is difficult to be conclusive on the speciation of uranyl in these mixed acid systems. The distribution ratios recorded for these systems increase as a function of increasing aqueous acid concentration. Uranium separated from mixed nitric and hydrochloric acid aqueous phases showed no improvement in the distribution ratios in comparison to those recorded for singular acid systems. However of the mixed acid systems analysed, the distribution ratio was observed to be lowest with equal concentrations of aqueous chloride and nitrate. This suggests that the formation of mixed chloride/nitrate complexes with uranyl is not favoured for extraction by TBP and pure anion uranyl coordination species are preferred for extraction.

Trace level neptunium (Np(V)) separation experiments in which the neptunium oxidation state was not manipulated, showed an increase in the distribution ratio as a function of aqueous acid concentration (where the aqueous phase consisted of various concentration nitric and hydrochloric acid). Distribution ratios observed for neptunium (Np(V)) separated from aqueous hydrochloric acid using TBP were higher overall than those observed for analogous nitric acid systems.

Neptunium, in which the oxidation state was manipulated to Np(VI), was separated from aqueous nitric acid using TBP. The distribution ratios were seen to increase as a function of aqueous nitric acid concentration. UV/vis/nIR spectra recorded for each phase post extraction, indicated that any residual Np(V) remained in the aqueous fraction whilst the Np(VI) was separated into the organic fraction. The amount of Np(VI) separated into the organic fraction increased with increasing aqueous acid concentration. The ^{31}P NMR spectra recorded for the organic phase post extraction for neptunium containing systems, showed what is thought to be a Np-NO_3-TBP type complexation signal in addition to the acid-TBP adduct signal. Further, the EXAFS spectra recorded for Np(VI) separated from 7.2 M aqueous nitric acid modelled excellently to the species $[NpO_2(NO_3)_2(TBP)_2]$.

For Np(VI) separated from aqueous hydrochloric acid, the data indicates an increase in the distribution ratios as a function of aqueous hydrochloric acid concentration. However, at low aqueous hydrochloric acid concentrations (~ 2 M), very little neptunium was separated, whereas almost 100 % separation was observed at higher aqueous hydrochloric acid concentrations (~ 10 M). UV/vis/nIR spectroscopic analysis of each phase post extraction showed that predominantly Np(VI) was separated into the organic fraction under these conditions. The amount of Np(VI) separated was observed to increase as a function of aqueous acid concentration. The ^{31}P NMR spectra recorded for the organic phase post extraction showed what is thought to be a Np-Cl-TBP type complexation signal in addition to the acid-TBP adduct signal. Further, the EXAFS spectra recorded for Np(VI) separated from 5 M aqueous hydrochloric acid modelled excellently to the species $[NpO_2Cl_2(TBP)_2]$.

Np(VI) separated from a mixed acid aqueous phase of 5 M HNO_3 and 5 M HCl gave a higher distribution ratio than analogous pure HCl or HNO_3 systems, which corresponded to around 95 % neptunium separation. The organic phase EXAFS spectra recorded for this system showed immediate reduction on the beam line to Np(IV). Modelling was therefore not successful despite many attempts. This may imply that in mixed chloride/nitrate systems, Np REDOX properties may be different to those in pure chloride and pure nitrate systems, but studies using, for example, electrochemical techniques would be necessary to confirm this interpretation.

Trace level plutonium (Pu(IV)) separated from various concentration aqueous nitric and hydrochloric acid using TBP, was enhanced with increasing aqueous acid concentration. Although the distribution ratios for both systems increased as a function of aqueous acid concentration, the distribution ratios for plutonium separated from hydrochloric acid were observed to be much higher than those for analogous nitric acid systems.

Further, plutonium was separated using TBP from aqueous nitric and/or hydrochloric acid and the resultant organic phases studied using NMR spectroscopy. This work was carried out at the INE, Karlsruhe Germany and was therefore a NMR study only. The data collected for each system analysed showed, at - 50 ^{o}C, evidence of Pu-acid-TBP type complexation. EXAFS studies of the organic phase post extraction for

these systems would corroborate any proposed speciation within these systems, however this was not possible in the time given.

It is apparent that for some systems modelled on PUREX style reprocessing, the M-Cl bond is stronger than the equivalent M-NO_3 bond (where M is a metal). For some systems then, it is possibly beneficial to have aqueous chloride present to enhance metal separation. If the presence of chloride can be used to manipulate the oxidation state of elements like Tc and Np and therefore control the path of these elements in a PUREX flowsheet, it may avoid the need to add further chemical REDOX agents.

It was found that third phase formation, in the studies conducted here, only occurred in pure chloride containing aqueous phases and seems to be suppressed in mixed nitrate/chloride systems. Consequently, it is improbable that a pure chloride solvent extraction process will be implemented based on third phase maloperation concerns, but if chloride is present in dissolved fuel feeds the use of a nitric acid based PUREX process is unlikely to result in third phase formation.

Batch experimentation surrounding the separation of the lanthanides from aqueous nitric acid using proposed GANEX type conditions was studied here. For the various solvent systems studied (TODGA, TODGA/TBP, TODGA/1-octanol, TODGA/DMDOHEMA and DMDOHEMA), the separation of each lanthanide increases as a function of increasing aqueous nitric acid concentration overall. The data recorded indicates a general trend of improved metal distribution ratio across the lanthanide series, thus indicating that higher atomic number lanthanides exhibit more effective separation under these conditions. Lanthanides separated using a range of TODGA concentrations from 2, 6, 10 and 14 M aqueous nitric acid all demonstrated similar trends; the distribution ratio of each lanthanide increased with increasing TODGA concentration in the organic fraction. The concentration of nitric acid in the initial aqueous fraction made little difference to the resultant lanthanide distribution ratios analysed. Although it is not essential for Ln extraction to be complete for GANEX to be successful according to the proposed EURO-GANEX flowsheet, it is worthy to note that the extent of Ln extraction does depend on the type of lanthanide, most likely relating to the Ln contraction and effective ionic charge, and not just on aqueous nitric acid and organic extractant concentrations. In the case of TODGA

organic phases, there are examples where within the Ln series there are Ln ions that effectively remain in the aqueous phase and some are entirely extracted.

For other heavy metals relevant to nuclear fuel reprocessing (Tc, Np, Am, Pu) that were separated from aqueous nitric acid (8 M) using a range of TODGA concentrations, there is an increase in distribution ratio with increasing organic TODGA concentration. Plutonium is most effectively separated; neptunium, and americium separate well over the TODGA concentration range analysed; technetium is not well separated at low TODGA concentrations but shows better separation at higher organic TODGA concentrations. Similarly, using 0.2 M TODGA in the organic fraction, the distribution ratios of Np, Am, Eu and Pu each increase over the aqueous nitric acid concentration range analysed. Again, plutonium separation is more effective under these conditions. Technetium separation decreases significantly from aqueous nitric acid concentrations of 1 to 14 M.

Lanthanides separated using DMDOHEMA from a range of aqueous nitric acid concentrations showed an initial increase in distribution ratio with increasing aqueous acid concentration. However the distribution ratios for lanthanides separated from aqueous nitric acid fractions above 6 M decreased with increasing aqueous nitric acid concentration. Unlike systems using the extractant TODGA, lanthanides separated using DMDOHEMA showed distinct optimum conditions for separation. The reasons why Ln extractions using DMDOHEMA have an optimum aqueous nitric acid concentration of 6 M, and do not, for example, steadily increase with increasing nitric acid concentrations, are not obvious. Possibilities may include competition of Ln binding between DMDOHEMA and nitrate where high ntrate concentrations start to detrimentally impact Ln coordination to DMDOHEMA reducing the extent of Ln extraction, or DMDOHEMA itself may hydrogen bond with HNO_3 at high nitric acid concentrations reducing its ability to bind to lanthanides.

Lanthanides separated using a range of DMDOHEMA concentrations from 2, 6, 10 and 14 M aqueous nitric acid showed a general trend of increasing distribution ratio as a function of increasing organic DMDOHEMA concentration; however, notable variations were observed at each aqueous concentration analysed. For lanthanides

separated from 2 M aqueous nitric acid, the distribution ratios across the series were low, showing little separation and no significant trend. The lanthanides separated from 6 and 10 M aqueous nitric acid showed increasing linear trends in distribution ratio as a function of organic DMDOHEMA concentration. Although both sets of data (lanthanides separated from 6 and 10 M aqueous nitric acid) gave higher distribution ratios overall *c.f.* data observed for lanthanides separated from 2 M aqueous nitric acid, those observed for all lanthanides separated from 6 M aqueous nitric acid were notably higher, indicating these conditions were optimal for the separation of the lanthanides analysed under these conditions.

The distribution ratio data calculated for lanthanides separated from 14 M aqueous nitric acid using a range of organic DMDOHEMA concentrations did not follow a clear trend. Very little lanthanide separation was observed under these conditions.

For heavy metals (Tc, Np, Am and Pu) separated using DMDOHEMA over a range of aqueous nitric acid concentrations, the trend observed was similar to those observed in analogous systems using TODGA *i.e.* the distribution ratios for the metals analysed generally increased as a function of aqueous nitric acid concentration. However, for technetium, the distribution ratio decreased as a function of aqueous nitric acid concentration and overall, very little separation was observed under these conditions. The distribution ratios observed for Np, Am, Eu and Pu were notably improved from aqueous acid concentrations above 6 M. Plutonium gave the highest distribution ratios over the aqueous acid concentration range analysed. These heavy metals were separated from 8 M aqueous nitric acid using a range of DMDOHEMA concentrations.

The calculated distribution ratios for the above metals, analysed as a function of increasing organic DMDOHEMA concentration increased over the extractant concentrations tested. The distribution ratios for plutonium over the range of DMDOHEMA concentrations analysed were notably higher than the remaining metals examined. Technetium exhibited the lowest distribution ratios overall and showed very little separation in general under these conditions. The distribution ratios calculated for the aforementioned metals separated using DMDOHEMA were overall lower than those calculated for analogous systems containing TODGA.

The distribution ratios for neptunium (Np(VI)) separated using various GANEX type solvent systems (DMDOHEMA, TODGA/DMDOHEMA, TODGA/TBP, TODGA/1-octanol) as a function of aqueous nitric acid concentration were recorded. The neptunium separated well using each solvent system with an increase in distribution ratios observed as a function of increasing aqueous nitric acid concentration. The proposed GANEX solvent of TODGA and DMDOHEMA gave the most effective neptunium separation *c.f.* the remaining solvent systems.
Post separation, the organic fractions for the aforementioned corresponding solvent systems were analysed via EXAFS spectroscopy. It was found that upon beam line analysis, the neptunium, previously determined to be in the +6 state, reduced immediately to Np(IV), as affirmed by the XANES spectra. Consequently, modelling for samples where the TODGA extractant was present was therefore not successful despite many attempts. However, modelling of the data produced for the sample containing only DMDOHEMA in the organic fraction was successful and was deemed to be in excellent agreement with the species $[Np(DMDOHEMA)_2(NO_3)_2]$ species.

Overall, these studies will aid the formation of a next generation reprocessing system that serves to remove and recycle the more radiotoxic isotopes, creating a waste liquor that facilitates proliferation concerns. The processes studied here will contribute to the development of an overall GANEX style process that will likley use a nitric acid aqueous dissolution feed and a series of cycles and extractants, each with a specific role. From the work shown here, the GANEX solvent consisting of TODGA and DMDOHEMA, shows excellent promise in the 'first cycle' in which the transuranic and lanthanide elements are separated. If the removal of both transuranic and lanthanide elements are desired in this manner, it is hoped the work illustrated here contributes to the novel separations processes that compliment the proposed Generation IV nuclear reactors.

8 Further Work

It is proposed that future work that directly stems from the studies presented in this thesis would include a comprehensive study of plutonium speciation in the PUREX process via the use of EXAFS. It would also be favourable to investigate the speciation of plutonium in the proposed GANEX process via EXAFS to indicate any possible complexation with TODGA and DMDOHEMA. If the use of TBP is chosen as a phase modifier in the GANEX solvent, the aforementioned investigation into plutonium speciation surrounding the PUREX process would also be relevant. Further work, in addition to the data presented here, surrounding neptunium chemistry in the post-separated organic phase of the proposed GANEX process would be carried out, as well as further EXAFS analysis in the hope that oxidation state stability is achieved.

Although much analytical data has been published surrounding the effectiveness of metal separation under certain conditions using a variety of extractants, little is known of the phase transfer process *i.e.* the chemistry of the aqueous-organic interface. This work seems to indicate that in general there is no obvious link between bulk organic phase speciation and extraction performance. However, speciation at the interface may be different to what is observed in the bulk organic phase and it is the behaviour at the interface that will most likely dictate extraction performance. It would however, be of interest to develop methods for aqueous-organic interfacial analysis, such as microfocus X-ray absorption spectroscopy, and further, provide data on the interfacial speciation for the transuranic elements intended for separation in the proposed GANEX reprocessing process.

It is hoped that the kinetic behaviour of these systems of a GANEX nature can be investigated in order to build a complete picture of any proposed future reprocessing systems. This work would complement the current work which explores metal distribution at equilibrium. Oxidation state behaviour of more problematic isotopes, such as neptunium, should also be investigated in a real time, industrial type set up.

Further, it is of paramount importance that this work is carried out within industrial facilities on contactor systems, such as centrifugal contactors, mixer settlers and pulsed columns. This will built a more real picture of the behaviour of the metals involved in these systems and whether proposed industrial separation routes will affect the extraction performance of these systems.

9 References

1. Interim Storage Facility Field Survey, http://www.fepc.or.jp/english/library/power_line/detail/12/02.html).
2. M. A. Brown, P. Tkac, A. Paulenova and G. F. Vandegrift, *Sep. Sci. Technol.*, 2009, **45**, 50-57.
3. J. Kang, F. Von Hippel, A. MacFarlane and R. Nelson, *Science and Global Security*, 2002, **10**, 85-101.
4. S. B. Krivit, J. H. Lehr and T. B. Kingery, *Nuclear Energy Encyclopedia: Science, Technology, and Applications*, John Wiley & Sons, 2011.
5. C. D. Ferguson, *Nuclear Energy: What Everyone Needs to Know*, Oxford University Press, 2011.
6. M. Kurtzhand, Y. Ronen, L. Droizman and E. Shwageraus, 2006.
7. L. E. McKinley, W. Russell Alexander, W. R. Alexander and L. E. McKinley, *Radioactivity in the Environment*, Elsevier, 2007.
8. M. Salvatores and G. Palmiotti, *Prog Part Nucl Phys*, 2011, **66**, 144-166.
9. A. Makhijani, H. Hu, K. Yih, I. P. f. t. P. o. N. War, I. f. Energy and E. Research, *Nuclear Wastelands: A Global Guide to Nuclear Weapons Production and Its Health and Environmental Effects*, MIT Press, 2000.
10. B. Weaver, *Anal. Chem.*, 1954, **26**, 474-475.
11. G. Modolo, H. Asp, C. Schreinemachers and H. Vijgen, *Solvent Extraction and Ion Exchange*, 2007, **25**, 703-721.
12. J. Plaue, A. Gelis and K. Czerwinski, *Separ Sci Technol* 2006, **24**, 271-282.
13. S. Tachimori, Y. Sasaki and S. Suzuki, *Solv Extr. Ion Exch.*, 2002, **20**, 687-699.
14. R. C. O'Brien, R. M. Ambrosi, N. P. Bannister, S. D. Howe and H. V. Atkinson, *Journal of Nuclear Materials*, 2008, **377**, 506-521.
15. F. Baumgaertner and L. Finsterwalder, *The Journal of Physical Chemistry*, 1970, **74**, 108-112.

16. V. Petitjean., C. Fillet., R. Boen., C. Veyer. and T. Flament., *Qualification of a Vitrified High Level Waste Product to Support Used Nuclear Fuel Recycling in the US.*, 2002.
17. A. Poczynajlo, *J Radioanal Nucl Ch*, 1988, **125**, 445-465.
18. J. Stas, A. Dahdouh and H. Shlewit, *Periodica Polytechnica Chemical Engineering*, 2005, **49**, 3-18.
19. A. Vértes, S. Nagy, Z. Klencsár, R. G. Lovas and F. Rösch, *Handbook of Nuclear Chemistry: Vol. 1: Basics of Nuclear Science; Vol. 2: Elements and Isotopes: Formation, Transformation, Distribution; Vol. 3: Chemical Applications of Nuclear Reactions and Radiation; Vol. 4: Radiochemistry and Radiopharmaceutical Chemistry in Life Sciences; Vol. 5: Instrumentation, Separation Techniques, Environmental Issues; Vol. 6: Nuclear Energy Production and Safety Issues*, Springer, 2010.
20. A. Dyer and S. Aggarwal, *Journal of Radioanalytical and Nuclear Chemistry*, 1997, **221**, 235-238.
21. C. Madic *Radiat. Prot. Dosim.*, 1989, **26**, 15-22.
22. T. V. Healy and H. A. C. McKay, *Trans. Faraday. Soc.* , 1956, **52**, 633.
23. P. R. Vasudeva Rao and Z. Kolarik, *Solvent Extraction and Ion Exchange*, 1996, **14**, 955-993.
24. M. Nakahara and Y. Sano, *Radiochim. Acta*, 2009, **97**, 727-731.
25. T. S. Rudisill, M. C. Thompson, M. A. Norato, G. F. Kessinger, R. A. Pierce and J. D. Johnson, *Westinghouse Savannah River Company*, 2003, **Rev. 1**.
26. K. D. Kok, *Nuclear Engineering Handbook*, CRC Press, 2009.
27. R. Chiarizia and E. Philip Horwitz, *Solv Extr. Ion Exch.* , 1987, **5**, 175-194.
28. E. P. Horwitz, D. G. Kalina, H. Diamond, G. F. Vandegrift and W. W. Schulz, *Solv Extr. Ion Exch.*, 1985, **3**, 75-109.
29. J. D. Law, T. G. Garn, D. H. Meikrantz and J. Warburton, *Separation Science and Technology*, 2010, **45**, 1769-1775.
30. E. P. Horwitz and W. W. Schulz, in *New Separation Chemistry Techniques for Radioactive Waste and Other Specific Applications*, Springer Netherlands, 1991, ch. 5, pp. 21-29.

31. G. R. Choppin, M. K. Khankhasayev and H. S. Plendl, *Chemical Separations in Nuclear Waste Management: The State of the Art and a Look to the Future*, Battelle Press, 2002.
32. C. Madic, P. Blanc, N. Condamines, P. Baron, L. Berthon, C. Nicol, C. Pozo, M. Lecomte, M. Philippe and M. Masson, *Actinide partitioning from high level liquid waste using the DIAMEX process*, CEA Centre d'Etudes de la Vallee du Rhone, 30-Marcoule (France). Dept. d'Exploitation du Retraitement et de Demantelement, 1994.
33. C. Madic, B. Boullis, P. Baron, F. Testard, M. J. Hudson, J. O. Liljenzin, B. Christiansen, M. Ferrando, A. Facchini, A. Geist, G. Modolo, A. G. Espartero and J. De Mendoza, *Journal of Alloys and Compounds*, 2007, **444–445**, 23-27.
34. B. A. Moyer, *Ion Exchange and Solvent Extraction: A Series of Advances*, Taylor & Francis, 2009.
35. H. H. Dam, D. N. Reinhoudt and W. Verboom, *Chemical Society Reviews*, 2007, **36**, 367-377.
36. D. Warin, *Mater. Sci. Eng.*, 2010, **9**.
37. A. Wilden, C. Schreinemachers, M. Sypula and G. Modolo, *Solvent Extraction and Ion Exchange*, 2011, **29**, 190-212.
38. E. Aneheim, C. Ekberg and M. R. StJ. Foreman, *Solvent Extraction and Ion Exchange*, 2013, **31**, 237-252.
39. D. Magnusson, A. Geist, A. Wilden and G. Modolo, *Solvent Extraction and Ion Exchange*, 2012, **31**, 1-11.
40. A. Bhattacharyya, P. K. Mohapatra and V. K. Manchanda, *Solvent Extraction and Ion Exchange*, 2006, **24**, 1-17.
41. A. Wilden, G. Modolo, C. Schreinemachers, F. Sadowski, S. Lange, M. Sypula, D. Magnusson, A. Geist, F. W. Lewis, L. M. Harwood and M. J. Hudson, *Solvent Extraction and Ion Exchange*, 2013, **31**, 519-537.
42. G. Modolo, A. Wilden, P. Kaufholz, D. Bosbach and A. Geist, *Progress in Nuclear Energy*, 2014, **72**, 107-114.

43. R. B. Gujar, S. A. Ansari, A. Bhattacharyya, A. S. Kanekar, P. N. Pathak, P. K. Mohapatra and V. K. Manchanda, *Solvent Extraction and Ion Exchange*, 2012, **30**, 278-290.
44. A. Geist, U. Müllich, D. Magnusson, P. Kaden, G. Modolo, A. Wilden and T. Zevaco, *Solvent Extraction and Ion Exchange*, 2012, **30**, 433-444.
45. D. Magnusson, A. Geist, R. Malmbeck, G. Modolo and A. Wilden, *Procedia Chemistry*, 2012, **7**, 245-250.
46. M. Miguirditchian, L. Chareyre, X. Heres, C. Hill, P. Baron and M. Masson, *GANEX: Adaptation of the DIAMEX-SANEX Process for the Group Actinide Separation, USA.*, 2007.
47. E. Aneheim, C. Ekberg, A. Fermvik, M. R. S. Foreman, T. Retegan and G. Skarnemark, *Solv Extr. Ion Exc.*, 2010, **28**, 437-458.
48. J. Brown, F. McLachlan, M. Sarsfield, R. Taylor, G. Modolo and A. Wilden, *Solvent Extraction and Ion Exchange*, 2012, **30**, 127-141.
49. M. Carrott, K. Bell, J. Brown, A. Geist, C. Gregson, X. Hères, C. Maher, R. Malmbeck, C. Mason, G. Modolo, U. Müllich, M. Sarsfield, A. Wilden and R. Taylor, *Solvent Extraction and Ion Exchange*, 2014, **32**, 447-467.
50. M. Taube, *Fast reactors using molten chloride salts as fuel*, INFCE (Switzerland), 1978.
51. R. Taylor, *Reprocessing and Recycling of Spent Nuclear Fuel*, Elsevier Science, 2015.
52. J. Hobbs, *Orphan Wastes*, *BNFL Report*, 2007.
53. R. P. Cox, H. C. Peterson and G. H. Beyer, *Industrial & Engineering Chemistry*, 1958, **50**, 141-143.
54. J. Lehto and X. Hou, *Chemistry and Analysis of Radionuclides: Laboratory Techniques and Methodology*, Wiley, 2011.
55. S. A. Ansari, R. B. Gujar, D. R. Prabhu, P. N. Pathak and P. K. Mohapatra, *Solv Extr. Ion Exch.* , 2012, 190.
56. I. Blazheva, Y. Fedorov, B. Zilberman, L. Mashirov and O. Shmidt, *Radiochemistry*, 2009, **51**, 149-155.
57. I. Blazheva, Y. Fedorov, B. Zilberman and L. Mashirov, *Radiochemistry*, 2008, **50**, 256-260.

58. O. Sinegribova, A. Sharkunova, T. Dvoryanchikova, E. Koparulina and M. Shtutsa, *Theoretical Foundations of Chemical Engineering*, 2010, **44**, 800-804.
59. A. Da Silva, E. El-Ammouri and P. A. Distin, *Canadian Metallurgical Quarterly*, 2000, **39**, 37-42.
60. M. Taghizadeh, R. Ghasemzadeh, S. N. Ashrafizadeh, K. Saberyan and M. G. Maragheh, *Hydrometallurgy*, 2008, **90**, 115-120.
61. M. Sypula, A. Wilden, C. Schreinemachers, R. Malmbeck, A. Geist, R. Taylor and G. Modolo, *Solvent Extraction and Ion Exchange*, 2012, **30**, 748-764.
62. A. Bleise, P. R. Danesi and W. Burkart, *J. Environ. Radioact.*, 2003, **64**, 93-112.
63. T. A. S. Devraj, *Trace Analysis of Uranium and Thorium*, Discovery Publishing House, 1997.
64. S. Fortier and T. W. Hayton, *Coord. Chem. Rev.*, 2010, **254**, 197-214.
65. J. R. Kumar, J.-S. Kim, J.-Y. Lee and H.-S. Yoon, *Sep Purif Rev*, 2011, **40**, 77-125.
66. K. L. Nash and G. R. Choppin, *Separ Sci Technol* 1997, **32**, 255-274.
67. X. Ye, R. B. Smith, S. Cui, V. de Almeida and B. Khomami, *Solv Extr. Ion Exch.*, 2010, **28**, 1-18.
68. J. Plaue, *Separ Sci Technol* 2006, **41**, 2065-2074.
69. M. Miguirditchian, C. Sorel, B. Cames, I. Bisel and P. Baron, *Extraction of uranium(VI) by N,N-di-(2-ethylhexyl)isobutyramide (DEHIBA): from the batch experimental data to the countercurrent process*, 2008.
70. J. Schramke, D. Rai, R. Fulton and G. Choppin, *Journal of Radioanalytical and Nuclear Chemistry*, 1989, **130**, 333-346.
71. P. Tkac and A. Paulenova, *J. Am. Chem. Soc.*, 2007, **234**.
72. H. C. Hodge, J. N. Stannard and J. B. Hursh, *Uranium · Plutonium Transplutonic Elements*, Springer Berlin Heidelberg, 2013.
73. A. Paulenova., G. F. Vandegrift. and K. R. Czerwinski., *Plutonium Chemistry in the UREX+ Separation Processes*, *U.S D.o.E.* , 2009.
74. G. L. Silver, *Applied Radiation and Isotopes*, 2003, **59**, 217-220.

75. J. Rydberg, M. Cox and C. Musikas, *Solvent Extraction Principles and Practice*, Marcel Dekker Incorporated, 2004.
76. J. Plaue, A. Gelis, K. Czerwinski, P. Thiyagarajan and R. Chiarizia, *Solvent Extraction and Ion Exchange*, 2006, **24**, 283-298.
77. M. Carrott, A. Geist, X. Hères, S. Lange, R. Malmbeck, M. Miguirditchian, G. Modolo, A. Wilden and R. Taylor, *Hydrometallurgy*, 2015, **152**, 139-148.
78. G. A. Burney and R. M. Harbour, *Radiochemistry of Neptunium*, Technical Information Center, Office of Information Services, United States Atomic Energy Commission, 1974.
79. R. K. Sjoblom, J. C. Hindman, U. S. A. E. Commission and L. Argonne National, *Spectrophotometry of neptunium in perchloric acid solutions*, Argonne National Laboratory, Chicago, III., 1950.
80. V. Marchenko, V. Koltunov and K. Dvoeglazov, *Radiochemistry*, 2010, **52**, 111-126.
81. H. Steele and R. J. Taylor, *Inorganic Chemistry*, 2007, **46**, 6311-6318.
82. M. J. Sarsfield, R. J. Taylor and C. J. Maher, *Radiochim. Acta*, 2007, **95**, 677-682.
83. N. Kumari, P. N. Pathak, D. R. Prabhu and V. K. Manchanda, *Separation Science and Technology*, 2012, **47**, 1492-1497.
84. O. Tochiyama, Y. Nakamura, Y. Katayama and Y. Inoue, *J. Nucl. Sci. Technol.*, 1995, **32**, 50-59.
85. Y. Ban, S. Hotoku and Y. Morita, *J Nucl Sci Technol*, 2012, **49**, 588-594.
86. K. Reinschmiedt, C. Sullivan and M. Woods, *Inorg. Chem.*, 1973.
87. A. Wilden, G. Modolo, M. Sypula, A. Geist and D. Magnusson, *Procedia Chemistry*, 2012, **7**, 418-424.
88. J. C. Mailen and J. T. Bell, *Separ Sci Technol*, 1987, **22**, 347-360.
89. E. Aneheim, C. Ekberg, M. R. S. Foreman, E. Löfström-Engdahl and N. Mabile, *Separ. Sci. Technol*, 2011, **47**, 663-669.
90. R. J. Silva, G. Bidoglio, P. B. Robouch, I. Puigdomenech, H. Wanner and H. Rand, *Chemical Thermodynamics of Americium*, Elsevier Science, 2012.
91. C. Rostaing, C. Poinssot, D. Warin, P. Baron and B. Lorraina, *Procedia Chemistry*, 2012, **7**, 367-373.

92. L. R. Morss, N. M. Edelstein and J. Fuger, *The Chemistry of the Actinide and Transactinide Elements (Set Vol.1-6): Volumes 1-6*, Springer, 2010.
93. P. J. Panak and A. Geist, *Chem. Rev.*, 2013, **113**, 1199-1236.
94. M. Nilsson, C. Ekberg, M. Foreman, M. Hudson, J. O. Liljenzin, G. Modolo and G. Skarnemark, *Solvent Extraction and Ion Exchange*, 2006, **24**, 823-843.
95. K. H. Lieser, *Radiochimca Acta*, 1993, **63**, 5.
96. D. Curtis, J. Fabryka-Martin, P. Dixon and J. Cramer, *Geochim. Cosmochim. Acta*, 1999, **63**, 275-285.
97. R. E. Wildung, K. M. McFadden and T. R. Garland, *J. Environ. Qual.*, 1979, **8**, 156-161.
98. J. P. Icenhower, N. P. Qafoku, J. M. Zachara and W. J. Martin, *American Journal of Science*, 2010, **310**, 721-752.
99. T. N. Jassim, J. O. Liljenzin, R. Lundqvist and G. Persson, *Solvent Extraction and Ion Exchange*, 1984, **2**, 405-419.
100. M. Takeuchi, S. Tanaka, M. Yamawaki and S. Tachimori, *Solvent Extraction and Ion Exchange*, 1995, **13**, 43-57.
101. A. M. Fedosseev, N. A. Budantseva, M. S. Grigoriev, K. E. Guerman and J. C. Krupa, *Journal*, 2003, **91**, 147.
102. Y. Kanchiku, *Bulletin of the Chemical Society of Japan*, 1969, **42**, 2831-2835.
103. V. A. Volkovich, I. May, J. M. Charnock and B. Lewin, *Physical Chemistry Chemical Physics*, 2002, **4**, 5753-5760.
104. J. Rothe, A. Denecke Melissa, K. Dardenne and T. Fanghänel, *Journal*, 2006, **94**, 691.
105. B. Ravel and M. Newville, *Journal of Synchrotron Radiation*, 2005, **12**, 537-541.
106. M. Baaden, R. Schurhammer and G. Wipff, *The Journal of Physical Chemistry B*, 2002, **106**, 434-441.
107. C. R. Blaylock and D. W. Tedder, *Solv Extr. Ion Exch.*, 1989, **7**, 249-271.
108. B. Mokili and C. Poitrenaud, *Solv Extr. Ion Exch* 1995, **13**, 731-754.

109. K. Alcock, S. Grimley, T. Healy, J. Kennedy and H. McKay, *Transactions of the Faraday Society*, 1956, **52**, 39-47.
110. R. Chiarizia and A. Briand, *Solv Extr. Ion Exch*, 2007, **25**, 351-371.
111. E. Hesford and H. A. C. McKay, *Journal of Inorganic and Nuclear Chemistry*, 1960, **13**, 156-164.
112. R. Chiarizia, M. P. Jensen, M. Borkowski, J. R. Ferraro, P. Thiyagarajan and K. C. Littrell, *Solvent Extraction and Ion Exchange*, 2003, **21**, 1-27.
113. R. Chiarizia, A. Briand, M. P. Jensen and P. Thiyagarajan, *Solv Extr. Ion Exch*, 2008, **26**, 333-359.
114. R. Chiarizia, P. G. Rickert, D. Stepinski, P. Thiyagarajan and K. C. Littrell, *Solvent Extraction and Ion Exchange*, 2006, **24**, 125-148.
115. R. K. Jha, K. K. Gupta, P. G. Kulkarni, P. B. Gurba, P. Janardan, R. D. Changarani, P. K. Dey, P. N. Pathak and V. K. Manchanda, *Desalination*, 2008, **232**, 225-233.
116. R. Shabana and F. Hafez, *Journal of Radioanalytical Chemistry*, 1975, **26**, 63-71.
117. T. V. Healy and H. A. C. McKay, *Transactions of the Faraday Society*, 1956, **52**, 633-642.
118. A. E. Levitt and H. Freund, *J. Am. Chem. Soc.*, 1956, **78**, 1545-1549.
119. N. Ishii, K. Tagami and S. Uchida, *Chemosphere*, 2004, **57**, 953-959.
120. Z. Kolarik and P. Dressler, *Solvent Extr. Ion Exc.*, 1989, **7**, 625-644.
121. J. Garraway and P. D. Wilson, *Journal of the Less Common Metals*, 1985, **106**, 183-192.
122. K. L. Nash and G. J. Lumetta, *Advanced Separation Techniques for Nuclear Fuel Reprocessing and Radioactive Waste Treatment*, Elsevier Science, 2011.
123. J. A. Rard, *Journal of Nuclear and Radiochemical Sciences*, 2005, **6**, 197-204.
124. T. Ishimori and K. Watanabe, *Bulletin of the Chemical Society of Japan*, 1960, **33**, 1443-1448.
125. D. J. Pruett, *Solvent extraction of heptavalent technetium by tributyl phosphate*, 1981.

126. S. K. Patil, V. V. Ramakrishna, G. V. N. Avadhany and M. V. Ramaniah, *Journal of Inorganic and Nuclear Chemistry*, 1973, **35**, 2537-2545.
127. E. Anders, *The Radiochemistry of Technetium*, Subcommittee on Radiochemistry, National Academy of Sciences-National Research Council, available from the Office of Technical Services, Department of Commerce, 1960.
128. J. Steigman, G. Meinken and P. Richards, *The International Journal of Applied Radiation and Isotopes*, 1975, **26**, 601-609.
129. P. Giridhar, K. Venkatesan, T. Srinivasan and P. Vasudeva Rao, *Journal of Radioanalytical and Nuclear Chemistry*, 2005, **265**, 31-38.
130. M. L. Dietz and D. C. Stepinski, *Talanta*, 2008, **75**, 598-603.
131. T. A. Todd, *Journal*, 2009.
132. F. Testard, T. Zemb, P. Bauduin and L. Berthon, *ChemInform*, 2010, **41**, i.
133. D. Peppard, G. Mason and M. Gergel, *Journal of Inorganic and Nuclear Chemistry*, 1957, **3**, 370-378.
134. H. Irving and D. N. Edgington, *Journal of Inorganic and Nuclear Chemistry*, 1959, **10**, 306-318.
135. K.-W. Kim, K.-C. Song, E.-H. Lee, I.-K. Choi and Y. J-H., *J. Radioanal. Nucl. Ch.*, 2000, **246**, 215-219.
136. C. Gregson, C. Boxall, M. Carrott, S. Edwards, M. Sarsfield, R. Taylor and W. D., *Procedia Chemistry*, 2012, **7**, 398-403.
137. T. Ishimori and E. Nakamura, *Bulletin of the Chemical Society of Japan*, 1959, **32**, 713-720.
138. M. J. Sarsfield, I. May, S. M. Cornet and M. Helliwell, *Inorganic Chemistry*, 2005, **44**, 7310-7312.
139. J. N. Mathur, M. S. Murali, M. V. Balarama Krishna, R. H. Iyer, R. R. Chitnis, P. K. Wattal, A. K. Bauri and A. Banerji, *Journal of Radioanalytical and Nuclear Chemistry*, 1996, **213**, 419-429.
140. A. S. Solovkin, *Soviet Atomic Energy*, 1971, **30**, 673-675.
141. A. Paulenova, I. George F. Vandegrift and K. R. Czerwinski, *Plutonium Chemistry in the UREX+ Separation Processes*, Report DOE/ID/14652; TRN: US1001317, 2009.

142. T. N. Jassim and A.-H. I., *J. For Pure & Appl. Sci.*, 2011, **24**, 183-192.
143. N. Souka, R. Shabana and F. Hafez, *Microchemical Journal*, 1976, **21**, 215-221.
144. A. Geist and G. Modolo, 2009.
145. Z.-X. Zhu, Y. Sasaki, H. Suzuki, S. Suzuki and T. Kimura, *Anal. Chim. Acta*, 2004, **527**, 163-168.
146. P. Deepika, K. N. Sabharwal, T. G. Srinivasan and P. R. Vasudeva Rao, *Solvent Extraction and Ion Exchange*, 2010, **28**, 184-201.
147. M. J. Carrot, C. R. Gregson and R. J. Taylor, *Solvent Extraction and Ion Exchange*, 2012, **31**, 463-482.
148. A. Wilden, G. Modolo, P. Kaufholz, F. Sadowski, S. Lange, M. Sypula, D. Magnusson, U. Müllich, A. Geist and D. Bosbach, *Solvent Extraction and Ion Exchange*, 2014, **33**, 91-108.
149. R. Taylor, F. Livens, A. Mount, L. Harwood, C. Rhodes and B. Hanson, *Actinide and Fission Product Partitioning and Transmutation*, 2013, 36.
150. A. Rout, K. A. Venkatesan, T. G. Srinivasan and P. R. Vasudeva Rao, *J. Hazard. Mater.*, 2012, **221–222**, 62-67.
151. R. J. Taylor, C. R. Gregson, M. J. Carrott, C. Mason and M. J. Sarsfield, *Solvent Extraction and Ion Exchange*, 2013, **31**, 442-462.